Multi Criteria Design Optimization and Control of Community Scale Photovoltaic based Reverse Osmosis Water Desalination System

BY

NASEER AHMAD

A Dissertation Presented to the

DEANSHIP OF GRADUATE STUDIES

KING FAHD UNIVERSITY OF PETROLEUM & MINERALS

DHAHRAN, SAUDI ARABIA

In Partial Fulfillment of the

Requirements for the Degree of

DOCTOR OF PHILOSOPHY

In

MECHANICAL ENGINEERING

DECEMBER 2014

KING FAHD UNIVERSITY OF PETROLEUM & MINERALS
DHAHRAN- 31261, SAUDI ARABIA

DEANSHIP OF GRADUATE STUDIES

This thesis, written by **Naseer Ahmad** under the direction his thesis advisor and approved by his thesis committee, has been presented and accepted by the Dean of Graduate Studies, in partial fulfillment of the requirements for the degree of **DOCTOR OF PHILOSOPHY IN MECHANICAL ENGINEERING**.

Anwar Khalil Sheikh

Dr. Anwar Khalil Sheikh
(Advisor)

Dr. Moustafa Elshafei Ahmed Elshafei
(Co-Advisor)

Dr. Zuhair Mattoug Gasem
Department Chairman

Dr. Palanichamy Gandhidasan
(Member)

Dr. Salam A. Zummo
Dean of Graduate Studies

Dr. Hussain Mohammad Al-Qahtani
(Member)

18/12/14
Date

Dr. Mohammed Ashraf Gondal
(Member)

Dedicated to

Allah (SWT) and His Last Prophet Muhammad

(PBUH)

For whom the whole universe and worlds are created

ACKNOWLEDGMENTS

Countless thanks to Allah (SWT), the most Merciful and Gracious. No good act and the deed of the life cannot be accomplished without His special permission. Peace be upon The Last Prophet, The Mohammad, the last connection between human kind and Allah SWT. His teachings are the evergreen source of guidance for human being in every aspect and race of life for the success in this life and hereafter.

I am highly indebted to my thesis supervisor Dr. Anwar Khalil Sheikh and Co-supervisor Dr. Moustafa Elshafei for their constant technical and moral support, encouragement and guidance during the successful accomplishment of this research work.

I would also like to present my grateful thanks to my thesis committee members, Dr. P. Gandhidasan, Dr. Hussain Al-Qahtani and Dr. Ashraf Gondal for their constant support, cooperation and involvement in reviewing the research work.

I would like to acknowledge the support of King Fahd University of Petroleum and Minerals through the Center for Clean Water and Clean Energy at KFUPM and MIT (R6-DMN-08- Design and Manufacturing of Solar Power Systems and Devices for Challenging Environments) for providing this excellent opportunity of research work.

I am also very thankful to my parents, wife, children (Zainab and Muhammad), brothers, sisters and friends for their constant support, love and prayers. Their encouragement and moral support always been a great source in the achievement of this goal.

TABLE OF CONTENTS

LIST OF TABLES

LIST OF FIGURES

NOMENCLATURE

A_i	Anisotropy index
A_{perm}	Permeability of the membrane, ($1.086x10^{-5}$ $m^3/(m^2$-h-bar))
B	Mean anomaly of the earth
B_{salt}	Salt permeability of membrane ($4.65x10^{-7}$ $m^3/(m^2$-h))
C_p	Permeate concentrate, (ppm, mg/l)
C_{fc}	Average salinity of feed and brine, (ppm, mg/l)
C_f	Feed water concentration, (ppm, mg/l)
C_c	Brine concentration, (ppm, mg/l)
CPF	Concentration polarization factor
C_{TCF}	Temperature correction factor
FF	Fouling factor
f	Modulating factor
G	Solar radiation
G_{ref}	Solar radiation of 1000 W/m^2
G_{sc}	Solar constant, $1367W/m^2$
G_{on}	Solar radiation received on the top of the earth's atmosphere, (W/m^2)
G_{oh}	Radiation collected on the horizontal surface on the tip of atmosphere
G_{dT}	Diffuse component of the solar radiation on inclined surface, (W/m^2)
G_T	Solar radiation on the tilted surface, (W/m^2)
$G_{T,NOCT}$	Solar radiation at NOCT, (W/m^2)
G_d	Diffuse component of the solar radiation on flat surface, (W/m^2)

$I_{sc,ref}$	Short circuit current at reference conditions (Amps)
n	Ordinal date of the year
P_{fc}	Average feed and brine pressure, (bars)
P_p	Permeate back pressure, (bars)
P_f	Feed/System pressure, (bars)
P_c	Brine/Concentrate pressure, (bars)
Q_p	Permeate flow rate, (m^3/h)
Q_b	Brine flow rate, (m^3/h)
Q_f	Feed flow rate, (m^3/h)
Q_c	Brine/Concentrate flow rate, (m^3/h)
R_b	Geometric factor
SEC	Specific energy consumption, (kWh/m^3)
S_e	Membrane active surface area, (m^2)
T_w	Feed water temperature, (^{o}C)
T_c	PV cell temperature, (^{o}C)
$T_{c,ref}$	PV cell reference temperature, 25 ^{o}C
$T_{C,NOCT}$	Cell temperature defined at NOCT, (^{o}C)
$T_{a,NOCT}$	Ambient temperature defined at NOCT, (^{o}C)
t_s	Solar time, (hours)
U_L	Overall loss coefficient to the environment
Y	Recovery ratio, (%)
φ	Latitude of the site where PVRO is installed, (degree)

θ_z	Zenith angle of the site, (degree)
α_s	Solar altitude angle, (degree)
γ	Solar azimuth angle, (degree)
γ_s	Surface azimuth angle, (degree)
β	Inclination of the surface/slope of PV panel, (degree)
θ	Angle between beam radiation and normal to the surface, (degree)
δ	Declination of the earth
ω	Hour angle, (hours)
τ	Solar transmittance of the PV module
α	Solar absorption of the module
η_C	Electrical conversion efficiency, (%)
ρ	Surrounding diffuse reflectance factor
π_f	Feed water osmotic pressure, (bars)
π_b	Concentrate osmotic pressure, (bars)
π_p	Permeate side osmotic pressure, (bars)
η_{MOTOR}	DC motor efficiency, (85.5 %)
η_{PUMP}	Pump efficiency, (75 %)
η_{ERD}	Energy recovery device efficiency, (80 %)
$\mu_{p,temp}$	Temperature coefficient for PV cell for output power
$\mu_{ocv,temp}$	Temperature coefficient for PV cell for open circuit voltage
$\mu_{scc,temp}$	Temperature coefficient for PV cell for short circuit current

ABSTRACT (English)

Full Name : Naseer Ahmad

Thesis Title : Multi Criteria Design Optimization and Control of Community Scale Photovoltaic based Reverse Osmosis Water Desalination System

Major Field : Mechanical Engineering

Date of Degree : December 2014

Access to safe, clean drinking water is a major challenge to many communities which reside near the seawater or brackish water resource. PV driven RO water desalination is a viable solution to this acute shortage of clean water for underserved communities in developing countries. The optimal design process of PVRO system encompasses different disciplines starting from energy harvesting from PV panels, optimal RO process operation under available energy, reduced RO membrane maintenance and environmental friendly water treatment issues.

In this thesis, optimal operational aspects of a designed community scale PVRO system are comprehensively discussed. A detailed set of physics based models of whole PVRO system are meticulously developed and solved to accomplish this task. This developed PV and RO system modeling technique (independent PV and RO, and integrated PVRO) is validated using the KFUPM experimental PVRO facility.

Electrical energy harvested from the solar radiation using PV panels is prone to be variable and fluctuating in nature throughout the whole day, but on the other hand desalination process needs certain amount of energy to keep it in operating state for the permeate production. The different parameters of PV system e.g. maximum available

power and its duration, power increasing and decreasing trends and total duration of power availability were studied for fixed, single and double axis tracked PV panels for different extreme days of all four seasons of the year.

For a single stage single pass RO configuration, its operational design space was determined by considering the RO membrane data provided by its manufacturer as membrane operational constraints. These constraints are the maximum allowable permeate flux, maximum feed flow rate, maximum recovery ratio and minimum concentrate flow rate for specific RO stage configuration. Within the developed RO operational design space, PV output power (ranging from minimum to maximum available power from PV source) lines are drawn to determine the feasible operational region of PVRO system. Within the operational design space, design variables (feed flow rate and system pressure) are manipulated in such a way to keep the RO at optimum operation methodology while taking the wide range of PV power utilization into consideration. The investigated operational methodologies are constant feed water flow rate, constant feed pressure, constant retentate flow rate, constant recovery ratio and constant permeate salinity. For each of this methodology specific energy consumption (SEC) of RO unit over the whole range of available PV power was acquired. The analysis of the results revealed that least SEC of the RO system is achieved by constant feed pressure methodology if the available PV power is sufficient enough to drive the RO pump. Constant Recovery Ratio methodology is preferable with slightly higher SEC than constant feed pressure methodology's SEC when the broad range of PV available power is to be utilized.

Among the possibilities of running the system either at constant pressure (CP), constant recovery ratio (CRR), or combined mode (CP + CRR), the best methodology can

be selected and the optimal set points for the RO system i.e. (RO system pressure and feed flow rate) are computed according to the available PV power for the fixed and tracked PV panels. These values are sent to the local feed flow control and pressure control loops as reference signals. The local controllers make use of feedback control system to track the reference values effectively.

To attain the sustainable and environment friendly PVRO operation, solar UV disinfection at pretreatment and at post treatment is also envisaged. In pursuit of this, two solar disinfection photo reactors, stair case and parabolic trough concentrator (PTC) were designed, fabricated and demonstrated for disinfection of E.Coli bacteria. The results revealed that adequate disinfection is attained using sunlight with the use of supported catalyst in both reactors. Experimental results revealed that 28% and 75% of the initial bacterial concentration is disinfected in stair case and PTC photo reactor, respectively during the first 20 minutes of operation. The fast decay in bacterial disinfection activity in PTC is attributed due to the high insolation flux at the tube leading to more photo catalytic activity.

ABSTRACT (Arabic)

ملخص الرسالة

الاسم الكامل: نصير أحمد

عنوان الرسالة: التصميم الأمثل والمتعدد المعايير و التحكم في نظام لتحلية المياه بالتناضح العكسي المدفوع بالطاقة الكهروضوئية على نطاق مجتمعي.

التخصص: الهندسة الميكانيكية

تاريخ الدرجة العلمية: : ديسمبر/2014

إن الحصول على مياه شرب مأمونة ونظيفة يمثل تحديا كبيرا لكثير من المجتمعات التي تتواجد بالقرب من مياه البحر أو موارد المالحة.إن تحلية المياه بالتناضح العكسي المدفوع بالكهروضوئية حل ناجع لهذا النقص الحاد في المياه النظيفة للمجتمعات المحرومة في البلدان النامية .عملية التصميم الأمثل لنظام التناضح العكسي المدفوع بالكهروضئية يشمل تخصصات مختلفة بدءا من جمع الطاقة من الألواح الكهروضوئية، و أمثل عملية تناضح عكسي بحسب الطاقة المتاحة، وخفض صيانة غشاء التناضح العكسي وكذلك قضايا معالجة المياه الصديقة للبيئة.

ففي هذه الأطروحة، سيتم التناول بشكل شامل للجوانب التشغيلية المثلى لنظام التناضح العكسي المدفوع بالكهروضئية المصمم لإنتاج المياه المحلاة على نطاق مجتمعي.تم تطوير مجموعة مفصلة من النماذج القائمة على الفيزياء من نظام التناضح العكسي المدفوع بالكهروضئية بأكمله بدقة متناهية لإنجاز هذه المهمة.إن التقنية المطورة لنمذجة نظامي التناضح العكسي و الكهروضوئية (نظام الكهروضوئية المستقل و نظام التناضح العكسي المستقل ونظام التناضح العكسي المدفوع بالكهروضئية المتكامل) قد تم التحقق من صحتها بإستخدام المنشأة التجريبية للتناضح العكسي المدفوع بالكهروضئية في جامعة الملك فهد للبترول والمعادن.

الطاقة الكهربائية التي تحصد من الأشعة الشمسية باستخدام الألواح الكهروضوئية عرضة لتكون متغيره ومتقلبة بطبيعتها على مدار اليوم كاملا، بينما عملية التحلية تحتاج كمية محددة من الطاقة لإبقائها في وضع التشغيل لإنتاج

التغلغل اللازم.المعايير المختلفة من النظام الكهروضوئي على سبيل المثال، الطاقة القصوى المتاحة ومدتها، واتجاهات زيادة الطاقة وخفضها والمدة الكلية لتوافر الطاقة، تمت دراستها للالألواح الكهروضوئية ذات محور التعقب الثابت و المفرد والمزدوج لمختلف الأيام من جميع الفصول الأربعة من السنة.

بالنسبة لتهيئة نظام التناضح العكسي ذات التمريرة الواحدة والمرحلة الواحدة، فقد تم تحديد مجال التصميم التشغيلي لها من خلال النظر في بيانات غشاء التناضح العكسي المقدمة من قبل الشركة المصنعة لها عن القيود التشغيلية للغشاء.هذه القيود هي الحد الأقصى المسموح به لتدفق التخلل ، الحد الأقصى لمعدل تدفق التغذية، ونسبة الإسترداد القصوى وأدنى معدل لتدفق التركيز وذلك لكل تهيئة لمراحل التناضح العكسي.في إطار فضاء التصميم التشغيلي المطور للتناضح العكسي، فإنه يتم سحب خرج خطوط الطاقة للنظام الكهروضوئي التي تتراوح من الحد الأدنى إلى أقصى قدر متاح من الطاقة من مصدر نظام التناضح العكسي المدفوع بالكهروضوئية ليتم تحديد المنطقة التشغيلية المجدية .ضمن مساحة التصميم التشغيلي، فإنه تتم معالجة متغيرات التصميم (معدل تغذية التدفق وضغط النظام) بطريقة ما للحفاظ على التناضح العكسي في منهجية التشغيل الأمثل في حين أخذ مجموعة واسعة من استخدام طاقة النظام الكهروضوئي في الاعتبار.المنهجيات التشغيلية التي تم بحثها هي معدل ثابت لتدفق مياه التغذية، تغذية ثابتة للضغط ، معدل ثابت لتدفق المياه المالحة المتبقية من المياه المحلاة، نسبة ثابتة للشفاء وملوحة ثابتة للتخلل.لكل من هذه المنهجيات، فإنه تم إكتساب إستهلاك الطاقة المحدد (SEC) لوحدة التناضح العكسي على كامل مدى طاقة النظام الكهروضوئي المتاحة.كشف تحليل النتائج أن أقل قيمة لإستهلاك الطاقة المحدد SEC لنظام التناضح العكسي يتحقق من خلال منهجية التغذية بالضغط الثابت إذا كانت طاقة النظام الكهروضوئي المتاحة كافية لدفع مضخة نظام التناضح العكسي.إن منهجية نسبة الاسترداد الثابت مفضلة مع الإرتفاع الطفيف في معدل إستهلاك الطاقة المحدد SEC على منهجية ضغط التغذية الثابت عندما يتم إستخدام النطاق الواسع من طاقة النظام الكهروضوئي المتاحة.

ومن بين خيارات تشغيل النظام إما في الضغط الثابت (CP) ، أو نسبة الاسترداد الثابتة (CRR) ، أو الوضع المدمج (CP + CRR) ، فإنه يمكن اختيار أفضل منهجية و أمثل نقاط التهيئة لنظام التناضح العكسي أي (ضغط النظام ومعدل تدفق التغذية لنظام التناضح العكسي) يتم إحتسابه وفقا للقوة المتاحة من النظام الكهروضوئي لكل من الألواح الكهروضوئية الثابتة والمتعقبة.يتم إرسال هذه القيم إلى عقد التحكم في تدفق التغذية المحلي و عقد التحكم في الضغط كإشارات مرجعية .وحدات التحكم المحلية تستخدم نظام التحكم بالردود لتتبع القيم المرجعية على نحو فعال .

لتحقيق عملية تناضح عكسي مدفوع بالكهروضوئية مستدامة وصديقة للبيئة ، فإنه تم توخي التعقيم بالأشعة الشمسة الفوق البنفسجية عند مرحلة قبل المعالجة وكذلك بعد المعالجة أيضا.وسعيا لتحقيق ذلك، فقد تم تصميم وتصنيع مفاعلين فوتوغرافيين للتطهير الشمسي، الأول سلمي الشكل و الثاني مكثِف على شكل قطع مكافئ(PTC) ، لإظهار القدرة على تعقيم بكتيريا إي.كولاي .أظهرت النتائج أن التطهير الملائم يتحقق باستخدام أشعة الشمس مع استخدام محفز مساند في كل مفاعل .أظهرت النتائج التجريبية أن 28٪ و 75٪ من تركيز البكتيريا الأولي تم تطهيره في حالة المفاعل السلمي الشكل و المفاعل المكثف على شكل القطع المكافئ PTC ، على التوالي خلال أول 20 دقيقة من التشغيل .ويعزى الاضمحلال السريع في نشاط التطهير الجرثومي في المفاعل المكثف على شكل القطع المكافئ PTC إلى الدفق ذي العزل العالي في الأنبوب ممايؤدي إلى المزيد من نشاط الحفازة الفوتوغرافية.

Chapter 1

Introduction and literature review

Water is life in the universe and clean water is essential to the human being for his good health. Water is the backbone of the global economy, quality, reliable, and sustainable supplies are vital for agriculture, industry, recreation, energy production, and domestic consumption [1]. In the past few decades, clean water supply has become more and more critical due to excessive use and increasing contamination of natural water sources. Globe is facing formidable challenge of scarcity of water due to the external draughts, population growth, health based regulations and competing demand from users. Moreover, the demand for drinking water in the world is increasing and regulations on drinking water quality have become a lot more stringent [2]. Improving the effectiveness and efficiency of water purification technology, to produce clean water and protect the environment in a sustainable manner, is considered by many as perhaps the main *challenge of the 21st century*. Frantic efforts are underway throughout the world to avert this looming crisis by conservation of the existing limited fresh water supply and conversion of the abundantly available seawater through various desalting technologies [3].

Rapid industrial growth, the worldwide population explosion and increase in the life style of the people have resulted in a large escalation of demand for fresh/clean water. Moreover the fossil fuels are exhausting as time is progressing and this alarming situation necessitates the technological development of water desalination processes driven by

renewable energies. Among the different renewable energy sources (geothermal, solar and wind), solar energy is ubiquitous and easily accessible to every human and it can effectively be used for the brackish or seawater desalination using thermal or membrane based filtration process. Along with other commercial available purification/treatment technologies i.e. multi effect distillation (MED), multi stage flashing (MSF), vapor compression (VC) and electro dialysis (ED), reverse osmosis (RO) is one of the primary means of the desalination of water [4]. Figure 1.1 depicts out different renewable energy sources, their conversions to electricity, heat and shaft energies connected with potential desalination technologies. In recent years, reverse osmosis (RO) has become a critical technology, which promises to greatly increase the supply of clean water through desalination and purification of nontraditional water sources such as brackish, sea, and wastewater [3]. RO is considered as the simplest and most efficient technique for seawater desalination purposes [5]. It is reported that membrane-based desalination accounts for about 53% of the installed capacity of water desalination all around the world [6]. PV-powered reverse osmosis is considered one of the most promising forms of renewable-energy-powered desalination, especially when it is used in remote areas.

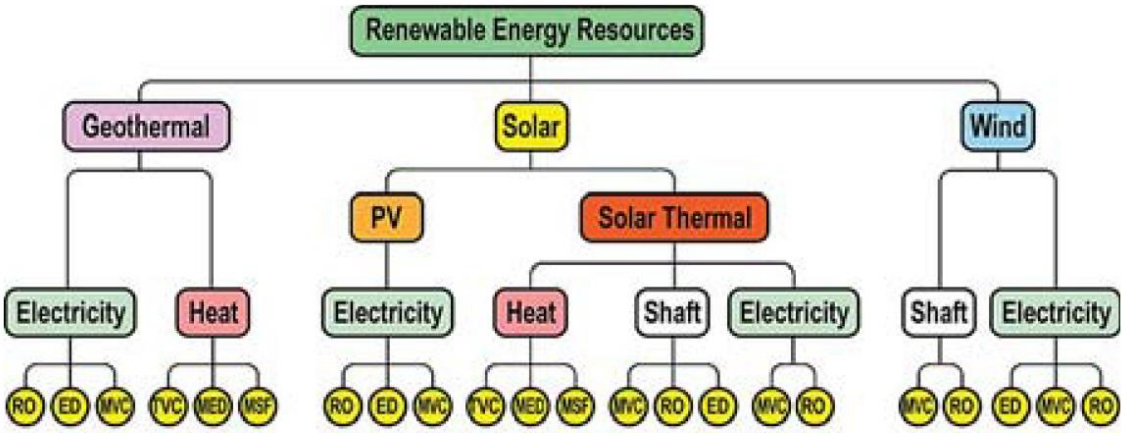

Figure 1.1: Renewable energy and desalination technologies [4]

PVRO is most cost-competitive for small-scale systems where other technologies are less competitive [7]. Among the renewable driven desalination technologies, PVRO has the maximum share of 40% and is shown in Figure 1.2.

1.1 PVRO desalination system

PVRO water desalination unit is composed of two modules, solar energy power system and RO desalination system as shown in the Figure 1.3. The basic building block element of PV cells is the semiconductor devices, which convert the sunlight energy directly into and electrical energy. To convert the maximum amount of solar radiation into electrical energy it is desirable to have solar tracker which ensures the PV panel in a position perpendicular to the solar radiation during the daylight. The output of the PV module is strong function on solar irradiation and module temperature. Due to the specific nature of the IV characteristics of the PV module, a maximum power point tracker (MPPT) is usually employed to harvest the maximum possible DC energy from the PV module. Batteries might be employed between MPPT and load to smooth out the variations in the power due to intermittent fluctuation in the insolation.

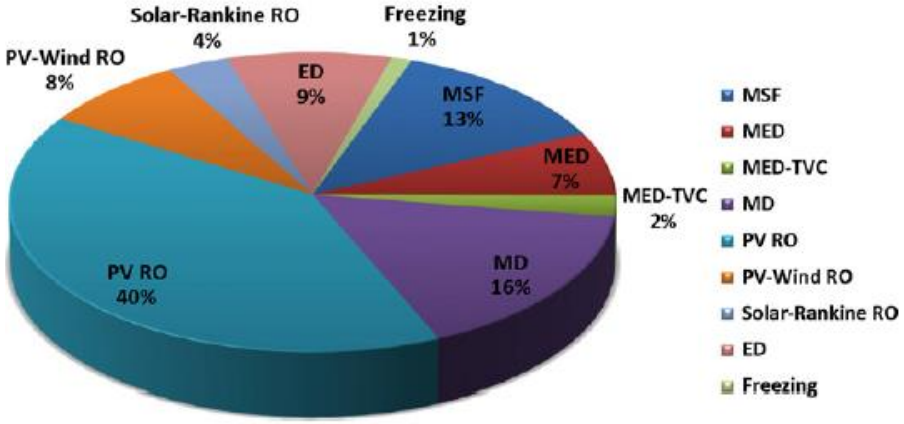

Figure 1.2: Renewable energy desalination technologies installed worldwide [8]

The disadvantages of the batteries are periodic maintenance and reduced life cycle when operated in deep discharge mode in hot climates. The DC power available from the MPPT is converted into AC power and may be utilized for certain applications. In RO desalination system low pressure pumps are used to suck the water from the source and provide sufficient amount of pressure to initiate the pre filtration process. High pressure pumps are used to move the feed water with a certain flow rate and pressure. The power available from the PV module is varying throughout the day and its proper study is essential to make full use of it for desalination purpose. Reverse osmosis is a pressure-driven membrane-based process, where the membrane acts as the heart of the process in separating the undesired constituents from the feed to obtain the desired pure product.

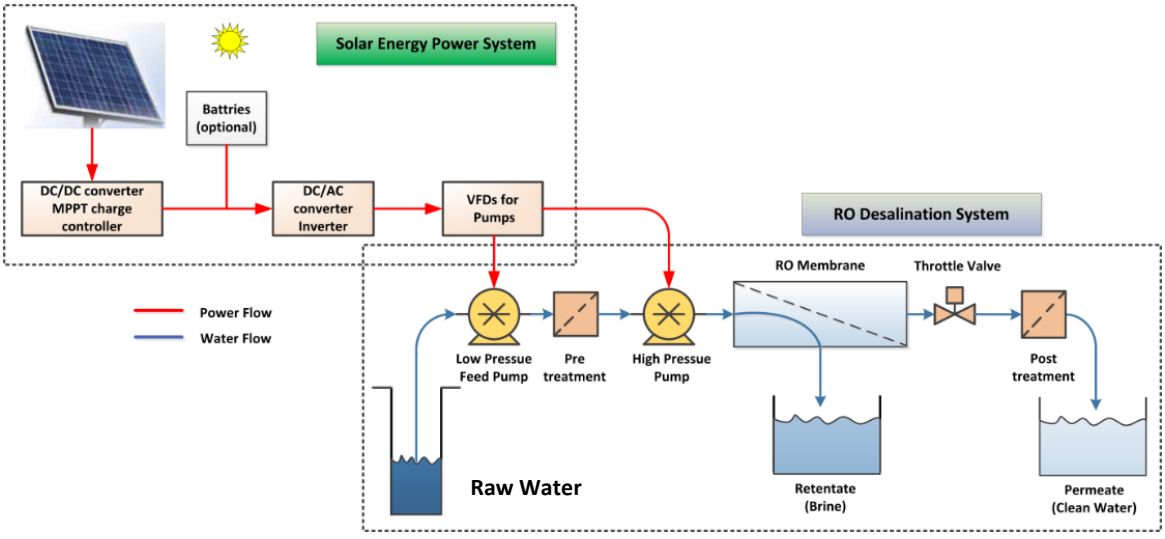

Figure 1.3: Photovoltaic based RO system

An RO membrane acts as the semi-permeable barrier that allows selective transport of a particular species (solvent, usually water) while partially or completely blocking other species (solutes, such as salt). Separation, most importantly, depends upon the properties of the membrane used in the process. These properties depend on the chemical nature and the physical structure of the membrane material. An ideal RO membrane should be resistant to degradation by chemicals and microbes, have good mechanical and structural stability over long operating periods, and possess desired separation characteristics. Most currently available RO membranes fall into two categories: asymmetric membranes containing one polymer layer and thin-film composite (TFC) membranes consisting of two or more polymeric layers. After the filtration process by the RO membrane, clean water known as permeate is stored in a tank, disinfected and remineralization is done to make it drinkable. The rejected water known as concentrate is disposed to the environment or send to energy recovery device to recover the stream energy.

1.2 Literature review

1.2.1 PVRO installed systems

Many of the installed PVRO systems composed of simple configuration, PV array, battery bank and RO facility. The experimental results prove the inefficiency of these systems and researchers has focused to increase the overall system's efficiency by numerous control techniques. The control techniques are employed to optimize the PV power harvesting and to utilize it by RO facility efficiently [9].

An early demonstration of PV RO system was installed and tested by Saleh et al, 1995 [10] in Sadous village near Riyadh, Saudi Arabia for the research purpose. Its simple design consists of 10 kW fixed PV panels, MPPT, batteries and single pass single stage

RO design without any energy recovery devices. The clean water production capacity was 15 m^3/day (600 L/h) and serves well the community for 24 hour. The system uses a data logger system connected to a computer and stores various process measurements for performance evaluation. Battery storage was used to smooth out the PV fluctuations and RO was operated for 24 hours on constant pressure and constant feed flow rate without usage of energy recovery devices [10]. During the experimental run, PVRO operation was carried out at fixed process parameters and no mechanism is involved to optimize the PVRO performance for wide range of PV power.

France et al, 2000 [11] have designed, developed and analyzed a small scale PV powered RO desalination to optimize the power needs and energy consumption. From the experimental results it was concluded that for the optimal operation of RO system, an appropriate control system is needed to adjust the RO pressure actively. This objective was attained by the installation of a special electrically operated valve, which ensures the pressure regulation and keeping the feed flow rate at steady condition while considering the variations of PV power. However in this work the determination of control system set points for the feed pressure and feed flow rates for the specific PV power is not discussed and it needs to be explored using parametric equations of PVRO system.

Herold et at, 2001 [12] designed and installed PVRO system with water production 1-5 m^3/day at Canary Islands Technological Institute. The plant is equipped with a standalone 4.8 kW PV system with an additional battery bank of 60 kWh storage. Three different regulation strategies for the energy management of the plant are compared. Based on the experimental results recommendations for an optimized operation to curtail the SEC, high potable water production and with sufficient permeate quality are provided. In this

setup state of charge (SoC) of the batteries is continuously monitored to select the mode of PVRO operation. During the experimental run, RO is operated ON for fixed system pressure with constant feed flow rate. If the battery power is not able to provide the sufficient amount of power then the RO is kept OFF for a certain time and batteries are allowed to charge to start the next cycle. Authors concluded that reduction in batteries' capacity and incorporation of energy recovery devices is envisaged to reduce the specific energy consumption of potable water.

Joyce et al, 2001 [13] described a small RO pilot unit powered by a PV system for a small capacity of 500 L/day. During the experiments the comparison of the permeate quality and specific energy consumption versus membrane working pressure for different feed salinities is carried out. Nevertheless, it can be concluded that for the small RO pilot the specific energy consumption decreases as feed water recovery and feed pressure increase. The detailed mathematical parametric analysis showing the interplay of different process parameters over the SEC is not discussed.

Thomson et al, 2003 [14] demonstrated another PVRO system to desalinate seawater without any battery storage facility. The developed system is operated for seawater desalination. The clean water production varies throughout the day according to the available solar power. During the experimental run, with the modest solar resource available in the UK, provided freshwater at approximately 1.5 m^3/day. Nearer to the equator and with a PV array of only 2.4 kWp empirical model estimates the production of over 3 m^3/day throughout the whole year. In this work feed water flow rate is varied according the PV power and the system pressure is adjusted automatically by the energy

recovery devices (clark pump). Frequent start/stop of the system is encountered due the pressure fluctuations caused by the reciprocating motion of piston in clark pump.

Espino et al, 2003 [15] investigated the experimental performance of PVRO system for capacity of 10 m^3/day. During the experiments, real results were used to optimize the RO plant operation by the coordination and timing of the PV system. The plant is fed with pre-heated seawater to optimize the overall energy consumption. The plant is operated automatically for an average of 8 hours during summer and 7 hours during winter time while the plant operation is adjusted to the changing energy production of the PV generator. The plant is equipped with a double flushing system with fresh water for the membranes and pumps during the daily periods.

Bryce et al, 2013 [16] designed and tested a photovoltaic (PV)-powered desalination system with hybrid membrane configuration, whereby an ultrafiltration (UF) module is used for removing particulates, bacteria and viruses, while a reverse osmosis (RO) or nanofiltration (NF) membrane retains the salts. The specific energy consumption ranged from 2 to 8 kWh/m^3 of disinfected and desalinated drinking water, depending on the salinity of the feed water and the system operating conditions. The optimum operating pressure when filtering bore water was determined experimentally and it is in the range of 6 to 7 bars.

Oliveira et al, 2005 [17] designed PVRO plant and is operated at variable flow/pressure in equatorial areas, enabling it to make efficient use of the naturally varying solar resource. A novel feed forward control algorithm was introduced to control the duty ratio of the DC/DC converter to ensure the maximum usage of available power from

meager PV source. A complete Simulink model of feed forward control was made and validated experimentally successfully.

Schafer et al, 2007 [18] has developed and demonstrated a PV hybrid membrane system comprising UF and NF or RO membrane. In this system four nano filtration and RO membranes (ESPA4, BW30, NF90, TFC-S) and a number of operational parameter (trans membrane pressure, feed flow rate, water salinities) combinations were investigated to find the best operating conditions for maximum drinking water production with minimum specific energy consumption (SEC). It was concluded that ESPA4 membrane performed best for this brackish source, producing 250 L/h of excellent drinking water (257 mg/L TDS) at an SEC of 1.2 kWh/m^3 for brackish water having 5300 TDS salinity.

The cost of the PVRO system is increased by the incorporation of storage batteries, more over the life cycle of the batteries is reduced in hot climates. Other thing in small PVRO systems is that, they do not incorporate ERD due to pressure and flow variations. In view of these, Mohamed et al, 2008 [19] has developed a battery less PV-SWRO system equipped with an ERD. The system was installed, tested and compared to a battery based system, producing 0.35 m^3/d in winter (feed water temperature 18°C) consuming only 4.6 kWh/m^3. It was concluded that SEC of direct coupled system is higher than battery based system by 7%. It was also concluded that large battery bank (>1500 Ah) could improve the system behavior, but will increase the environmental effects and operating cost will be very high in isolated areas.

Richards et al, 2008 [20] demonstrated PV desalination system to evaluate the performance due to the process fluctuations during the operation. The system was battery less, hybrid in configuration (ultrafiltration-nanofiltration/reverse osmosis UF-NF/RO)

powered by photovoltaic treating brackish ground water in outback Australia. The performance of the system over four different solar days was evaluated using four different NF membranes (BW30, NF90, ESPA4 and TFC-S). It was concluded that batteryless operation is a simple and robust way to operate such systems under conditions ranging from clear skies to medium cloud cover.

Kim et al, 2009 [21] has proposed a temperature control methodology for the feed water temperature to optimize the RO desalination process using genetic algorithm. It was concluded that in temperature controlled operation of RO, permeate flow rate can be increased by 57 % if the feed water temperature is increased from 15 ^{o}C to 40 ^{o}C.

Qiblawey et al, 2009 [22] investigated the usage of photovoltaic as a power source to operate a small RO for clean water production. Experiments on the developed unit were performed using saline water with two different concentrations (350 mg/L and 720 mg/L). During the experimental run, the unit was entirely powered by photovoltaic cells and operated with and without storage batteries. Average specific energy consumption is measured to be 1.3 kWh/m^3 for the battery less operation and 2.7 kWh/m^3 for battery based operation. However, during this PVRO operation, feed pump speed is controlled by the PV available energy and the retentate valve is kept fixed at constant position.

Douglas et al, 2009 [23] designed, simulated and implemented a feedback and feed forward control methodology to vary the pressure and feed flow rated to track the maximum power point of the PV panels. It is reported that, operation of PVRO system using this controller improves the daily permeate production by 60% and daily operation time period by 30%.

Khayet et al, 2010 [24] constructed a solar thermal and PVRO desalination system and optimized it for brackish water desalination. Solar thermal system was used to heat the feed water whereas the PV power is used to drive the feed pump and high pressure pump. The central composite experimental design of orthogonal type and response surface methodology (RSM) has been used to develop predictive models from the experimental data. These black box models were used for optimization of different responses of the PVRO system. The optimized plant guarantees a potable water production of 0.2 m^3/day with specific energy consumption lower than 1.3 kWh/m^3.

Kelley et al, 2013 [25] have proposed an active thermal management control system to enhance the performance of PVRO desalination system. For a given level of solar radiation, a photovoltaic panel produces more power at a lower temperature. For a certain amount of power, an RO system produces more clean water at higher feed water temperature. An active thermal management system is used to exploit these complementary characteristics by cooling the solar panel and warming the RO feed water. This concept is validated by simulation and experimentation. An increase of 57% in fresh water was achieved in experiments using active thermal management control system and solar concentrators with PV panels.

Penate et al, 2011 [26] has discussed the gradual operation mode of the RO to adapt the variable energy source (wind energy). It was concluded that power fluctuation caused pressure and feed flow variation and high quality components are to be used to withstand the process variation during filtration process. In this mode of operation, multiple RO units are installed in parallel and each unit is operated on fixed feed pressure and flow rate. The numbers of RO units are switched ON according to the available wind energy. The

available wind energy is monitored and based upon this data RO units are switched ON/OFF accordingly.

Forstmeier et al, 2008 [27] has discussed the design challenges and methods to integrate the fluctuation power source (renewable energy source especially wind and PV) to conventional membrane process. Gandhidasan and Sultan 2009 [28] had discussed the effect of feed pressure on the performance of PVRO seawater desalination system under the variable energy sources.

1.2.2 RO control systems

The control techniques used for conventional RO system are well established and discussed in the literature. During the operation of these systems, power variation or fluctuation is not a concern because they are connected to grid. Commonly used control techniques are PID control, Fuzzy logic control, Dynamic Matrix Programming methods, model predictive control and fault tolerant control [29]-[32]. In all these control methods the set point for feed flow rate and system pressure are considered to be constant and they are determined from the RO configuration and process parameters. Other process variables such as feed temperature, feed salinity and water chemistry are considered as disturbance variables. Control system tracks the set points (feed flow rate and feed pressure) by rejecting the process disturbances actively.

Despite of the good research work in the designing and field testing of the PVRO system, very little research work is carried out to compute the optimal and effective way to operate the whole PVRO system. Control schemes in the battery based PVRO system focuses on the maximum power transfer from the batteries and operate the RO system on fixed pressure and feed flow rate of raw water. Some simple battery less system operate

are operated with only one pump to maximize the power transfer. In summary, specifically for the PVRO system, the following methods are employed for the optimized operation to enhance the overall system performance.

- The brine valve is kept at constant position so the membrane pressure is dictated by the feed flow rate. Moreover the feed water flow rate is changed by varying the pump speed according to the PV available power. [10]-[15]
- Feed flow rate is kept constant and system pressure is varied by changing the brine valve position to track the maximum power point of the PV curve [32]-[33].
- PVRO systems comprising energy recovery devices, the feed flow rate is altered to track the maximum power point (MPP) of the PV panel and the pressure is adjusted automatically on a certain point as dictated by the energy recovery device (ERD).
- For the gradual capacity operation, parallel RO sections are installed and the number or RO sections are turned ON/OFF according to the PV available power. The RO section in ON state will be operated on fixed feed flow rate and fixed system pressure. [26]

In all the above mentioned literature, the researchers have adopted different operational methodologies on the PVRO experimental set ups to come up with the optimal operation point, but no one has made the detailed analytical/mathematical analysis of PVRO system to come up with the optimal point of operation of RO system under the given PV power. Our intention is to develop a comprehensive parametric model of whole PVRO system. Based on the developed model, complete analysis of the PV and RO section will

be carried out. The analysis will be used to carve out the optimum operational methodology of RO section that will ensure the optimum utilization of available PV power while minimizing the SEC of the RO plant.

1.3 Thesis objective

The basic design of RO system can be developed in view of recommendations given by membrane manufacturing and selecting the best compatible RO parts such as membrane filters, valves, and low and high pressure pumps. For large RO Plants driven by grid connection, companies have developed optimized control for specific applications , but for small plants driven by PV or wind or operating in hybrid manner, which are the focus of this study, only some initial efforts to develop appropriate control strategies are reported in literature, which are still continuing to make further improvements. The design process of PVRO encompasses different disciplines starting from energy harvesting from PV panels, optimal RO process operation under available energy, reduced RO membrane energy consumption (reduced SEC) and environmental friendly water treatment issues. The proposed research is to design each phase of the system for optimum operation and then integration of these optimized phases will culminate into state of the art PVRO system. Appropriate objectives based on different criteria like energy (harvesting and consumption) optimization, RO process optimization along with associated constraints will be developed and solved for different process variables. The resulting optimized system will need to have an intelligent control to run it at or near optimal operating points. Smart control systems might use collective knowledge taken from the studies and will be capable to operate, control and optimize, and to evaluate the performance of PVRO system. The control system will comprise both energy management control system and process control system.

Electrical energy harvested from the solar radiation using PV panels is prone to be variable and fluctuating in nature throughout the whole day. But on the other hand desalination process needs certain amount of power to keep RO in operating state. The research scheme will utilize the information of different variables in the process i.e. available power from the PV panel, feed salinity and feed temperature. This information will be processed by the controller in an intelligent way and will provide the optimal set points for the process i.e. feed pressure and feed rate according to the available power form the PV source while accounting the variations in the feed water quality and system energy utilization.

1.4 Problem statement

In short the description of the research problem statement may be written as

"To determine the optimal hydraulic parameters (feed flow rate and feed pressure) by minimizing the specific energy consumption (SEC) of fixed RO network design (single stage and single pass) while satisfying the given PV power profile (with available range) requirements and RO operational constraints at a given feed water temperature and feed concentration".

"Based upon the solution a ***controller*** *is to be designed that will generate* ***the optimal set points for feed and pressure control loop*** *that will be used for RO system with either be used with variable ERD or without ERD."*

In order to come up with the solution of this research problem following research methodology is used.

- Comprehensive Modeling of PV and RO system independently (and combined) with its experimental validation is carried out.
- Validated PVRO model is used to predict the permeate flow rate for flat and tracked PV panels.
- Optimization problem is formulated using design variables, constraints and parameters of PVRO system.
- A graphical approach is used to construct the feasible design space of RO system by satisfying the RO operational constraints.
- Within the feasible RO design space, PV power lines (contours) are drawn to define the corresponding PVRO feasible area.
- Defining the appropriate multi criteria objective functions (max Permeate, min SEC, Max use of PV power) for complete PVRO system optimization evaluation to come up with the best solution.
- Different strategies are used to sweep the maximum PV power lines in design space.
- Best possible methodology (min SEC and max PV usage) is used to generate Feed flow and Pressure reference signals for control purposes.

In this optimization different cost functions will be defined and constraints will be imposed to solve the optimization problem. General form of the optimization problem is described in Table 1.1.

Table 1.1: General form of PVRO optimization problem

Objective function:	to minimize the specific energy consumption (SEC) of RO unit
Design Variable:	hydraulic parameters of RO system (feed flow rate, feed pressure in the Pressure vessel)
Constraints:	The different operation methodologies, constant pressure, constant recovery ratio, constant feed flow rate, constant retentate flow rate. Operational limits imposed by the RO network design e.g., maximum pressure of the membrane, minimum retentate flow rate, maximum feed flow rate, maximum recovery of membrane and maximum salinity of the permeate. Available PV power profile and available range.
Parameters:	Feed water salinity and concentration.

In this optimization problem, solution is envisaged to come up with optimal feed flow rate and optimal system pressure while minimizing the specific energy consumption and considering all physical and computational constraints. The major constraint which is imposed in the problem is the limited amount of available energy harvested from the PV panel. Heuristic search might be used to explore the generated data to come up with the solution of the problem. From the solution optimal feed flow rate and optimal pressure are to be used for the local controllers as set points. These local controllers will be responsible to regulate the system variables according to the set points. This phenomenon is evidenced from the Figure 1.4 and Figure 1.5 for without ERD and with RED operation respectively.

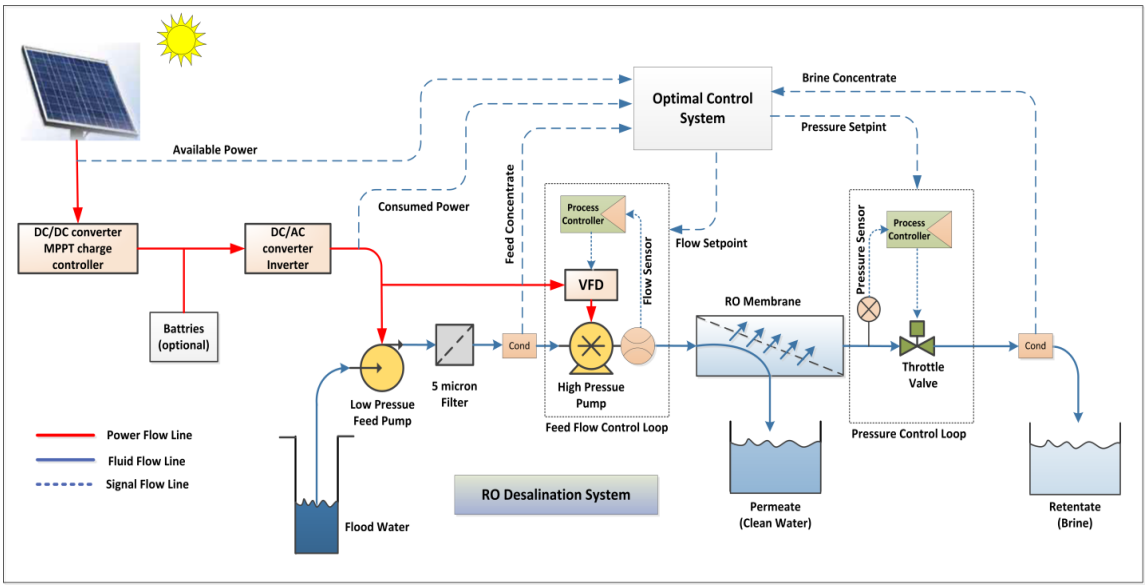

Figure 1.4: Towards an optimal operation of PVRO system without ERD

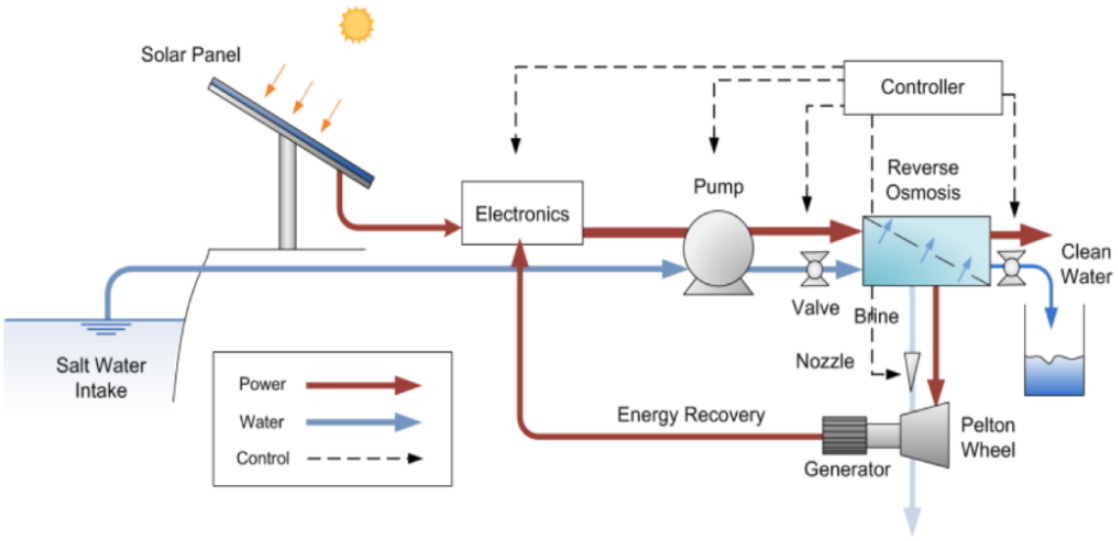

Figure 1.5: Optimal operation of PVRO with ERD

1.5 Thesis organization

The thesis is organized in six chapters. This chapter includes the introduction to PVRO system, its different components and its technical and economic feasibility in the solar radiation rich areas. Different installed PVRO systems in the various locations of the globe are reviewed and their configuration and control aspects are explored. Based upon this literature review research objectives are determined.

In Chapter 2, complete analytical modeling, simulation with experimental verification of photovoltaic system driving reverse osmosis water desalination is presented. In photovoltaic system, solar radiation and PV generation modeling is done and investigation of the effect of fixed and tracking PV panel on the collected insolation and PV power is carried out. In the RO section, complete model of RO membrane is developed that estimates the feed water pressure and permeate flow rate. The developed PV and RO models are validated individually as well as integrated (combined PVRO) by experimental data and show good agreement. By using this validated model the effect of slope and azimuth angle of the PV panel is studied on the permeate flow rate for the whole year. The increments in the clean water flow rate for the yearly tilt, monthly tilt, single and double axis tracking PV panels with respect to traditional flat panel is computed.

Chapter 3 illustrated the designing and development of instrumentation, data acquisition and graphical user interface of photovoltaic driven reverse osmosis system for monitoring and performance evaluation purposes. Proper instrumentation is carried out in PV system to measure the irradiation, temperature, voltage and current at various points. Moreover various sensors are used to measure the pressures, flows, salinities at RO unit. The experimental investigation of PVRO system is carried out by using LabVIEW

interface capabilities. The developed system reveals and stores the pronounced impact of measured variables on the PV output power and specific energy consumption of the RO filtration system.

Chapter 4 presents some literature review of RO network optimization work and based on this optimized RO network for the community scale PVRO system in selected. For the selected RO network, RO process optimization is carried out for the effective utilization of available PV power by RO unit by using different RO operational methodologies. The RO process parameters (feed flow rate and system pressure) are optimized in such a way to keep the RO operation at specific methodology while taking the PV power into consideration. The investigated operational methodologies are constant feed water flow rate, constant feed pressure, constant retentate flow rate and constant recovery ratio. For each of this methodology specific energy consumption (SEC) of RO unit over the whole range of available PV power is simulated.

Chapter 5 presents the overview of conventional and sustainable environmental friendly pretreatment methods for the disinfection of the feed water. Conventional water treatment and its environmental effects are elaborated. UV photo catalysis based pretreatment process is discussed in detail. To validate the viability of the photo reactors two experimental setups (stair case and parabolic designs) are evaluated by experimental trials. Chapter 6 summarizes the thesis and presents some avenues for further research.

Chapter 2

PVRO modeling and performance analysis

In this chapter complete analytical modeling, simulation with experimental verification of PVRO water desalination is presented. In photovoltaic system, solar radiation and PV generation modeling is done and investigation of the effect of fixed and tracking PV panel on the collected insolation and PV power is carried out. In the RO section, complete model of RO membrane is developed that estimates the feed water pressure and permeate flow rate. The developed PV and RO models are validated individually as well as integrated (combined PVRO) by experimental data and show good agreement. By using this validated model the effect of slope and azimuth angle of the PV panel is studied on the permeate flow rate for the whole year. The increments in the clean water flow rate for the yearly tilt, monthly tilt, single and double axis tracking PV panels with respect to traditional flat panel is computed. The estimated results reveal that yearly optimal tilt angle of PV panels due south is close to the 0.913 times latitude of the Dhahran city. Yearly permeate gain with the yearly optimal tilt, monthly optimal tilt of PV panel relative to flat panel installation is 10% and 19% respectively. The optimization of photovoltaic system suggests the adjustment of the PV orientation (tilt angle and azimuth angle) by using a single and dual axis tracking system installations. The yearly permeate gain made by single and double axis continuous tracking PV panels is 43% and 62%, respectively.

2.1 Introduction

In the PVRO system the workhorse is the PV system that needs to be studied to harvest the maximum possible power. The amount of solar energy incident on a PV panel in various time scales is a complex function of many factors including the local radiation climatology, the orientation and tilt of the exposed panel surface and the ground reflection properties [34]. The performance of solar PV panel is strong function of surface azimuth angle and angle of inclination with the horizon and it is due to the fact that both orientation angles influence the incidence angle of solar radiation reaching the PV panel. The analysis of the influential parameters on the PV power generation is vital to harvest the maximum possible power from PV panel.

Empirical correlations are proposed in the specialized literature to estimate the optimal tilt angle of the solar collector for different environmental conditions. It is reported that the yearly optimal tilt angle of PV panel to maximize the output power is in the range of $20-30°$ due south [35]. Shariah et al, 2002 [36] showed that the yearly optimum tilt angle for solar collector in Jordan (an Arab country located at north of Saudi Arabia) is less than the latitude by about $5-8°$ degrees. Duffie and Beckman has suggested the use of ($\varphi \pm 15°$), where the plus and minus signs corresponds to the use in winter and summer solstice days respectively [37].

Nijegorodov et al, [38] has proposed formulations which consists of 12 expressions for determining the monthly optimal tilt angles for latitudes between $60°N$ and $60°S$. Huseyin and Arif, 2007 [39] found that the monthly optimal angles for solar collector in Izmar, Turkey were in good agreement with those calculated by the expressions proposed by Nijegorodov. More optimization of PV system suggests the use of single or double axis

tracker systems with PV panels to collect more solar radiation. Energy gain by making use of tracking systems with PV panels in good insolation areas is typically between 30 and 40% [40]. Pen Zhang et al, 2013 [41] have built a two axis tracker system and come up with a model to simulate the instantaneous PV power from the fixed as well as two axis tracked panels and applied this work on the street lighting applications.

Şenpinar el al, 2012 [42] compared the performance of two PV panel modules, one fixed and the other fitted with a two-axis tracking system which enables the collector to move and be controlled to follow the Sun's radiation. The instantaneous PV output power was computed and plotted, it was found that the daily output power of the tracking module was 13–15% higher than the fixed module.

Eka et al, 2012 [43] has made the comparison of two double axis sun tracking PV systems feeding the grid. For both cases an instantaneous PV output power is plotted against the time and concluded that 30.79% more PV electricity is obtained in the double axis sun-tracking system when compared to the latitude tilt fixed system.

Qiblawey et al, 2011 [44] investigated the usage of PV as a power source to operate a small RO for clean water production. Experiments on the developed unit were performed using saline water with two different concentrations (350 mg/L and 720 mg/L). During the experimental run, the unit was entirely powered by PV modules and operated with and without storage batteries. In this work instantaneous insolation, PV temperature, PV power and permeate flow rate is plotted versus day time. However in this work prediction models for the PV and RO systems are not provided and system is driven with fixed PV panels.

Ayber et al, 2010 [45] have investigated the pilot PVRO project. Plots of the experimental data for the insolation, PV power and permeate flow rate against the time are plotted. All the measurements were recorded after 15 minutes of interval. However in this work, the detailed modeling of PV and RO systems are not discussed for the prediction of PV and RO performance parameters.

Achies et al, 2010 [46] has modelled the RO system in the Dymola simulation environment using the modeling language Modelical and discussed an operating control strategy under variable available power. Based upon PV power variation dimensioning of PV driven desalination plants is carried out. The system is simulated to see the special requirements relating to the operating control strategy during the whole day operation of PVRO system.

In the above mentioned literature different authors have used radiation models to estimate the hourly mean or instantaneously values of solar insolation and applied their work in heating, lighting, grid and RO applications. For the PVRO application, experimental investigations are carried out with fixed PV panels. But comprehensive modeling of PVRO system and its experimental validation with different fixed or tracked PV panels is necessary for its performance analysis.

The combined PV driven RO system, also needs a proper understanding of RO process and mathematical models to describe the behavior of a proposed /designed RO unit, after grasping such a model both PV and RO models can be integrated in to a complete PVRO system model. The following provides the introduction to various RO models.

Models that adequately describe the performance of RO membranes are important and needed in the design of RO process. Different models are proposed in literature for RO membrane filtration process. Membrane transport models focuses on top thin skin of asymmetric membranes layer of composite material and steady state phenomena (equilibrium) is described. Lumped parameter models describe the transient as well as the steady state behaviors of the process and used for the control purposes [47]. Theoretical (parametric) models are based on fundamental knowledge of RO process and its irreversible thermodynamic properties. These models fall into two categories; porous models (such as finely-porous, preferentially sorption capillary flow models) and non-porous or homogeneous membrane models (all models based on diffusion based). Another type of models are empirical (non-parametric) models that do not involve the fundamental principles and can be modeled by soft computing methodologies by making use of experimental data i.e. artificial neural networks (ANN) and response surface methodology (RSM) etc [47].

Sundaramoorthy et al, 2011 [48] has provided solution diffusion model that incorporates the spatial variation of pressure, flow and solute concentration in the membrane unit. This model works well under the uniform conditions and provides parameter profiles along the membrane but this model is not applicable for dynamical system. Kaghazchi et al, 2010 [49] has given a solution diffusion model in which membrane is assumed as nonporous media and steady state operational conditions are assumed. In this model one dimension transport phenomenon is assumed and is suitable for uniform conditions but not applicable for dynamic systems for control purposes. Pranay et al, 2009 [50] has provided a predictive model for boron rejection in pilot and full-scale

RO desalination process. This model is suitable for varying water quality and operating conditions and it can be used for RO process design and optimization.

Abbas et al, [51] have reported the model of an RO water desalination unit using neural networks approach. Feed forward neural network are trained to predict the performance of RO. A series of 63 experiments were conducted and collected data is used to train the ANN. Input parameters are feed temperature, feed pressure and feed concentration whereas permeate rate is the response variable. However the achieved model is only applicable to the plant on which experiments are conducted and it cannot be generalized for other RO systems.

Jamal et al, 2004 [52] has proposed a model that combines material balance on membrane and feed tank with mass transfer models. Nonlinear differential equations having feed concentration as a function of operating time are evolved and solved numerically. Bartman et al, 2009 [53] has proposed a dynamic model by considering mass balance around the entire system and energy balance around the actuated retentate valve. A nonlinear differential equation having the dynamics of retentate stream under the influence of value resistance is developed. The developed model is used for the implementation of advanced control algorithms for overall process optimization. Gambier et al, 2007 [54] has proposed a dynamic model by decomposing of the RO system into brine subsystem, membrane subsystem and permeate subsystem. Mass, momentum and energy conservation principles are used to evolve the equations for each subsystem. However, this model requires a lot of parameters that hinders its application for the implementation of advance control system.

Riverol, et al, 2005 [55] developed the model by identification method using the step response of the RO system. System pressure and feed water pH are taken as inputs and permeate flow and its concentration is considered as output variables. The developed model is only applicable to particular setup at which the experiments are carried out for identification purpose. Abderrahmen et al, 2011 [56] proposed a MIMO (multi input multi output) model with state space realization and an empirical transfer function is achieved. Khayat et al, 2011 [57] has used response surface methodology (RSM) and artificial neural network (ANN) for the predictive models of PVRO system. Concentration, temperature, feed flow and pressure are taken as inputs and permeate flux and salt rejection is considered as outputs in the predictive models. The achieved model is used to solve an optimization problem to maximize the salt rejection and permeate flux.

As our work is not to design a control system for the RO unit, rather than we are just making the prediction of permeate flow rate based upon instantaneous PV available power. In this work feed concentration, temperature and pH are assumed constant (for a specific locality having brackish water). PV power changes very slowly and it is assumed that for a certain PV power, RO process operates near equilibrium conditions. By taking these consideration into account, the solution diffusion model using the thin film approach for the spiral wound RO membranes can be nicely used in predicting the steady state RO filtration performance.

In this study an overview of basics of solar radiation, PV power generation and RO system is presented for the instantaneous performance evaluation of PVRO system under different azimuth and inclination angles of PV panels. The factors affecting the instantaneous PVRO performance of flat panel, yearly optimal tilt and monthly optimal

tilted PV panels are analyzed for specific days in the year for the city of Dhahran, Saudi Arabia. Moreover the additional permeate collected by single axis and double axis tracked PV panels is computed and compared to the performance of conventional flat PV panel for one complete whole year.

2.2 Solar radiation modeling

2.2.1 Solar angles

The sun, with the diameter of $1.39x10^{9}$m is the center of our solar system and emits total energy of $3.8x10^{20}$ MW. A tiny fraction $1.7x10^{14}$kW of this radiated energy from the sun is captured by the earth after traveling a mean distance of $1.496x10^{11}$ m [37]. The earth revolves around the sun in an elliptical orbit with the sun as foci and the plane of this orbit is known as ecliptic. The eccentricity of the earth's orbit is such that the distance between the sun and earth varies by 1.7% [37] . The true anomaly is an angular parameter that defines the position of the earth moving along a Keplerian orbit and is defined as the angle between the direction of the periapsis and the current position of the earth as seen from the sun. The mean anomaly B is parameter relating position and time for the earth moving in a Kepler orbit and it is given by the following formula.

$$B = 360\frac{(n-1)}{365} \tag{2.1}$$

n is the ordinal date and is one for 1st January and $n = 365$ for December 31st. The earth obliquity or the earth axial tilt is the angle between the rotational axis of the earth and perpendicular to the orbital plane. The actual value of earth obliquity is 23.45^{o}. The declination of the sun is the measure of angle between sun rays and plane of the earth's equator. Figure 2.1 shows the schematic representation of solar angles. Solar declination

changes with the season, at solstices it has the maximum value of 23.45. At summer solstice $\delta = 23.45$ and at winter $\delta = -23.45$ and at equinoxes is become zero. It can be calculated by mean anomaly *B* or by ordinal day *n* by using following equation [36].

$$\begin{aligned}\delta = {} & 0.006908 - 0.399912\cos B + 0.070257\sin B \\ & -0.006758\cos 2B + 0.0000907\sin 2B \\ & -0.002679\cos 3B + 0.00148\sin 3B\end{aligned} \tag{2.2}$$

By using the ordinal date n the declination is given by the following expression.

$$\delta = 23.45^{o}\sin\left(360\frac{284+n}{365}\right) \tag{2.3}$$

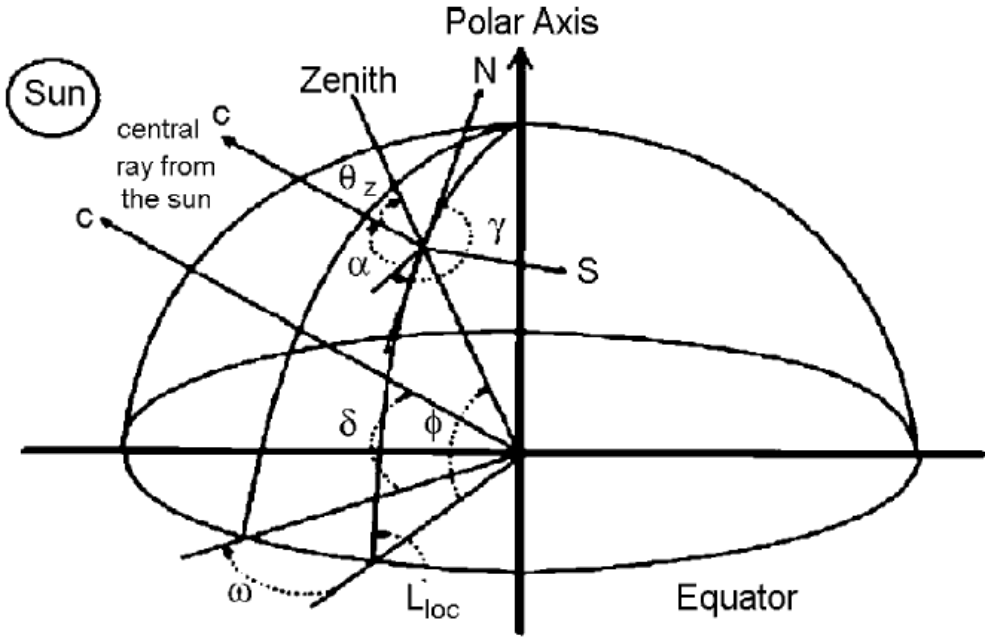

Figure 2.1: Schematic representation of solar angles [58]

Latitude φ is the angular location north or south of the equator; north is positive and south is negative and its range for any site on the globe is $-90 < \varphi < +90$. Longitude is the geographic coordinate that specifies the east west position on the surface of the earth. Latitude and Longitude are the angular measurement to locate a specific site on the earth and are usually expressed in degrees, minutes and seconds.

Standard time zone is defined by geometrically dividing the earth's sphere in 24 lunes, and each lune in bordered by meridian having 15 degrees. The hour angle ω is the solar angular displacement east or west measured from the local meridian due to the earth's rotation and it is $15°$ per hour. Hour angle is taken as –ve in the morning and +ve in the afternoon and is expressed in the following equation.

$$\omega = (t_s - 12).15° \tag{2.4}$$

2.2.2 Zenith, solar azimuth angle, solar altitude angle

The zenith angle θ_z is the angle between the vertical and the line to sun, that is the angle of incidence of beam radiation on a horizontal surface. Solar altitude α_s is the measure of angle between horizontal and the line to the sun. Zenith angle is the compliment to the solar altitude angle and is given in term of latitude, declination and hour angle by the following equation [36].

$$\theta_z = 90 - \alpha_s = \cos^{-1}(\cos\varphi\cos\delta\cos\omega + \sin\varphi\sin\delta) \tag{2.5}$$

The solar azimuth angle γ_s is defined as the angular displacement of the projection of beam radiation on the horizontal plane from the south. This angle is zero on south, negative on east and positive on west and its range is $-180° < \gamma < +180°$.

Surface azimuth angle γ is the deviation of the projection on a horizontal plane of the normal to objective surface from the local meridian and is shown in Figure 2.2. Surface azimuth angle is zero on south, negative on east and positive on west and its range is $-180° < \gamma < +180°$. Slope β is the inclination of the surface, is the angle between the plane of surface in question and the horizontal. The range of surface slope angle is $0° < \beta < +180°$. Angle of incidence θ is defined as the angle between beam radiation and normal to the surface in question in any orientation. It can be expressed in following equation [36].

$$\cos\theta = \sin\varphi\sin\delta\cos\beta - \cos\varphi\sin\delta\sin\beta\cos\gamma + \cos\varphi\cos\delta\cos\beta\cos\omega + \sin\varphi\cos\delta\sin\beta\cos\gamma\cos\omega + \cos\delta\sin\beta\sin\gamma\sin\omega \quad (2.6)$$

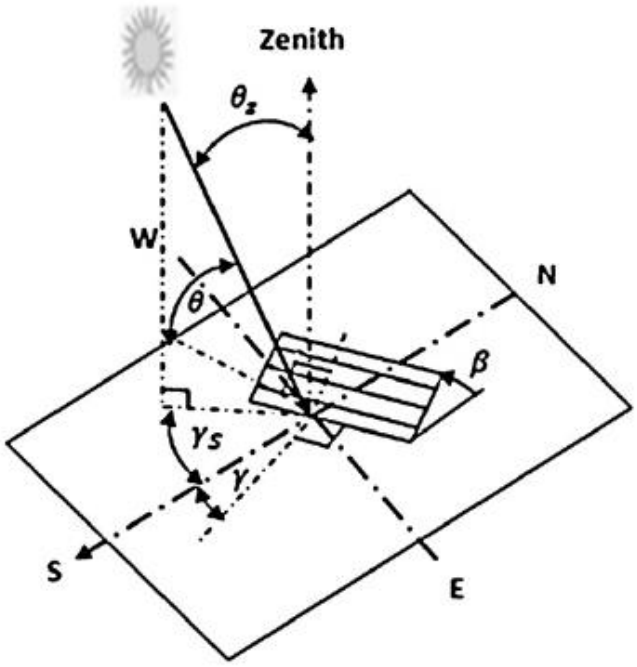

Figure 2.2: Solar and surface angels [59]

2.2.3 Radiation on horizontal and inclined surface

The solar constant, also known as the extraterrestrial radiation constant is the measure of the energy collected per unit time and per unit area of surface perpendicular to the direction of propagation of the radiation at a mean sun earth distance outside the atmosphere [36]. The value of solar constant is G_{SC} = 1367W/m^2 as adopted by the World Radiation Center (WRC). The normal extraterrestrial radiation G_{on} in defined as the solar radiation received on the top of the earth's atmosphere and it can be calculated by equation (2.7) [36].

$$G_{on} = \begin{Bmatrix} G_{sc}(1.00011 + 0.034221\cos B + 1.0001280\sin B \\ +0.000719\cos 2B + 0.000077\sin 2B) \end{Bmatrix} \quad (2.7)$$

Whereas B is the mean anomaly and is calculated by equation (2.1). The horizontal extraterrestrial radiation G_{oh} is the amount of radiation collected on the horizontal surface on the tip of the atmosphere and is calculated by equation (2.8).

$$G_{oh} = G_{on}(\cos\theta_z) \quad (2.8)$$

The global radiation is the sum of beam radiation and diffuse radiation. The beam radiation G_b are the solar radiation that travels from the sun to the surface of the earth without being scattered by the atmosphere. Different models are available in the literature to estimate the beam and diffuse radiation on the horizontal surface. Mondol et al, 2008 [60] suggested the relationship between diffuse and global radiation by using the clearness index *k* but to estimate its value, measured radiation data is needed or its value is to be assumed for simulation purpose. This relationship is given in equation (2.9).

$$\frac{G_d}{G} = \begin{Bmatrix} 0.98k\ (k \le 0.2) \\ 0.61092 + 3.6259k - 10.171k^2 + 6.388k^3 (0.22 \le k \le 0.8) \\ 0.672 - 0.474k\ (k > 0.8) \end{Bmatrix} \quad (2.9)$$

From the above mentioned set of equation global radiation on flat collector plate or surface is estimated. Several models are presented in the specialized literature to calculate the solar radiation for a tilted surface from the radiation for a horizontal surface. All these models use the same method to calculate the beam and ground reflected radiation for tilted surface but the only difference exists in the calculation of diffuse radiation [34].

2.2.4 Beam and diffuse radiation

Beam radiation on the tilted surface is calculated by multiplying the beam radiation on flat surface (G_b) by the shape factor of the inclined surface (R_b), that is function of zenith and beam ray incident angle. Geometric factor is calculated using equation (2.10).

$$R_b = \frac{\cos\theta}{\cos\theta_z} \quad (2.10)$$

In this expression, angle of incidence θ is defined as the angle between beam radiation and normal to the collector surface. It is a function of solar angles and the orientation of collector surface in question. The beam radiation on tilted surface G_{bT} is calculated by equation (2.11).

$$G_{bT} = G_b . R_b = G_b \frac{\cos\theta}{\cos\theta_z} \quad (2.11)$$

It has been pointed out in the literature that the sky diffuse component of the radiation is considered to be largest potential source of computational error [61]. The most challenging problem in the estimation of the diffuse radiation on tilted surface is due to the

fact that diffuse component does not have an isotropic distribution in sky and this distribution is not uniform over the time. Many others have evaluated this component and classified basically into three types: Isotropic model, circumsolar model and anisotropic models.

Isotropic model presume that the intensity of diffuse radiation is uniform over the entire hemisphere of the sky and it could be true in overcast skies [34]. Circumsolar model presume that all the radiation come from the sun and the surroundings, and therefore diffuse component can be calculated as analogy to the direct component [62]. This model can only be applied in case of clear skies and generally it overestimates the diffuse component of the radiation [62].

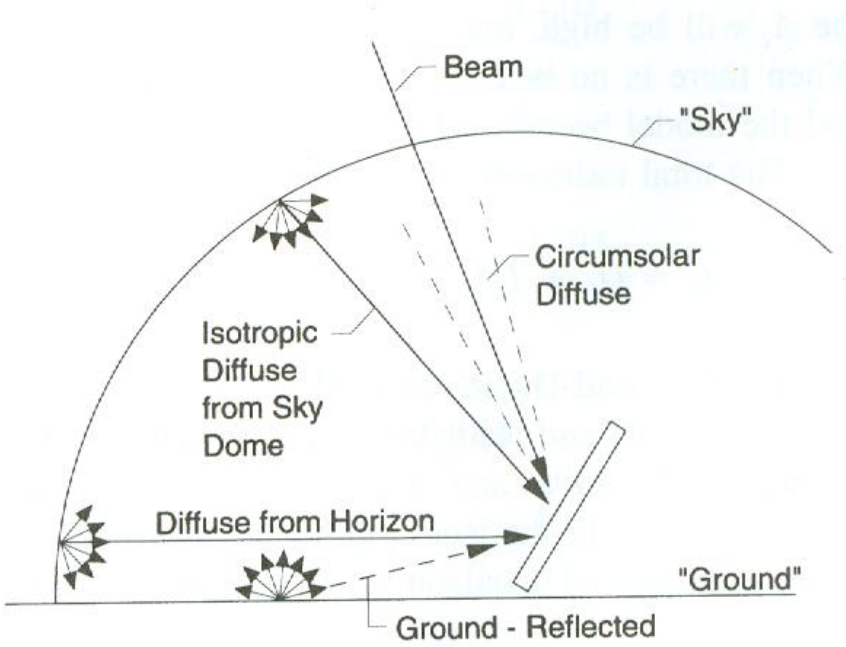

Figure 2.3: Beam, diffuse and ground reflected radiation on a tilted surface [37]

The anisotropic model presumes the anisotropy of the diffuse sky radiation in the circumsolar region and isotropy diffuse component distribution from the rest of the sky. This model is widely accepted and is used for clear, cloudy and partial cloudy skies. Based on this context, one of the most popular anisotropic sky model is the HDKR, Hay-Davis-Klucker-Reindl model [63]. This model assumes three components of diffuse radiation: an isotropic component which comes from all parts of the sky equally, secondly circumsolar diffuse component which is concentrated near the sun in the sky and third is horizontal brightening component which comes from the sky near the horizon as shown in the Figure 2.3. According to anisotropic sky model the diffuse component of the solar radiation on inclined surface is calculated using equation (2.12).

$$G_{dT} = G_d R_b A_i + G_d (1 - A_i) \left(\frac{1 + \cos \beta}{2} \right) \left[1 + f \sin^3 \left(\frac{\beta}{2} \right) \right] \tag{2.12}$$

A_i is the anisotropy index and is used to estimate the forward scattered radiation, also known as the circumsolar diffuse radiation. This index is a ratio of beam radiation on a horizontal ground surface to extraterrestrial radiation and is calculated using equation (2.13).

$$A_i = \frac{G_{bn}}{G_{on}} = \frac{G_b}{G_o} \tag{2.13}$$

The modulating factor f accounts for the cloudiness and is expressed by equation (2.14).

$$f = \sqrt{\frac{G_b}{G}} \tag{2.14}$$

The entire radiation model assume that ground reflected term is isotropic and is given by equation (2.15).

$$G_r = G\rho\left(\frac{1-\cos\beta}{2}\right) \tag{2.15}$$

ρ is the surrounding diffuse reflectance for the total solar radiation and ρ = 0.15 for road laid by asphalt [64] and ρ = 0.20 for desert surroundings [34].

2.2.5 Global radiation

The solar radiation on a tilted surface G_T is the sum of beam radiation G_b, diffuse radiation G_d and ground reflected radiation G_r. Therefore the global incident radiation on tilted surface are given by the equation (2.16).

$$G_T = G_{bT} + G_{dT} + G_r \tag{2.16}$$

In this case study anisotropic sky diffuse model will be used and final expression for the calculation of solar radiation on the tilted surface is given by equation (2.17).

$$G_T = G_b.R_b + G_d.R_b.A_i + G_d(1-A_i)\left(\frac{1+\cos\beta}{2}\right)\left[1+f\ \sin^3\left(\frac{\beta}{2}\right)\right] + G\rho\left(\frac{1-\cos\beta}{2}\right) \tag{2.17}$$

2.2.6 Simulink model of solar radiation

All the pertinent modeling equations of solar radiation as described above are translated into Simulink/Matlab Environment and is shown in Figure 2.4. The developed Simulink model accepts the latitude of the site, day of the year, PV panel slope and azimuth angle and clock as input arguments and finally calculates the global radiation incident on the collector surface. The model encompasses numerous blocks. Each block contains matlab code that accepts the input arguments and computes the output. The “Normal Extraterrestrial Radiation block”, “Declination Block” and “Hour angle Block” calculates

the extraterrestrial radiation, declination of the earth and hour angle of the sun respectively. These outputs along with the PV panel slope and azimuth angles are provided to the "Solar Angle Calculator Block" to compute the solar zenith angle, solar altitude angle, incidence angle of beam radiation, day shining hour and shape factor of the collector surface. "Clear sky radiation block" is used to calculate the transmittance of beam and diffuse radiation for the different seasons. At last the computed solar angles and transmittance of beam and diffuse radiation are fed to the "An isotropic sky calculation block" and total radiation falling the PV panel or collector plate is calculated.

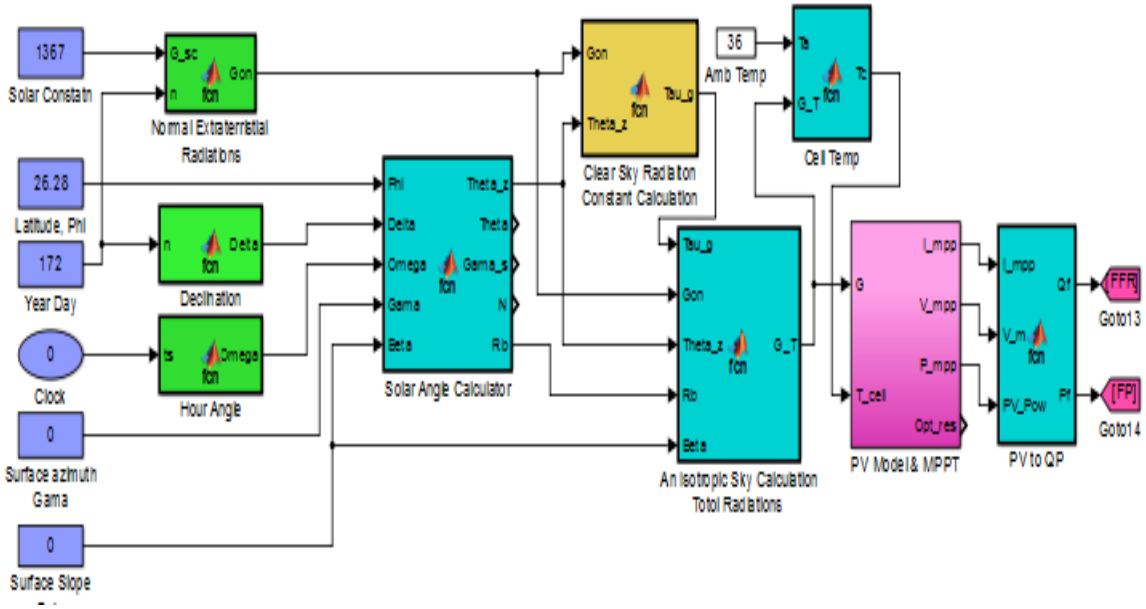

Figure 2.4: Simulink model of solar radiation

2.3 PV modeling

The PV generation is strong function of solar incident radiation and cell temperature. Increase in the radiation increases the short circuit current but increase in cell temperature reduces the open circuit voltage of the module. In this section PV cell temperature and PV output power will be estimated.

2.3.1 PV cell temperature

The absorbed solar energy by the PV module is converted partly into thermal energy and partly into electrical energy which is removed from the cell through the external circuit. So the temperature of the module is to be estimated through energy balance, on one side energy absorbed by the module and on the other hand power production and heat transmitted to atmosphere is considered. The energy balance for unit area of the module which is cooled by losses to the surroundings can be written as equation (2.18) [37].

$$\tau\alpha G_T = \eta_C G_T + U_L (T_c - T_a) \tag{2.18}$$

Where $\tau, \alpha, G_T, \eta_C, U_L$ and T_a are solar transmittance of the PV module, solar absorption of the module, solar radiation striking the PV, electrical conversion efficiency, overall loss coefficient to the environment and ambient temperature respectively. According to the equation (2.18) the cell temperature can be written as equation (2.19).

$$T_c = T_a + G_T \left(1 - \frac{\eta_C}{\tau\alpha}\right)\left(\frac{\tau\alpha}{U_L}\right) \tag{2.19}$$

To estimate the value of $(\tau\alpha / U_L)$, nominal operating cell temperature (NOCT) is introduced which is defined as the cell temperature that results at an incident radiation of 800W/m^2, an ambient temperature of $20℃$ and no load operation (η_C = 0) with an average

wind speed of equal to 1m/s [65]. By the substitution of these standard values in equation (2.18) the value of $\left(\tau\alpha/U_L\right)$ can be written as in equation (2.20).

$$\frac{\tau\alpha}{U_L}=\frac{T_{C,NOCT}-T_{a,NOCT}}{G_{T,NOCT}} \tag{2.20}$$

Where $T_{C,NOCT}, T_{a,NOCT}$ and $G_{T,NOCT}$ are the nominal cell temperature, ambient temperature and the solar radiation at which NOCT is defined. With the assumption that $\left(\tau\alpha/U_L\right)$ is constant and its substitution in the equation (2.19) yields equation (2.21).

$$T_c=T_a+G_T\left(1-\frac{\eta_C}{\tau\alpha}\right)\left(\frac{T_{C,NOCT}-T_{a,NOCT}}{G_{T,NOCT}}\right) \tag{2.21}$$

It is assumed that PV module is always operated at maximum power point, which means the cell efficiency is always equal to the MPP efficiency of the PV module ($\eta_C=\eta_{mp}$). MPP efficiency η_{mp} depends on the cell temperature T_c and it is inferred [59] that cell efficiency varies linearly with the cell temperature according to following equation.

$$\eta_{mp}=\eta_{mp,std}\left[1+\alpha_p\left(T_c-T_{c,std}\right)\right] \tag{2.22}$$

Where $\eta_{mp,std}, \alpha_p$ and $T_{c,std}$ are maximum efficiency of the PV module under standard reference conditions (radiation of 1kW/m^2, cell temperature of $25℃$,wind velocity zero and air mass ratio of 1.5), temperature degradation coefficient and cell temperature at standard conditions. Putting the efficiency equation (2.22) into equation (2.21), the cell temperature becomes.

$$T_c = T_a + G_T \left(1 - \frac{\eta_{mp,std}\left[1+\alpha_p\left(T_c - T_{c,std}\right)\right]}{\tau\alpha}\right)\left(\frac{T_{C,NOCT} - T_{a,NOCT}}{G_{T,NOCT}}\right) \tag{2.23}$$

Rearranging the equation (2.23) we get the cell temperature equation (2.24) and it will be used to estimate the PV cell temperature.

$$T_c = \frac{G_T\left(T_{C,NOCT} - T_{a,NOCT}\right)\left(\tau\alpha - \eta_{mp,std} - \eta_{mp,std}T_{c,std}\alpha_p\right) + T_a G_{T,NOCT}\tau\alpha}{G_{T,NOCT}\tau\alpha - \eta_{mp,std}\alpha_p G_T\left(T_{C,NOCT} - T_{a,NOCT}\right)} \tag{2.24}$$

PV cell temperature equations are written in a Simulink block and is shown in Figure 2.5. This block accepts the solar insolation and ambient temperature and calculates the PV cell temperature.

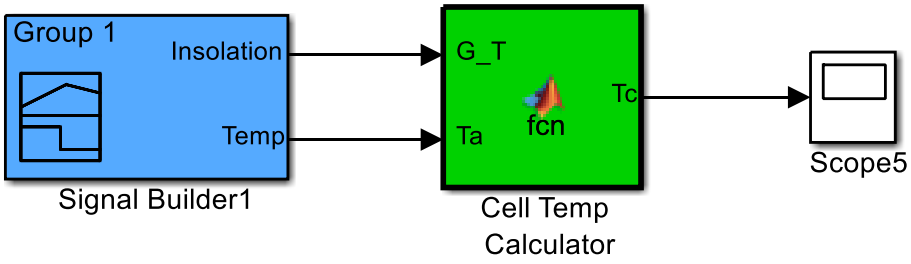

Figure 2.5: Simulink block for cell temperature calculation

2.3.2 PV output power

Photovoltaic cell is a semiconductor device that transforms solar radiation in electrical energy and this phenomenon is termed as 'Photovoltaic effect'. PV cells are assembled in form of series and parallel configuration to form a PV panels and these panels are concatenated in different configurations (series or parallel) for different energy capacities. The electrical power generated by the PV panels is strong function of field conditions (i.e. day time, irradiation level, environment temperature and orientation of the panel) and operating conditions (i.e. type and intensity of load) [37]. PV cell is highly nonlinear device and typically its behavior is represented as current source. In the literature various models of solar cell are presented: one-diode and one-resistance model, one diode and two resistances model and more than one-diode models [66].

An equivalent circuit of a typical PV cell is shown in Figure 2.6 having one diode and two resistors. At fixed temperature and solar radiation the relation between current and voltage of this model is given by equation (2.23) [37] .

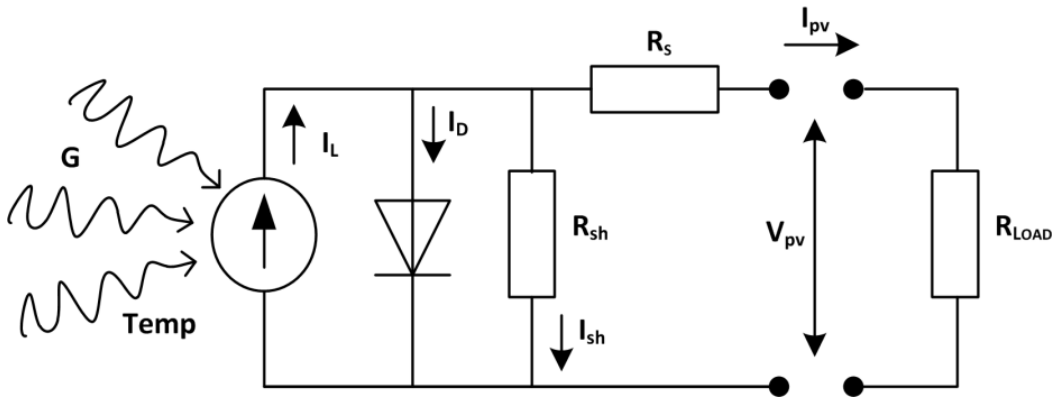

Figure 2.6: PV cell model

$$I_{PV} = I_L - I_D - I_{sh} = I_L - I_0 \left[\exp\left(q \frac{V_{PV} + I_{PV} R_s}{nkTN_s} \right) \right] - \frac{V_{PV} + I_{PV} R_s}{R_{sh}} \quad (2.25)$$

The circuit requires five parameters to be known:

- Light current I_L
- Diode reverse saturation current I_0
- Series resistance R_s
- Diode Ideality factor n
- Shunt Resistor R_{sh}

The diode ideality factor n has the value (typical between 1 and 2 for real diodes, 1 is for an ideal diode); T is the cell temperature, k = $1.38*10^{-23}$ J/K the Boltzmann's constant and q=$1.6022*10^{-19}$C the elementary charge. Ns is the number of cells in series. In a practical PV cell, R_s series resistance is the current path through the semiconductor material, the metal grid, contacts, and current collecting bus [67]. These resistive losses are lumped together as a series resister (R_s). Its effect becomes very conspicuous in a PV module that consists of many series-connected cells, and the value of this resistance is multiplied by the number of cells. Parallel Resistance also known as shunt resistance causes a loss associated with a small leakage of current through a resistive path in parallel with the intrinsic device [67]. Its effect is much less conspicuous in a PV module compared to the series resistance, and it will only become noticeable when a number of PV modules are connected in parallel for a larger system.

The five parameters in the model are taken from the current and voltage measurement of module at reference conditions provided by the manufacturer. Electrical characteristics of the PV module are usually measured at standard reference conditions of

incident radiation of 1000 W/m2, cell temperature of 25C and air mass ratio of 1.5. Following parameters are usually provided by the manufacturer of the PV panel.

- Open circuit voltage, V_{oc}
- Short circuit current, I_{sc}
- Maximum power point conditions, V_{mp} and I_{mp}
- Temperature coefficient of short circuit current
- Temperature coefficient of open circuit voltage

To determine the five parameters, five different conditions need to be known. Open circuit voltage is taken when the current flowing through cell is zero and short circuit current is measured when the voltage across the PV cell is zero. The condition of maximum power point is taken where the derivative of power w.r.t voltage becomes zero. Remaining two parameters can be calculated by temperature coefficients. Resulting five simultaneous equations are to be solved numerically to determine the five parameters at reference conditions.

Some other simple methods are also reported in the literature with significant accuracy and low computational burden. The study done by Walker [68] uses the electric model with moderate complexity with the assumption of shunt resistance infinity and provides fairly accurate results. The diode ideality factor (n) is determined by estimation. It takes a value between one and two; the value of n=1 (for the ideal diode) is, however, used until the more accurate value is estimated later by curve fitting [68].

The series resistance (R_s) of the PV module has a large impact on the slope of the *I-V* curve near the open-circuit voltage (V_{oc}), hence the value of R_s is calculated by

evaluating the slope *dI/dV* of the *I-V* curve at the V_{oc} [68]. The equation for R_s is derived by differentiating the equation (2.25) and then rearranging it in terms of R_s yields equation (2.26).

$$R_s = -\left.\frac{dV}{dI}\right|_{V_{oc}} - \frac{nkT/q}{I_o.e^{\frac{qV_{oc}}{nkT}}} \tag{2.26}$$

Where: $-\left.\frac{dV}{dI}\right|_{V_{oc}}$ is the slope of the I-V curve at V_{oc} (taken from the datasheet of the module). As most of PV manufacturers give only three operating points (short-circuit current I_{SC}, the maximum power point defined as maximum power current I_{MPP} and maximum power voltage V_{MPP} and open-circuit voltage V_{OC}) and since this work is not based on a PV intrinsic study, the one-diode model is considered satisfactory and easy to implement under MATLAB Simulink environment.

Finally, it is possible to solve the equation of *I-V* characteristics equation (2.25). It is, however, complex because the solution of current is recursive by inclusion of a series resistance in the model. Although it may be possible to find the answer by simple iterations, the Newton's method is used for rapid convergence of the answer [68]. The Newton's method is described as:

$$x_{n+1} = x_n - \frac{f(x_n)}{f'(x_n)} \tag{2.27}$$

Rewriting the equation (2.25), the function for the I_{pv} is expressed in equation (2.28).

$$f(I_{pv}) = I_L - I_{pv} - I_0\left(e^{q\left(\frac{V_{pv}+I_{pv}R_s}{nkT}\right)} - 1\right) \tag{2.28}$$

By writing the I_{pv} function in terms of numerical formulation yields equation (2.29).

$$I_{pv(n+1)} = I_{pv(n)} - \frac{I_L - I_{pv(n)} - I_0\left(e^{q\left(\frac{v_{pv}+I_{pv}R_s}{nkT}\right)} - 1\right)}{-1 - I_0\left(\frac{qR_s}{nkT}\right)e^{q\left(\frac{v_{pv}+I_{pv}R_s}{nkT}\right)}} \tag{2.29}$$

The photo current I_L is given by equation (2.30) and diode saturation current I_0 is given by equation (2.31) [37].

$$I_L = \frac{G}{G^*}\left(I_{SC} + K(T - T^*)\right) \tag{2.30}$$

$$I_o = I_0^*\left(\frac{T}{T^*}\right)^{3/n} \exp\left(\frac{-V_G T^*}{nV_T}\left(\frac{1}{T} - \frac{1}{T^*}\right)\right) \tag{2.31}$$

The input parameters are the solar radiation G (W/m^2), G* (1000 W/m^2) the reference solar radiation, cell temperature T and K temperature coefficient for current. V_T is the thermal voltage. For polycrystalline cells, the band gap energy semi-conductor, here noted as V_G, is equal to 1.12 eV. Under the G* reference irradiance and the T* reference temperature reverse saturation current at reference temperature is given by equation (2.32).

$$I_0^* = \frac{I_{SC}}{(e^{qV_{OC}/nkT} - 1)} \tag{2.32}$$

By putting the concerned parameters in the equation (2.25) and solving it iteratively will provide the converged solution of I_{pv}. Output power of the PV panel is then calculated by equation (2.33).

$$P_{PV} = I_{PV} * V_{PV} \tag{2.33}$$

All of the above equations were programmed in the Matlab/Simulink environment and is shown in Figure 2.7.

The results obtained from the model were plotted. Figure 2.8 shows the different voltage current characteristics of the panel for different insolation at constant temperature. It is evident from the figure that short circuit current produced by the panel is a strong function of the intensity solar radiation. As the solar radiation intensity increases the short circuit current of the panel also increases and has little effect on the open circuit voltage of the module. Figure 2.9 reveals the power characteristics of the panel for different insolation at constant temperature. Figure 2.10 shows the different curves drawn at different temperature (insolation is kept constant) to observe the effect of temperature on the performance of PV panel. As the panel temperature increases, open circuit voltage is reduced and there is negligible effect on the short circuit current of the module. Figure 2.11 reveals the effect of temperature on the output of panel power. Increase in the panel temperature drastically decreases the panel output power.

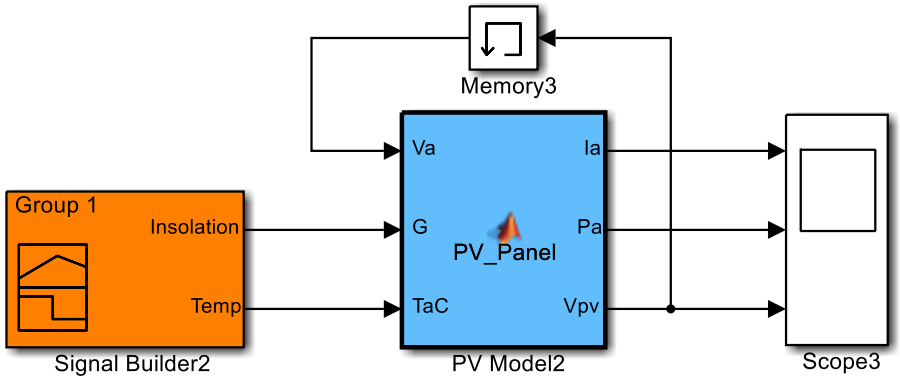

Figure 2.7: Simulink model of PV cell

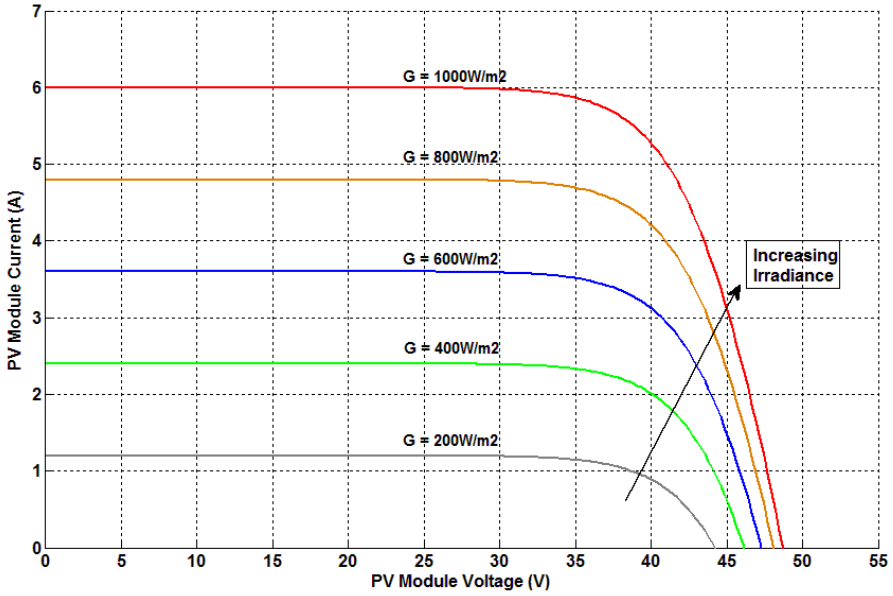

Figure 2.8: PV panel IV curves for different insolation

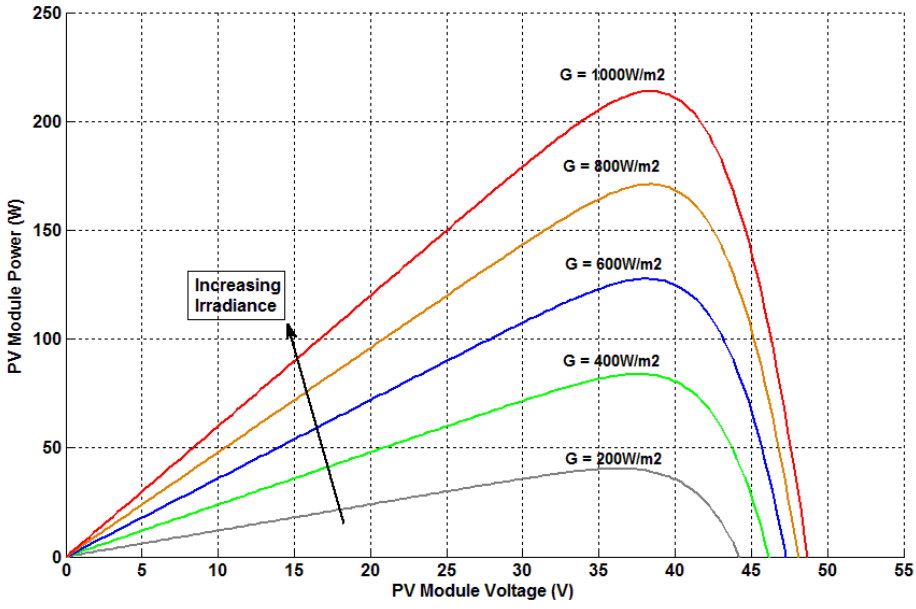

Figure 2.9: PV panel power curves for different insolation

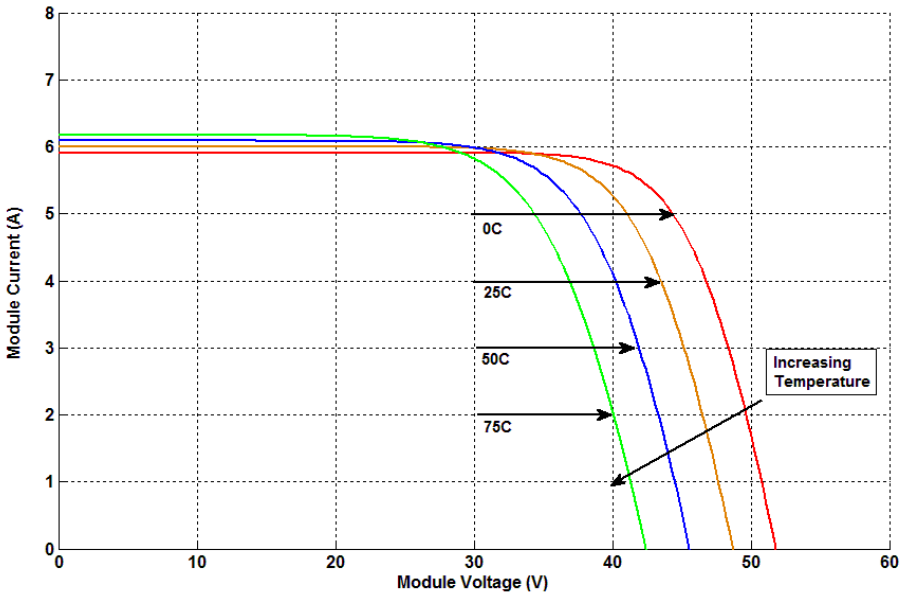

Figure 2.10: Effect of temperature on panel IV curve

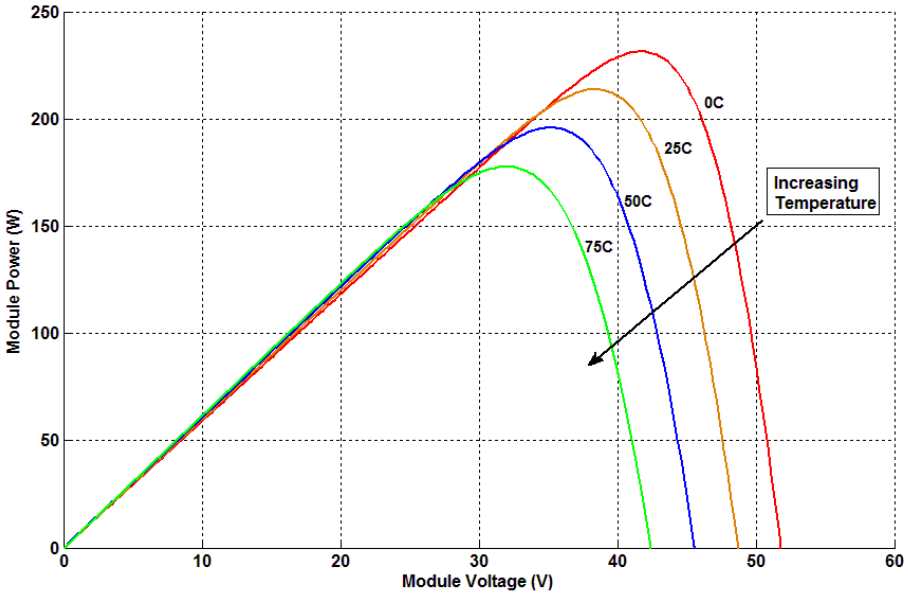

Figure 2.11: Effect of temperature on panel power Curve

2.3.3 Maximum power point tracker (MPPT)

The current and voltage relationship of photovoltaic module is inherently nonlinear and it needs an online search and identification point for the maximum power point tracking. Load can extract the maximum power form the photovoltaic panel only and only if load line is intersecting with the maximum power point of the voltage current curve of the photovoltaic panel. MPPT (maximum power point tracker) is an electronics converter which tracks the maximum power point in the VI curve of the PV module. It is inserted between the photovoltaic panel and the load to achieve the optimum characteristic matching and is shown in Figure 2.12. Basic purpose of MPPT is to harvest the maximum energy from the photovoltaic module and deliver it to the load. MPPT is a power electronics converter having the following main three parts.

- DC/DC converter
- Current and Voltage sensing circuits
- Controller for MPPT algorithm

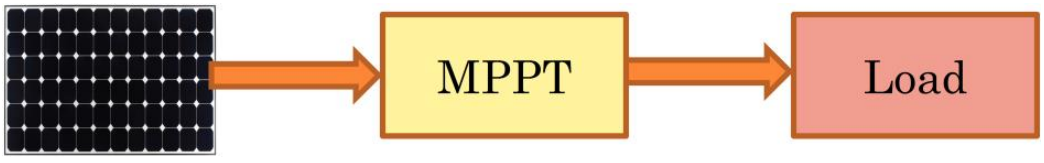

Figure 2.12: Placement of MPPT in the PV source and load

DC/DC converter is the main power unit of the MPPT and it converts the direct current power to direct current power. Its basic principle is to chop the input signal and store the electric energy in the inductor or capacitor. This stored energy is then delivered to the load depending upon its load characteristic and maximum current is drawn from photovoltaic module. To calculate the amount of power delivered by the PV module, output voltage and current drawn from the PV module is measured. A software algorithm is usually employed to acquire the required signals and process them according to some MPP tracking algorithms and implement the decision on power electronic converters. A review of these MPP tracking techniques is given in [69]. Commonly used MPP tracking algorithms are following

- Open circuit voltage method
- Perturb and observe methods
- Incremental conductance method (IC)

IC method provides good dynamic tracking over other algorithms but its implementation is more complex. This algorithm's flowchart with output sensing direct control is shown in Figure 2.13. The Simulink implementation of the CI algorithm is depicted out in Figure 2.14.

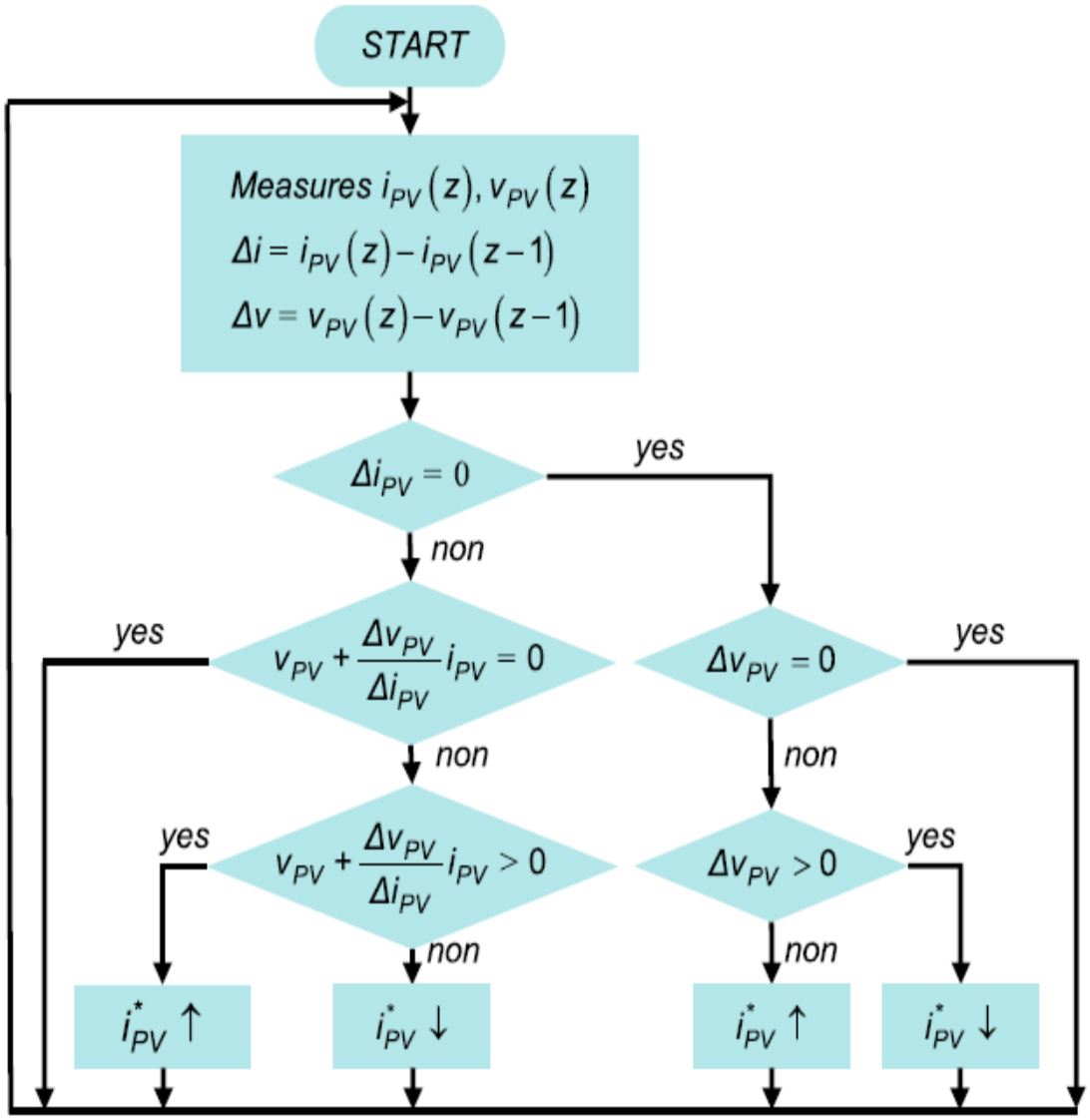

Figure 2.13: Incremental conductance (CI) algorithm with output sensing [70]

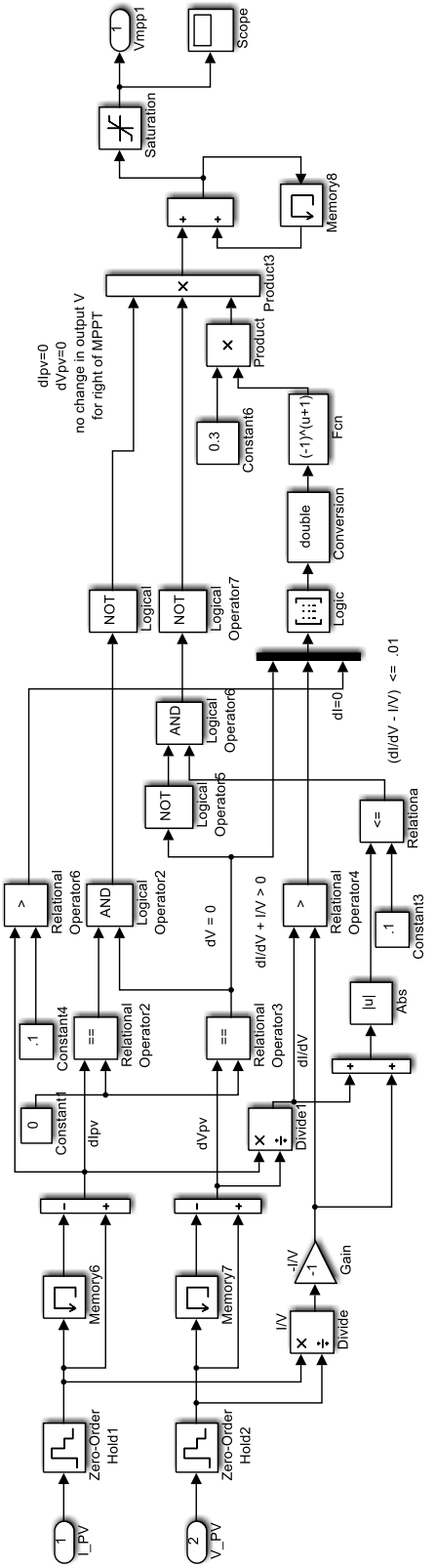

Figure 2.14: Simulink implementation of MPPT algorithm

The Simulink model of the PV/MPPT is simulated under different insolation to get the current and voltage profile of the module. Perturb and observe (P&O) algorithm is used with the PV IV curves to track the maximum power point. The results of the algorithm is given in the Figure 2.15 . In figure different power curves are drawn for different insolation of the sun and the green line is the locus of maximum power points tracked by MPPT algorithm.

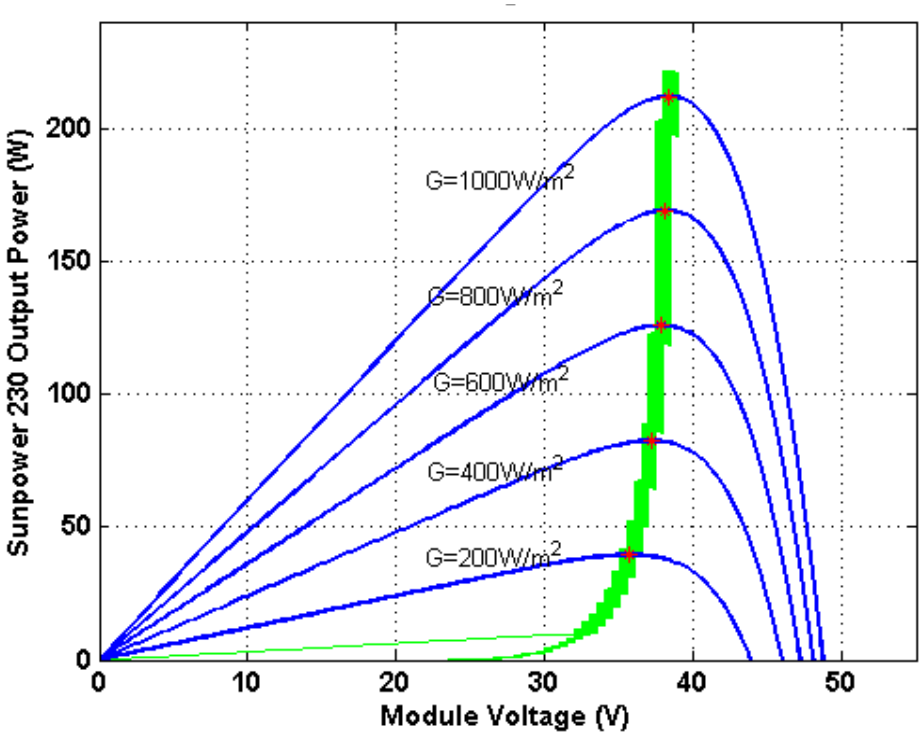

Figure 2.15: Maximum power point tracking of MPPT algorithm

2.4 Reverse osmosis model

Brine/brackish water is an unsaturated solution of salt and water. When we try to separate water from the solution through a semipermeable membrane, the water passes through the membrane and dilutes the salt solution. The membrane rejects most of the dissolved salts and allowing the water to permeate, known as natural osmosis as depicted in Figure 2.16. When sufficient time is provided to the solution in the osmosis apparatus and water passes through the membrane, the pressure on the dilute side drops and the pressure of the concentrated solution increases. The osmotic flux continues and an equilibrium is reached, consequently, water flux through the membrane diminishes. At the equilibrium stage, the liquid level in the concentrated water side is higher than that on the waterside. The amount of water passing in either direction will be equal. The hydrostatic pressure difference is called osmotic pressure and is equal to the effective driving force causing the flow. Osmotic pressure is dependent on the solute concentration, solute temperature and on the type of ionic species in the solution [71].

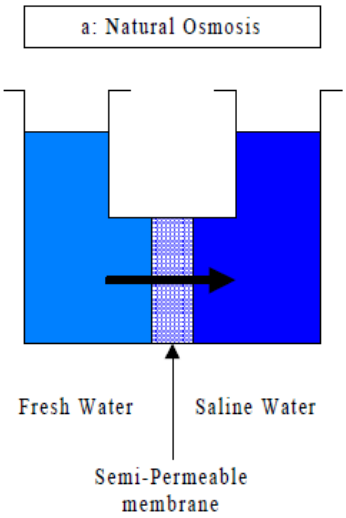

Figure 2.16: Natural osmosis [71]

If the pressure is applied in excess of the osmotic pressure to the concentrated water section, then its effect is to slow down the osmotic flow and forces the water to flow from the salt solution into the waterside. Therefore, the direction of flow is reversed, and that is why this separation process is called reverse osmosis [71]. An RO membrane module is an essential element for the commercial filtration process. The spiral wound membranes are commonly used in the RO water desalination systems. In these membranes the feed channel, ploy amide active layer for filtration process, feed spacer and retentate channel are fabricated in a form of sheet and then wounded in spiral configuration to increase the compact density of membrane. Feed water is forced to pass through the feed channel from one end of membrane with high pressure.

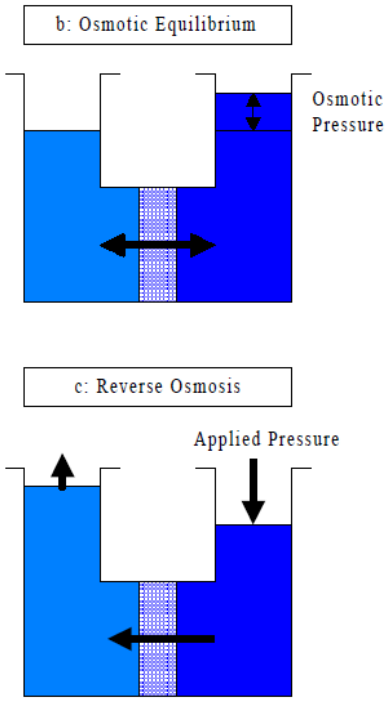

Figure 2.17: Osmotic equilibrium and reverse osmosis [71]

Due to the filtration process clean water passes through the polyamide active layer and after travelling through the spiral permeate channel, it is collected from the central tube of the membrane. High concentration brine is collected from the other end of the membrane for disposal or energy recovery. This filtration process is depicted out in the Figure 2.18.

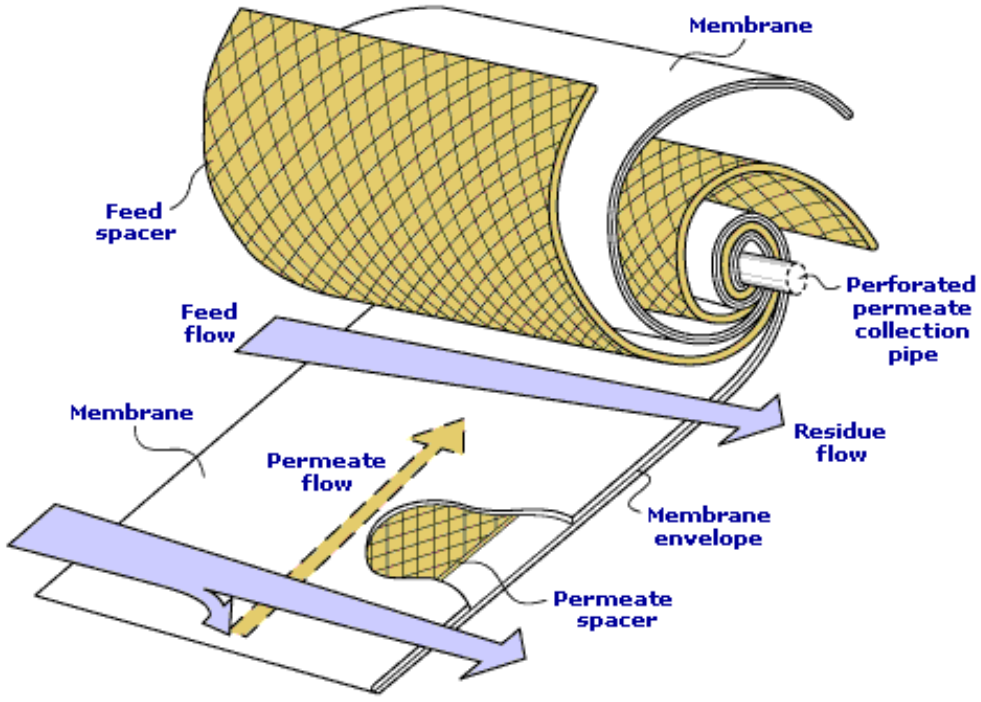

Figure 2.18: Schematic representation of spiral wound membrane module (courtesy of MTR)

Spiral wound membranes are usually considered as cross flow separator to model its filtration process. The permeate flow rate through the membrane is strong function of the difference between feed pressure and osmotic pressure and is estimated by solution diffusion model. In this model the clean water flow rate passing through the membrane is given by equation (2.34) [72].

$$Q_p = A_{perm} S_e (TCF)(FF)\left[(\mathrm{P_f} - \frac{\Delta P_{fc}}{2} - \mathrm{P_p}) - (CPF\ \frac{\pi_f + \pi_b}{2} - \pi_p) \right] \qquad (2.34)$$

Where A_{perm} the water permeability of the membrane is, S_e is the membrane active surface area and both parameters are available from the RO membrane data sheet. In the RO process, higher the feed water temperature, higher the permeate flow rate. So a temperature correction factor (TCF) is introduced in the equation and it is approximated by the formulae provided by the DOW membrane manufacturer company [72].

$$TCF = \begin{Bmatrix} \exp\left[2640\left(\frac{1}{198} - \frac{1}{273+T_w} \right) \right], Tw \geq 25°C \\ \exp\left[3020\left(\frac{1}{198} - \frac{1}{273+T_w} \right) \right], Tw < 25°C \end{Bmatrix} \qquad (2.35)$$

T_w is the feed water temperature. FF is the membrane fouling factor. Its value is unity for new membrane and decreases as the RO filtration time increases. P_f is the pressure of feed water entering the membrane module. ΔP_{fc} is the pressure drop along the membrane module (feed side pressure – concentrate side pressure) during the filtration process and is approximated by empirical formula [72].

$$\Delta P_{fc} = 0.756\left(\frac{Q_c + Q_f}{2}\right)^{1.7} \tag{2.36}$$

P_p is permeate side pressure and is usually taken as unity. *CPF* is concentration polarization factor and is given by following empirical relation [72].

$$CPF = e^{(0.7\,\mathrm{Y})} \tag{2.37}$$

Y is the water recovery ratio (ratio between permeate flow rate to feed flow rate). π is the osmotic pressure of solution at a given salinity and temperature and is calculated by following practical short approximation reported in the [72].

$$\pi = \left\{ \begin{array}{l} \dfrac{C\,(\mathrm{T}+320)}{491000}, C < 20000 mg\ /\ l \\ \dfrac{0.0117C - 34}{14.23} . \dfrac{(\mathrm{T}+320)}{345}, C > 20000 mg\ /\ l \end{array} \right\} bars \tag{2.38}$$

T is the feed water temperature and C is the salinity in PPM or mg/l. By putting all the concerned values in equation (2.34), permeate flow rate is calculated. Concentration of the salt in the filtered water is calculated by using equation (2.39).

$$C_p = B_{salt} S_e (TCF)\left[CPF\left(\frac{C_{fc}}{Q_p}\right) \right] \tag{2.39}$$

B_{salt} is the salt permeability of the membrane and is evaluated from manufacturer's data. S_e is membrane active area. C_{fc} is the average concentration of the water on the concentrate side of the membrane module and is calculated by following formula.

$$C_{fc} = \frac{C_f + C_c}{2}, C_{fc} = C_f \ln\left(\frac{1}{1-Y}\right)/Y \tag{2.40}$$

Y is recovery ratio for a membrane module and is calculated as follows.

$$Y = \frac{PermeateFlowRate}{FeedFlowRate} = \frac{Q_p}{Q_f} \tag{2.41}$$

By making use of above equations, permeate flow rate and its concentration can be calculated. All flow rates are considered to be incompressible so conservation of flow is used to calculate the concentrate flow rate by using equation (2.42).

$$Q_f = Q_p + Q_c \tag{2.42}$$

By making use of mass balance equation brine concentrate is calculated by equation (2.43).

$$Q_f C_f = Q_p C_p + Q_c C_c \tag{2.43}$$

Power consumed by the high pressure pump is the difference between power feeding the raw water and power recovered by the energy recovery device (Pearson Pump). Equation (2.44) is used to calculate the net consumed power.

$$Power = \frac{Q_f P_f}{\eta_{HPP}} - Q_c P_c \eta_{ERD} \tag{2.44}$$

All of the above mentioned equations are programmed in MATLAB/Simulink environment and is shown in Figure 2.19, and are solved within the operational constraints. Different flow rates along with their concentrations and pressures are computed according the PV available power.

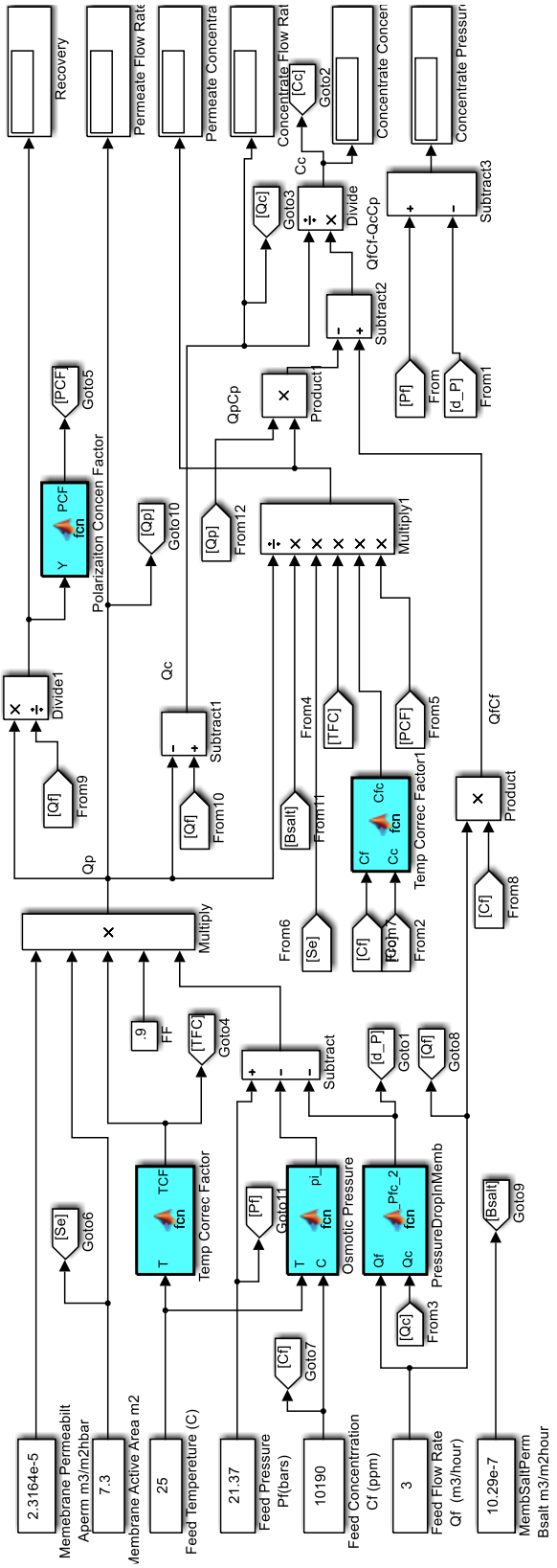

Figure 2.19: Simulink model of RO membrane

2.5 PVRO configuration and experimental setup

PVRO system consists of two sections, PV and RO section. PV system consists of PV Panels, sun trackers, charge controllers, batteries (optional) and inverters/motor drives. RO section comprises of feed pump, pretreatment filters, water storage buffers, high pressure pumps, membrane modules and PX (pressure exchangers for energy recovery devices). PV generator converters the sunlight into electrical energy, and is dependent on the solar insolation and module temperature. Figure 2.20 illustrates the schematic description of the PVRO system.

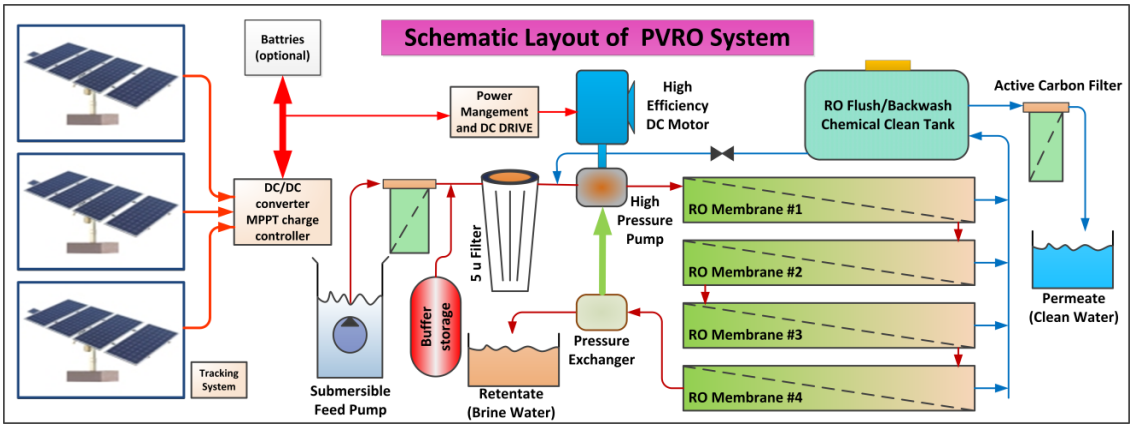

Figure 2.20: Schematic description of PVRO system

Table 2.1: Electrical specifications of megasol panel modules

Parameter	Symbol	Value
No of PV Modules	N	12
Dimension of PV Module		800mm x 1600mm
Peak Power (+/- 5%)	P_{max}	185 W
Rated Voltage (at Pmax)	V_{mpp}	41.0 V
Rated Current (at Pmax)	I_{mpp}	5.61 A
Open Circuit Voltage	V_{oc}	48.7 V
Short Circuit Current	I_{sc}	5.99 A
Power Temperature coefficient	$\mu_{p,temp}$	-0.38 % / K
Voltage Temperature coefficient	$\mu_{ocv,temp}$	-132.5 mV / K
Current Temperature coefficient	$\mu_{scc,temp}$	3.5 mA / K
NOCT (Nominal Operating Cell Temperature)	T_{noct}	25^{o} C+/-2^{o} C

All the PV modules are installed on two axis trackers to enhance the output power production by maximizing the received insolation. In this configuration, the received insolation and hence power production can be accessed for flat plat, single axis and double axis mode of operations. Table 2.1 shows the electrical specifications of the used panels. PV panel's output is connected to maximum power point trackers (MPPT)/charge controller, which tracks the maximum power point on the current voltage (IV curves) of PV panel for a given irradiation level and module temperature. PV output voltage and current both are varying in nature due to the variation of environmental variables. Output

of the charge controller/MPPT is stabilized on constant voltage at 24 volt and current is changed according to the available PV output power. Typical conversion efficiency of the MPPT/charge controller is about 92%. Regulated power provided by MPPT is used to drive the motor of high pressure pump. To utilize the maximum amount PV available energy, motor load line must coincide with the load characteristic of MPPT/charge controller, otherwise the MPP will not be tracked and energy will be lost due to mismatch of impedances of the PV source and the RO load. So a motor drive is incorporated in the design to vary the motor speed that changes the position of load line. The current drawn by the motor/HPP is function of system pressure that is adjusted by bleed valve available at the pearson pump.

Quality and quantity of produced clean water is a function of feed water chemistry, RO configuration, and feed flow rate and membrane pressure. Different RO configurations are evaluated for different feed water chemistry in [73], and it is reported that the optimum configuration of RO for feed water salinity ranging from 35000-48000 ppm is single pass single stage. In the single pass single stage configuration, RO membranes are connected is series and the brine output of the first membrane unit is taken as the feed for the next membrane. The output of the last membrane is sent to the PX (energy recovery device) to recover the potential energy. Efficiencies of the feed pump and energy recovery device along with booster pump are also considered in the calculation. The description of PVRO arrangement with different process variables at different points is depicted out in Figure 2.21. The Simulink model of this RO network with different modeling blocks is shown in Figure 2.22. Feed water characteristics and RO membrane specifications are enumerated in Table 2.2 and Table 2.3 respectively.

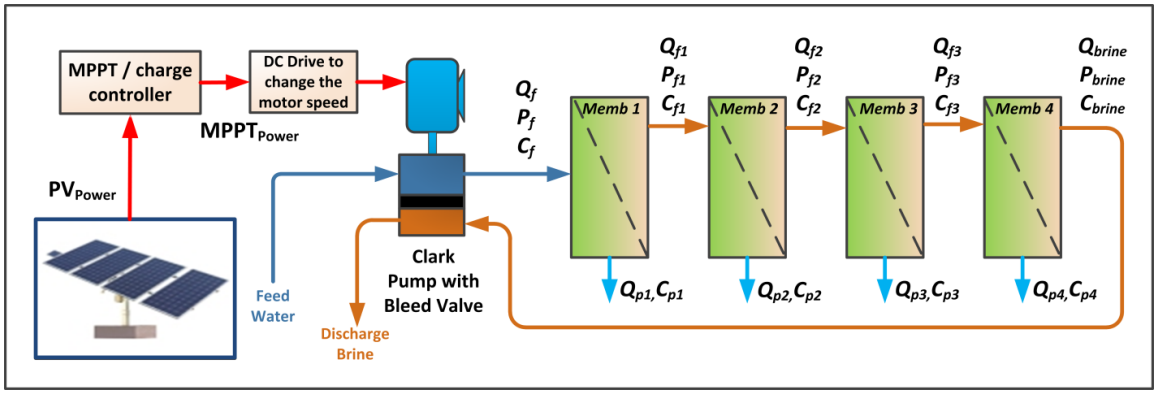

Figure 2.21 : Single stage, single pass RO configuration for PVRO system

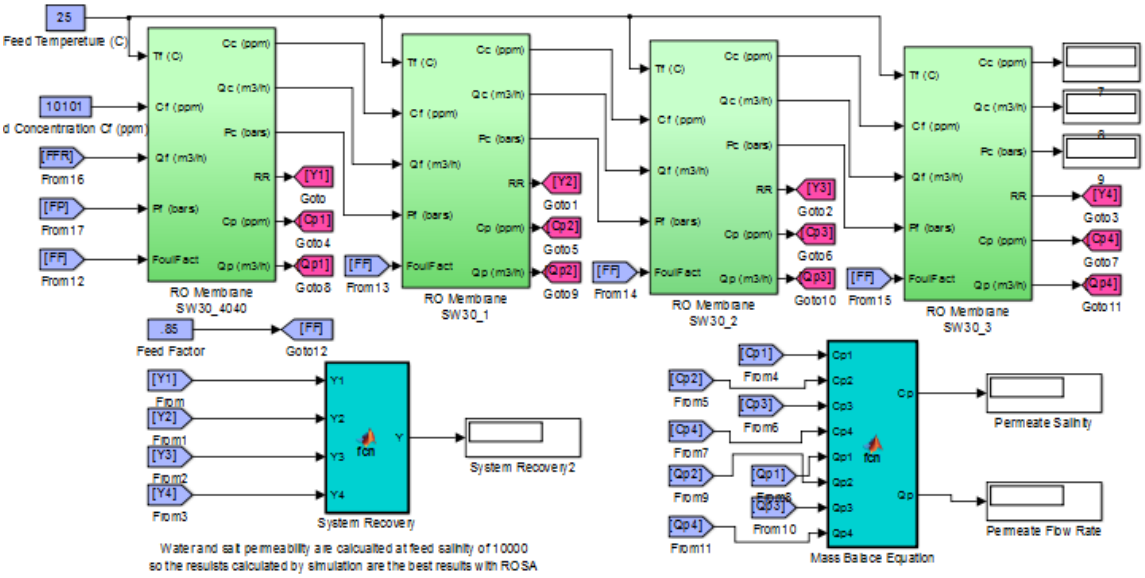

Figure 2.22: Simulink model of the RO membranes in single stage single pass configuration

In this configuration the different process parameters are listed below.

Table 2.2: Feed water flow characteristics

Feed water Characteristics and RO Configuration.	
Typical Concentration of brackish water	10342 mg/L, TDS, ppm
Silt Density Index (SDI) , after pretreatment of feed water using micro and ultra-filtration	Less than 5, [72]
RO system configuration	Single Pass, Single Stage, One pressure vessel having four membranes in series. Membrane type SW30-4040. Flow Factor = 0.85, some aged system.

Table 2.3: Detailed specification of SW30-4040 membranes

Detailed Specifications of RO membrane [73].	
Make and Model	Dow Chemical, SW30-4040
Active Layer Material	Polyamide thin-film composite
Active Area ft^2 (m^2)	78 (7.2)
Membrane Length, meter	1.016
Membrane Diameter, mm	99
Operating Pressure (Maximum), bars	41
Operating Temperature (Maximum), ^oC	45
Operating Pressure Drop (Maximum), bar	1.0
Operating pH Range, Continuous Operation	2-11
Maximum Feed Silt Density Index	SDI 5

Chlorine Tolerance, mg/l, ppm	< 0.1
Clean Water Permeability, $m^3/(m^2\text{-h-bar})$	1.086×10^{-5}
Salt Permeability, $m^3/(m^2\text{-h})$	4.65×10^{-7}

To validate the proposed model of complete PVRO system a state of the art lab for the PV systems and RO units is established. The PVRO desalination system is installed in the premises of KFUPM University, Saudi Arabia. The system is modular and contains three main sections, (1)-Solar Energy Power System, (2)-Pretreatment System and (3)-RO Desalination System. All of three modules encompass the state of the art high efficiency components to ensure the enhanced performance of the system. The process flow diagram of the installed system is according to Figure 2.20. To measure the different parameters and process variables of the PV and RO systems, data acquisition system is developed and installed. A computer having LabVIEW software installed is connected to data acquisition system via USB cables. The complete experimental setup is shown in Figure 2.23.

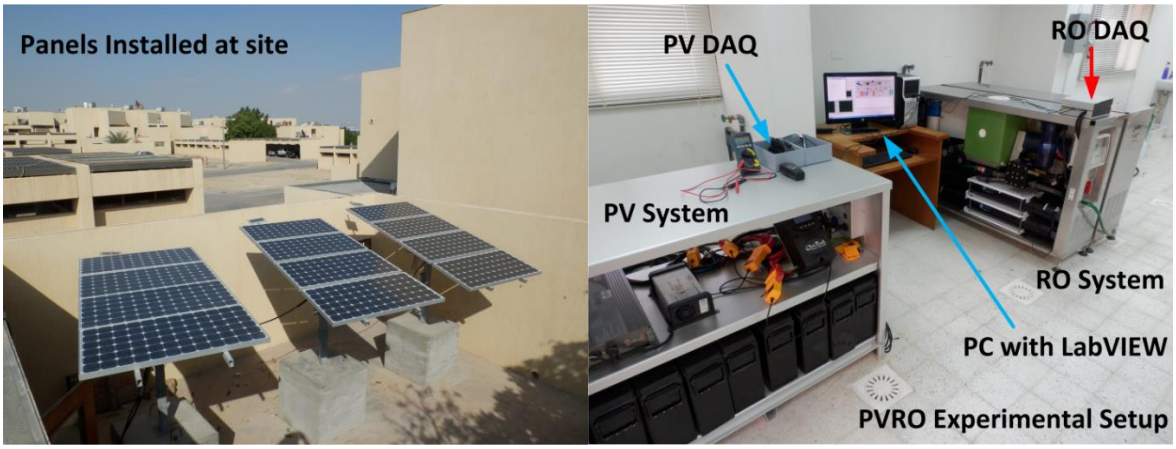

Figure 2.23: PVRO experimental setup for model verification

A day of 5 December 2013 was selected to run the PV system for data collection. All the current transducers were calibrated to ensure the correct reading. Sampling time of 10 seconds was selected to record the readings. The test was started before 15 minutes of sun rise and continued until 15 minutes after the sunset. The collected data was available in spread sheet compatible to the excel format. Figure 2.24 shows the theoretical and experimental instantaneous solar insolation profiles. The theoretical solar radiation curve exhibits the smooth variation from dawn to dusk. The behavior of the experimental data is slightly different from the theoretical curve but it follows the same trend. The theoretical and experimental power extracted from the panels through maximum power point tracker is shown in Figure 2.25. The average percentage error of experimental power from the predicted one is -16.5%. It is obvious that the measured PV output power is closely following the predicted PV power. During the whole day 7.5kWh of energy was provided to charge the batteries and its voltage was raised from 23.7V to 27.4V. The charged batteries from the PV system operation were used to run the RO system. The developed data acquisition system for PVRO was used to collect the data for the different variables in the RO system. The salinity of the feed water was set to 10350 ppm. Speed of the motor was changed from the DC drive to vary the feed flow rate of the input water. High speed of the motor corresponds to the more power consumption and vice versa. For a certain motor speed, consumed power, feed flow rate, feed salinity, permeate flow rate, system pressure and permeate salinity is recorded.

The experimental and simulated permeate flow rate results v/s PV power are plotted and shown in Figure 2.26. In this plot, curves are fitted on simulation and experimental results to see the trend of the data. Equations of the both fitted curves are second order

polynomials which reveal that neither simulated nor are experimental values linear in relation to the PV power. Experimental results are in close match with the predicted one with the average percentage error of -6.77%, which is quite fair for the validation of the model. Figure 2.27 shows the experimental and theoretical permeate flow rate for a whole day with an average percentage error of -4.91%. In this figure for the low power 700-900 W, the experimental data exhibits some mismatch to the predicted one. This mismatch is due to the increased losses of the DC drive, motor and ERD at low speeds. For the high power range 900-1400 watts the experimental values are in good match with the predicted ones. All the figures reveal that the experimental data of solar insolation, PV power and permeate flow rate are in good agreement to the predicted data from the theoretical formulations. The experimentally validated model is further used for the prediction of clear water production for peak days of different seasons with different PV panel configurations.

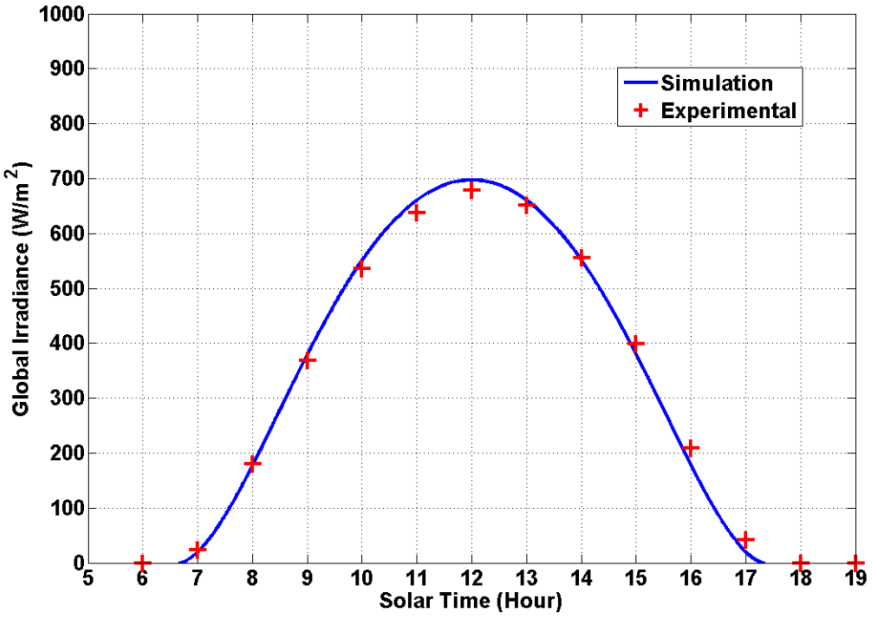

Figure 2.24: Theoretical and experimental plots of solar radiation 5 dec

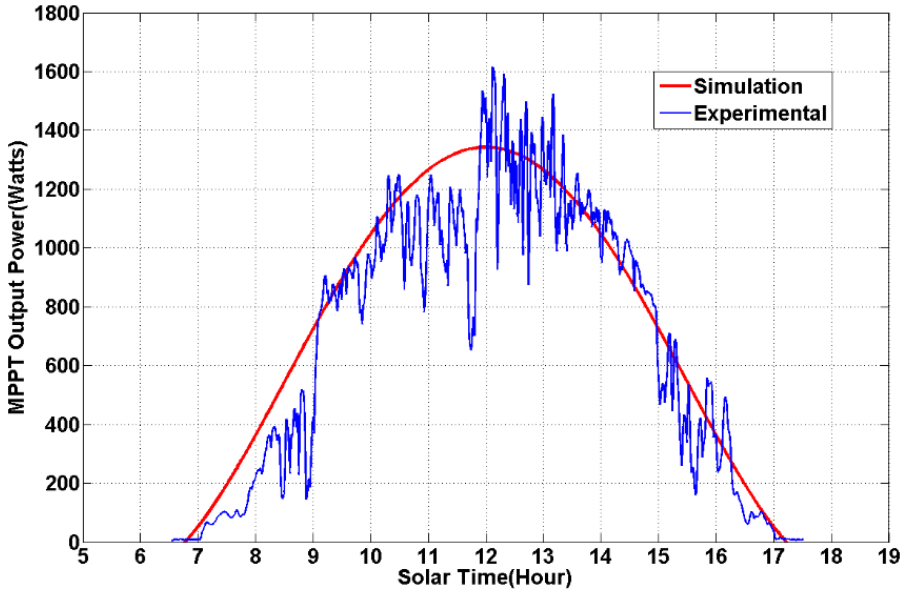

Figure 2.25: Theoretical and experimental plots of PV output power

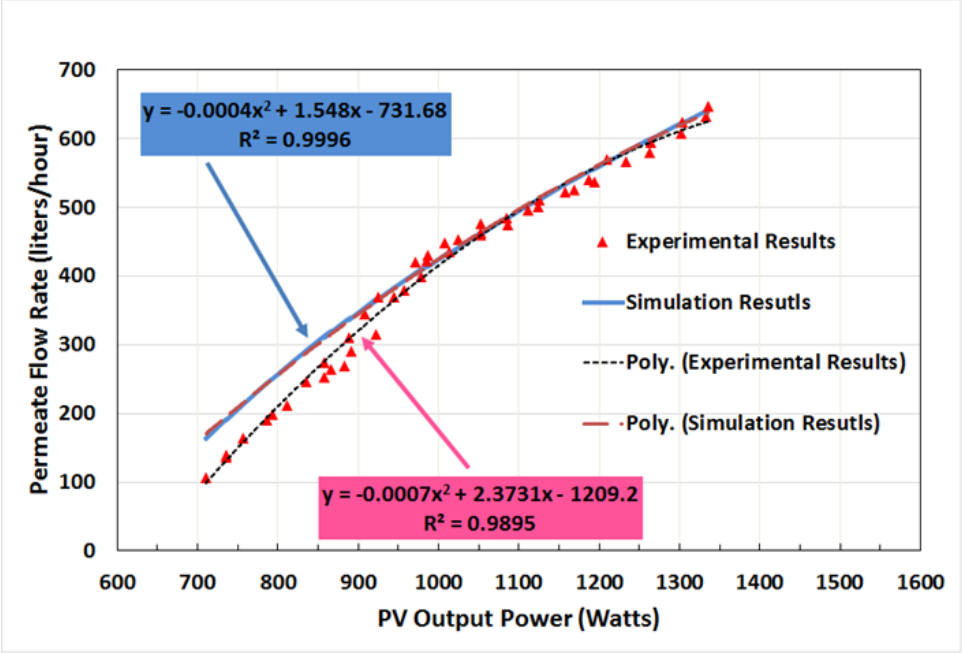

Figure 2.26: Experimental data of clean water flow rate for different PV power

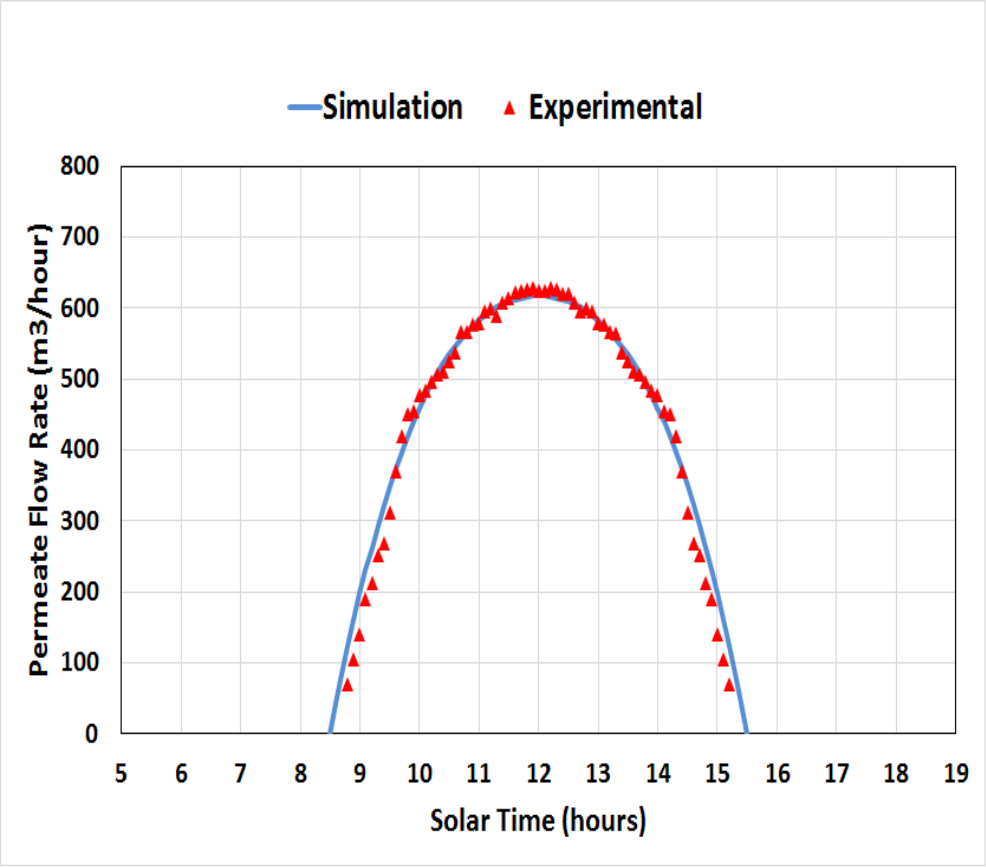

Figure 2.27: Theoretical and experimental plots of clean water flow rate for a whole day

2.6 Results and discussion

This case study is carried out for Dhahran City, situated on eastern coast of Saudi Arabia. The latitude and longitude of Dhahran is 26.2794^{o} N and 50.2038^{o} E respectively and altitude is 16.77 meters above the sea level. Experimentally verified modeling equations (1-34) of whole PVRO system were programmed in MATLAB/Simulink environment. All parameters mentioned above for the PV and RO systems are used in the program. The solution of the equations provides solar radiation, panel temperature, PV power and permeates flow rate results for any selected day of the year. Simulation step is set equal to (1/10) hour in this simulation work. The calculation flow chart of different parameters is presented in Figure 2.28.

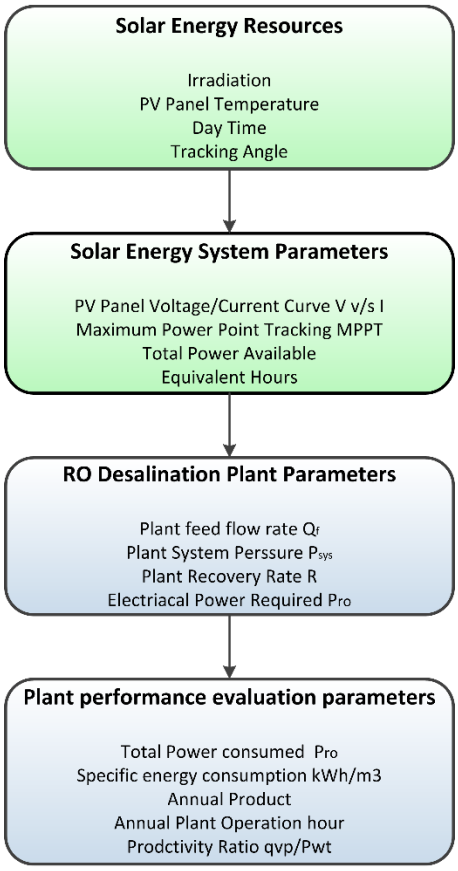

Figure 2.28: Flowchart for PVRO parameters calculation

2.6.1 Effect of day on the instantaneous PV power and permeate flow rate

To analyze the PV output power and permeate flow rate for the different days of the year, four extreme days of the four seasons are considered in the year i.e. vernal equinox (n = 80), autumnal equinox (n = 266), summer solstice (n = 172) and winter solstice (n = 356) days. The simulations are carried out for horizontal PV panels having slope β and surface azimuth angle γ equal to zero. The results of the simulation in terms of instantaneous irradiance, PV output power and permeate flow rate for the four seasons are shown in Figure 2.29, Figure 2.30 and Figure 2.31 respectively. Due to the difference in the day light hours in winter and summer, it is obvious that the solar radiation available on PV panels are slightly more than 10 hours in winter solstice day and slightly less than 14 hours in summer solstice day. During the day irradiation begins with the sunrise and gradually increases to maximum value at solar noon and then decline gradually until sunset. Maximum radiation received at solar noon differs from day to another and it is due to fact that how high sun appears in the sky. During the winter (Nov, Dec and Jan) sun's elevation angle is lower and in summer (May, June and July) sun's elevation is maximum than the other seasons. During the vernal equinox (n = 80, spring season) and autumnal equinox (n = 266), sun’s elevation is almost same due to that the solar radiation profiles in these days are very close to each other in the Figure 2.29.

Figure 2.30 shows the PV power output profiles for the different peak days of four seasons for the whole year. It is obvious that the peak power produced in summer season and winter season is 1850 and 1390 W respectively, and this difference of power is attributed to the different insolation levels in the summer and winter days. Maximum power produced in spring and autumn days is 1660 and 1575 W but the insolation level for both

respective days is almost 860W/m^2. This variation of PV output power for same insolation level is due to the different temperature for both seasons. Average temperature for the March (spring season) and September (autumn season) is 21.9 and 33.1 ^oC respectively. Due to high temperature in September PV output power is low and due to reduced temperature in March PV power is high.

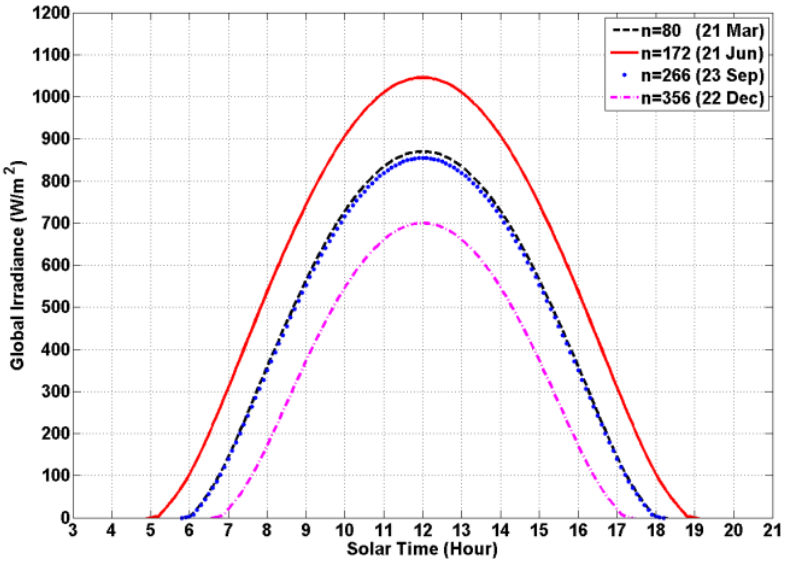

Figure 2.29: Instantaneous irradiation for different days of the year at Dhahran

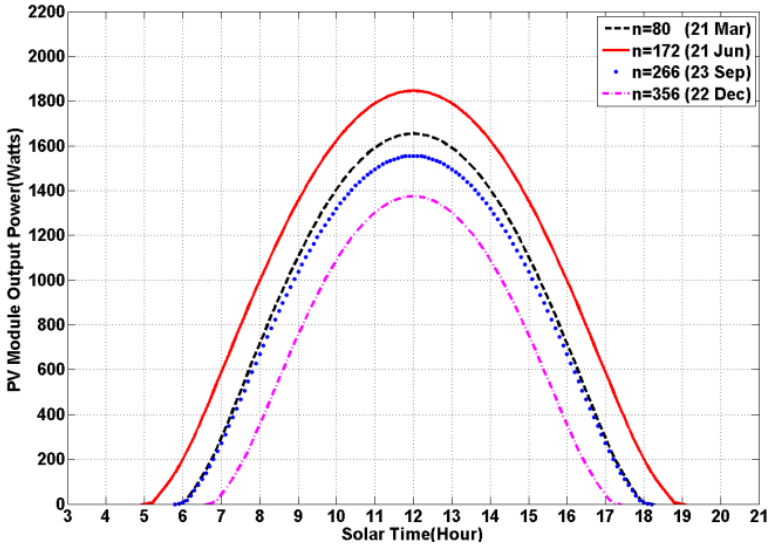

Figure 2.30: Instantaneous PV output power during different equinox and solstice days

PV output power is provided to the RO section to drive the high pressure pump. Pump speed is controlled by DC drive to match the load and source impedance for maximum power flow. Due to the motor speed variation, feed flow rate is changed whereas the system pressure is adjusted automatically due to the pearson pump (working as energy recovery device). The permeate flow rate for different PV power profiles for different seasons is depicted out in Figure 2.31. Maximum permeate flow rate for summer and winter days is noted to be at 925 and 650 L/h respectively. The permeate flow rate profiles in Figure 2.31 for different seasons shows the same trend as that of their corresponding PV power profile in Figure 2.30. It is concluded that the clean water production is in linear relation to the PV available power.

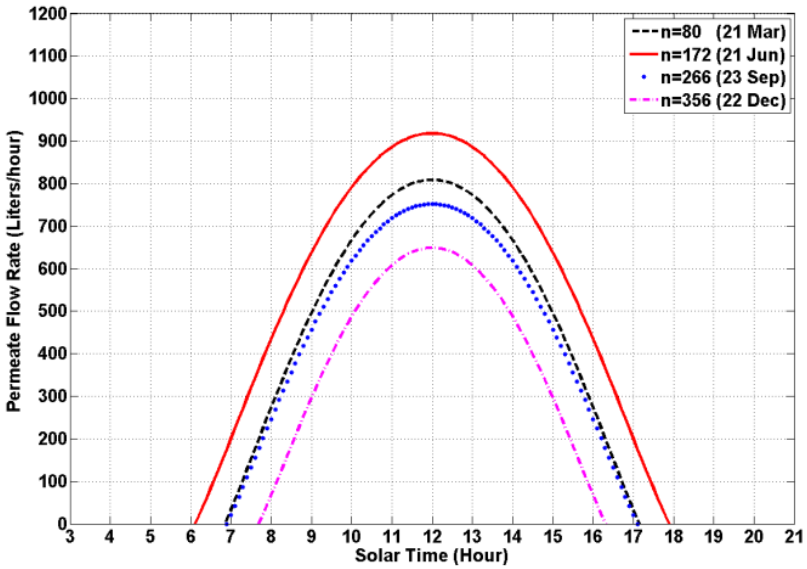

Figure 2.31: Instantaneous permeate flow rate during different equinox and solstice days

2.6.2 Effect of slope on the instantaneous permeate flow rate

Slope of the PV panels is an important parameter that effects the permeate flow rate and it is due to the fact that variation of the slope changes the amount of solar radiation reaching the PV panel. Figure 2.32 shows the instantaneous permeate flow rate at the different inclination of the PV panels for winter solstice, vernal equinox day, summer solstice day and autumn solstice days of the year. For the analysis of the simulation results PV panel slope is changed from zero to 90 with the increment of 15^{o}.

It is obvious that the inclination angle of the PV panel has significant effect on the permeate flow rate during the summer solstice day as compared to the results of winter solstice day. The zenith angle of the sun varies form 90 (at sunrise) to almost zero at solar noon and then gradually increase to 90 (at sunset) in summer solstice day but during winter solstice day zenith angle decrease to 50 (at solar noon) and then gradually increases to 90 at sunset.

The permeate flow rate in winter solstice day is 550 L/h for flat PV panel, and it increases to 870 L/h when PV slope is 45. Further increase in the PV slope decreases the permeate flow rate to 680 L/h for PV slope of 90. So PV panel slope ranging from 45-50, the permeate flow rate is more attractive than other slopes. This phenomenon is due to the fact that the sun zenith angle at noon is 45, and if the PV slope is set to this angle then it collects maximum radiation causing more PV power consequently increased permeate flow rate. This phenomenon is shown in the Figure 2.32a.

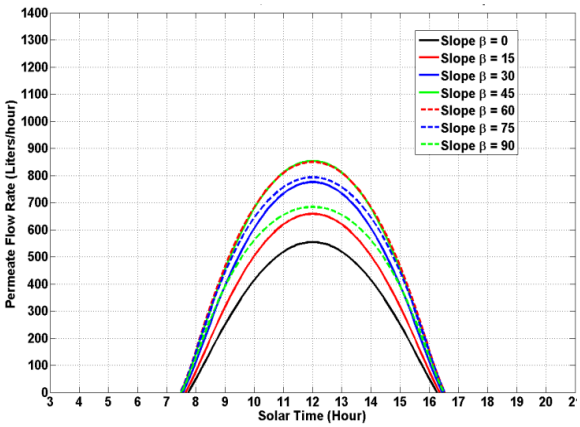

Figure 2.32a:

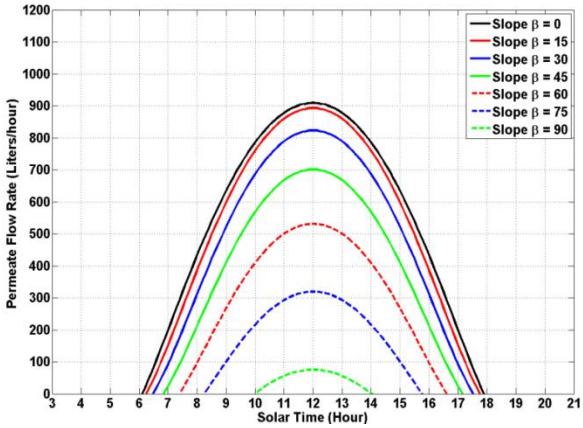

Figure 2.32b:

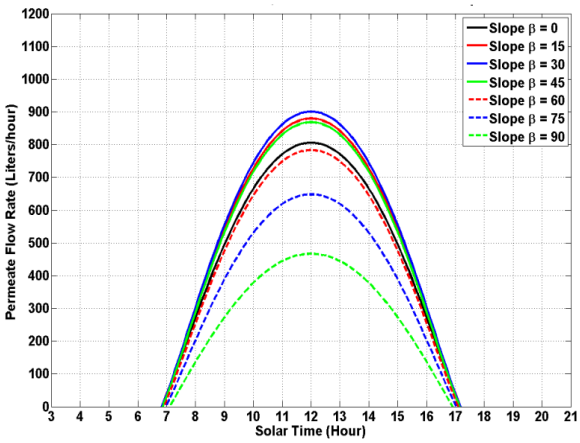

Figure 2.32c:

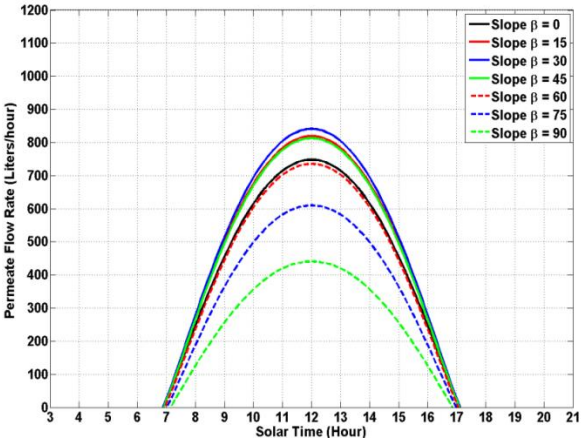

Figure 2.32d:

Figure 2.32: Instantaneous permeate flow rate with different slopes during winter solstice days (a), summer solstice days (b), vernal equinox day (c) and autumn equinox day (d).

The permeate flow rate in winter solstice day is 550 L/h for flat PV panel, and it increases to 870 L/h when PV slope is 45. Further increase in the PV slope decreases the permeate flow rate to 680 L/h for PV slope of 90. So PV panel slope ranging from 45-50, the permeate flow rate is more attractive than other slopes.

In the both equinox days, maximum permeate flow rate is 800 and 750 L/h for vernal equinox and autumnal equinox days respectively for flat PV panels and is shown in Figure 2.32c and 13d. In these both days the solar radiation profiles are almost (as shown in Figure 2.29) same and the permeate flow rate difference is attributed to the difference in PV panel temperature. During the vernal equinox season monthly average temperature is less than the autumnal equinox monthly average temperature. In these both days increase in PV panel angle up to 30 degree shows the increase in the permeate flow rate, and after then it declines to minimum that corresponds to PV panel slope of 90. Analysis of the permeate flow rate results for different seasons of the year indicates that for a specific day, certain inclination angle for PV panel exists that ensures the maximum permeate flow rate and that is azimuth angle of the sun at solar noon at that day.

2.6.3 Yearly optimal tilt angles for south facing collector

Due to the inconveniences of the cost and other technological aspects of the tracking system, researchers have proposed to find out the yearly optimal slope for PV panel. Figure 2.33 shows the yearly collected permeate for PV panels at different inclinations (0 to 90) with surface azimuth angle zero.

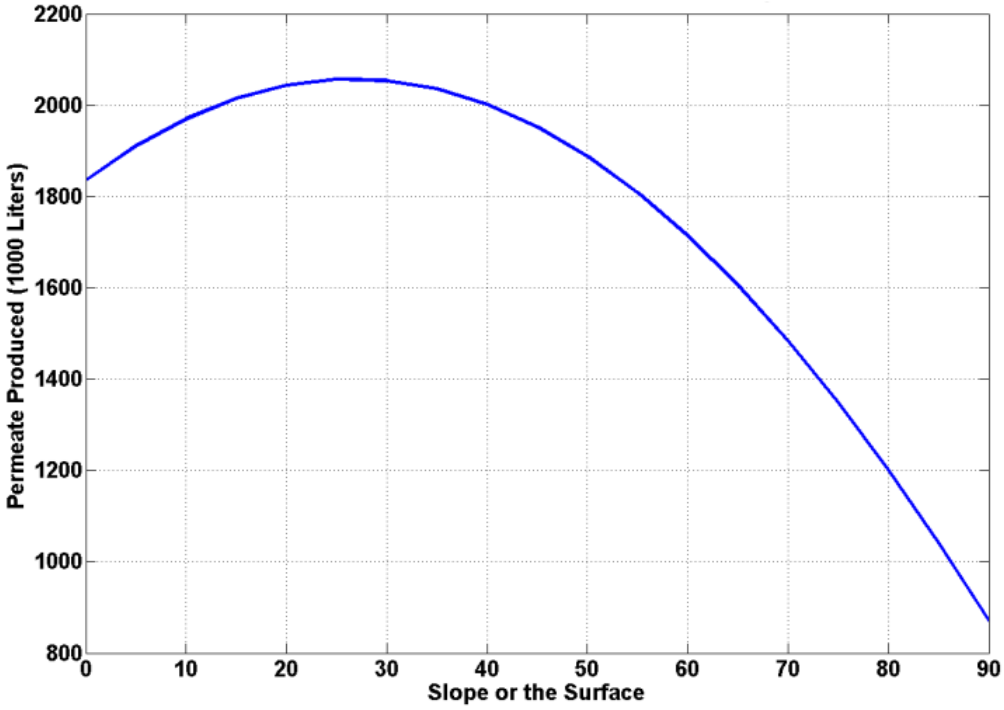

Figure 2.33: Yearly collected clean water for different PV panel slope angles

The computed yearly permeate is 1850 thousand liters for the horizontal PV panel configuration (inclination is zero) and 890 thousand liters when the PV inclination is 90. It is evident that the maximum yearly collected permeate is 2050 thousand liters that is obtained when the PV inclination angle is of 24 degrees. This result is in agreement with the result of Chang and Tian, 2009 [75], who predicted that yearly optimal tilt angle for south facing PV panels in northern hemisphere for latitudes below 65 degrees is 0.9 times the latitude of the site. From the results yearly optimal angle is 24 and corresponds to 0.913 times the latitude of the Dhahran.

2.6.4 Monthly optimal tilt angles for south facing collector

To enhance the PV panel's output power, single axis or double axis tracking system is usually employed in PV systems. Gunerhan et al, 2007 [76] recommends that PV panel's slope/inclination has to be adjusted optimally every month. Monthly optimal angles are calculated in such a method that during the mean average day of the month, the PV panel or the solar collector surface must have the beam incidence angle (at solar noon) equal to zero to ensure the maximum solar radiation. This condition can be achieved by setting the inclination of the south facing panel equal to solar azimuth angle at solar noon for the average mean day of the month.

Table 2.4 recapitulates the monthly optimal tilt angle of the PV panels facing south for Dhahran city. The optimal panel tilt varies form 3.2 degrees in June to 49.3 in December. Figure 2.34 illustrates the variation of optimal tilt angle during the whole year. It is obvious that during the first six months the optimal tilt angle has the decreasing trend form 47 to 3.2, but in second half of the year it is increasing up to 49.3 for December. It is

concluded that optimal angle variation have the same trend as that of the solar zenith angles (at solar noon) for the whole year.

Table 2.4: Monthly optimal tilt angles for PV panels

Month	Jan	Feb	Mar	Apr	May	Jun	Jul	Aug	Sept	Oct	Nov	Dec
Optimal Tilt	47.2	39.2	28.7	16.9	7.5	3.2	5.1	12.8	24.0	35.9	45.2	49.3

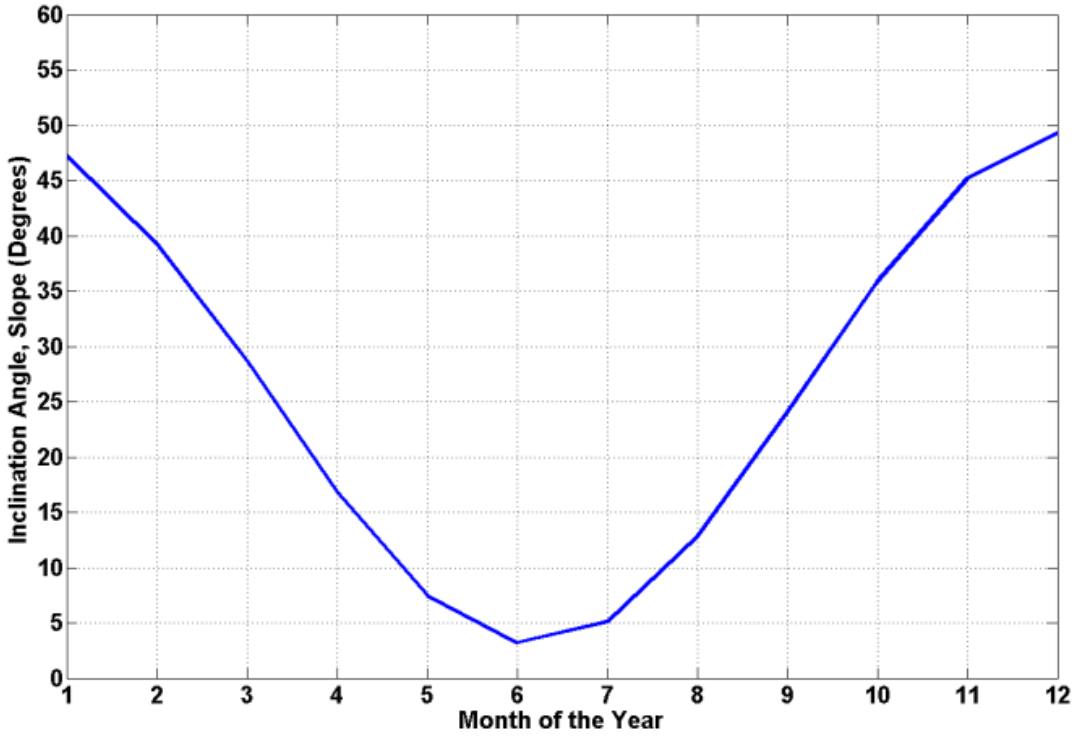

Figure 2.34: Monthly optimal tilt angles for PV Panels

2.6.5 Tracking angles for single axis and double axis trackers

In the previous section, investigations of the variations of PV panel inclination angle on the PV power generation and permeate flow rate is made. On the same way if the PV panel azimuth angle is changed and keeping the inclination angle of PV panel fixed, the peak of the PV power generation and permeate flow rate will be shifted from the solar noon. This peak shift will be towards morning time if the surface azimuth is negative and towards evening time for positive values. To optimize the PV power gain and permeate flow rate, single or dual axis tracker are usually employed. In the solar trackers, the first axe is the horizontal one to adjust the slope or the inclination of the PV panel surface and the second axe is the vertical one to adjust the surface azimuth angle of the PV panel.

In single axis tracker the slope of the collector is kept constant and usually equal to the yearly optimal tilt angle or to the latitude of the site [75], but the surface azimuth angle is adjusted continuously to track the solar azimuth angle.

$\beta = const = \varphi$ PV panel slope = Latitude of the site

$\gamma = \gamma_s$ PV panel azimuth angle = Sun azimuth angle

In double axis tracking system, slope and azimuth angle of the solar PV panels are continuously adjusted to harvest the maximum possible solar radiation. Surface slope and azimuth angle are to track the sun zenith and sun azimuth angle respectively to ensure the beam incidence angle θ equal to zero at any time during the whole day.

$\beta = \theta_z$ PV panel slope = Sun zenith angle

$\gamma = \gamma_s$ PV panel azimuth angle = Sun azimuth angle

Figure 2.35 and Figure 2.36 illustrate the variation of tracking angles of PV panels for single and double axis tracking systems respectively for the city of Dhahran, Saudi Arabia. Four extreme days of the year, vernal equinox day, summer solstice day, autumn equinox day and winter solstice day are selected to depict out the tracking angle variation for both types of tracking systems.

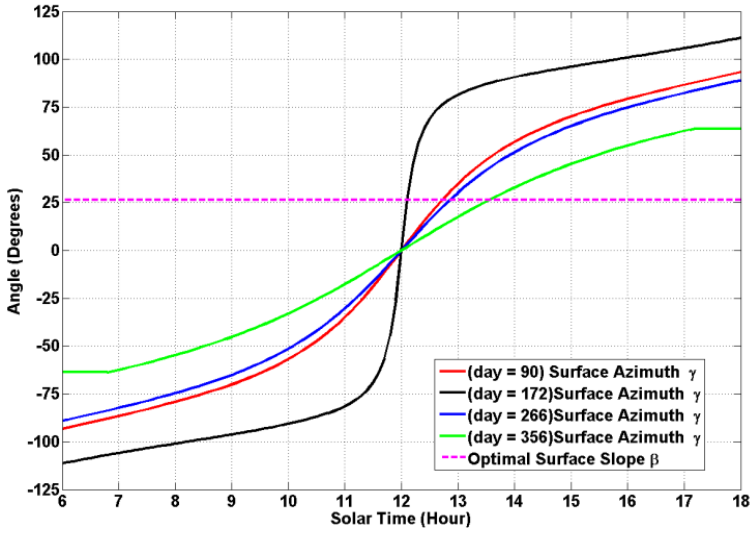

Figure 2.35: Tracking angles for single axis continuous tracker

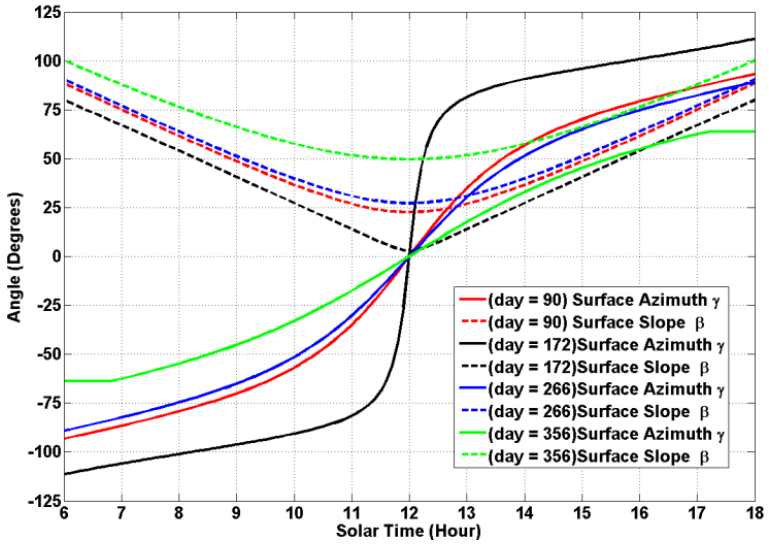

Figure 2.36: Tracking angles for double axis continuous tracker

From the Figure 2.36 it is obvious that the PV inclination angle is 90 at sunrise and at sunset, and these positions corresponds to vertical orientation of the PV panel at dawn and dusk in double axis tracking system. During the first half of the day the inclination angle β decreases from 90 gradually and approaches to minimum value at solar noon, but in the second half it increases until 90 at sunset time. This phenomenon in evidenced by Chang 2009 [77] and illustrated that slope of the tracked panel is minimum at solar noon and increases towards dawn or dusk. PV panel slope at solar noon depends on the day number of the year and its highest value is $49.3°$ in winter solstice day and minimum value $3.2°$ on summer solstice day in our case study.

For the tracking panels, the negative surface azimuth angle corresponds towards the east and positive value towards the west. During the whole day operation of double axis tracker, the surface azimuth angle increases from negative extreme value (at dawn time) to positive extreme values (at dusk time). In the summer solstice day it varies from -110 to +110 while in winter solstice day it varies from -62 to +62 degrees. From the Figure 2.36 it is obvious that the PV panel azimuth angle is more important between 10^{th} to 14^{th} hour of solar time during the day. During this period (around the solar noon) solar path in the sky is perpendicular to line joining the sun and PV panel and this results in the highest displacement of the sun in the sky. This large displacement of the sun causes the significant variation of the sun azimuth angle.

2.6.6 Comparison of collected permeate for fixed and tracking PV panels

Based on the analysis of tracking angles for single axis and double axis trackers for PV panels, the permeate flow rate of PVRO system when driven by tracked panels is also analyzed. Figure 2.37 shows the permeate collected for horizontal PV panel (β and γ =

0), yearly optimal tilt (β = 24.5), monthly optimal tilt, single axis and double axis tracking PV panels for the vernal equinox, summer solstice, autumn equinox and winter solstice days for Dhahran city. It is found that least amount of permeate is received by the horizontal PV panels and maximum is received by the double axis tracking surface. Among the fixed PV panels, monthly optimal tilt configuration produce more permeate than the yearly tilt and flat PV panels. Among the tracked surfaces double axis tracked surface receives more insolation and produce more permeate than single axis tracking system and fixed panel configurations due to the optimal incidence angle of beam radiation throughout the whole day.

Figure 2.38 and Table 2.5 summarizes the collected permeate for different fixed and tracked PV panels for each month of the year. Permeate collected for flat PV panel is taken as reference for gain calculation for other PV panel configurations. For the yearly optimal tilt surface, the maximum gain is 53% for December and minimum gain is -12% in the month of June. For the other monthly optimal tilt, single axis and double axis tracked surface it is noticeable to comment that maximum gain is in December and minimum gain is in June. Yearly comparison illustrates 10% and 19% increase in insolation for yearly optimal tilt and monthly optimal tilt surfaces respectively. Noticeable yearly increment of 43 % and 62 % is estimated for single axis and double axis tracking surfaces respectively. If the permeate produced by yearly optimal tilted PV panels is taken as reference then yearly permeate gain is 8 %, 30 % and 47 % for the monthly optimal tilted, single axis and double axis tracked PV panels respectively.

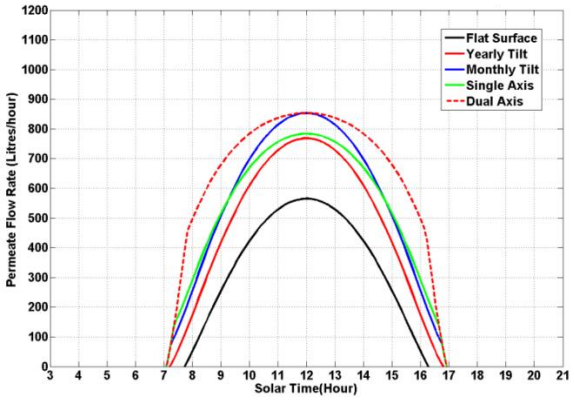

Figure 2.37a

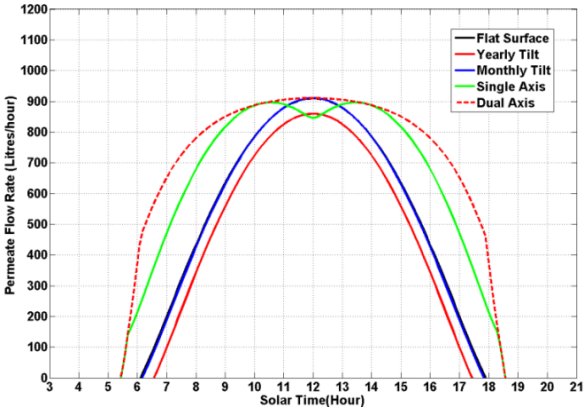

Figure 2.37b

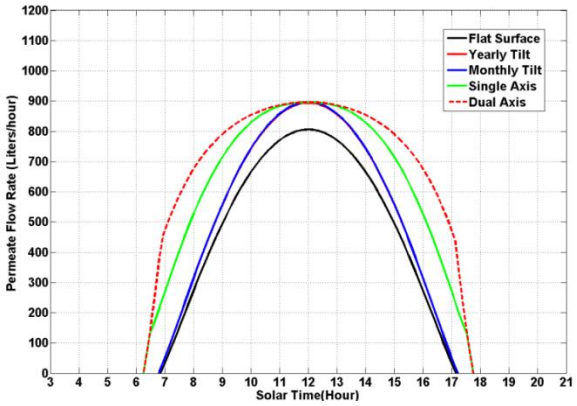

Figure 2.37c

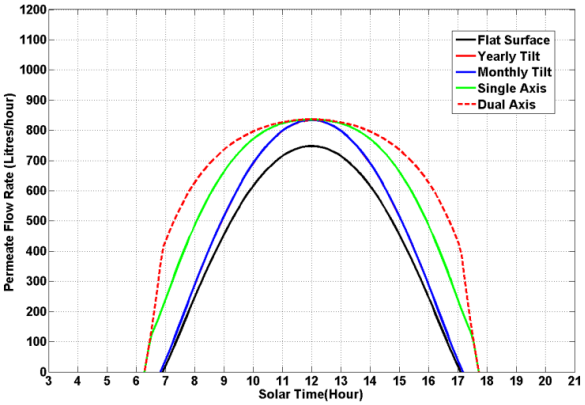

Figure 2.37d

Figure 2.37: Instantaneous permeate flow rate with different fixed and tracked PV panels during winter solstice days (a), summer solstice days (b), vernal equinox day (c) and autumn equinox day (d).

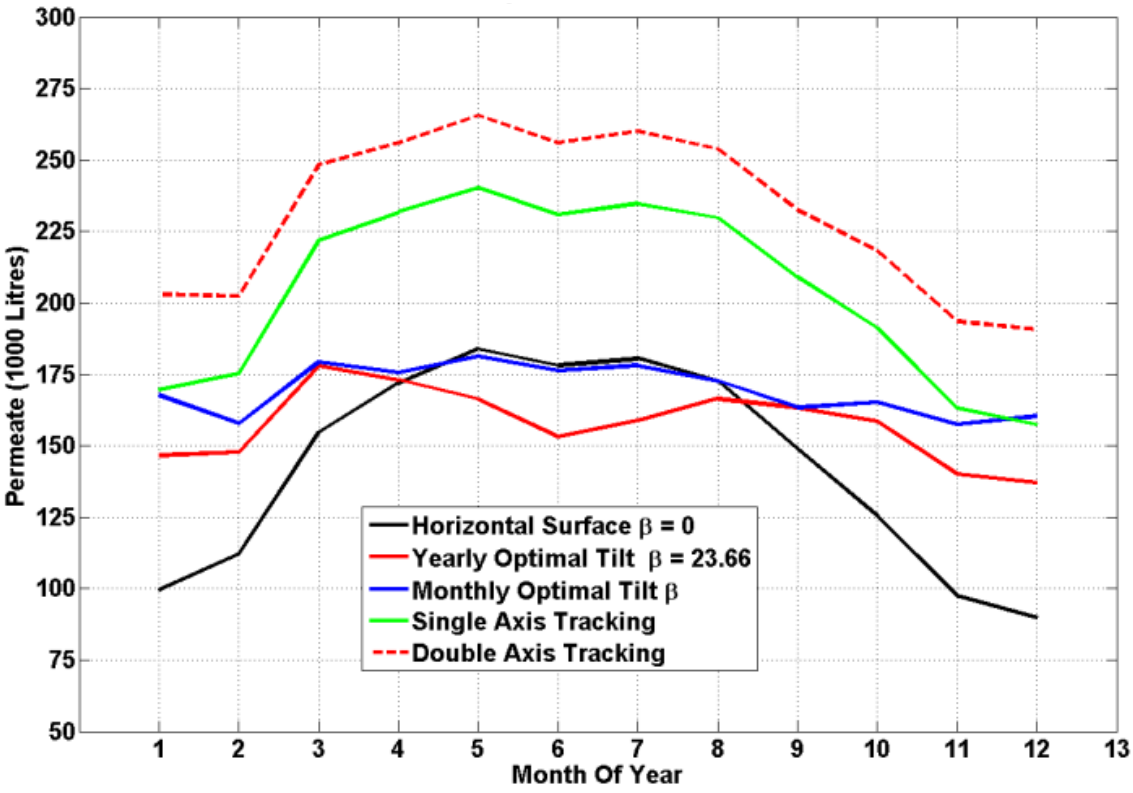

Figure 2.38: Monthly collected permeate for different fixed and tracked PV panels

Table 2.5: Comparison of collected permeate by fixed and tracked PV panels

	Flat Plate	Yearly Optimal Tilt	%age gain	Monthly Optimal Tilt	%age gain	Single Axis Tracking	%age gain	Double Axis Tracking	%age gain
Month	(1000 liters)	(1000 liters)		(1000 liters)		(1000 liters)		(1000 liters)	
	(Base Values for Comparison)		(Comp to FlatPlate)		(Comp to FlatPlate)		(Comp to FlatPlate)		(Comp to FlatPlate)
January	100	147	47 %	168	68 %	170	70 %	203	103 %
February	112	148	32 %	158	41 %	175	56 %	202	80 %
March	155	178	15 %	179	16 %	222	43 %	248	61 %
April	172	173	1 %	176	2 %	232	35 %	256	49 %
May	184	166	-10 %	181	-1 %	240	31 %	265	44 %
June	178	153	-14 %	176	-1 %	231	30 %	256	44 %
July	181	159	-12 %	178	-1 %	235	30 %	260	44 %
August	173	166	-4 %	173	0 %	230	33 %	254	47 %
September	149	163	10 %	163	10 %	209	40 %	233	56 %
October	125	158	26 %	165	32 %	191	52 %	218	74 %
November	98	140	44 %	157	61 %	163	67 %	194	98 %
December	90	137	53 %	160	79 %	157	76 %	191	113 %
Yearly Comp (based on Flat Plate)	1715 (Base Value)	1889	10 %	2035	19 %	2454	43 %	2780	62 %
Yearly Comp (Based on Y Optimal Tilt)	--	1889 (Base Value)	0 %	2035	8 %	2454	30 %	2780	47 %

2.7 Summary

In this chapter an overview on the basics of PVRO system is presented with detailed modeling of radiation, PV panels and RO system. The developed PVRO model is validated experimentally. Based on validated PVRO model system configuration is discussed and simulations are carried out to estimate the permeate flow rate. Moreover the effect of PV panel inclination angle and azimuth angle on the permeate flow rate is discussed in detail. Developed models are used to access the permeate flow rate when RO system is driven by flat panels, yearly optimal tilt, monthly optimal tilt, single axis and double axis tracked PV panels. These formulation and performance investigations are important in the prediction of monthly and yearly clean water production when RO is driven by different PV configurations. This case study is carried out for the city of Dhahran and some concluding remarks are inscribed below.

- The yearly optimal tilt angle of solar panel for the city of Dhahran faced due to south is 24.50 degrees and it is very close to the 0.9 times the latitude of the site. Yearly permeate gain made by PVRO having the yearly optimal tilt panels is 10% as compared to conventional flat plate PV panels for Dhahran city.
- Monthly optimal tilt angles for the PV panels are investigated; the maximum optimal tilt angle is 49.3 for December and 3.2 for the month of June. It is also estimated the permeate gain made by monthly optimal tilted panels due south is 19% as compared to the flat conventional PV panel.
- Single axis azimuth type continuous tracker is investigated while keeping the tilt angle of the PV panel equal to yearly optimal tilt angle. The monthly

maximum gain in permeate is 70% during in winter season and minimum gain is 30 % in summer solstice days. Yearly gain using this type of tracker is estimated as 43% as compared to the flat PV panel.

- More optimization is carried out by using the continuous dual axis tracker systems, having the capability to change the surface azimuth and tilt angle throughout the whole day. The permeate gain made by this tracker relative to flat plate PV panel is 44 % and 103 % in the summer and winter solstice days respectively. Yearly permeate gain is estimated to be 62 % relative to flat plate configuration.
- This case study provides a guide for the selection of the yearly optimal tilt, monthly optimal tilt, single axis and double axis continuous tracking angles of the PV panels for the PVRO system. Moreover the monthly and yearly permeate production estimation of PVRO system when driven by any fixed or tracked panel is also carried out for Dhahran city of Saudi Arabia.
- Though the use of trackers clearly demonstrate a substantial gain in energy harvesting and corresponding increase in production of clean water. The actual decision of using a tracker or not will be governed by many technical and economic factors. It will be necessary to compare Life Cycle Costing (LCC) of PVRO system with and without single and double tracking. It will need proper estimate of maintenance costs and parts replacements of mechanical items prone to failures of trackers and all other related costs of installations and acquisition of trackers.

Chapter 3

PVRO experimental setup with DAQ

This chapter is related to the design and development of instrumentation, data acquisition and graphical user interface of photovoltaic driven reverse osmosis system for monitoring and performance evaluation purposes. Installed PV system comprises of 12 PV panels, trackers, batteries and inverter whereas RO system is equipped with pre filters, pumps, energy recovery devices and filtration membranes. Proper instrumentation is carried out in PV system to measure the irradiation, temperatures, voltage and current at various points. Moreover various sensors are used to measure the pressures, flows, salinities at RO unit. Signal conditioning circuits are designed to adjust sensor output signals for computer interface. A simple moving average filter is used to suppress the measurement noise. The experimental investigation of PVRO system is carried out by using LabVIEW interface capabilities. The developed system reveals and stores the pronounced impact of measured variables on the PV output power and specific energy consumption of the RO filtration system. The online data display in multi-scale window frame is very informative for system operation and analysis. During the experimental run of PVRO system using the developed DAQ system, the PV system generated 7.5 kWh of energy during the whole day operation. Feed water having 7100 ppm salinity and its flow rate was set to 850 L/h by adjusting the RPM of the high pressure pump. Clean water flow rate is recorded to be at 465 L/h having salinity of 115 ppm during the RO operation. Specific energy consumption of RO system comes out to be 2.1 kWh/m3 for 7100 ppm salinity of feed water.

3.1 Introduction

Due to the rapid development of PV technology with declining cost, coupling PV with desalination methods has increased considerably in the last few years. PVRO systems are excellent devices for clean water for small remote communities having no grid connections but have access to brackish water or seawater. The reason behind the interest in PVRO system is its economic benefit and system's modularity, low noise level, low maintenance, long life and non-emissions of greenhouse gases [78].

In the literature various research groups have worked on to measure the renewable energy parameters using dedicated data acquisition methods. Development of a low cost wireless data acquisition system for remote PV pumping water system using single board computer is reported in [79]. A low cost concept for data acquisition system applied to decentralized renewable energy plants with a USB interface is reported by Sandro et al, 2011 [80]. A water environmental monitoring system based on a wireless sensor network is also reported that contains three parts: data monitoring nodes, data base station and remote monitoring center [81]. This system is suitable for the complex and large-scale water environment monitoring, such as for reservoirs, lakes, rivers, swamps, and shallow or deep groundwater. A data acquisition system for photovoltaic modules characterization by using a microcontroller and an electronic load under the metrological conditions is provided [82]. Another attempt of data acquisition is carried out for weather station monitoring at Madina city, KSA [83]. Qiblawey et al, 2011 [84] have developed basic instrumentation system to investigate the performance of the household photovoltaic driven RO desalination system. Experiments on the laboratory household unit were performed using water with two different total dissolved solid (TDS) concentrations (350

mg/L and 720 mg/L) and results were achieved but the designed instrument system is not capable to collect the data for long time operations during field tests. Most recent attempt to develop an empirical model based on experimental data for photovoltaic driven RO is reported by Daniel et al, 2013 [85]. In this work a laboratory based data collecting unit is established using NI DAQ board and the effect of different process intricate parameters is carried out.

Significant amount of research is being carried out to enhance the efficiency of individual components such as PV panels (solar cell materials), RO membrane materials and its packing strategies and energy recovery devices but little work is carried out to optimize the overall system performance [86]. PVRO system efficiency can be enhanced by taking the process optimization and control methods into account. Designing and developing advanced optimization and control strategies for PVRO system demand reliable and efficient instrumentation and data acquisition system to collect the system data and to monitor the process dynamics. Designing of an efficient data acquisition system for PVRO system is an elaborative work and it involves many complicated and interacting choices to meet the technical and economic requirements. The main focus of this work is to design, develop and install the reliable and efficient data acquisition system having the capability to collect the short term data for performance indication and long term data to monitor the field test performance of the PVRO deployed system. The complete PVRO system with developed data acquisition system will be suitable for the field testing purposes and an experimental setup for the implementation of advanced optimization techniques and control methodologies.

3.2 PVRO system description

The PVRO Desalination system is installed in the premises of KFUPM University, Saudi Arabia. The system is modular and contains three main sections, (1)-Solar Energy Power System, (2)-Pretreatment System and (3)-RO Desalination System. All of three modules encompass the state of the art high efficiency components to ensure the enhanced performance of the system. The process flow diagram of the system is shown in Figure 3.1. The PV energy harvesting system comprises of 12 PV panels, which convert the sunlight energy directly into and electrical energy. Output power of the PV module is strong function on solar irradiation and module temperature. Singe axis solar trackers are used with PV panels to keep the PV position perpendicular to the solar radiation during the daylight to collect maximum insolation. A charge controller having the high efficiency DC/DC converter with maximum power point tracker (MPPT) is employed in the system. Its output is 24 V and can be used for battery charging or to drive any other load. Batteries are also employed between MPPT and load to smooth out the variations and to store the additional energy available from the PV panels. A selector switch is used to disconnect the batteries form the system for battery less autonomous operation of the RO system.

In pretreatment section a low pressure pump is used to suck the water from the source and provides sufficient amount of pressure to initiate the pre-filtration process. Three phase brush less direct current (BLDC) motor is used to drive progressive cavity positive displacement pump to suck the saline water. A motor drive is used to adjust the feed pump RPM to control the flow rate. The pre filtration unit consists of 3 self-cleaning cartridge filter assemblies to block undissolved solids, coarse dirties and floating particles. The first prefilter is equipped with a cartridge mesh size of 100 μm and it filters the first

incoming crudes and particles bigger than 100 µm. The water flows further to the next 2 prefilters which works parallel and have a cartridge mesh size of 25 µm. A 25 liter buffer tank is installed to store the high pressure water for prefilter backwash process. Controller, an automatic drive and brushes inside the filter housing make sure a periodically backwash process when certain pressure is build up across the filters due to dirties.

In the RO desalination section a 60 liter RO buffer tank is used for water storage to ensure the continuous supply of water while pretreatment backwash process is in progress. Then the water is allowed to pass through paper filter having pore size of 5um for the safe operation of RO membranes. State of the art Spectra Pearson Pump is a device which performs the pumping and energy recovery functions simultaneously at the same time. Unlike the Clark pump, its operation is smooth and does not induce pressure fluctuations in fluid stream during its pumping operation.

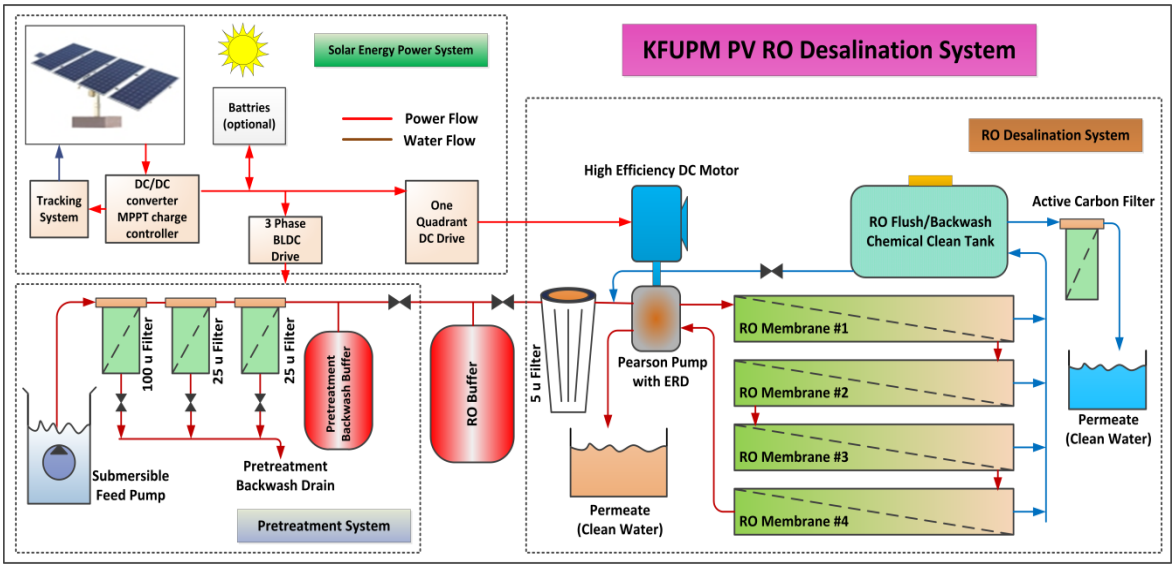

Figure 3.1: Process flow diagram of KFUPM PVRO system

Feed water pressure is boosted by Pearson pump and allowed to pass through the membrane for the filtration process. Reverse Osmosis membranes removes dissolved solids (salt, inorganic contamination etc.) as well as virus and bacteria without requiring toxic chemical treatment. Permeate is collected from the central port of the membrane whereas the retentate stream is send back to Pearson pump to recover the energy. Moreover, permeate is passed through activated carbon filter to eliminate chlorine, bad tastes and unpleasant smells. Technical specifications of the components in the system are detailed in the Table 3.1.

Table 3.1: Technical specifications of PVRO system

PV System Specifications
PV Panels: MEGASOL Technology; No of modules = 12; Peak Power = 12*185=2220 Watts; Mono crystalline type
Solar Tracker: ETATRACK active 600, EAST WEST Continuous Tracking, Due South Manual Adjustment.
Solar Charger: Outback Power Systems, FLEXmax 80 MPPT; Power handling Capability @ 24V = 2500W; Efficiency = 97%
Inverter: MEANWELL, TS-1500; Input = 24Vdc, Output = 110V ac; Pated Power = 1500 Watts max, Efficiency = 89%
Batteries: 12Volt, 180Ah sealed Lead Acid Batteries. Total storage capacity is 180x24x4 = 720Ah @ 24Volts
Pretreatment Section Specifications

Feed Pump: LORENTZ PS150-HR14; Type = Positive Displacement submersible type; Pump capacity = 1100 L/h
Feed Pump Controller: Input Voltage = 12-24Vdc; Output = 4-18V EC PWM 3-Phase, Efficiency = 92 % (motor + controller)
Pretreatment Filters: Permatrade 1x100um & 2x25um Filters (Germany); With self-cleaning mechanism.
Pretreatment Buffer Tank: VAREM; Capacity 25 Litres, Max Pressure 10 bar;
Reverse Osmosis Specifications:
RO Buffer Tank: VAREM, Capacity 60 Litres, Max Pressure 10 bar.
RO Prefilter: Filtration: 5 micron; Cartridge: Pleated Paper Filter,
High Pressure Pump: Pearson Pump with Energy Recovery Devices; Maximum Flow rate = 1100 L/h; Feed Water Recovery = 50%; Required inlet pressure = 1.5 bar (20 psi)
HPP Motor: LEESON 2HP, 1800RPM, 24Volt, FLoad 70Amps With DC Drive to control the speed of the motor.
Membranes: Type: M-B4040 (DOW Filmtech); Operation Pressure max: 41 bar (4.1 MPa); Salt Rejection: 99 %; Series Configuration, single stage, single pass.
Activated Carbon Filter: Pentair CFB Plus-10 (5-10um),Flow: 720 L/h

3.3 Instrumentation and signal conditioning

Proper instrumentation is a vital work to have the accurate data from the different sensors to measure the process variables for the performance evaluation of an experimental prototype. In the solar power section panel position, solar insolation, PV cell temperature, ambient temperature, panel voltage and current, MPPT current, battery voltage, battery current and RO load current are measured by different sensors. In the pretreatment section feed water temperature, feed flow rate and pressures are measured. Pressures sensors are used to measure the differential pressure across prefilters and 5μm RO filter. In the RO Desalination section pump RPM, membrane pressure, permeate flow rate, feed salinity and permeate salinity are measured by appropriate transducers. Sensors output signals are conditioned to make them compatible with the input specifications of the NI Data Acquisition board. LabVIEW software is used as an interface to configure, communicate and acquire the measurement data from NI board using graphical programming capability. Moreover the measured variables are shown on computer display for monitoring purpose in real time. The measurements are also recorded in a spread sheet for analysis purposes. The position of different sensors and transducers installed in the PVRO system are depicted out in the Figure 3.2.

3.4 Solar power system instrumentation

Instrumentation carried out in solar power system encompasses the measurement of solar panel position, panel temperature, environmental variables (solar insolation and ambient temperature), PV panel voltage and battery voltage. Moreover current measurements from PV panel, MPPT, battery and RO load is also an integral part of this work. Measurement of environment variables and voltages needs some signal conditioning

circuits to adjust the signal strength to cope with the technical aspects of NI board. In these measurements analog channels of NI board are configured in single ended mode with 13 bit resolution of ADC. This configuration provides measurement accuracy of 20/8*1024 = 2.4mV with input measuring range of ±10 Volts. Outputs of current sensors are directly connected to DAQ card in differential mode configuration with 14 bit ADC resolution. This configuration provides measurement accuracy of 2/214 = 0.122mV with input measuring range of ±1 volt, which corresponds to 0.122A current resolution. A general schematic of sensors, conditioning circuits with their input and output signal range is shown in Figure 3.3. The developed signal conditioning circuits for PV system along with NI DAQ board are depicted out in Figure 3.4.

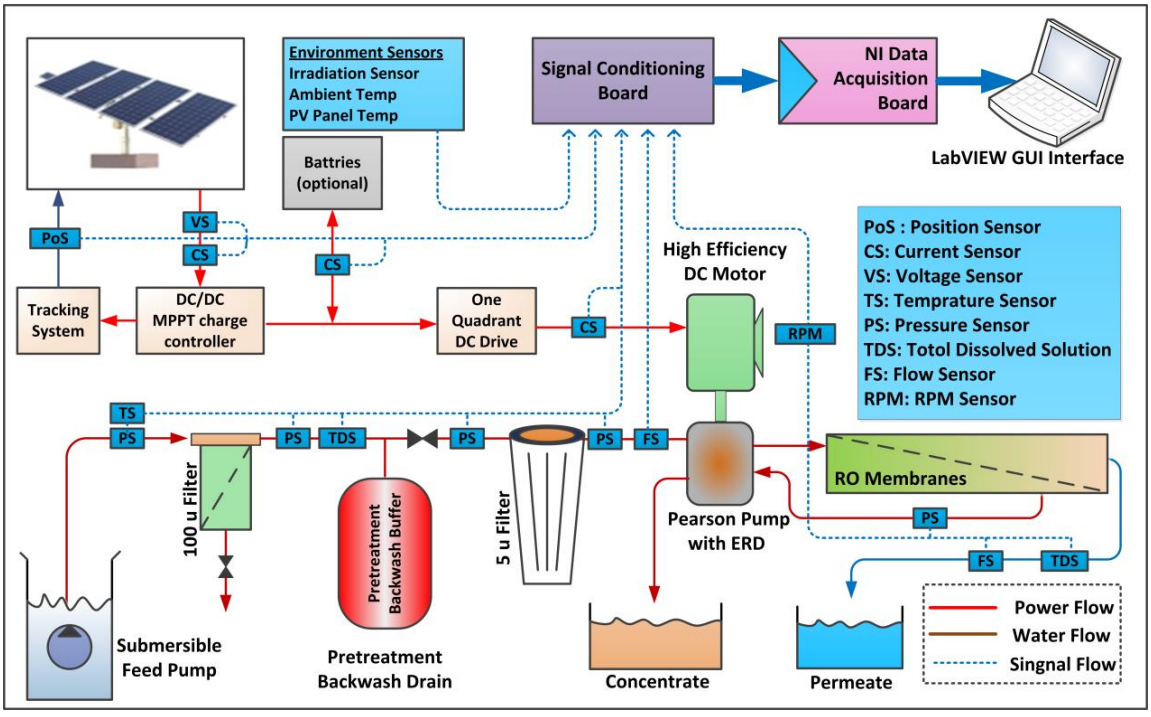

Figure 3.2: Position of different sensors and transducers in PVRO System

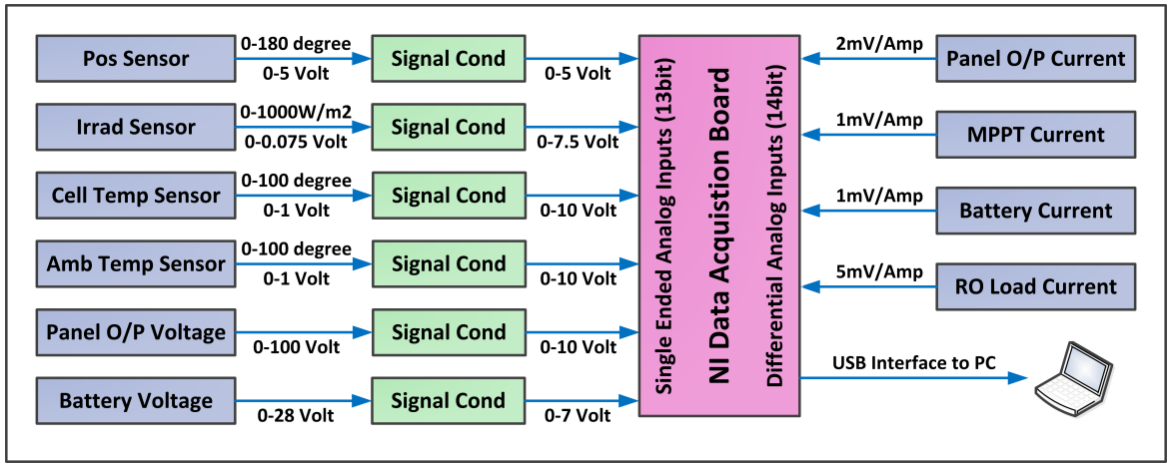

Figure 3.3: Sensors and conditioning circuits with their signal ranges for PV System

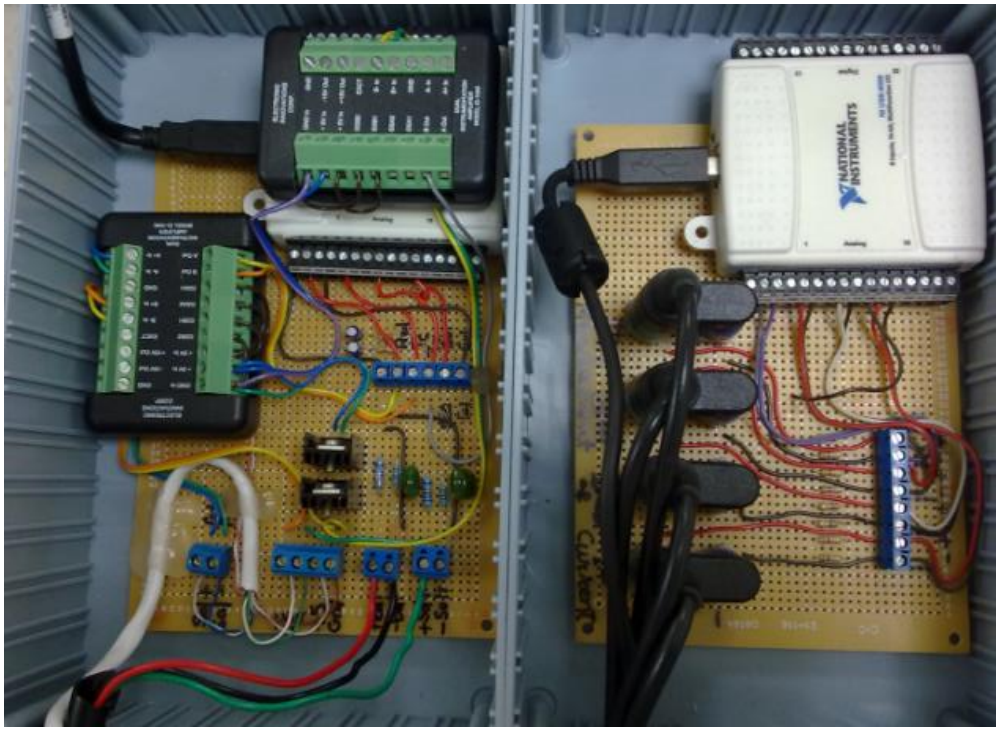

Figure 3.4: Developed signal conditioning circuits for PV System and NI DAQ

3.4.1 Solar radiation measurement

A separate 5W solar panel is used to measure the solar insolation and panel temperature. Short circuit current passing through PV module is function of solar irradiation and cell temperature. Short circuit current and cell temperature are measured and then irradiation is calculated based upon this sensory information. Relation between panel current, insolation and PV cell temperature is evidenced form the equation (3.1).

$$I_L = \frac{G}{G_{ref}}\left\{I_{sc,ref} + \mu\left(T_c - T_{c,ref}\right)\right\} \tag{3.1}$$

In this equation I_L is the light current, G is solar insolation, G_{ref} is solar insolation of 1000 W/m2 and used for short circuit reference current I_{ref} calculation. μ is temperature coefficient of current, T_c is the PV cell temperature and $T_{c,ref}$ is the reference temperature of 25 ^{o}C. By knowing the short circuit current and PV cell temperature, G insolation can be estimated by using the equation (3.2).

$$G = \frac{I_L G_{ref}}{I_{sc,ref} + \mu(T_c - T_{c,ref})} \tag{3.2}$$

By putting the reference values of insolation and temperature, short circuit reference value and temperate coefficient value of the 5W (5W PV module have the *Isc* = 0.3 A and *Voc* = 21.6 V when measured under standard condition of 1000W/m^2 insolation) measuring panel in equation (3.2), following equation (3.3) is obtained and finally is used for the measurement of insolation.

$$G = \frac{1000 I_L}{0.30 + 0.0035(T_c - 25)} \tag{3.3}$$

To measure the short circuit current of PV module a shunt resistor is connected across the PV terminals. This shunt resistor behaves like a resistive load for the PV panel.

For the proper selection of shunt resistor value different IV curves are drawn for different insolation level along with different load lines. Intersection of load line to the IV curve dictates the current flowing through the load resistance. From the Figure 3.5 it is obvious that for R=100 Ω, current flow is less than the short circuit current for insolation of 500W/m^2. It is also obvious that by decreasing the load resistance, load line becomes steeper and approaches to the vertical axis of the graph and this phenomenon is shown in Figure 3.5. Eventually load shunt resistance of R=0.225 Ω is selected ensuring the flow of short circuit current under any value of insolation. The voltage induced by flowing the short circuit current through the shunt resistance is measured. For G=1000W/m^2 short circuit current is 0.3 A and it produces 0.0675 V. This small voltage is amplified by instrumentation amplifier with a gain of 100.

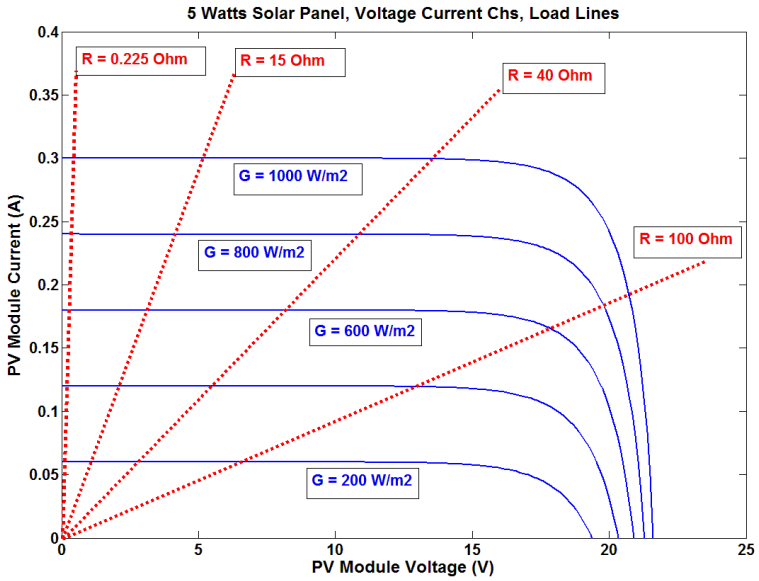

Figure 3.5: IV curves and load lines for shunt resistor selection

Burr Brown PG204 chip is used having two instrumentation amplifiers with programmable gain options of 1, 10, 100 and 1000. Gain 100 is selected by connecting A0 pin to +V and A1 to ground as shown in the Figure 3.6. This signal conditioning circuit produced the voltage of 0-6.75V which corresponds to the 0-1000W/m^2 insolation. Output of the instrumentation amplifier is connected to the NI DAQ board.

3.4.2 Temperature measurement

Cell temperature is measured by making use of semiconductor temperature sensor LM35. It is precision sensor and provides output of 10 mV/C. Its output is also amplified by making use of another PGA204 instrumentation amplifier configured in the gain of 10. Moreover ambient temperature is also measured because of its profound effect on the cell temperature. Again LM 35 sensor is used to measure ambient temperature and its output is amplified by gain 10 by using PG204 instrumentation amplifier. The schematic of PV short circuit current sensing, cell temperature and ambient temperature is shown in the Figure 3.6.

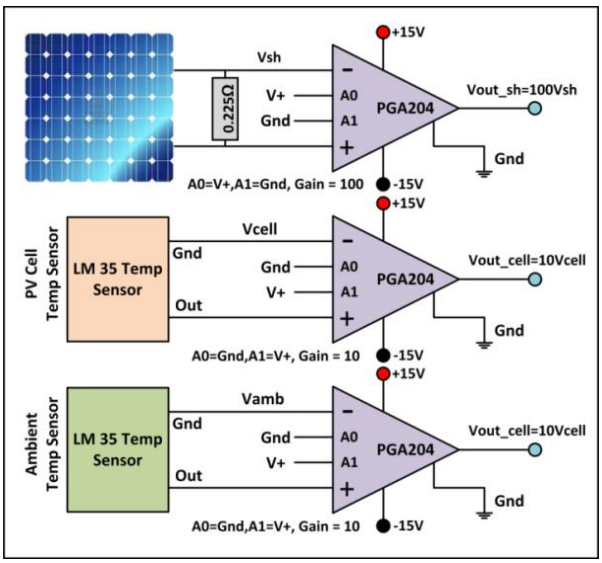

Figure 3.6: Schematic for environment variables measurement

3.4.3 PV voltage and current measurement

PV string open circuit voltage is 96.8 V and decreases when load is applied. A voltage divider circuit is used reduce the PV output voltage by factor of 10 for measurement purpose. Battery output voltage varied between 24 and 27.4 V depending on the state of charge and load. This voltage is reduced by factor of 4 by voltage divider circuit for measurement purpose. For the measurement of current clamp type meters are used and provides 1 mV/A for DC current. PV panel output current, MPPT output current, battery current for charging and discharging and RO load current are measured. Measurement of voltage and placement of current sensors in PV power system is shown in Figure 3.7.

3.5 Pretreatment and RO unit instrumentation

Instrumentation in pretreatment section is carried out by installing a pair of pressure sensors across the pretreatment filters for its condition monitoring purpose to initiate back wash process. In the RO section a pair of pressure transmitters is installed across RO filter for its status checking. Another pressure sensor is installed at high pressure vessels containing membrane modules for the system pressure measurement. Two flow sensors are installed to measure the feed flow rate and permeate flow rate.

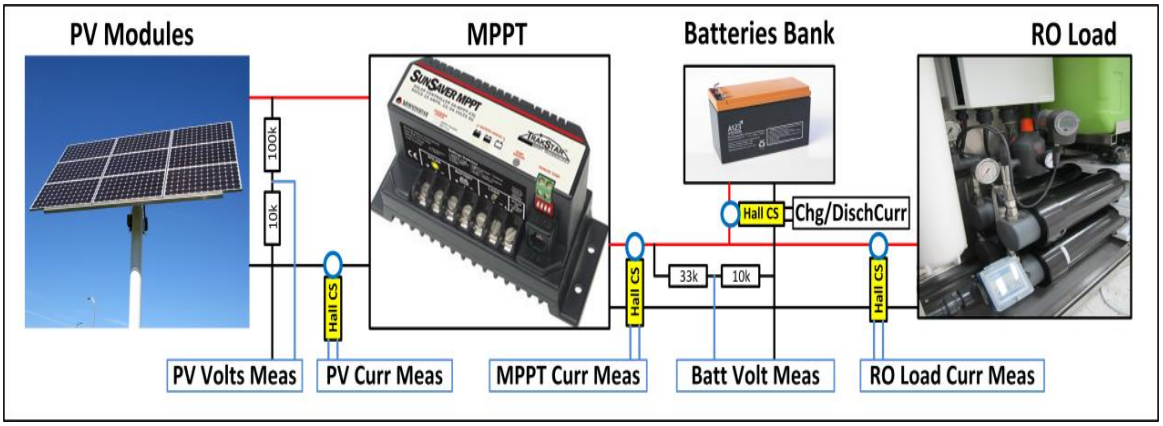

Figure 3.7: Voltage and current measurements in PV system

Two conductivity transmitters are used to measure the salinities of feed water and produced clean water. A proximity inductive sensor is used to measure the revolution of high pressure pump. A general schematic of sensors with their measuring range, output signal type and associated signal conditioner are depicted out in Figure 3.8. The developed signal conditioning circuits along with NI DAQ board are depicted out in Figure 3.9.

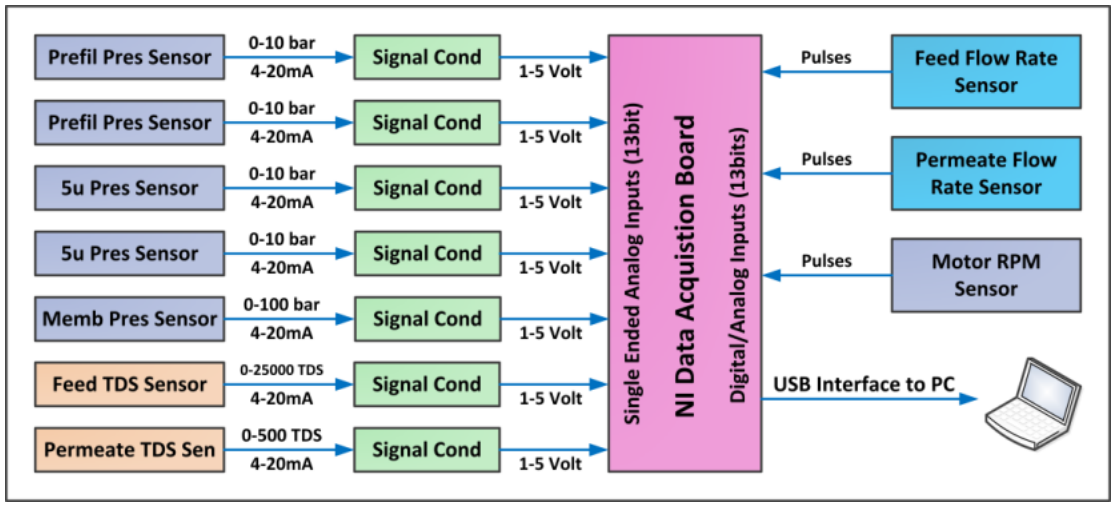

Figure 3.8: Sensors and conditioning circuits with their signal ranges for RO System

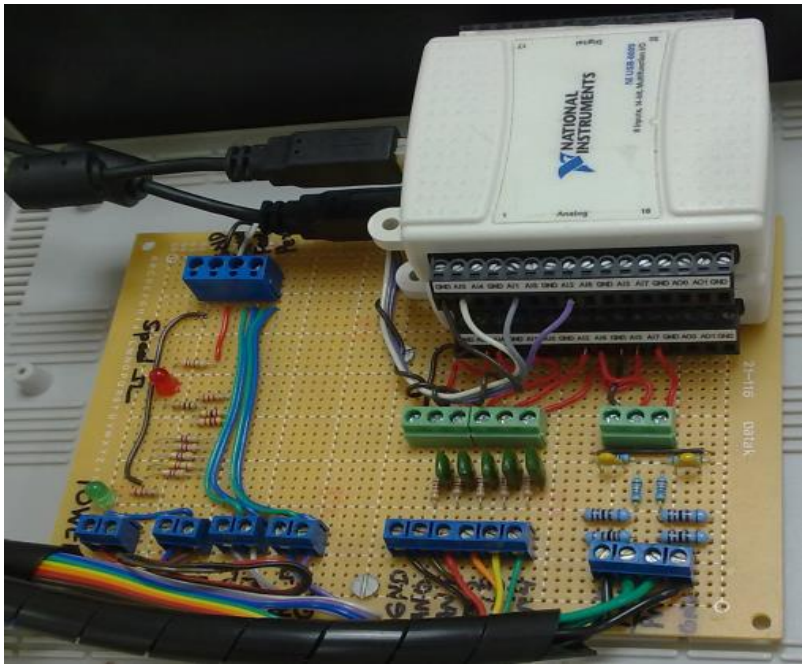

Figure 3.9: Experimental setup showing signal conditioning circuits for RO system

3.5.1 Pressure sensing

Pressure sensors (Burkert, Type 8314 pressure transmitter) are installed across the pretreatment filters, RO filter and at the high pressure vessel for pressure measurement. These transmitters meet the highest requirements with regard to mechanical loading, operational reliability and most suitable for rugged industrial applications. Relative pressure measurements with a range of 0-10 bar is carried out for pretreatment and RO filter section and 0-100 bar for system pressure. These transmitters are accurate up to 0.3% of full scale measurement. It is two wire version, operates on 8-33V DC unregulated power supply and output is 4-20mA current signal drawn through power supply terminals. A simple precision resistor is used to convert the current signal into corresponding voltage. 500 Ω resistor (or two parallel 1000 Ω resistors) and a voltage divider circuit convert the 4-20 mA signals to 1-5V. An operation amplifier configured into unity gain voltage follower may be employed to improve the signal strength. Output signal 1-5 V is conditioned by RC filter as shown in Figure 3.10. The conditioning signal is fed to the NI DAQ board for measurement.

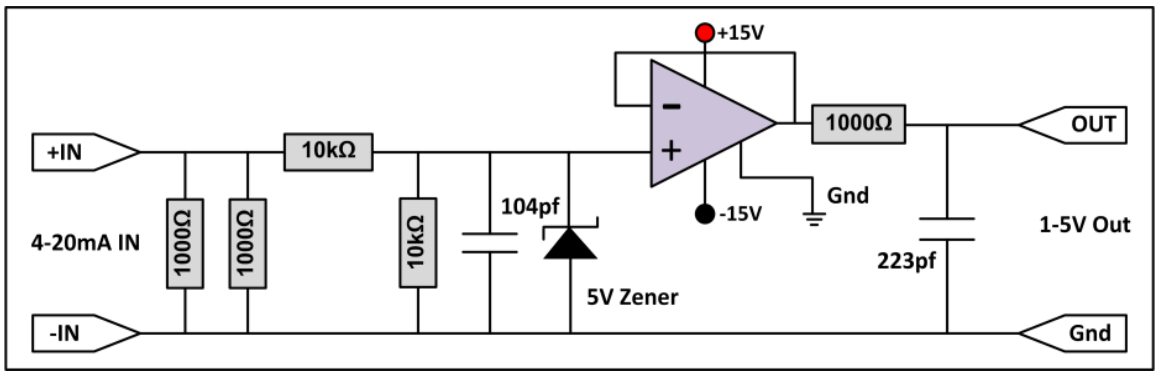

Figure 3.10: 4-20mA to 1-5 volt conversion circuits

3.5.2 Salinity sensing

In a desalination system salinity measurement of feed water and produced clean water is important to analyze the salt rejection ratio of the plant. Salinity is usually measured by conductivity transmitters, which measures the conductivity in the solution due to ionization of dissolved salts. For our desalination system feed water may have the salinity 0-25000 TDS. For this measurement a conductivity transmitter (Burkert Type 8220, with cell constant K=10) is used. Its measuring range is 0.5-200mS/cm (250-100000 TDS). This sensor is programmed to measure 0.5-50mS/cm (250-25000) and its corresponding output signal is 4-20mA. This output signal is converted to voltage by appropriate signal conditioner same as used for pressure measurement putpose. Permeate/produced clean water have the salinity 0-400 TDS. For this measurement a conductivity transmitter (Burkert Type 8222, with cell constant C=1.00) is used. Its measuring range is 5-10000uS/cm (2.5-5000 TDS). This sensor is programmed to measure 0-1000uS/cm (0-500 TDS) and its corresponding output signal is 4-20mA. After proper signal conditioning, voltage signal is send to DAQ system.

3.5.3 Flow rate sensing

Paddle wheel flow meters (Burkert Type 8011) are used for continuous flow measurement of feed and clean water flow rate. Flow meter produces a frequency pulse signal, proportional to flow rate that can be processed by transmitter/controller for the required information. Flow sensors are operated on 24V. Amplitude of output pulse train is the supply voltage and it can be reduced by voltage divider circuit and shaped by a Schmitt trigger. A counter is used to acquisition these pulse trains by a strobe signal of one

second to measure the frequency of the pulse signal. This frequency is multiplied by a factor K to yield fluid flow rate.

3.5.4 Pump speed sensing

A DC motor is used to drive the high pressure pump with a 2:1 reduction using a cog belt drive mechanism. The driven pulley is fitted with a metal object for the detection purpose for RPM measurement. A proximity inductive sensor is installed to sense the presence of installed metal object without physical contact. Inductive sensors basically comprises an oscillator whose windings generate magnetic field on the sensing face. When a metal object is placed within the magnetic field, the resulting currents induced from an additional load changes the oscillation frequency. This causes the output driver to operate and normally open or normally close output signal is produced. Signal due to metal object detection can be taken from the voltage across the resistor, which is placed in the supply line of the sensor. After proper conditioning of the pulses, it is used to drive a counter for frequency measurement purpose, eventually which is the revolution per seconds of the pulley. Figure 3.11 show the installation of sensor and its block diagram for pump speed measurement.

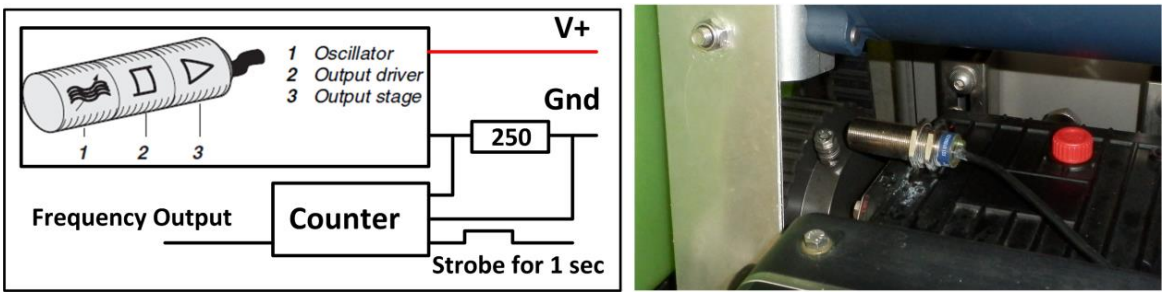

Figure 3.11: Block diagram for proximity inductive sensor and its installation

3.6 Programming and GUI interface development

The data acquisition system uses four modules of USB-2009 DAQ devices. Each DAQ has the following features.

- 8 single ended or 4 differential analog channels (software selectable) with maximum 48kS/sec sampling rate.
- Measuring range is of ±10V for single ended configuration and ±1V, ±2V or ±5V measuring range for differential mode configuration.
- 2 analog outputs with 12 bit resolution.
- 8 digital input/output channels and one event counter.

The DAQ device USB-2009 is configured and controlled by a properly developed program/interface in LabVIEW environment. The interface consists of two parts, first a graphical interface that show and process layout of the system, displays for sensor outputs, control elements and data charts to provide a convenience for the operator. Secondly a program code, programmed in visual programming format that contains blocks and built in virtual instruments, which performs analog channel selection, its configuration, math functions and program flow control elements.

All outputs of conditioning circuits except current probes are connected to analog input channels configured in RSE mode with 13 bit resolution. Current probes outputs are connected to analog channels with differential mode configuration, 14 bit resolution for better measurement resolution. Initially, all analog channels are scanned sequentially and the read voltage is calibrated according to the physical process variables. General form the calibration equation is of the following form

$$y_i = a_i x_i + b_i \tag{3.4}$$

Where x_i is voltage read by analog channel, y_i is physical variable and a_i, b_i are calibration constants. These calibration constants are determined by using the simulation function of the transducers. For the prefiltration and RO filter pressure transducers following calibration equation is achieved.

$$y_1 = 2.5x_1 - 2.5 \tag{3.5}$$

Range of x_1 is 1-5 volts whereas range of y_1 is 0-10 bars. Calibration equation for membrane pressure is

$$y_6 = 25x_6 - 25 \tag{3.6}$$

Range of x_6 is 1-5 volts whereas range of y_6 is 0-100 bars. Calibration equation for feed water salinity is

$$y_7 = 5682x_7 - 6250 \tag{3.7}$$

Range of x_7 is 1.1-5.5 volts whereas range of y_7 is 0-25000 PPM. Calibration equation for clean water salinity is

$$y_8 = 114x_8 - 125.4 \tag{3.8}$$

Range of x_8 is 1.1-5.5 volts whereas range of y_8 is 0-500 PPM.

PV system variables and process parameter change slowly, so the measured voltage by DAQ device is passed through the low pass filter to pass the low frequency signals while attenuating the high frequency measurement noise. Filtered voltage signals are converted into physical variables by using corresponding calibration equations. Physical variables

values are provided to "Relay" block which is enabled by a switch from the front panel view of VI program to enable the data collection option. When the "Relay" block is enabled, all values are reached to "Trigger and Gate" block which accumulates the 1000 measurement samples in one second, consequently a digital signal is triggered to enable the "case structure" branch of the program. During the execution of "case structure" branch of the code, 1000 samples are sent to "Statistics" block for arithmetic mean calculation which is sent to "Write To Measurement" block to store data entry in an external file for data analysis. Moreover the final data entry is send to "Build Table" block to construct a table in the front panel of VI program. Above mentioned program instances are shown in the Figure 3.12.

In the front panel view a complete graphical user interface of the PV RO system is developed to monitor the process variable. This graphical view mostly mimics the original PV RO system, comprising PV Solar system and RO Desalination system. Complete process lay out with the installations of different sensors within the whole system is delineated and is shown in the Figure 3.13. In the GUI, V1 and V2 are the solar panel and battery volts respectively, C1-C4 are current sensor installed at different location in PV system and display the value is Amps.

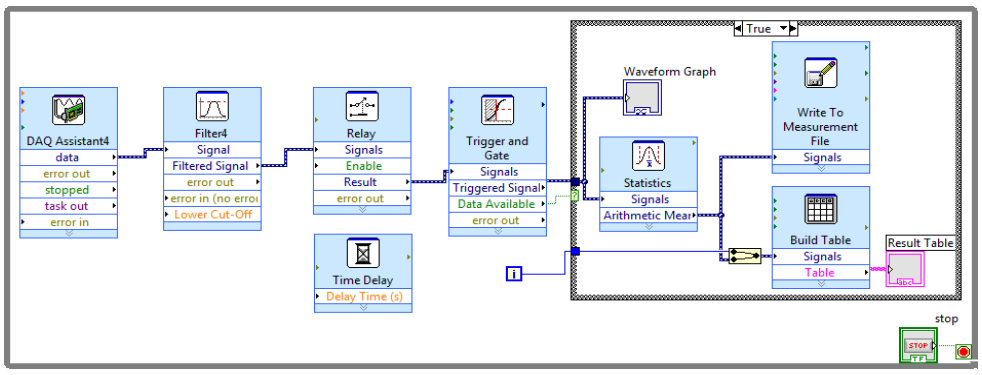

Figure 3.12: Part of LabVIEW program code

Environmental variables window shows the insolation, PV cell temperature and ambient temperature. P1-P5 are pressure sensors installed at different locations and displayed values is in bars. TDS-F and TDS-P provide the information of the salinities of the feed water and permeate in PPM. F_{in} and F_{out} are the feed rate (L/h) of the intake feed water and produced clean water. RPM shows the rotation speed of the pump pulley. Moreover a table at the bottom of GUI is also developed to grab the data entries for visualization purpose. From these measured variables other parameters like, PV power production, PV efficiency, MPPT efficiency, battery state of charge and overall PV system performance can be calculated. On the RO desalination section, RO power consumption, recovery ratio and specific energy can be calculation for process analysis and performance evaluation of the RO system.

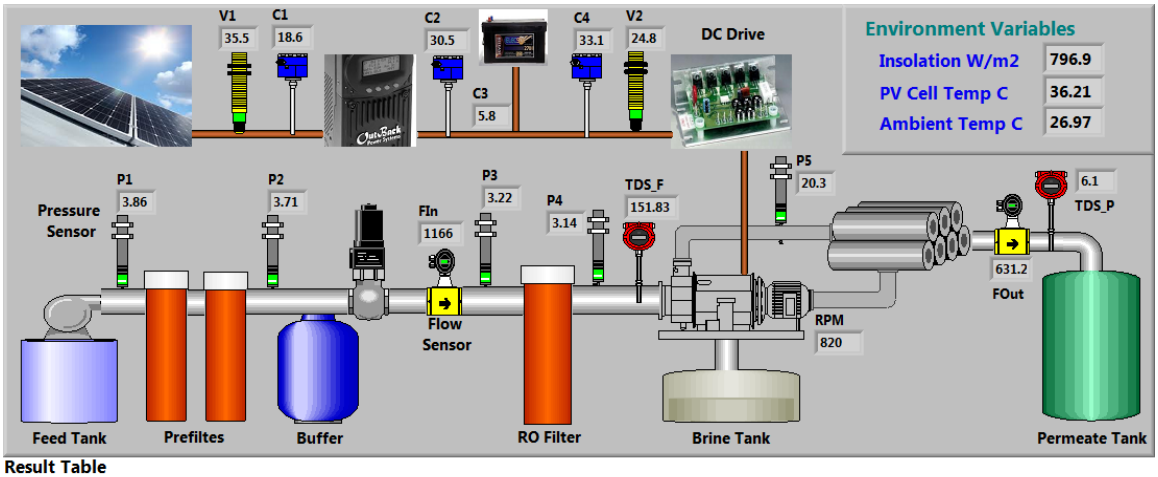

Result Table

Cycle	Rad(W/	PV T C	PV Volt	PV Curr	PV Pow	Batt Vol	Batt Cur	Sys Cur	Sys Pow	Feed Ter	BefPF Pr	AftrPF Pr	Bef5m Pr	Aft5m Pr	SysPres	FeedPPM	FeeduS/	Perm PP	RPM	FeedF
85.00	79.20	11.61	40.91	30.5	2506.47	24.83	29.12	33.29	826.41	25.00	3.82	3.67	3.18	3.08	20.34	158.94	0.32	6.57	815.16	1140.1
86.00	79.21	11.60	40.91	30.6	2503.78	24.82	29.18	33.29	826.28	25.00	3.82	3.67	3.18	3.08	20.35	159.02	0.32	6.59	814.66	1136.6
87.00	79.24	11.59	40.91	30.7	2504.78	24.82	29.18	33.31	826.75	25.00	3.82	3.67	3.19	3.08	20.35	159.94	0.32	6.57	815.16	1140.0
88.00	79.26	11.60	41.07	30.8	2515.51	24.82	29.08	33.29	826.39	25.00	3.82	3.68	3.19	3.09	20.35	158.46	0.32	6.58	815.09	1145.6
89.00	79.31	11.60	41.18	30.56	2521.46	24.82	29.02	33.29	826.34	25.00	3.82	3.68	3.19	3.09	20.34	159.38	0.32	6.56	815.64	1147.7

Figure 3.13: Developed GUI for PVRO system in LabVIEW

3.7 Results and discussion

The developed data acquisition system was successfully installed to PVRO plant. PV and RO DAQ modules were connected to a PC having LabVIEW software via USB cables. The complete experimental setup ready for experimentation is shown in Figure 3.14. A day of 5 December 2013 was selected to run the PV system for data collection. During this test batteries were connected as load and were charged successfully by the MPPT charge controller. All the current transducers were calibrated to ensure the correct reading. Sampling time of 10 seconds was selected to record the readings. The test was started before 15 minutes of sun rise and continued until 15 minutes after the sunset. The collected data was available in spread sheet compatible to the excel format. Different graphs were plotted for analysis purpose. Ambient temperature, cell temperature and their difference is shown in Figure 3.15. It is obvious that the both temperature increases as time progresses and achieved the maximum value at noon and then decreases until the sunset. Variations in the temperature are due to the variation in solar insolation and wind blow effect. Solar radiation measurement is shown in Figure 3.16.

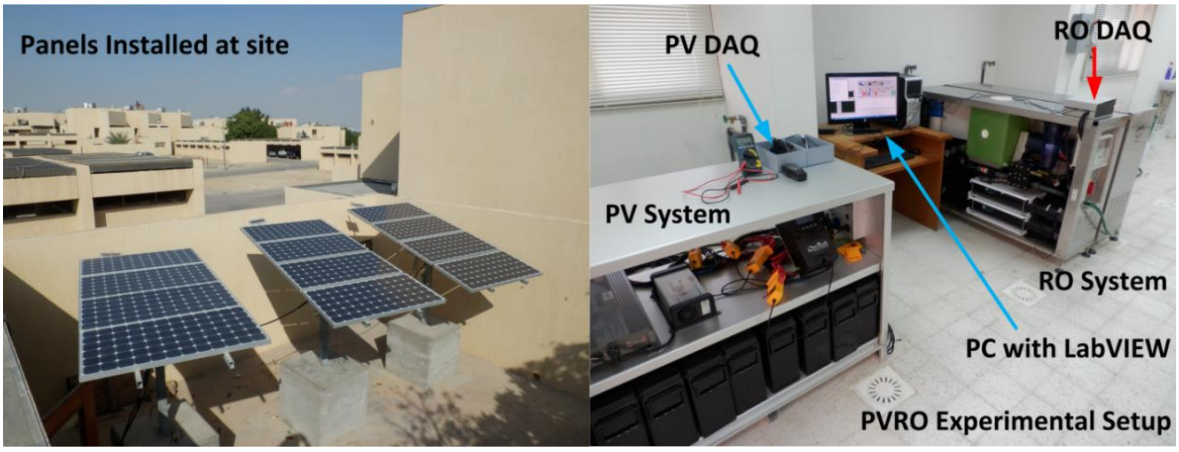

Figure 3.14: Complete PVRO experimental setup with developed DAQ system

It increases from dawn up to noon time and reached up to 740 W/m^2. The radiation decreases as time progresses until dusk. Panel voltage and panel current measurements are shown in Figure 3.17. Panel current is direct function of solar insolation and its variation is obviously directly related to the solar insolation and is illustrated in the Figure 3.17. MPPT output voltage and current are shown in Figure 3.18, and it is obvious that output voltage is controlled to charge the batteries but current injected is varied according the maximum power point of the PV panels. The extracted power from the panels and MPPT output power is shown in Figure 3.19, with the illustration that MPPT output power is closely following the input available power from the PV panels. MPPT is dynamically following the power curve very actively and efficiently. The difference between these two powers is due to the switching losses of the linear current booster and DC/DC power electronic converter of the MPPT module. Efficiency of the MPPT module is calculated and shown in Figure 3.20. During the morning and evening period MPPT efficiency is varying between 60-80% due to low radiation and low panel output current but between 8.00am to 4.00pm its efficiency is almost constant around 95% with a maximum record of 96.2% efficiency at some times. During the whole day 7.5kWh of energy was provided to charge the batteries and its voltage was raised from 23.7V to 27.4V.

The charged batteries from the PV system operation were used to run the RO system for 50 minutes. The developed data acquisition system for RO was used to collect the data for the different variables in the RO system. The salinity of the feed water was set to 7100 ppm. Acquired data during the test was plotted for analysis. Figure 3.21 shows the system voltage and current drawn by the RO unit during experiment run.

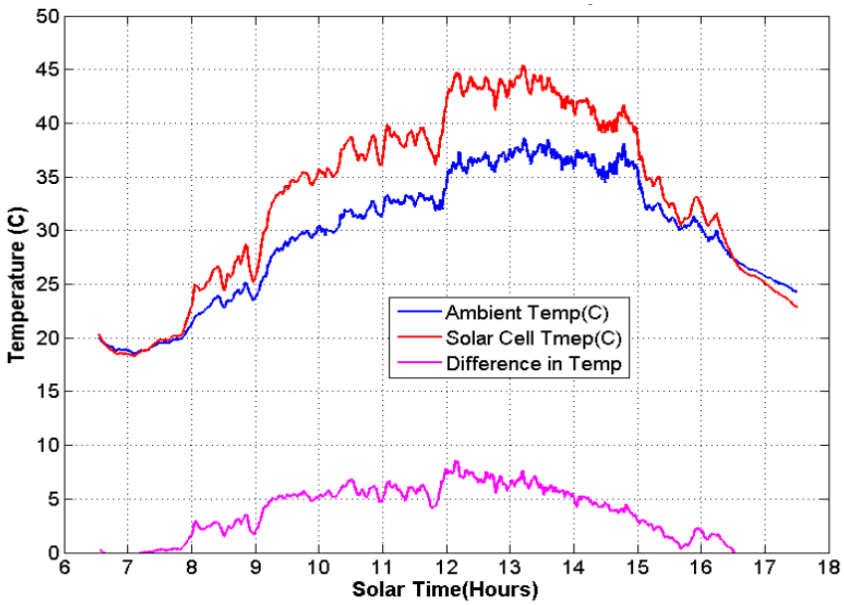

Figure 3.15: Ambient and PV temperature measurement results

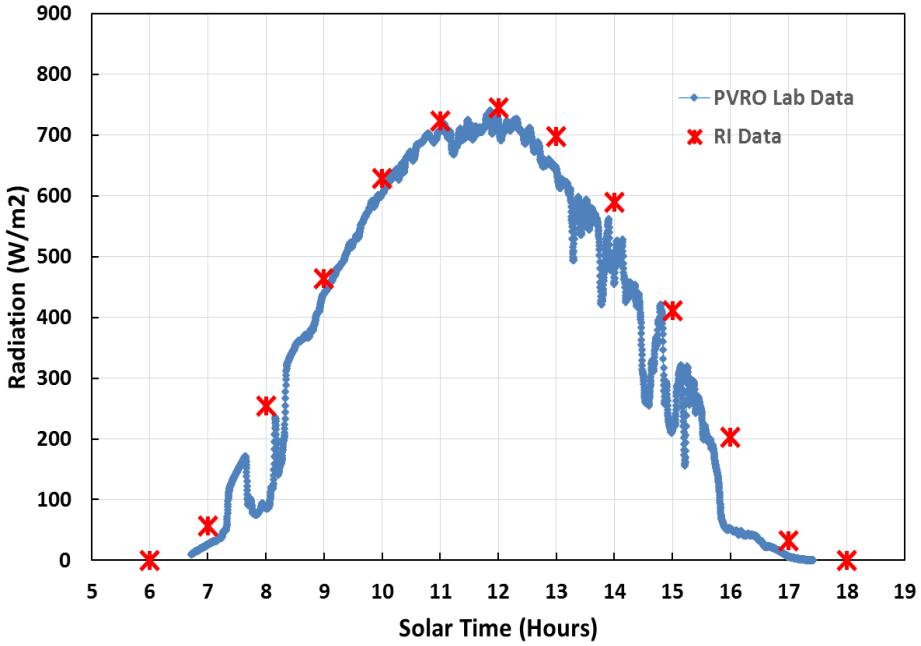

Figure 3.16: Solar radiation measurement results

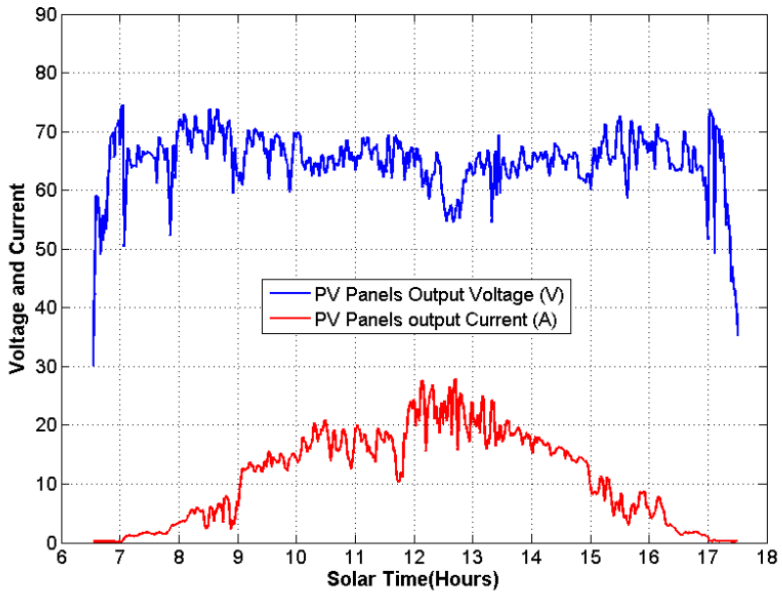

Figure 3.17: Panel voltage and current measurements

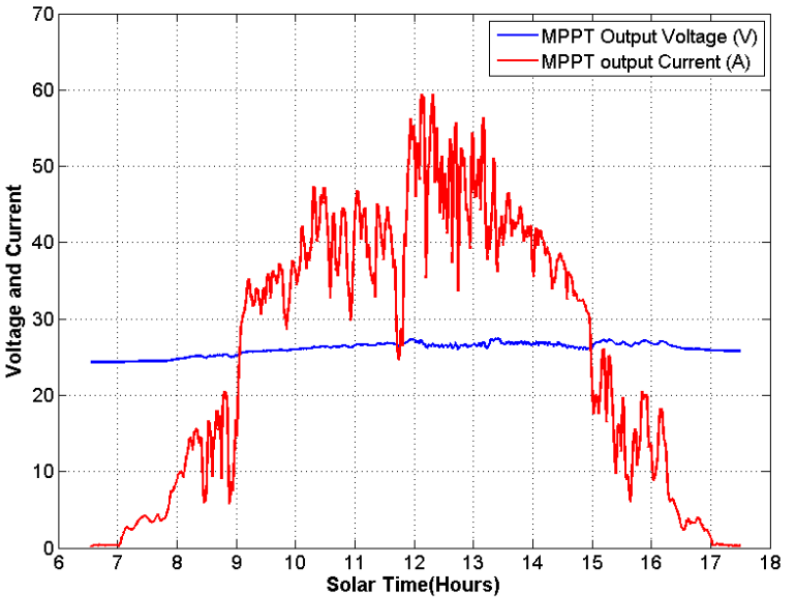

Figure 3.18: MPPT output voltage and current measurements

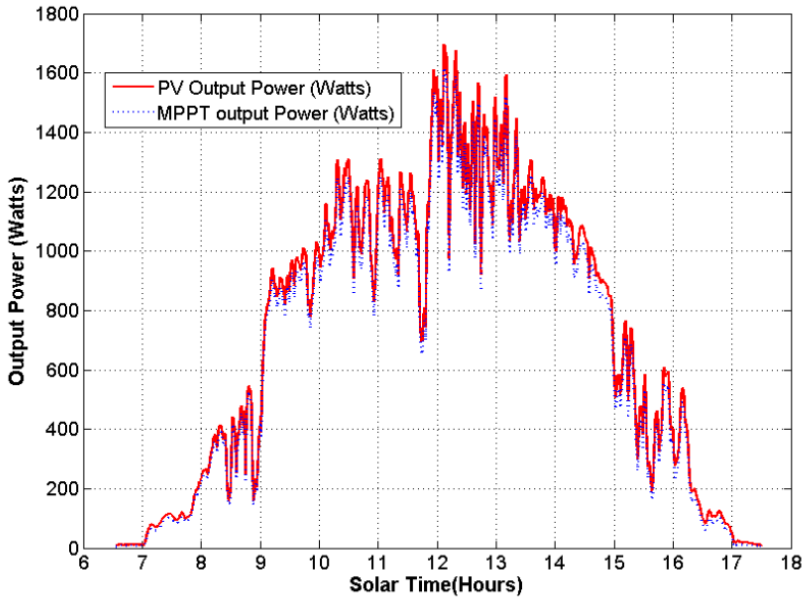

Figure 3.19: Measured panel and MPPT output power

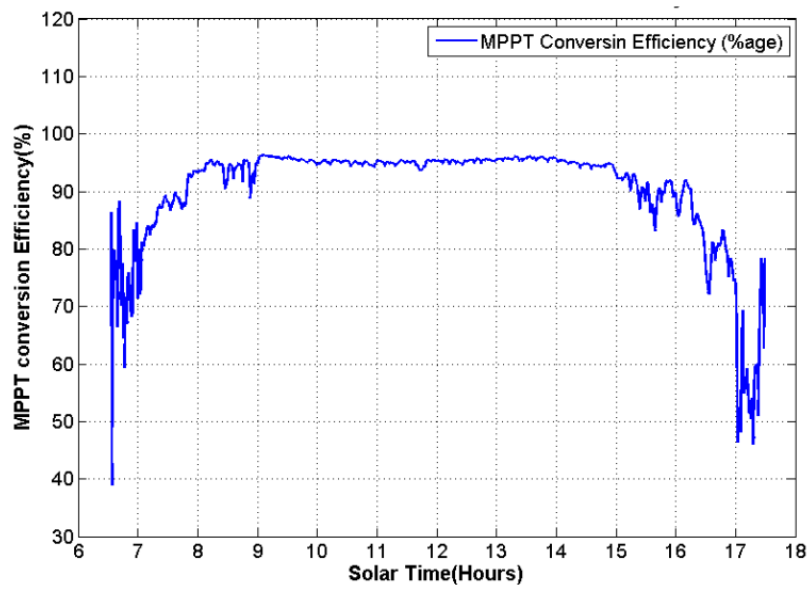

Figure 3.20: MPPT output power measurement

Current fluctuations are due to the frequent on/off of the feed pump to fill the RO buffer tank. RO pump is continuously running during the whole experiment. The minimum drawn current 27A is of the RO pump but the peaks illustrate the current drawn by feed pump and RO pump motor cumulatively. Figure 3.22 details the power consumed during the experiment. Figure 3.23 provides the information of pressure variations across the prefilters and 5u RO filter. Rise and fall in the graph is again attributed to the on/off state of the feed pump. When the controller switches on the feed pump, pressure of the RO buffer tank starts increasing. After achieving the required pressure pump is switched off and RO buffer provides water to the RO section and pressure starts decreasing. Feed water and clean water salinities along with their flow rates of the RO unit are depicted out in Figure 3.24. Feed water flow rate of the system was set to 850 L/h by adjusting the revolution of the high pressure pump. Clean water flow rate is recorded to be at 465 L/h having salinity of 115 ppm during the operation. At last overall system performance in terms of recovery ratio with specific energy consumption is shown in Figure 3.25. During the experiment run of RO system recovery ratio of 56.76% was recorded with specific energy consumption of 1.54 kWh/m^3. If both powers consumed by feed pump and RO pump are considered then the SEC comes out to be 2.1 kWh/m^3. During the test all sensors and data acquisition circuits functioned well and provided signals with significant accuracy. Moreover a comparison analysis of SEC of different capacities PVRO reported in the literature is also carried out. Table 3.2 illustrates the important findings of the different authors in their work during their experimental work. It is obvious that the SEC increases as the TDS of the feed water increases. From the following table SEC for BW5300PPM is 2.3 kWh/m^3 but in our case with the BW7100 TDS it is 2.1 kWh/m^3.

However, salinity of the feed water in our experiment is more than by 1800 PPM but SEC is less by 0.217 kWh/m^3, which concludes that the performance of our system is better than the other installed system.

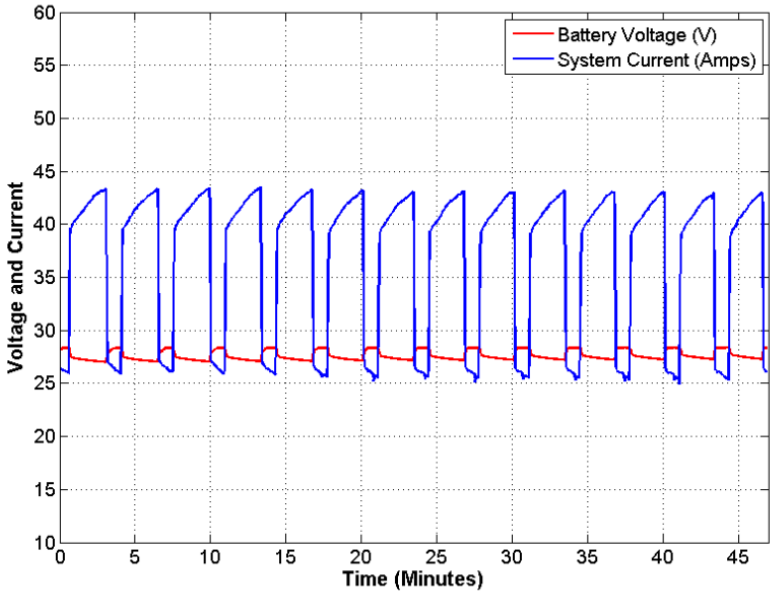

Figure 3.21: System voltage and current measurement

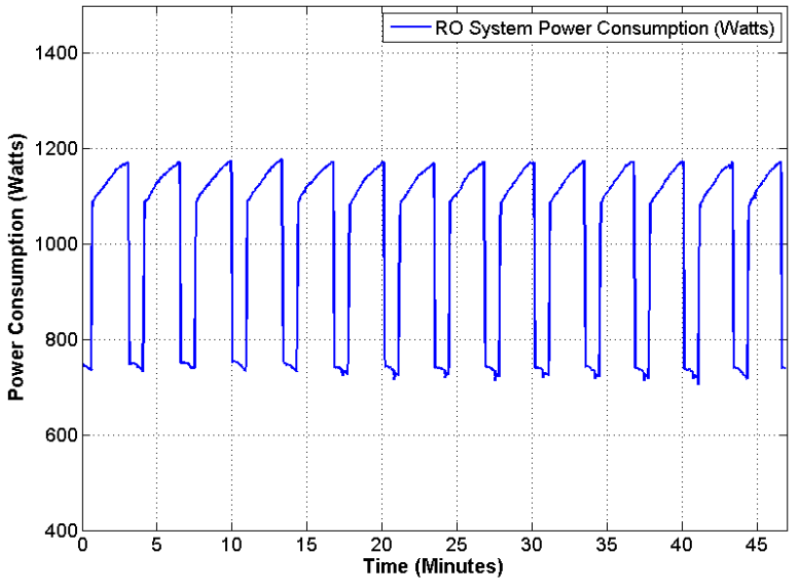

Figure 3.22: RO system consumed power

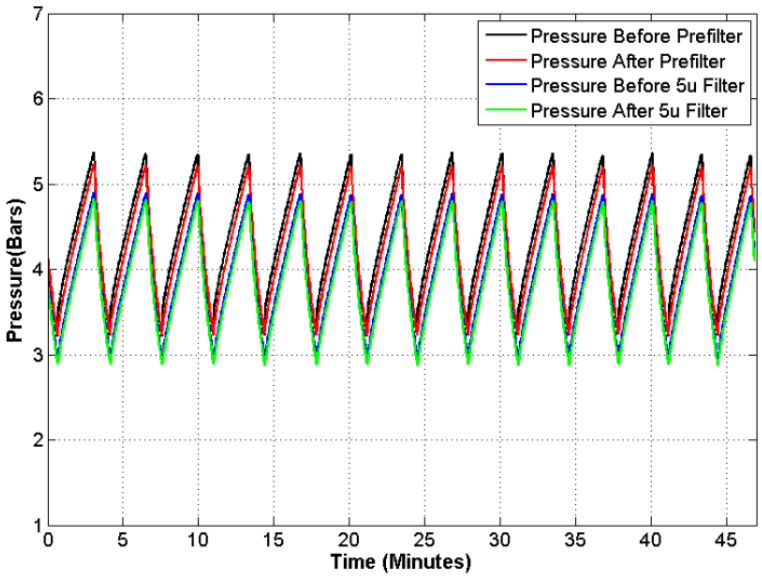

Figure 3.23: Pressure variation across prefilter due to feed pump ON/OFF

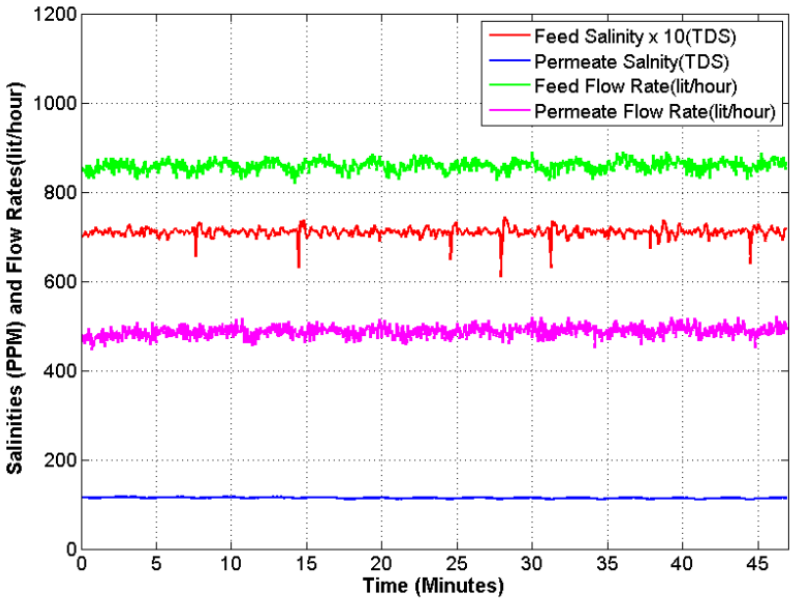

Figure 3.24: Feed salinities and flow rates for RO system

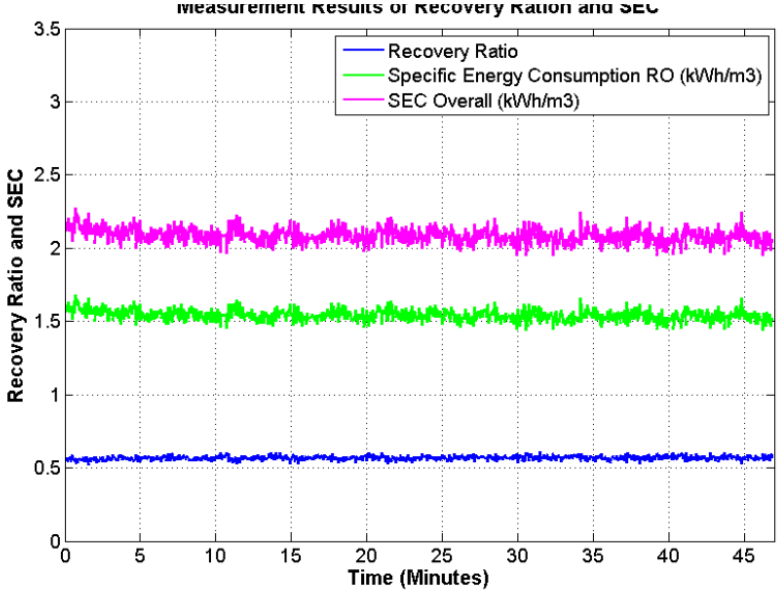

Figure 3.25: Recovery ratio and specific energy consumption

Table 3.2: Performance evaluation comparison of different PVRO systems

Author/Year	Feed Salinity (PPM)	Permeate Flow Rate (L/h)	Specific Energy Consumption (kWh/m^3)	Reference
Richards et al, 2008	Brackish Water 5300	250	2.3	[86]
Qiblawey et al, 2009	Brackish Water 720	10	1.1	[88]
Riffel et al, 2009	Brackish Water 800	30	1.50	[89]
Qiblawey et al, 2011	Brackish Water 1700	333	1.9	[84]
Our Work	Brackish Water 7100	465	2.083	-

3.8 Summary

The work presented in this chapter depicts the design, development and testing of data acquisition system for performance evaluation of a community scale PVRO desalination system. A complete instrumentation is carried out of PVRO system by different sensors with their associated signal conditioning circuits to measure the environment variables, voltages, currents, pressures, salinities, flow rates and RPM of the pump. NI DAQ boards are used as an interface between LabVIEW software and real system for measurement data transfer. Moreover a complete graphical user interface which mimics the real system processes is developed to monitor and process variables. Experimental runs were carried out for PV and RO systems and generated data was plotted for analysis purposes. During the whole day test PV generated the power of 7.5 kWh and charged the batteries. During the RO test its performance indicator; SEC comes out to be 2.1 kWh/m^3 for the 7100 ppm salinity of brackish feed water. The developed system is very useful for monitoring and performance evaluation of the PV and RO systems and can be used to implement advance control methodologies.

Chapter 4

Optimization of PVRO system

One of the most promising challenges in the PVRO system design is to integrate the RO section to PV system. Batteryless PV systems provide intermittent power due to the insolation variation and change in environmental variables. It is of necessary need to search for an optimal operation methodology of RO system having the capability to use the wide range of available PV power in an optimum way. In this pursuit complete PVRO system is modeled. From the PV system modeling, PV output power is analyzed in detail for a summer day. The effective utilization of available PV power by RO unit is investigated by using different RO operational methodologies. The RO process parameters (feed flow rate and system pressure) are manipulated in such a way to keep the RO operation at specific methodology while taking the PV power into consideration. The investigated operational methodologies are constant feed water flow rate, constant feed pressure, constant retentate flow rate and constant recovery ratio. For each of this methodology specific energy consumption (SEC) of RO unit over the whole range of available PV power is simulated. The analysis of the results reveals that least SEC of the RO system is achieved by constant feed pressure methodology if the available PV power is sufficient enough to drive the RO pump. Constant Recovery Ratio methodology is preferable with slightly higher SEC than constant feed pressure methodology's SEC when the broad range of PV available power is to be utilized.

4.1 RO network optimization

Efforts to minimize the operational cost of the desalination system are sought due to increase in the fossil fuel (diesel, energy, electricity) cost. In order to reduce this cost, nowadays considerable attention is given to the optimization and energy management of energy in various engineering systems, including water desalination systems [90]. In pursuit of this systematic optimization work of RO network to minimize the operational cost is considered well in the specialized literature. Kim et al, 2009 [91] have provided a detailed survey of numerous papers in RO design to minimize the permeate production cost using systems engineering approach. Lu et al, 2006 [92] optimized the single stage RO system for minimum annual production cost, considering rather complete capital and operation cost estimating schemes which included for instance the cost of membrane cleaning and replacement. The same author extended the research work to investigate the system of multiple stage RO system under different feed concentrations and product specifications. In a similar work, Zhu et al, 1997 [93] optimized the operation of an RO network operating under several variable operating conditions, e.g., time-dependent fouling, which in turn results in a time-dependent system performance.

See et al, 1999 [94] optimized the network structure (i.e., the staging and arrangement of membrane module) in RO section. Furthermore, they optimized the operation of a fixed network structure. In this work particular attention was given to the decay in membrane permeability, the increase in the membrane fouling with the membrane life, and the optimal membrane cleaning schedule. Authors used time intervals of 60 days to establish the optimal cleaning schedule for a 1080-day operation plan. Marcovecchio, et al, 2005 [95] used GAMS/CONOPT to find the optimal operating conditions that resulted

in minimum specific production cost for several cases assuming constant operation conditions.

Villafafila and Mujtaba, 2003 [96] optimized both the design (e.g., vessel's internal diameter and total number of vessels) and operation (e.g., feed flow rate and feed pressure) of RO for several objective functions including maximum recovery ratio, minimum energy consumption and minimum number of vessels in the system. Wilf and Bartels, 2005 [97] considered several possible system configurations, and energy recovery options to minimize the energy consumption of RO. The same author established the optimal recovery ratio for different seawater salinity levels to minimize the production cost, assuming constant operation conditions and electricity cost [98]. Lu et al, 2007 [99] presented the design of various multistage RO systems under different feed concentration and product specification. In this work an optimization method using the process synthesis approach to design an RO system has been developed.

Lu et al, 2012 [100] have described reverse osmosis (RO) desalination process with multiple-feed and multiple-product. The main focus of this work to explore synthesis-based optimization technique for the design of the RO system while taking the pressure drop and stage concentration changes into account.

Sassi and Iqbal, 2012 [101] have designed and optimized reverse osmosis (RO) network for desalination for a wide range of salinity and seawater temperature. A flexible superstructure that contains all possible alternatives of a RO network is synthesized using model based optimization technique. In this optimization problem power consumption of RO system was considered constant.

Following are some point to summarize the RO network Optimization work:

- Most of the optimization work in RO design considers constant operation only and it consume constant power during filtration process.
- Variable parameters such as feed salinity, temperature variation in feed stream, system pressure drop and concentration changes at different RO stages are taken as input parameters to optimize the RO network.
- The cost function in the optimization problems is the overall plant capital, operational and maintenance cost.

Based on the literature survey the optimal configuration for small community scale RO is the single stage and single pass is described below in Table 4.1. Its process stage diagram is shown in Figure 4.1.

Table 4.1: Optimum design for community scale RO system [97]

Optimized Design for Community Scale (10,000 lit/day) for sea water concentration up to 48000 ppm	
RO network for process flow	One stage system
Feed flow rate (maximum) Q_f, m^3/h	6.6
Overall recovery (maximum) %age	45%
Permeate salinity, C_p (ppm)	380
Membrane type	SW30XLE-400
Number of membranes in pressure vessel	5
Operating pressure in stage one, P, (MPa)	8.1
SEC	4.35 kWh/m^3

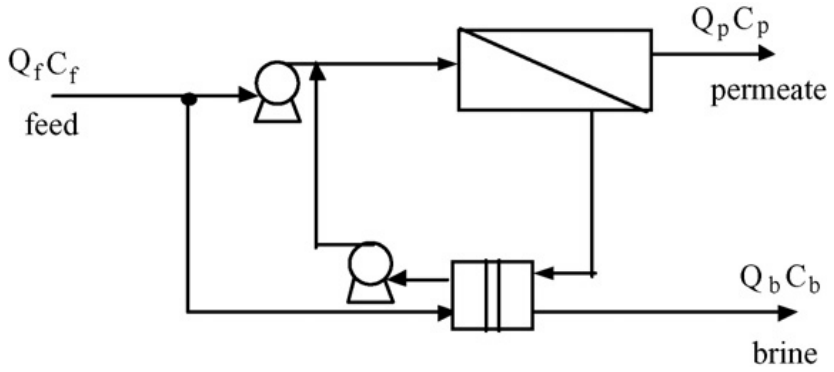

Figure 4.1: Optimized Stage design for salinity up to 48000 ppm [97]

A key issue that has been over looked in optimization of RO operation in previous work is the variable available power. Researchers have often looked into minimizing the energy consumption of RO, neglecting the variability in power.

4.2 RO process optimization

Once the RO network is designed to meet the design objectives, next step is to optimize the RO process driven by PV power for optimized performance. The development of models for operation of the RO systems under variable PV power is also valuable for the analysis of RO systems powered by renewable energies. The power produced through renewable energy has a variable rate. As such, it is of great interest to develop RO systems which can be readily operated under variable loading conditions. In the literature researchers have attempted to optimize the RO process driven by variable power. Some of them are elaborated here.

Labode et al, 2001 [102] has described the optimization strategy for the design and operation of a small scale solar powered RO desalination system. Detailed analysis and optimization is carried out for the power needs and energy consumption and concluded that

it is linear with the concentration in the feed solution. In the design it is reported that energy consumption is function of stage design and for the permeate flow rate (300 L/h with recovery 25%) the optimum configuration is single stage single pass. For the process optimization, feed pressure is analyzed and reported that SEC of the permeate decreases as the feed pressure is increased. So for certain amount of available power the system pressure is to set high as possible. In this work feed flow rate analysis is not elaborated and its effect on the SEC is not discussed.

Miranda et al, 2003 [103] has developed and analyzed the performance of a small scale wind powered RO system. In this work single stage single pass RO configuration is used. To accommodate the variability of wind power, RO operational window is defined to analyze the valid range of the RO operation. Different lines depicting out the maximum pressure, maximum brine flow rate, minimum brine flow rate and maximum allowed concentration of permeate are drawn. The region enclosed by lines shows the valid operational range for the RO network. This RO membrane operation window is shown in Figure 4.2. Based upon the input available power a control strategy is determined which imposes a fixed operating point on the system that lies within the allowed region.

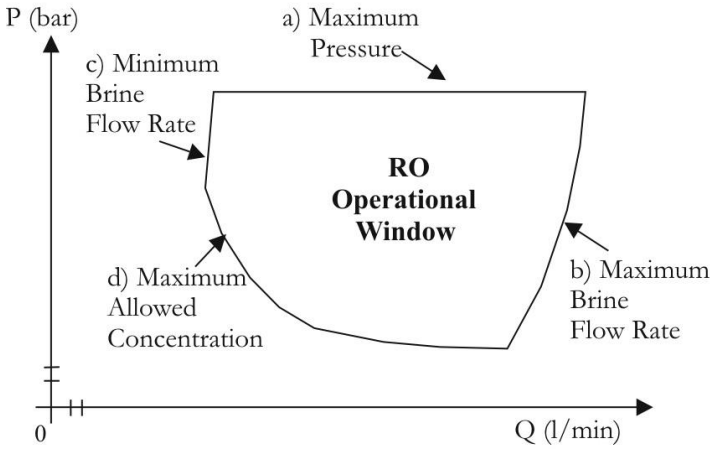

Figure 4.2: RO membrane operational window [103]

Liu et al, 2001, [104] has demonstrated a prototype wind driven RO desalination system with feedback control. The control scheme is employed to maximize the utilization of wind power. A pressure stabilizer system is used to retain the pressure of the feed water. Wind power is used to boost the feed pressure and stored in hydraulic jigger. Based up the accumulated pressure, different valves are opened to supply the pressurized water to RO unit. In this work it was concluded that the energy efficiency of the system is a function of wind speed. Energy utilization efficiency (P_{water}/P_{wind}) decreases as the wind speed increases.

Manth et al, 2003 [105] have demonstrated a sophisticated and comprehensive approach that accounts for the effects of variable parameters of operation on SEC by introducing the concept of the "hydraulic envelope". The variable parameters may be dictated due to the change of the available energy usually form the renewable energy sources. The Variable parameters include feed flow rates at variable recoveries, feed temperature and salinity with their resulting pressure requirements, pressure losses caused by membrane fouling, and pressure losses caused by system controls such as feed throttle valves. The concept of hydraulic envelop for the RO system is shown in Figure 4.3.

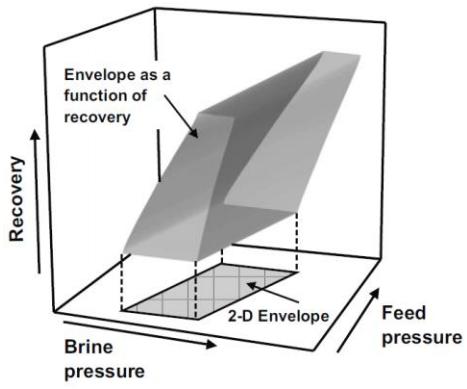

Figure 4.3: Hydraulic envelop of RO system [104]

Epp and Michael, 2004 [106] have illustrated key points and challenges for the autonomous desalination units driven by renewable energy sources. Among the major requirements of the aforementioned system, advanced management and control system is one of those. In this system the unsteady power supply from the renewable sources must be balanced against constant energy demand of the RO desalination system by advanced management system. Some objectives of this system are

- Efficient maximum power point tracking.
- Control to achieve the optimum use of variable power.
- Simplification of energy storage (storage of water not electricity)

Nuez, et al, 2004 [107] have performed the optimization study of an RO system driven by variable energy provided by wind mill and without energy storage element. The experimental data obtained confirm the wide spectrum of operation of the plant with respect to the power available and operation of the system. In the developed experimental set up feed flow control loop and system pressure control loop are used with PID compensator. During the experimental run feed flow rate is set at constant value by keeping the motor speed at 1500 rpm. The pressure is set at 39, 49 and 60 bar for different experiment trials. The results obtained reveal that optimum control for the reduction of the energy consumption in this type of design is to drive the system at recovery of (40-43%).

Gilau et al, 2008 [108] have analyzed the cost-effectiveness of a standalone small-scale renewable energy-powered seawater reverse osmosis (SWRO) system for developing countries. In this work authors have introduced a new methodology; an energy optimization model which simulates hourly power production from renewable energy sources. It is concluded that use of a booster pump, energy recovery turbine and an appropriate

membrane, allows the specific energy consumption to be decreased by about 70% compared to less efficient design without these features. However in this the optimum operating point (feed flow rate, recover and system pressure) for a certain amount of power is not discussed.

Khayet et al, 2010 [109], have constructed solar thermal and photovoltaic-powered reverse osmosis (RO) desalination plant has and optimized it for brackish water desalination. The central composite experimental design of orthogonal type and response surface methodology (RSM) have been used to develop predictive models for simulation and optimization of different responses such as the salt rejection coefficient, the specific permeate flux and the RO specific performance index that takes into consideration the salt rejection coefficient, the permeate flux, the energy consumption and the conversion factor. The input variables are feed flow rate, feed temperature and feed pressure. The RO optimized plant guarantees a potable water production of 0.2 m^3/day with SEC of 1.3 kWh/m^3.

Poullikkas 2010 [110] has developed an optimization model using a genetic algorithm technique for the desalinated water production cost using PV. In order to demonstrate the applicability of the method a parametric study is carried out for the optimum reverse osmosis (RO) desalinated water cost. It was concluded that production cost of desalinated water is increased with the degree of integration of PVs for partial and/or total electricity requirements of the RO plant.

In an effort to develop a general road map for the future of RO desalination using renewable energies (especially PV or wind), in the literature review it is identified that development of advanced control and management systems “to achieve optimum use of

variable power" for operation of the RO systems is vital. However, no clear approach is offered for developing such control systems. Optimization of RO operation by considering variable power and operating conditions, is a step towards the optimum use of RO units powered by renewable energies. In the following section optimum operation methodology or RO unit driven by PV system will be explored using the operation window method.

4.3 Objectives and methodology

The salient objective of this work is to determine the optimal operational methodology of RO desalination system that would be suitable to withstand the variation and fluctuations of PV power. Different design criteria are evaluated for different operational strategies to achieve the required objectives. Possible different criterions are the reduced SEC of the RO in the wide range of available energy from PV panel and small variations of the feed pressure during the operation. The required investigations are carried out by modeling the whole PVRO system in detail. First a complete range of available energy from PV panel is estimated for different peak days of the seasons during the year. Based upon the PV available energy profile, investigations of different operational methodologies are carried out by simulation of complete PVRO system.

The different operational methodologies are investigated while considering the different RO process parameter states within the broad PV power profile during the whole day operation. This investigation will be very helpful in the selection of hydraulic components for the optimum PVRO desalination process design. Thus this analysis provides solid background for the development of optimal/adaptive control systems for PVRO system having the capability to be operated within the wide range of PV power during the whole day within some aspect of uncertainty.

In this analysis, for simplicity, hydraulic parameters are used as process parameters of RO section, and are changed to investigate their effect on specific power consumption of desalination system. Motors, pumps and ERDs are assumed to be operated on constant efficiencies and the power requirement for pretreatment section and auxiliaries are neglected. The investigation of different operational methodologies is carried out with following steps.

- The determination of important aspects of PV system with respect to power is carried out for different extreme days of all four seasons of the year by taking the solar insolation and panel temperature into consideration. Analysis of PV power profiles is carried out for fixed and tracking panels. Within the PV profile the different parameters e.g. maximum available power and its duration, power increasing and decreasing trends and total duration of power availability will be studied.
- Based on the range of available PV power, RO process operational limits are determined by considering the RO section (pumps, membranes and ERDs) data provided in the datasheets. The RO operational limits are defined as the maximum allowable permeate flux, maximum feed flow rate, maximum recovery ratio and minimum concentrate flow rate for specific RO stage configuration.
- The RO operating point is strong function of feed water flow rate and system pressure. Each operational point corresponds to certain feed flow rate and system pressure. For a given PV power, different operational points for RO are located within the operational limits.

- Within the RO operational limits, RO operating points referring the maximum energy consumption (as provided by maximum energy point by PV, usually at noon time) is considered as set point or objective point. Within these, an appropriate operating point is to be approached by all methodologies while satisfying all the RO operational constraints and PV available power.
- The different operational methodologies i.e. constant feed flow rate operation, constant feed pressure operation, constant recovery ratio operation and constant retentate flow rate operation will be defined. For each strategy variable process parameters will be determined and changed to consume the whole range of PV power by keeping the operational points within the operational limits.
- For each strategy, RO process parameters (feed flow rate, feed pressure, permeate flow rate, permeate salinity, recovery ratio and retentate flow rate) and specific energy consumption is computed against the power consumption. This analysis will be helpful to identify the operational strategy which has the best match to cope with the PV power variability.
- The analytical results provided by the behavior of RO process parameters versus RO power consumption delineate the detailed behavior of RO operation over a wide range of available PV energy.
- All the simulations are carried out by modeling the whole PVRO system and putting all the pertinent equations in the MATLAB/Simulink environment for detailed analysis.

4.4 Seawater PVRO system design & configuration

According the World Health Organization (WHO), a human needs about 20L of clean water per day to meet the requirements. Assuming a community having 500 persons, total need of the water per day is 10,000 liters. PVRO system configuration is designed to meet this need of water. PVRO system consists of two sections PV system and RO section. PV system consists of PV Panels, sun trackers, charge controllers, batteries (optional), batteries chargers and inverters/motor drives. RO section comprises of feed pump, pretreatment filters, water storage buffers, high pressure pumps, membrane modules and PX (pressure exchangers for energy recovery devices) and a disinfection unit. PV generator converters the sunlight into electrical energy, and is dependent on the solar insolation and module temperature. Following figure illustrates the schematic description of the PVRO system.

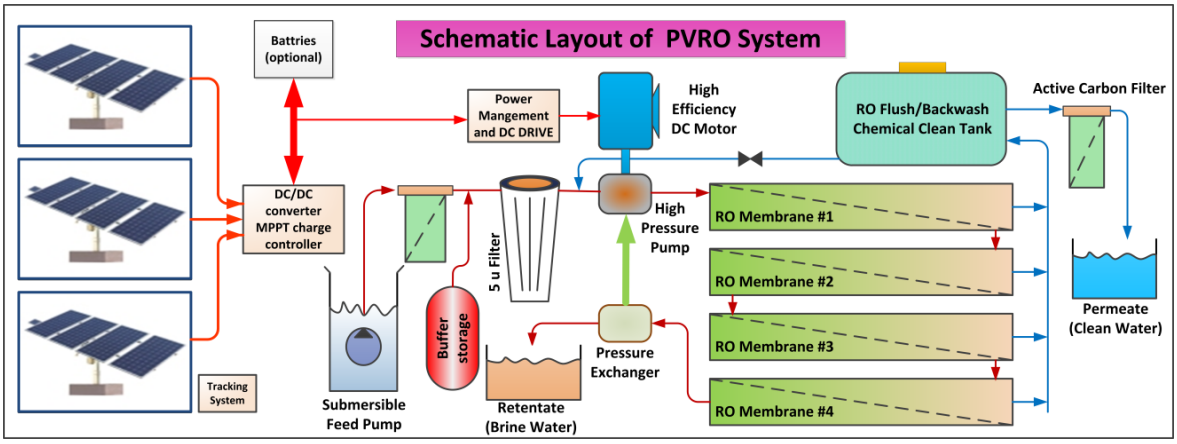

Figure 4.4: Schematic description of PVRO system

Table 4.2: Electrical specifications of sunpower 230 panel module [111]

Parameter	Symbols	Value
No of PV modules	N	64
Open circuit voltage	V_{oc}	48.7 V
Open circuit current	I_{sc}	5.99 A
Rated voltage (at P_{max})	V_{mpp}	41.0 V
Rated current (at P_{max})	I_{mpp}	5.61 A
Peak power (+/- 5%)	P_{max}	230 W
Power temperature coefficient	$\mu_{p,temp}$	-0.38 % / K
Voltage temperature coefficient	$\mu_{ocv,temp}$	-132.5 mV / K
Current temperature coefficient	$\mu_{scc,temp}$	3.5 mA / K

All the PV modules are used with double axis trackers to enhance the output power production by maximizing the received insolation. In this configuration, the received insolation and hence power production can be accessed for flat plat, single axis and double axis mode of operations. PV panel's output is connected to maximum power point trackers (MPPT)/charge controller, that tracks the maximum power point on the current voltage (IV curves) of PV panel for a given irradiation level and module temperature. PV output voltage and current both are varying in nature due to the variation of environmental variables. Output of the charge controller/MPPT is stabilized on constant voltage at 24 volt and current is changed according the available PV output power. Typical conversion efficiency of commercial scale MPPT/charge controller is about 98% [112]. This amount

of PV power is used to drive the motor of high pressure pump. To utilize the maximum amount PV available power, load line of the motor must coincide with the load characteristic line of MPPT/charge controller. Otherwise the MPP will not be tracked and energy will be lost due to mismatch of impedances of the PV source and the RO load. So a motor drive is incorporated in the design to vary the motor speed that changes the position of load line, consequently the feed flow rate is adjusted according the requirement. The current drawn by the motor/HPP is function of system pressure that is adjusted by bleed valve provided at the brine side on the energy recovery device.

Quality and quantity of produced clean water is a function of feed water chemistry, RO configuration, feed water flow rate and membrane pressure. Different RO configurations are evaluated for different feed water chemistry in [113] and it is reported that the optimum configuration of RO for feed water salinity ranging from 35000-48000 ppm is single pass single stage. The description of this arrangement with different process variables at different points is depicted out in Figure 4.5.

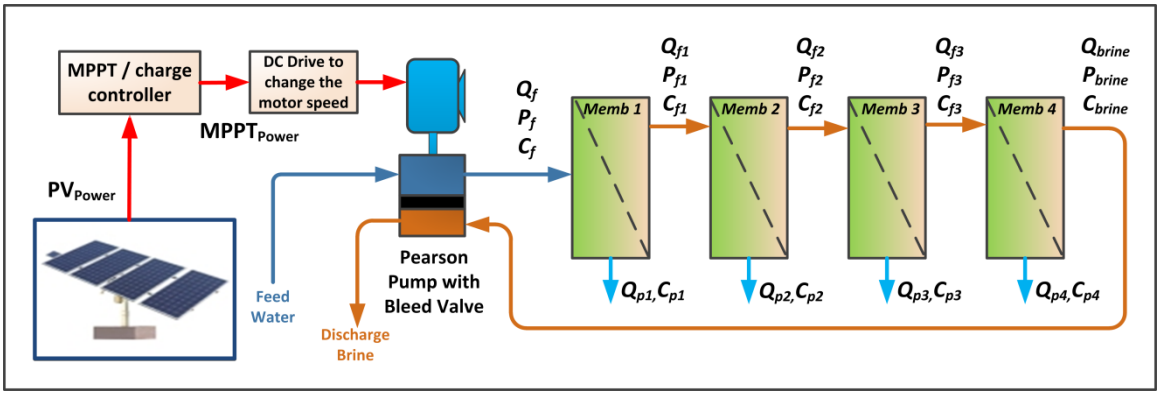

Figure 4.5: Single stage, single pass RO configuration for PVRO system

In this configuration the different process parameters are listed below.

Table 4.3: Feed water flow characteristics

Feed water Characteristics and RO Configuration:	
Typical Concentration of standard seawater	35647 mg/L, TDS, ppm [113]
Silt Density Index (SDI) , after pretreatment of feed water using micro and ultra-filtration	Less than 5, [113]
RO system configuration	Single Pass, Single Stage, One pressure vessel having four membranes in series. Membrane type SW30HRL-400i. Flow Factor = 0.85, some aged system.

Table 4.4: Detailed specification of SW30HRL-400i membranes

Detailed Specifications of membrane [115]:	
Make and Model	DOW, SW30HRL-400i
Active Layer Material	Polyamide thin-film composite
Active/Filtration Area	400 (37), ft^2 (m^2)
Membrane Length	1.016 meter
Membrane Diameter	201 mm
Operating Pressure (Maximum)	83 bars
Operating Temperature (Maximum)	45 ^oC
Operating Pressure Drop (Maximum)	1.0 bars
Operating pH Range, Continuous Operation	2-11
Maximum Feed Silt Density Index	SDI 5

Chlorine Tolerance	<0.1 mg/l, ppm
Clean Water Permeability	1.086×10^{-5} $m^3/(m^2\text{-h-bar})$
Salt Permeability	4.65×10^{-7} $m^3/(m^2\text{-h})$
Membrane Operational Constraints:	
Maximum Feed Flow Rate	14.08 m^3/h
Maximum Permeate Flow Rate per element	1.2 m^3/h
Minimum Concentrate Flow Rate	3.41 m^3/h
Maximum Permeate Concentration,	500 ppm, mg/l
Maximum Recovery per element, percent	13 %

All of the above membrane date and system configuration and its associated equations taken from the previous chapter are used. Matlab and ROSA (version 9.1) software are used to generate the data. The design warnings in ROSA software and data is searched to meet the objective function by satisfying the operation constraints. Flow rates, concentrations, pressures and recovery ratio for every membrane module is calculated. In the single pass, single stage, series RO membrane configuration brine output of the first membrane unit is taken as the feed for the next membrane. So in the calculations, brine flow rate and its concentration (for the first membrane) is taken as the feed flow rate and feed salinity for the next membrane. The output of the last membrane is sent to the PX (energy recovery device) to recover the potential energy. Efficiencies of the feed pump and energy recovery device along with booster pump are also considered in the calculation.

4.5 Results and discussion

4.5.1 PV output power profiles

The simulated radiation profiles for Dhahran city, Saudi Arabia on horizontal surface (slope β and surface azimuth angle γ is equal to zero) for different peak seasons are shown in Figure 4.6. Maximum insolation is received on 21st June and minimum on 22nd Dec at the noon time.

These radiation profiles and panel temperature estimation are further used to calculate the PV output power for PVRO system. The simulation results in terms of instantaneous PV output power for the four peak seasons is shown in Figure 4.7. Due to the difference in the day light hours in winter and summer, it is obvious that the radiation availability on surface slightly more than 10 hours in winter solstice day and slightly less than 14 hours in summer solstice day.

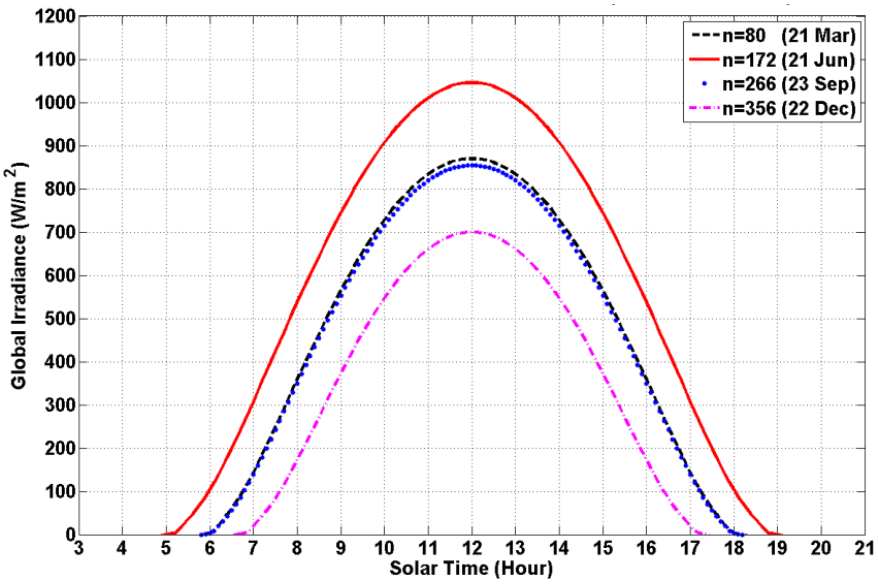

Figure 4.6: Global radiation for different seasons at Dhahran

During the day PV power starts with the sunrise and gradually increases to maximum value (13.2kW) at solar noon and then decreases gradually until sunset. Maximum PV power received at solar noon differs from day to another and it is due to fact that how high sun appears in the sky. During the winter (Nov, Dec and Jan) sun's elevation angle is lower and in summer (May, June and July) sun's elevation is higher than the other seasons.

Single axis and double axis trackers for the PV panels are usually used to increase the output power. The simulation results of PV output power in summer season (21st June) for the fixed, single axis and double axis tracked panels is shown in the Figure 4.8. Power produced in single axis and double axis tracker is 25% and 36% more than the power produced by the flat PV panels.

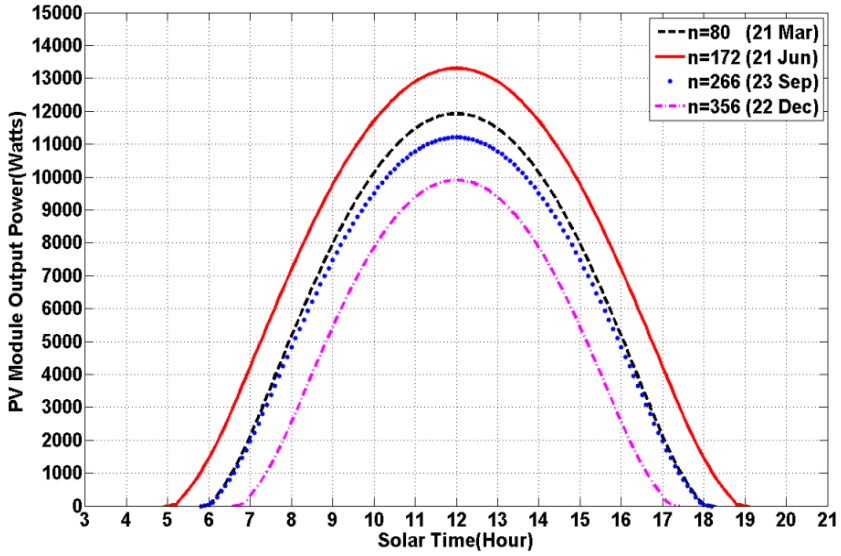

Figure 4.7: PV Output Power for Flat Panels in Different Seasons (No of panels = 64)

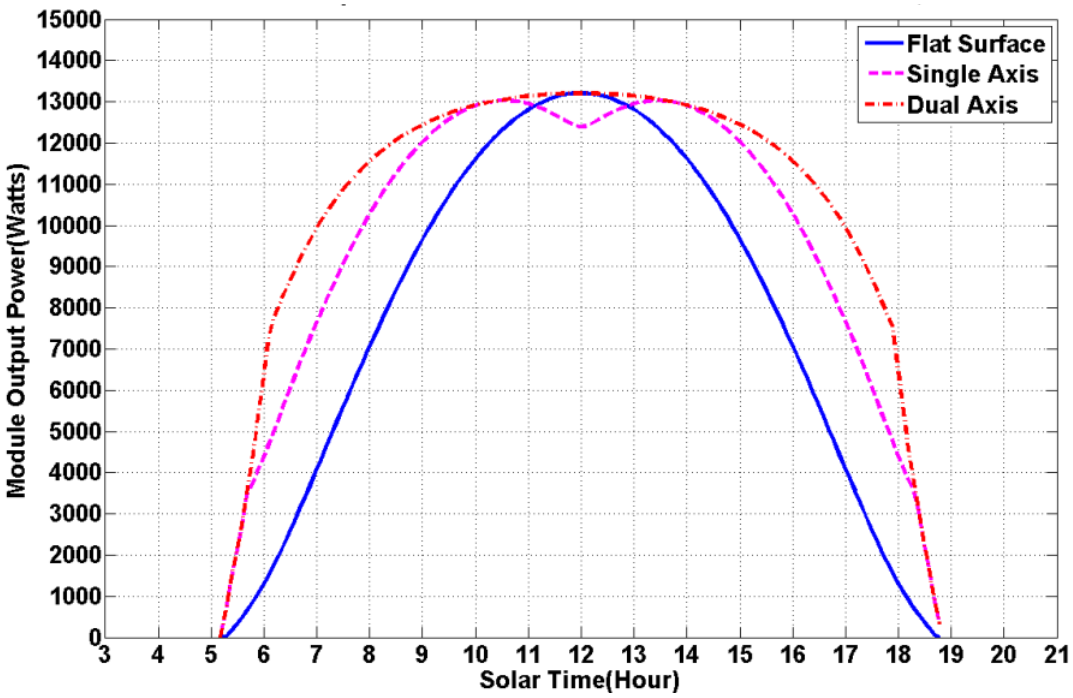

Figure 4.8: PV Output Power profiles by Flat and Tracked Panels

4.5.2 RO operational design space

The determination of RO design space, operational limits are carried out to analyze the RO performance under variable parameters conditions. The different extreme operating points are evaluated to define the operational limits by satisfying the constraints imposed by the membrane's manufacturer. The computed operational points and limits from the simulation results are depicted out in Figure 4.9. The area encompassed by the operational limits is known as operational window, which contains the all possible operational points of RO system for the designed system. Each point in the operational window corresponds to power consumption and it is function of feed flow rate and feed pressure. The PV power is varying in nature and for specific PV power different possible RO operational points are determined in the operation window and joined together to draw constant power consumption curve. Different PV power curves ranging from 17 kW to 3 kW are drawn in the RO operational window. The inclusion of PV power curves in the operational window are shown in Figure 4.10.

In Figure 4.9 the operational limits defined by point 1-4 depict the maximum feed flow rate of Q_f = 14.05 m^3/h for first membrane in the pressure vessel. All the membranes are configured in series so the feed flow rate for the second and next membranes is less the first one (as the permeate water leaves out form the first membrane). The higher feed flow rate than the permissible range (14.08 m^3/h) would induce the high mechanical stress that might damage the membrane permanently. So for the safe operation of the RO the feed flow rate should be kept less than the maximum permissible values (usually provided by the membrane manufacturer). At this maximum feed flow rate we have the option to change the system pressure. Data points 1-4 corresponds to system pressure of 33.5-66.5 bar.

Operation power of RO system is function of feed flow rate and feed pressure so less power is required to operate the system at point no 1 (less than 9 kw power is needed) and high power is required to operate at point 4 (more than 17 kW power is needed). So if the RO operation is to be carried out at constant feed flow rate, pressure increase will demand more power to maintain the RO operation at specified point. So the RO operation at variable PV power can be ensured by driving the RO system at constant feed flow rate and changing the system pressure according to available PV power.

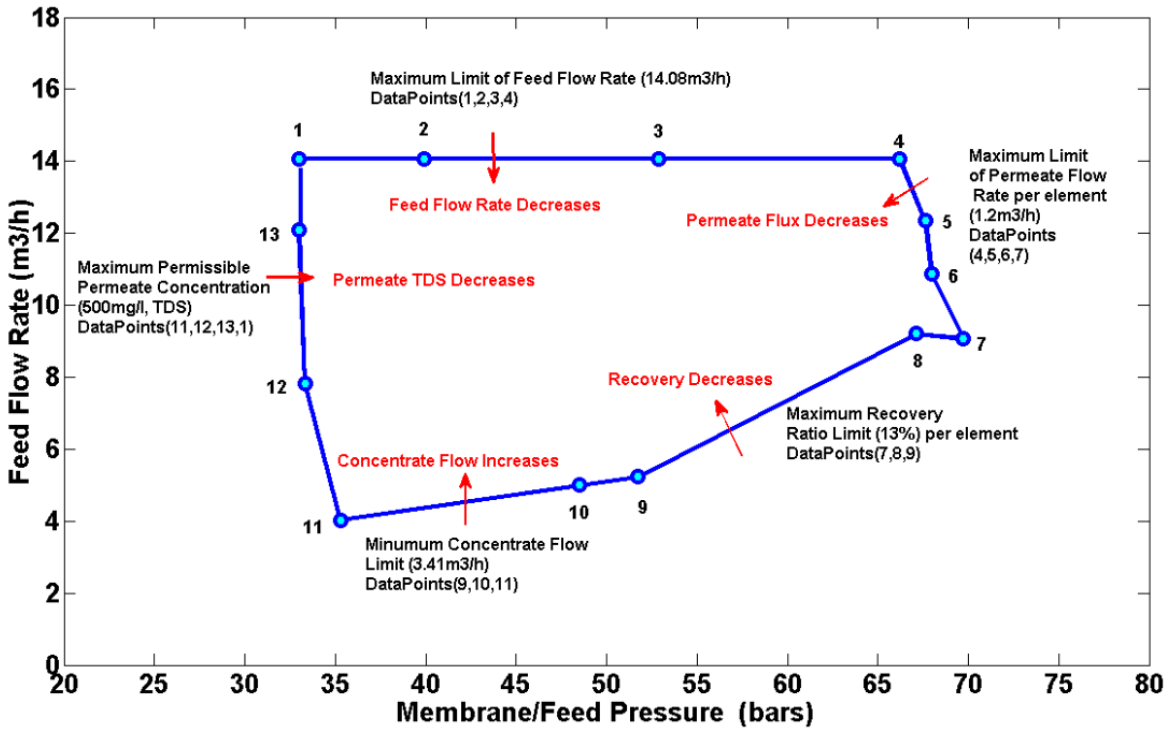

Figure 4.9: RO feasible operational design space

In the operational window points 4-7 shows the operational limit for maximum permeate flow rate for at least one membrane (first membrane) and it corresponds to the maximum recovery of membrane (13%). The maximum permeate flow rate corresponding to 13% recovery comes out to be 1.2 m^3/h. Efforts to increase the clean water flow rate than this limit will demand the pressure increase higher than the membrane specifications and it might damage the membrane permanently. Point 4 correspond the maximum permissible feed flow rate and feed pressure and it corresponds to the maximum RO power consumption. Moving form point 4 to point 7, feed pressure is slighting increasing and feed flow rate in decreasing. Due to decrease in feed flow rate, the power consumption has decreasing trend. Figure 4.10 shows the different PV power curves along the line (point 4-7). Points 7-9 illustrates the limit for the maximum recovery (13%) per membrane/element. Point 9-11 provides the limit for the minimum concentrate flow rate for the RO system.

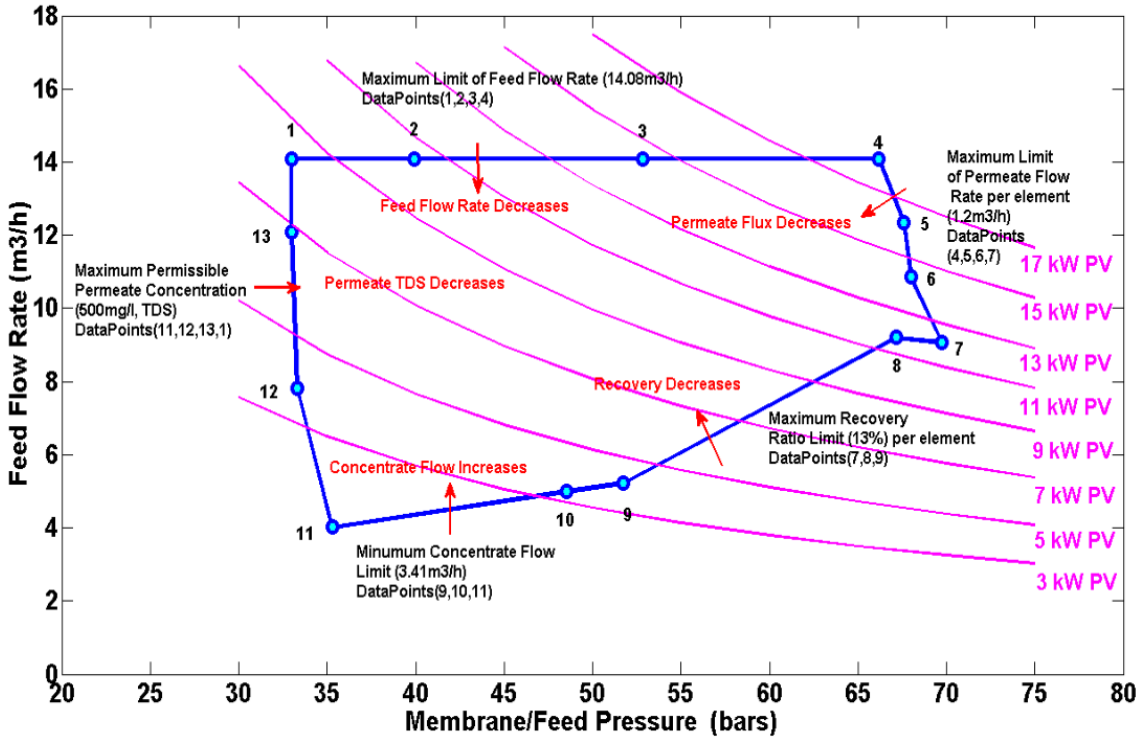

Figure 4.10: PVRO feasible operational design space

Lastly points 11-1 deciphers a limit, the maximum clean water/permeate concentration. In this work this limit is set to 500 ppm (TDS) as recommended by the WHO. The permeate concentration is strong function of water chemistry and is sensitive to variation in feed salinity, feed water temperature and salt rejection capability of the membrane.

The operational window defined by the different operational limits encompasses the numerous possible RO operating points which can be located by taking the feed flow rate and feed pressure as coordinates of the graph. In our PVRO design the peak power delivered by PV panels is 13 kW at noon. So a point is selected that corresponds to the power consumption provided by the peak time of solar panel. Any operational point along 13 kW PV power curve may be selected. Section of operation point with high feed flow rate (and low feed pressure) will yield into low recovery ratio. A point with high pressure and low feed flow rate will provide low room for the utilization of wide range of PV power. So an objective point (feed flow rate and feed pressure are moderately selected) is selected with a recovery ratio of 30%, feed flow rate of Q_f = 11.0 m^3/h and feed pressure of 60.81 bars that corresponds to the 13 kW PV power consumption. Selection of this recovery ratio reduces the scaling and fouling issues by minimal usage of antiscalant and anti-fouling chemicals in the pretreatment section. All the important parameters relevant to objective point are summarized in Table 4.5. As the PV available power is varying from 0 to 13KW from morning to the noon time, so this peak power RO operating point can be approached using different control methodologies under wide range of available PV power.

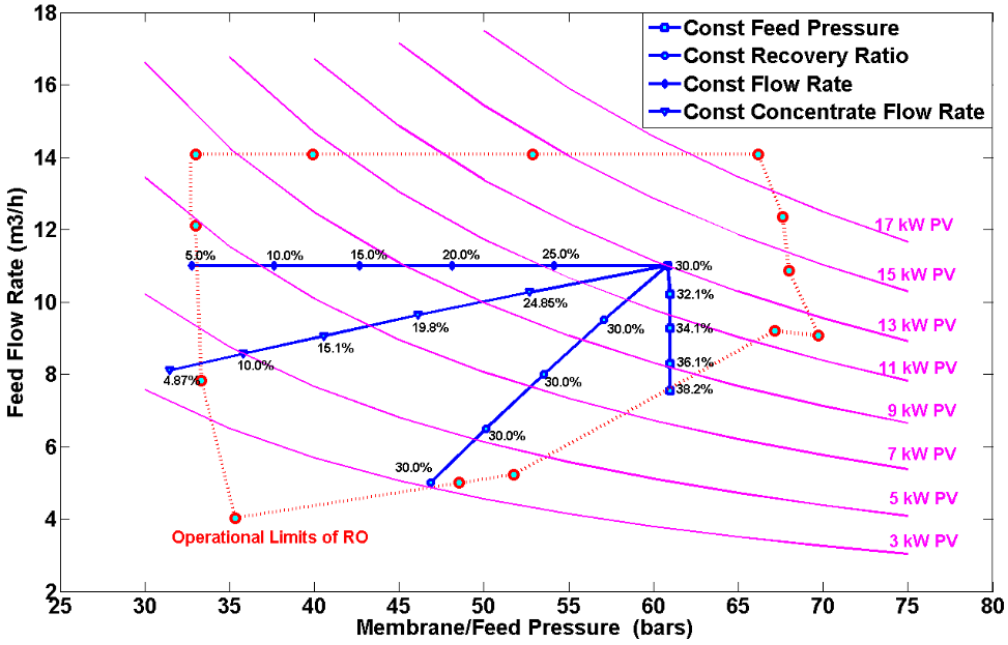

Figure 4.11: RO operational limits, PV power lines and objective point on 13 kW PV power

Table 4.5: Parameters of objective point

Symbol	Parameter	Value
Q_f	Feed Flow rate [m^3/h]	11.00
P_f	Feed Pressure [bar]	60.81
Y	Recovery Ratio [%age]	30
J_w	Permeate Flux [m^3/m^2-h]	22.2
Q_p	Permeate Flow Rate [m^3/h]	3.30
C_p	Permeate Concentration [ppm]	116
P	Overall Power Consumption [kW]	13

4.6 Operational Design Choices

As the maximum available power from the PV panels is varying with time during the day, variation of RO process/hydraulic parameters are needed to match the power consumption to the available PV power. The power consumption variation within the operational window can be achieved by different operational methodologies. Analysis of various operational strategies is carried out by keeping the one hydraulic parameter as constant while varying the others which effects the power consumption over the entire PV power available range. Following table shows the various strategies and their constant and variable parameters.

Table 4.6: Description of different operational strategies

Design Criteria	Description
Constant Feed Flow Rate	In this strategy the recovery ratio and feed pressure will be changed.
Constant Retentate Flow rate	In this methodology the feed pressure and feed flow rate will be simultaneously changed to keep the brine flow rate constant.
Constant Recovery Ratio	It can be achieved by changing the feed flow rate and feed pressure to keep the recovery ratio constant.
Constant Feed Pressure	To achieve this condition feed flow rate and the recovery is to be changed.

For each strategy, within the operational limits, different points are computed by changing the variable process parameters. To analyze the behavior of each strategy different operating points are computed within the operational window of RO system. Figure 4.12 illustrates the locus of operational points for different strategies which are defined by feed flow rate and feed pressure within the prescribed RO process limits.

For each operational point, feed, concentrate and permeate flow rates along with their pressures and salinities are recorded in spreadsheet and net power consumption is computed by equation (4.1).

$$Power = \frac{Q_f P_f}{\eta_{HPP}} - Q_c P_c \eta_{ERD} \tag{4.1}$$

The detailed process parameter aspects for every methodology are discussed in the following sections.

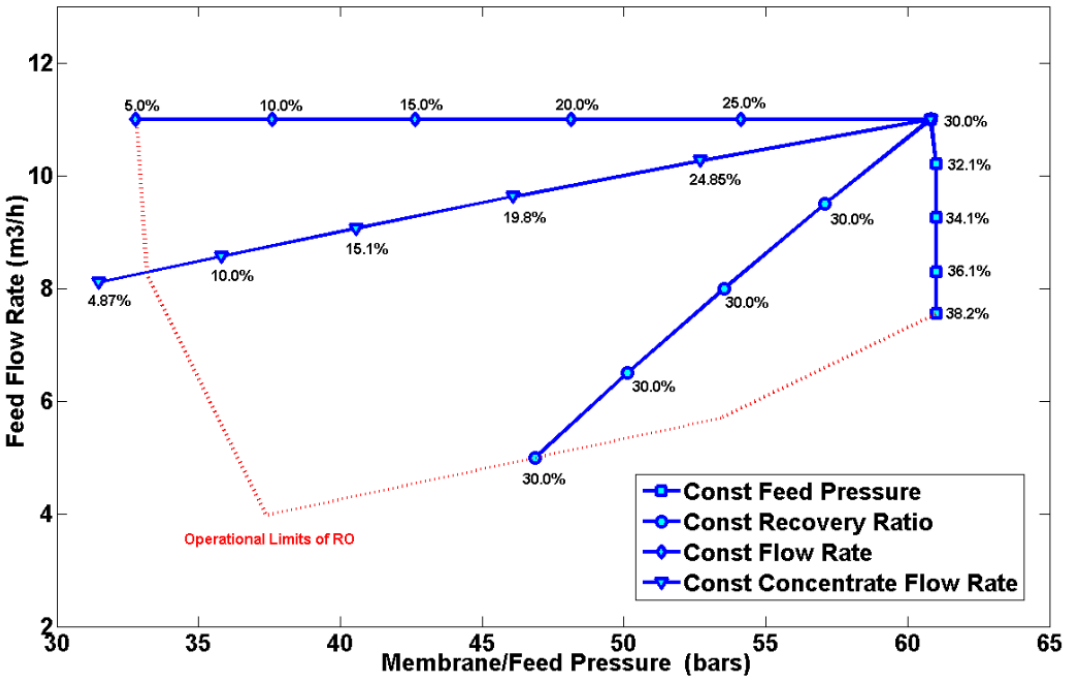

Figure 4.12: Different operational strategies

4.6.1 Design criteria 1: Constant feed flow rate

In this methodology the feed flow rate is kept constant over the entire range of PV power availability. Other parameter like the feed pressure is changed to approach the objective point. While the variation of the pressure, recovery ratio, permeates flow rate and its salinity are to keep within the operational limits. In terms of mathematical form this problem can be written in following form.

Table 4.7: Mathematical description of constant feed methodology

	Mathematical Description
To Compute:	$SEC = \frac{\text{Energy Consumed}}{\text{Recovery Ratio}}$
Equality Constraints	RO_model_*equations* $Q_f = 11.0 m^3/h (const)$
Inequality Constraints	$PV_{Power} = (0 - 13kW)$ $0 < P_f < 83 bars$ (max_membrane_pressure) $0 < Q_p < 1.2 m^3/h$ (per_membrane) $0 < Y < 13\%$ (per_membrane) $Q_c > 1.2 m^3/h$ (minimum_concentrate_flow_rate) $C_p < 500 mg/l$ (maximum_limit_for_clean_water_salinity)

The solution of this problem reveals as shown in Figure 4.12 that, by keeping feed flow rate constant the valid range of feed pressure varies from 32.78 to 60.81 bars. Feed pressure lower than the 34 bars will drive the RO system outside the operational limits, producing the permeate having higher TDS than the 500 ppm. To operate the RO system in this methodology at permissible limit of permeate quality (500 ppm) minimum 5.2 kW

of PV energy is required. As the PV power ranges from 5.2 kW to 13 kW, feed pressure is varies from 34 to 61 bars while keeping the feed flow rate constant at 11m^3/h. Due to increase in feed pressure, permeate flow rate increases from 0.55 to 3.3 m^3/h and retentate flow rate decreases from 10.47 to 7.7 m^3/hour. Different flow for this strategy are shown in Figure 4.13. Variation of permeate TDS, feed pressure and recovery as a function of PV power consumption is shown in Figure 4.14.

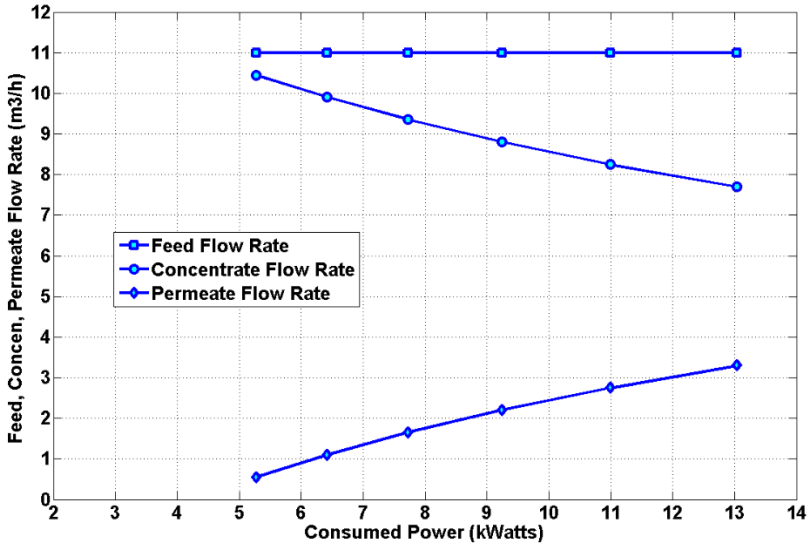

Figure 4.13: Different flow rates for constant feed flow rate methodology

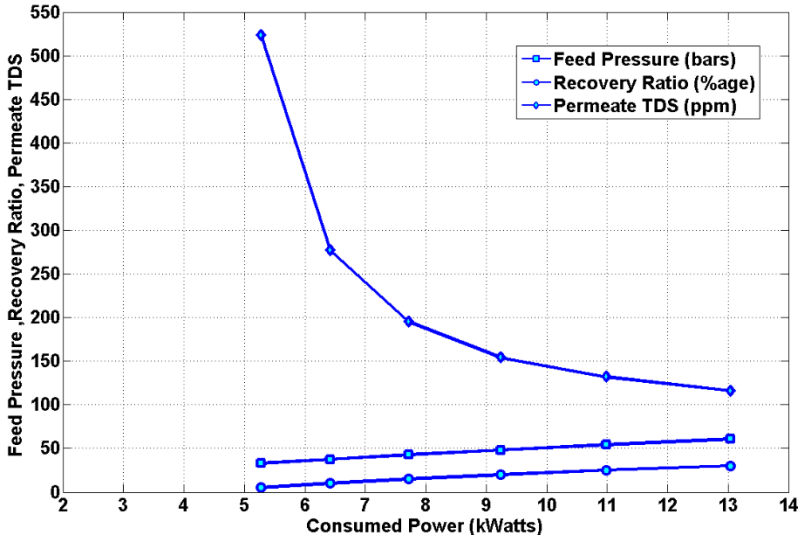

Figure 4.14: Pressures, permeate TDS and RR for constant feed flow rate methodology

4.6.2 Design criteria 2: Constant retentate flow rate

In this methodology the retentate flow rate is kept constant during the operation of RO system. This is accomplished by changing the feed flow rate and feed pressure simultaneously and objective point is approached. While the variation of the feed pressure and feed flow rate; recovery ratio, permeates flow rate and its salinity are to keep within the operational limits. In terms of mathematical form this problem can be written in following form.

Table 4.8: Mathematical description of constant brine methodology

	Mathematical Description
To Compute:	$SEC = \frac{\text{Energy Consumed}}{\text{Recovery Ratio}}$
Equality Constraints	RO_model_*equations* $Q_c = 7.7 m^3/h (const)$
Inequality Constraints	$PV_{Power} = (0 - 13kW)$ $0 < Q_f < 14.0 m^3/h$ (maximum_feed_flow_rate) $0 < P_f < 83 bars$ (max_membrane_pressure) $0 < \mathrm{Q_p} < 1.2 m^3/h$ (per_membrane) $0 < Y < 13\%$ (per_membrane) $C_p < 500 mg/l$ (maximum_limit_for_clean_water_salinity)

The solution of this problem as shown in Figure 4.12 reveals that the feed pressure less than 33.5 bar drives the RO system outside the operational limits and provides permeate higher than 500 ppm TDS. Minimum amount of PV energy required to keep the RO system at lower operational limit is 3.6kW which corresponds to feed flow rate of 8

m^3/h and feed pressure of 33.5bars. The valid operational region for this methodology consumes the PV energy range of 3.5 kW to 13 kW. Different flow rates of RO system for this methodology are shown in Figure 4.15. Feed pressures, RR and permeate TDS are illustrated in Figure 4.16. This methodology is more favorable for the usage of ERD i.e. works exchanger or pressure exchanger due to the constant brine flow. Less efficient operation of ERDs is usually observed for a variable retentate flow rate.

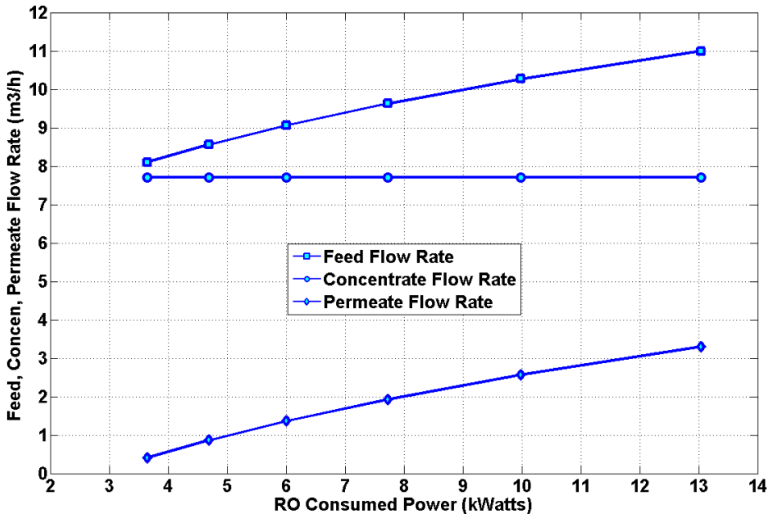

Figure 4.15: Different flow rates for constant concentrate rate methodology

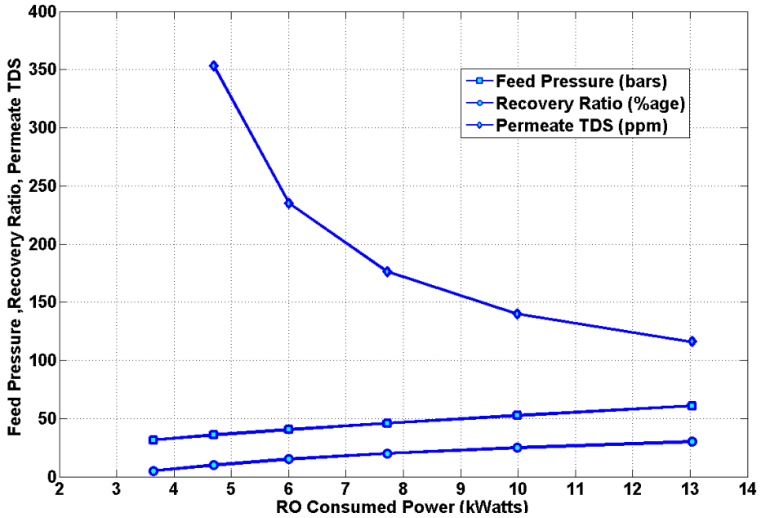

Figure 4.16: Pressure, permeate TDS and RR for constant concentrate rate methodology

4.6.3 Design criteria 3: Constant recovery ratio

In this methodology the overall recovery ratio of RO system is kept constant. This methodology is accomplished by changing the feed flow rate and feed pressure simultaneously and recovery ratio is kept constant. While the variation of the feed pressure and feed flow rate; permeates flow rate and its salinity are to keep within the operational limits. The recovery ratio is kept 30% and in mathematical form this problem can be written in following form.

Table 4.9: Mathematical description of constant recovery methodology

	Mathematical Description
Minimize:	$SEC = \frac{\text{Energy Consumed}}{\text{Recovery Ratio}}$
Equality Constraints	$\text{RO\_model\_}equations$ $Y = 30\%(\text{constant\_RR})$
Inequality Constraints	$PV_{Power} = (0-13kW)$ $0 < Q_f < 14.0m^3/h(\text{maximum\_feed\_flow\_rate})$ $0 < Y < 13\%(\text{per\_membrane})$ $0 < \text{Q}_\text{p} < 1.2m^3/h(\text{per\_membrane})$ $\text{Q}_c > 1.2m^3/h(\text{minimum\_concentrate\_flow\_rate})$ $C_p < 500mg/l(\text{maximum\_limit\_for\_clean\_water\_salinity})$

The solution of this problem as shown if Figure 4.12 reveals that the lower operational limit is defined by the minimum energy of 3kW which corresponds to minimum concentrate flow rate of 2.5 m^3/h. This strategy ensures the PV energy usage ranging from 3kW to 13kW. In this operating range the pressure is increased from 43.71bars to 60.81bars whereas the feed flow rate is increased from 3.5 m^3/h to 11 m^3/h. The permeate concentration is 351 TDS at lower operational point and decrease to 116 TDS due to increase in pressure. The permeate flow rate is increased from 1.05 m^3/h to 3.3

m^3/h when measured from the lower operational point to objective point. Obviously by keeping RR fixed, increase of feed flow rate will provide the variable flow rate of retentate. To restore the potential energy in brine stream at variable flow rate, special energy recovery devices are required which should have the fixed ratio for feed and retntate flow rate. Within the valid operational limits, different feed flow rates, pressures, TDS and permeate RR are show in Figure 4.17 and Figure 4.18.

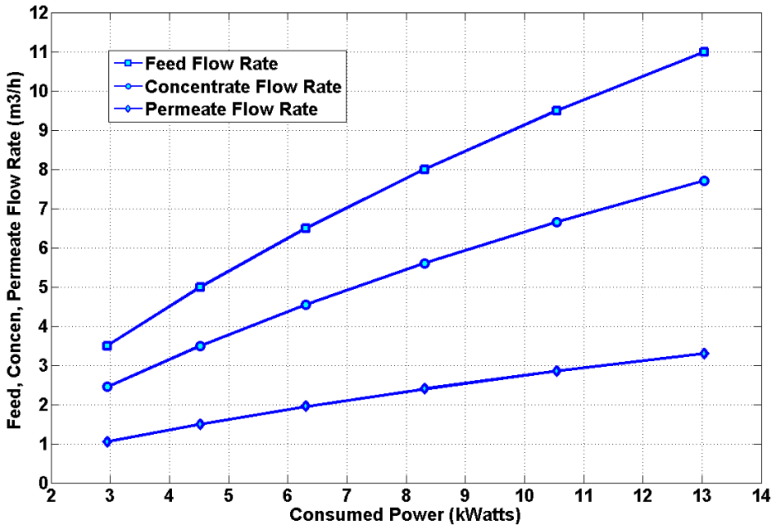

Figure 4.17: Different flow rates for constant recovery ratio methodology

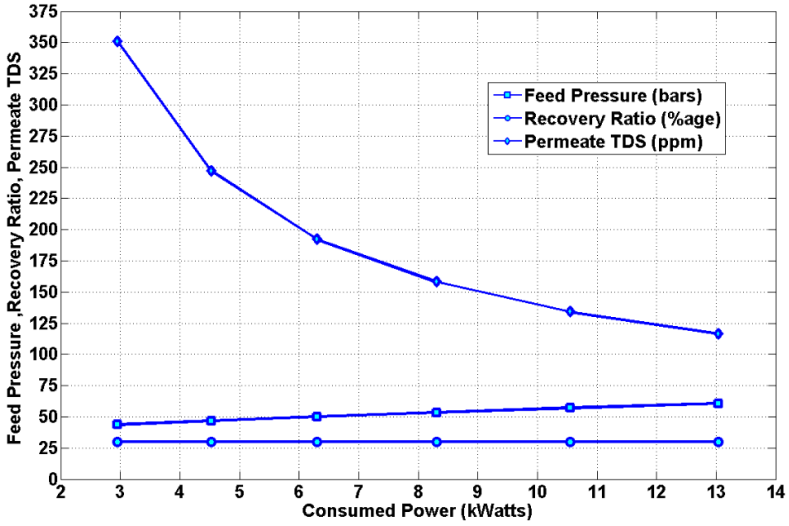

Figure 4.18: Pressure, permeate TDS and RR for constant recovery ratio methodology

4.6.4 Design criteria 4: Constant feed pressure

This methodology is based upon the idea to change the feed flow rate and recovery ratio to keep the membrane pressure constant during the broad range or PV available energy. Conventional RO desalination systems are usually operated at constant feed pressure. Since now, it is not investigated, if and how a variable feed pressure affects the long term performance of RO membrane, this operational methodology is assumed as "membrane friendly" [116]. The problem formulation for this strategy is as follows.

Table 4.10: Mathematical Description of Constant Feed Methodology

	Mathematical Description
To Compute:	$SEC = \frac{\text{Energy Consumed}}{\text{Recovery Ratio}}$
Equality Constraints	RO_model_*equations* $P_f = 61.39 bars\,(constant\ \text{\_pressure})$
Inequality Constraints	$PV_{Power} = (0-13kW)$ $0 < Q_f < 14.0 m^3/h\,(\text{maximum\_feed\_flow\_rate})$ $0 < \mathrm{Q_p} < 1.2 m^3/h\,(\text{per\_membrane})$ $0 < Y < 13\%\,(\text{per\_membrane})$ $\mathrm{Q_c} > 1.2 m^3/h\,(\text{minimum\_concentrate\_flow\_rate})$ $C_p < 500 mg/l\,(\text{maximum\_limit\_for\_clean\_water\_salinity})$

Solution of this problem reveals as shown in Figure 4.12, that the lower operational point in this methodology corresponds to feed flow rate of 6.7 m^3/h and recovery 40% with constant feed pressure of 61.39 bars, and it required minimum amount of 8.85kW of PV power. Below this power, RO system would be operated outside the RO operational limits,

which is not recommended. Starting from the lower operational point and approaching towards the peak power point, the feed flow rate is increased from 6.7 m^3/h to 11.4 m^3/h, recovery ratio is decreased from 40% to 30%.and power consumption varies from 8.85kW to 13.75 kW. This operational strategy provides lower operational range over a wide range of PV available energy.

In this methodology the net driving pressure (difference between the osmotic pressure and feed pressure) that causes the permeate flow through membrane is strong function of deposited salt concentration over the membrane due to the concentration polarization. Decrease in the feed flow rate while increasing the permeate recovery ratio increases the concentration polarization. So the increased osmotic pressure at membrane surface due to CP slightly curtails the driving pressure. Therefore the increase in permeate flow rate is observed by 28 % while its concentration is reduced by 29% when the RO operation from lower operational limit to objective point is considered. Figure 4.19 and Figure 4.20 depict out the important findings of different flow rates, RR, permeate TDS and RR for constant pressure methodology.

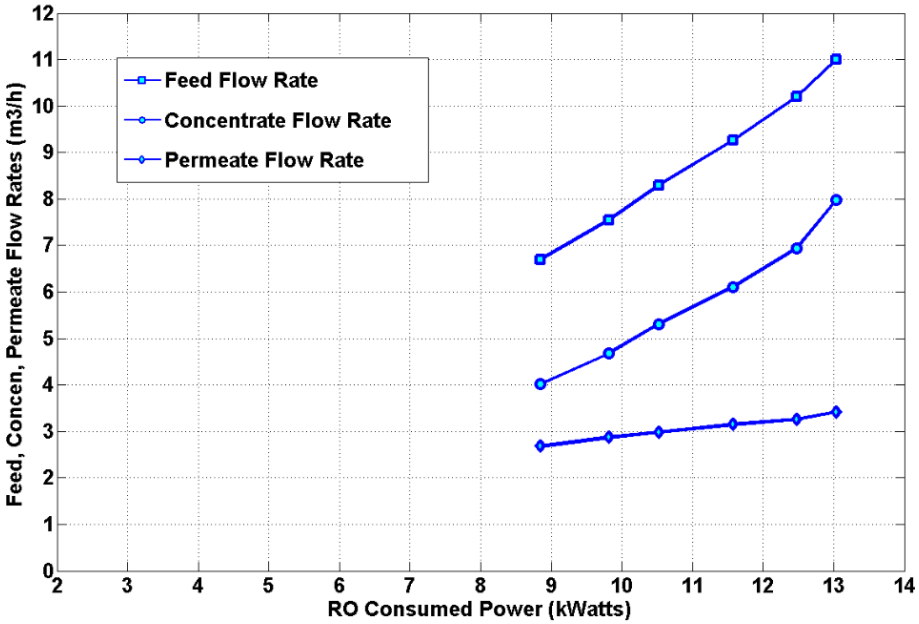

Figure 4.19: Different flow rates for constant pressure methodology

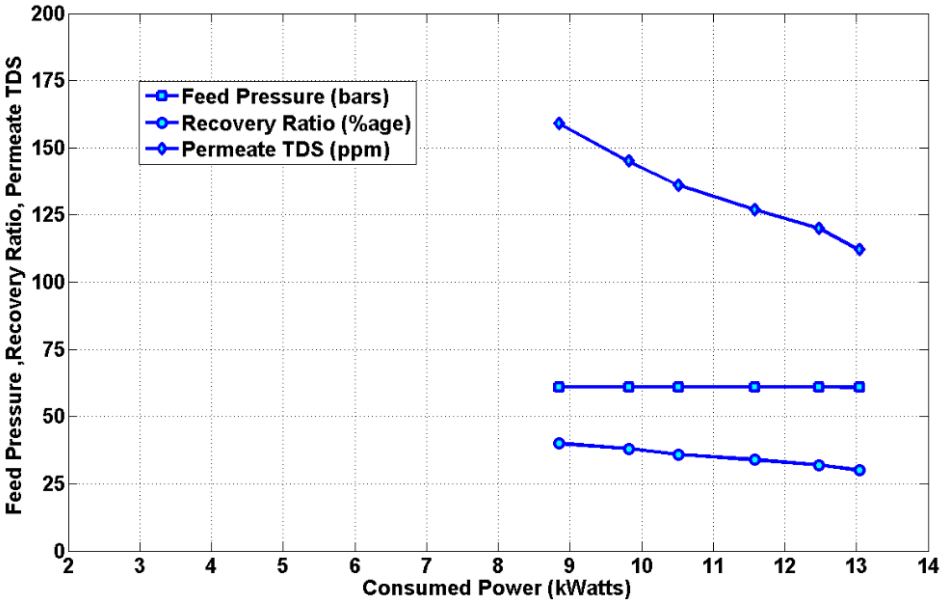

Figure 4.20: Pressure, permeate TDS and RR for constant pressure methodology

4.7 Comparative analysis of designs for PV available power

For the comparison of different operational strategies, permeate flow rate and specific energy consumption (ratio between the consumed energy and permeate flow rate) against the PV available energy range is taken as the selection criteria. So the operational methodology having the capability to use the maximum range of PV power with minimum SEC would be most appropriate for the optimal operation of PVRO system. Figure 4.21 presents the permeate flow rate of all operational strategies against the PV power (linear scale). Figure 4.22 shows the SEC of all operational strategies against the PV power (again linear scale). In the following section according the PV available power (profile) for the fixed PV, single axis and double axis tracked panel will be considered for the analysis of permeate flow rate and specific energy consumption.

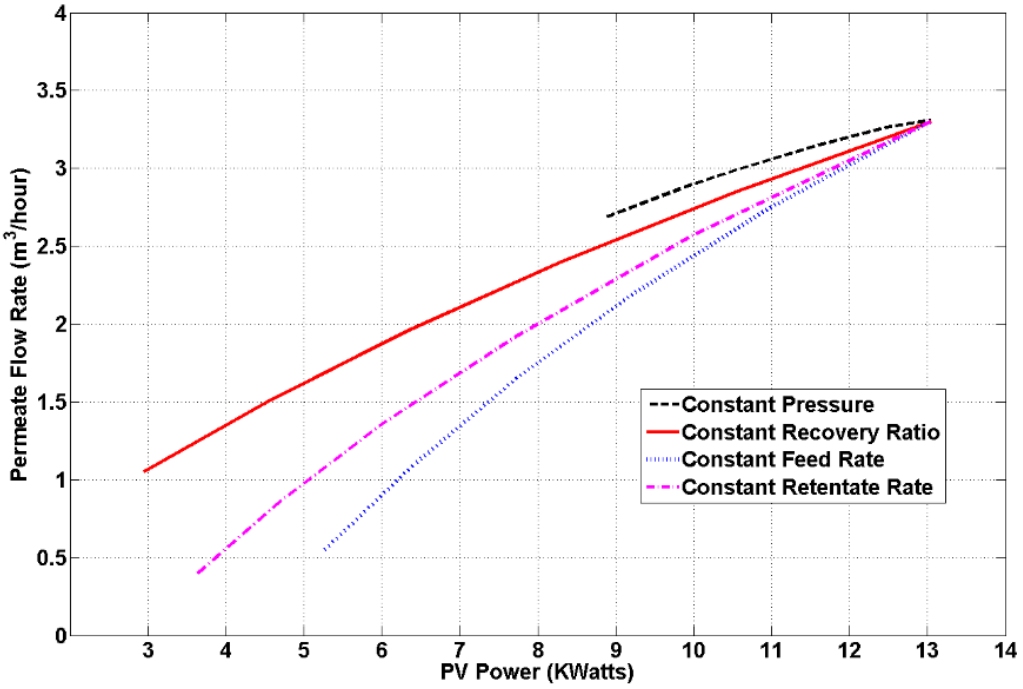

Figure 4.21: Permeate flow rate for different methodologies

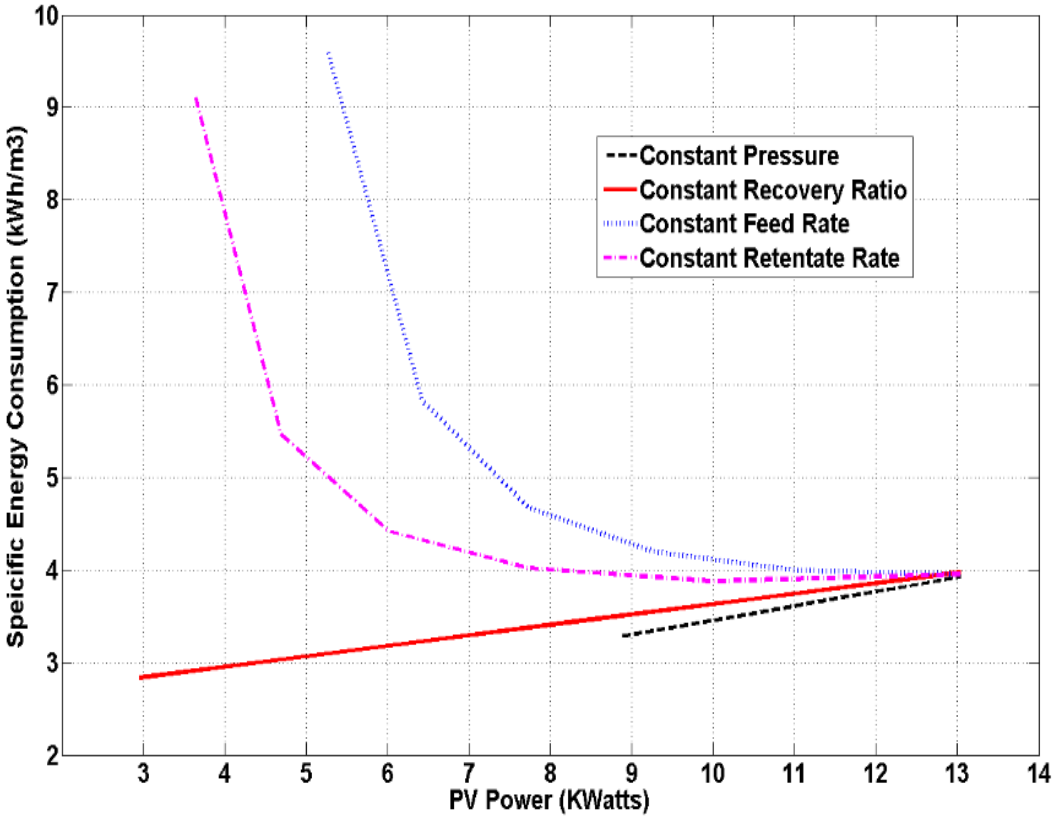

Figure 4.22: SEC comparison of different methodologies

4.7.1 Comparative analysis of methodologies for fixed PV panels

The power profile produced by the flat PV panel for the 22nd June for Dhahran city is shown in Figure 4.23. In this profile the sun shining time is 13.8 hours from dawn to dusk and amount of received electrical PV energy is 105.4 kWh. Within this PV power profile the permeate collected using different operational methodologies is shown in Figure 4.24. Based upon permeate flow rates and PV power (for the whole day power profile) SEC of all four operational methodologies is shown in Figure 4.25.

Constant feed pressure methodology offers the highest permeate flow rate with lowest specific energy consumption over the upper power range of PV system. This power range spans from the 8.8 kW to 13 kW and is available only at peak times of insolation. Total permeate produced in this scheme is 20.91 m^3 with energy consumption of 78.46 kWh and operational time of 6.8 hours during the whole day. The times providing the power less than 8.8 kW, RO operation at constant pressure will be driven outside the operational limits. Another noticeable advantage of this strategy is the small variation of permeate concentration. In this methodology, in the whole day operation, 50% day time is used and 74.44% of total available PV energy is utilized. Disadvantages of this technique is the narrow range of PV power usage and increased propensity of fouling and scaling due to and increased permeate recovery ratios.

Constant permeate recovery ratio strategy exhibits the longest operational line in Figure 4.24, which corresponds to the effective utilization of wide range of PV power. Total permeate produced in this scheme is only 27.981 m^3 with energy consumption of 102.52 kWh with operational time of 11 hours during the whole day. In this methodology 79.7% day time is used and 97.23% of total available PV energy is utilized. In contrary to

the constant feed pressure methodology, this strategy consumes slightly more SEC for upper values of PV power. The overall consumable PV power range in this strategy spans from 2.95 kW to 13.04 kW. The RO operation below 2.95 kW PV energy is not feasible due to the restriction imposed by the minimum retentate flow rate. At lower operational points the permeate concentration is more (but within the range of 500mg/l) and it decreases as the feed pressure and feed flow are increased.

Constant retentate flow rate strategy provides the utilization of PV power range that is comparable to the constant recovery ratio methodology (3 kW to 13 kW). Total permeate produced in this scheme is only 25 m^3 with energy consumption of 100.27 kWh with operational time of 10.30 hours during the whole day. In this methodology 74.64% day time is utilized and 95.13% of total available energy is consumed. At the low operational point the recovery is only 8.5% which causes the increased SEC at this point. Optimal SEC is exhibits when the PV power production is within the 90% of the peak PV power. With the reduction in PV power, SEC increases sharply to an unacceptable value. Another disadvantage of this strategy is increase in the clean water salinity when RO is operated at lower PV power.

As for as the constant feed flow rate methodology is concerned, it's SEC is significantly high, even higher than the constant retentate flow rate, when RO is operated at low PV power. Total permeate produced in this scheme is 22.92 m^3 with energy consumption of 96.35 kWh and operational time of 9.40 hours during the whole day. In this methodology 68.12% day time is utilized and 91.40% of total available energy is consumed. Moreover, the utilization of wide range of PV power is less than the constant

recovery and constant retentate flow rate strategies, but better than the constant pressure methodology.

The analysis clearly illustrates the pros and corns for each methodology. Utilization of broad range of PV power can be ensured by varying the feed pressure and feed flow rate accordingly to achieve the optimum operation. For the low variation of PV power around the noon time, constant feed pressure methodology is more feasible. For flat panels where the variation of PV power is more significant, the constant recovery ratio methodology is more appropriate for optimal operation. A third option can also be considered, that will make use of constant pressure and constant RR methodology together. In this option at lower PV power RO system is to be operated at constant recovery ratio methodology and for the higher PV power constant pressure methodology is more feasible choice. The combined operation methodology is depicted out in Figure 4.26 along with other methodologies. In combined methodology, total permeate produced is 28.60 m^3 with energy consumption of 102.52kWh and operational time of 11 hours during the whole day. In this methodology 79.71% day time is utilized and 97.27% of total available energy is consumed. In summary, the permeate collected for all methodologies during the whole day PVRO operation is shown in Figure 4.27. The overall energy consumption, day time usage, SEC and total permeate collected is detailed in Table 4.11.

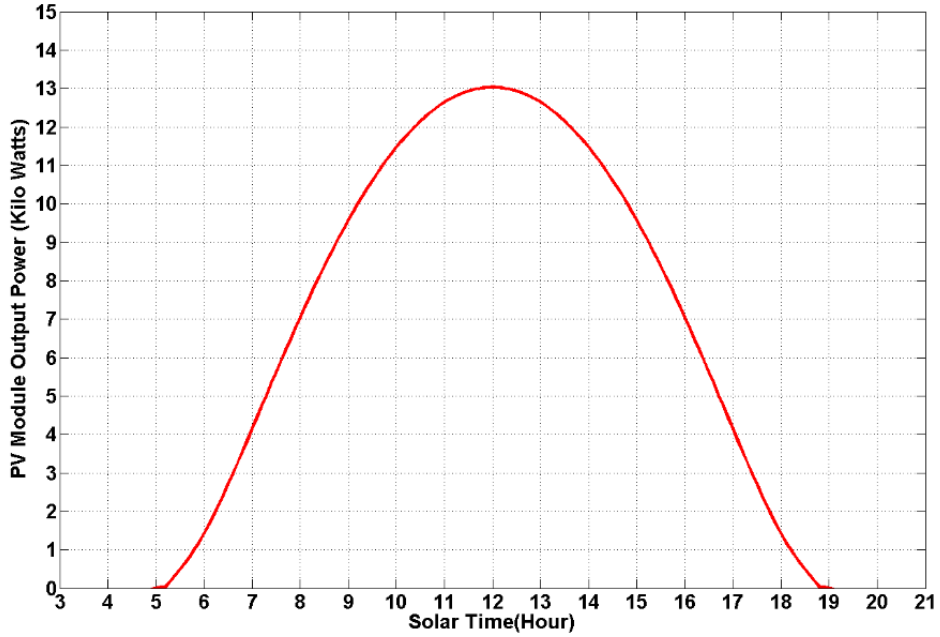

Figure 4.23: Flat PV output power profile

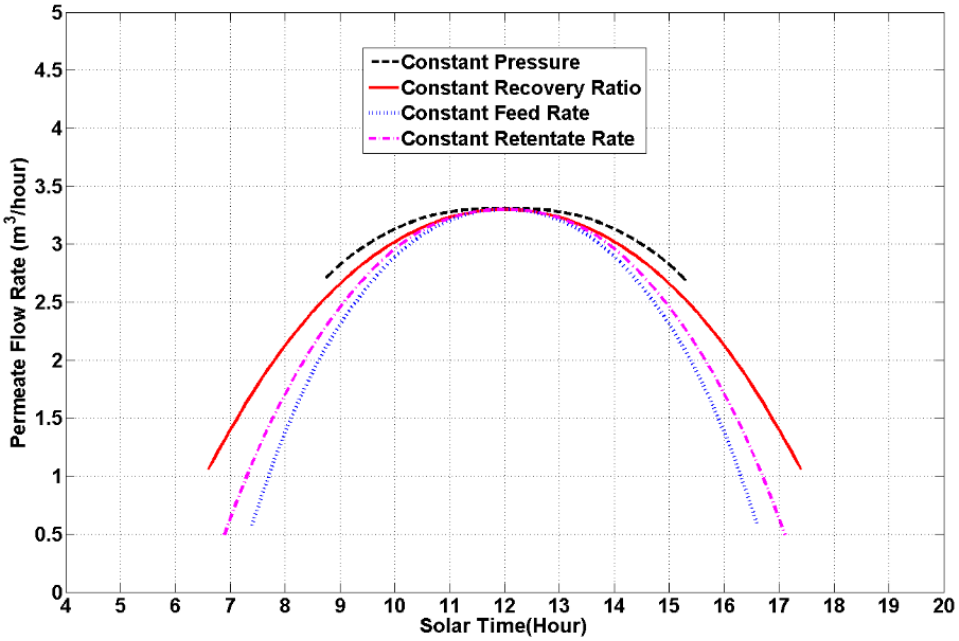

Figure 4.24: Permeate flow rate for different methodologies during the whole day

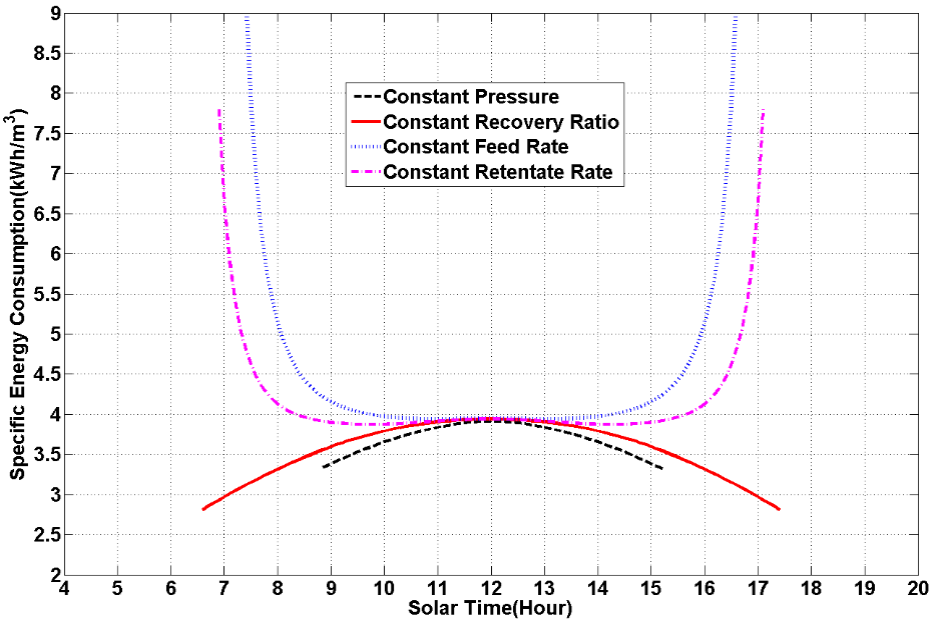

Figure 4.25: SEC Comparison of different methodologies for fixed PV panels

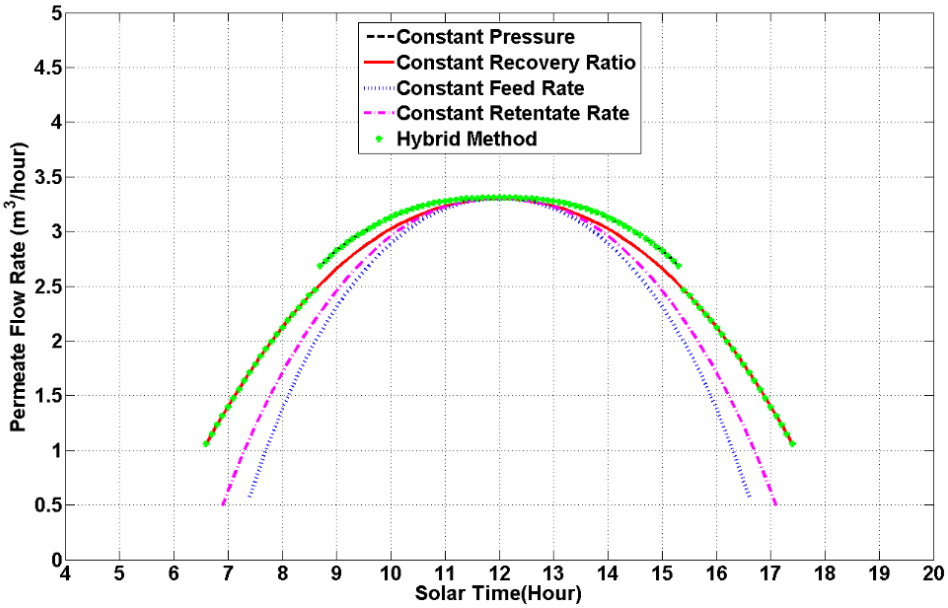

Figure 4.26: Permeate flow rate analysis of hybrid methodology with other methodologies

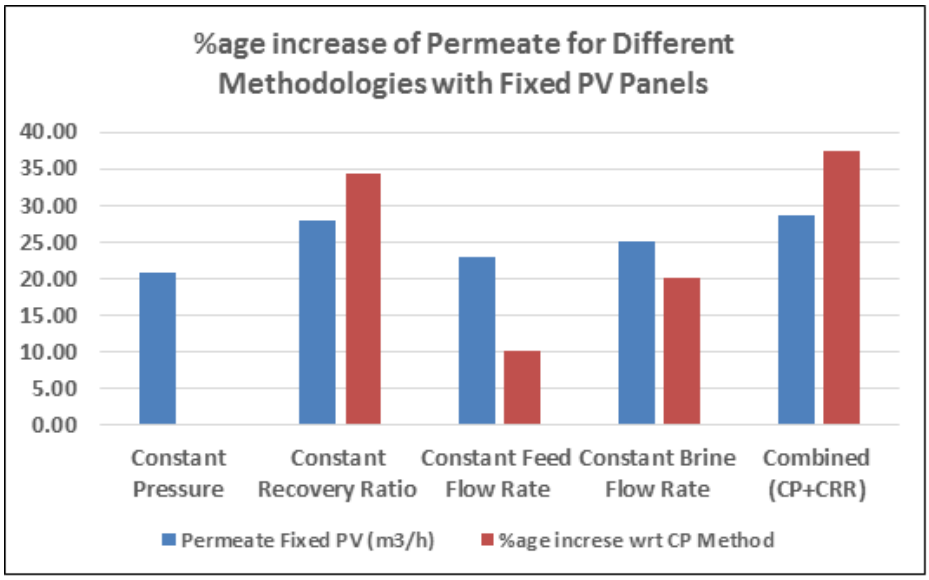

Figure 4.27: Percentage increase of permeate for fixed PV panels

Table 4.11: Permeate and SEC for different methodologies for fixed PV panels

	Permeate Produced (1000 Liters)	Energy Consumed (kWatt Hour)	Day Time Consumed (Hours)	Average SEC (kWatt Hour/m3)	%age Energy Used	%age Day Time Used
Constant Pressure Methodololy	20.82	78.46	6.80	3.77	74.44	49.28
Constant Recovery Ratio Methodology	27.98	102.52	11.00	3.66	97.27	79.71
Constant Feed Flow Rate Methodology	22.92	96.35	9.40	4.20	91.41	68.12
Constant Brine Flow Rate Methodology	25.00	100.27	10.30	4.01	95.13	74.64
Combined (CP+CRR) Methodolgy	28.60	102.52	11.00	3.58	97.27	79.71

4.7.2 Comparative analysis of methodologies for single axe PV panels

The power profile produced by the single axe PV panel for the 22nd June for Dhahran city is shown in Figure 4.28. In this profile the sun shining time is 13.8 hours from dawn to dusk and amount of received electrical PV energy is 130.60kWh. Within this PV power profile, the permeate collected using different operational methodologies is shown in Figure 4.29. Based upon permeate flow rates and PV power (for the whole day power profile) SEC of all four operational methodologies is shown in Figure 4.30.

Constant feed pressure methodology offers the highest permeate flow rate with lowest specific energy consumption for the high PV power production. This power range spans from the 8.8 kW to 13 kW and is available only at peak times of insolation. Total permeate produced in this scheme is 28.76 m^3 with energy consumption of 108.13 kWh and operational time of 9.20 hours during the whole day. The times providing the power less than 8.8 kW (corresponds to time before 7.30am and after 4.30pm), RO operation at constant pressure will be driven outside the operational limits. Another noticeable advantage of this strategy is the small variation of permeate concentration. In this methodology 66.67% day time is used and 82.79% of total available energy is utilized. This methodology uses quite good range of PV power with average SEC of 3.76 kWh/m^3.

Constant permeate recovery ratio strategy exhibits the longest operational line as shown in the Figure 4.29. It corresponds to the effective utilization of wide range of PV power. Total permeate produced in this scheme is 34.71 m^3 with energy consumption of 129.40kWh and operational time of 12.80 hours during the whole day. In this methodology 92.75% day time is used and 99.08% of total available PV energy is utilized. In contrary to the constant feed pressure methodology, this strategy exhibits slightly higher SEC for

upper values of PV power. The overall consumable PV power range in this strategy spans from 2.95kW to 13.04kW. The RO operation below 2.95 kW (time before 5.40 am and after 6.20pm) PV power, will not be possible due to the restriction imposed by the minimum retentate flow rate.

Constant retentate flow rate strategy provides the utilization of PV power range that is comparable to the constant recovery ratio methodology (2.95kW to 13.04kW PV power). Total permeate produced in this scheme is only 32.23 m^3 with energy consumption of 128.76kWh with operational time of 12.60 hours during the whole day. In this methodology 91.30% day time is utilized and 98.59% of total available energy is consumed. At the low operational point the recovery is only 8.5% which causes the increased SEC at this point. Optimal SEC is exhibited when the PV power production is high. With the reduction in PV power, SEC increases sharply to an unacceptable value. The noticeable disadvantage of this strategy is increase in the clean water salinity when RO is operated at lower PV power.

Constant feed flow rate methodology exhibits the high SEC, even higher than the constant retentate flow rate, when RO is operated at low PV power. Total permeate produced in this scheme is 30.20 m^3 with energy consumption of 124.60 kWh and operational time of 11.40 hours during the whole day. In this methodology 84.06% day time is utilized and 95.40% of total available energy is consumed. Moreover, the utilization of wide range of PV power is less than the constant recovery and constant retentate flow rate strategies, but better than the constant pressure methodology.

Utilization of broad range of PV power can be ensured by varying the feed pressure and feed flow rate accordingly to achieve the optimum operation for the selected

operational methodology. For the high PV power around the noon time, constant feed pressure methodology is more feasible due to its least SEC. For single axis tracked PV panels, the variation of PV power is more significant at morning and evening time. To accommodate the RO operation at reduced PV power, the constant recovery ratio methodology is more appropriate for optimal operation. A third option can also be considered, that will make use of constant pressure and constant RR methodology together. In this option at lower PV power RO system is to be operated at constant recovery ratio methodology and for the higher PV power constant pressure methodology is more feasible choice. The combined operation methodology is depicted out in Figure 4.31. In this combined methodology, total permeate produced is 35.50 m^3 with energy consumption of 129.40kWh and operational time of 12.80 hours during the whole day. In this methodology 97.75% day time is utilized and 99.08% of total available energy is consumed. In summary, the permeate collected for all methodologies during the whole day PVRO operation is shown in Figure 4.32. The overall energy consumption, day time usage, SEC and total permeate collected of all operational methodologies is detailed in Table 4.12.

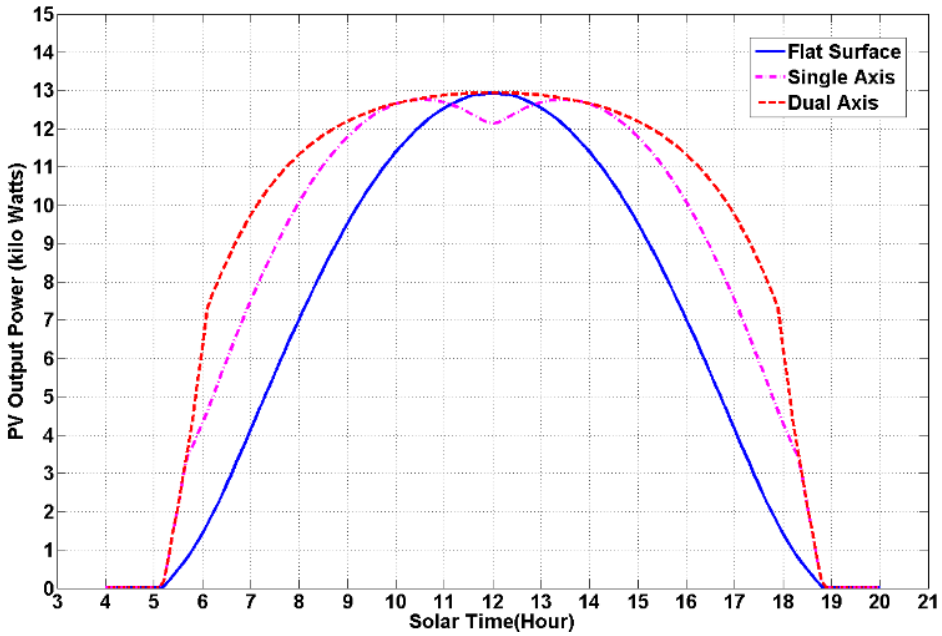

Figure 4.28: Flat and tracked PV output power profile

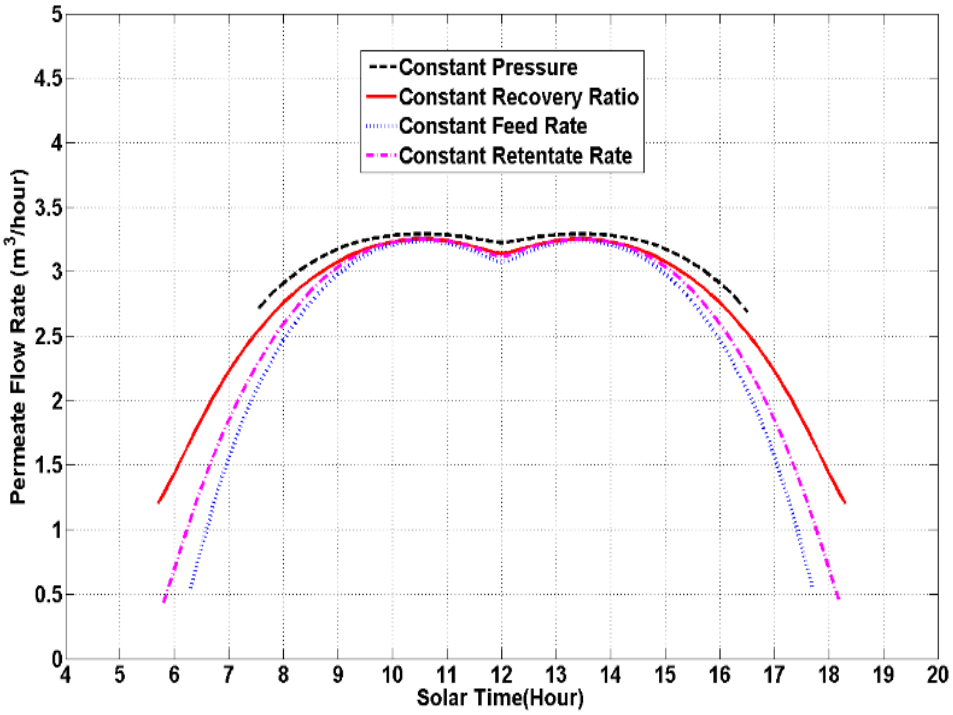

Figure 4.29: Permeate flow rate for different methodologies during the whole day (Single axis PV tracking)

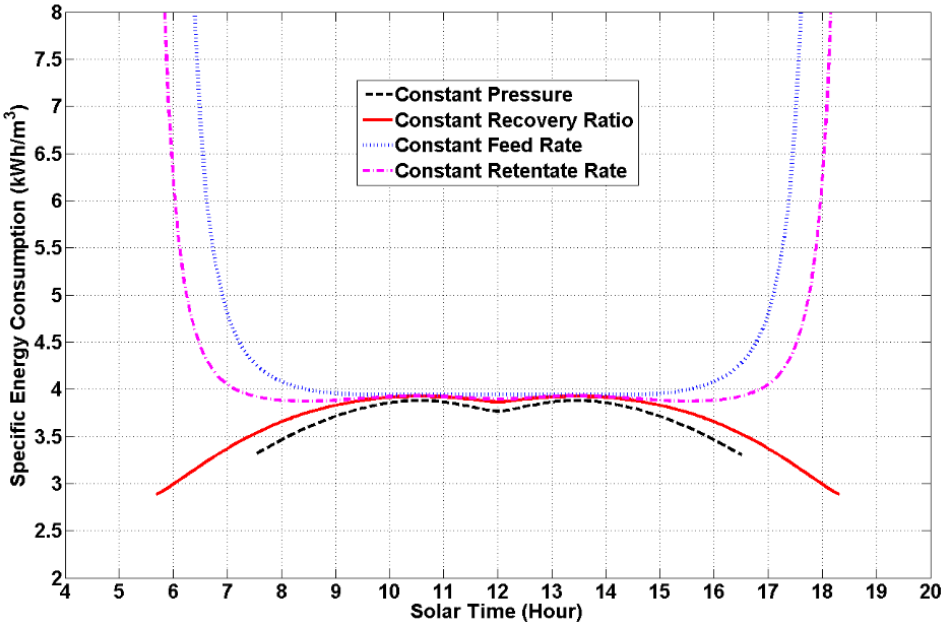

Figure 4.30: SEC comparison of different methodologies for single axe tracked PV panels

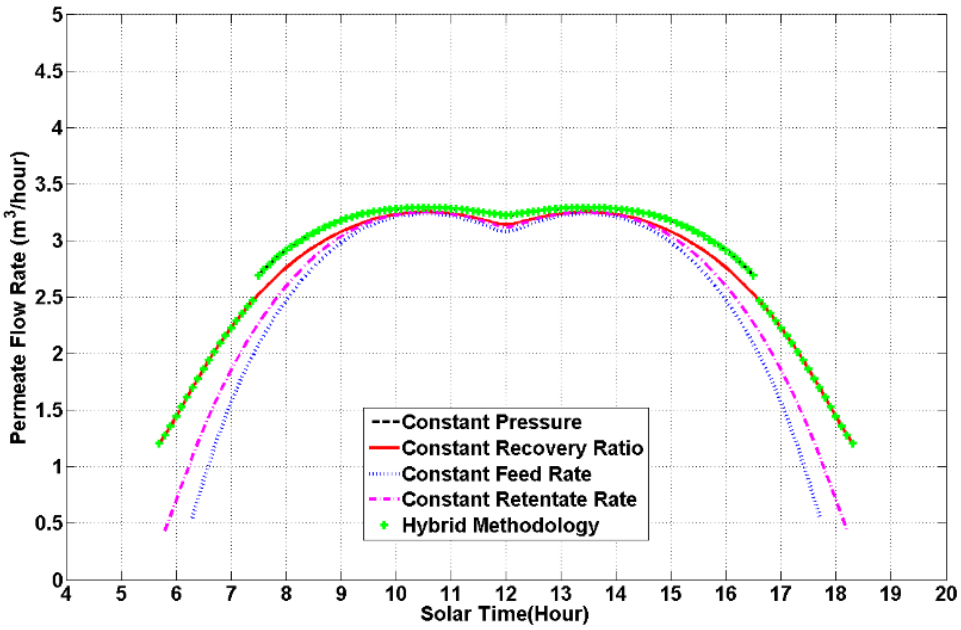

Figure 4.31: Permeate flow rata analysis of hybrid methodology with other methodologies (single axis PV tracking)

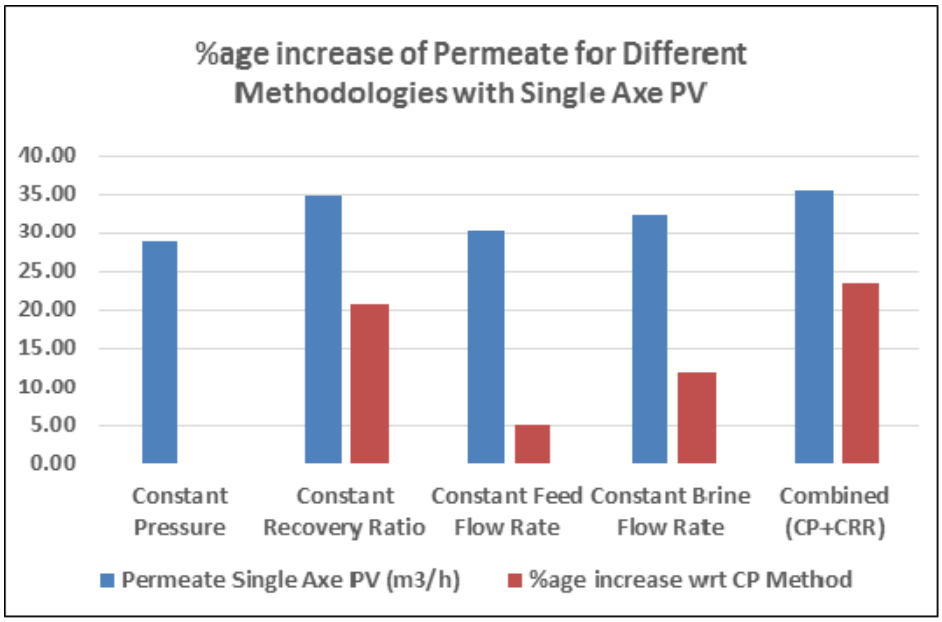

Figure 4.32: Percentage increase of permeate for single axe PV panel tracking

Table 4.12: Permeate and SEC for different methodologies for single axe tracking PV panels

	Permeate Produced (1000 Liters)	Energy Consumed (kWatt Hour)	Day Time Consumed (Hours)	Average SEC (kWatt Hour/m3)	%age Energy Used	%age Day Time Used
Constant Pressure Methodololy	28.76	108.13	9.20	3.76	82.79	66.67
Constant Recovery Ratio Methodology	34.71	129.40	12.80	3.73	99.08	92.75
Constant Feed Flow Rate Methodology	30.20	124.60	11.60	4.13	95.41	84.06
Constant Brine Flow Rate Methodology	32.23	128.76	12.60	4.00	98.59	91.30
Combined (CP+CRR) Methodolgy	35.50	129.40	12.80	3.65	99.08	92.75

4.7.3 Comparative analysis of methodologies for double axis PV panels

The power profile produced by the double axis tracked PV panel for the 22nd June for Dhahran city is shown in Figure 4.33. In this profile the sun shining time is 13.8 hours from dawn to dusk and amount of received electrical PV energy is 142.80kWh. Within this PV power profile the permeate collected using different operational methodologies is shown in Figure 4.34. Based upon permeate flow rates and PV power (for the whole day power profile) SEC of all four operational methodologies in Figure 4.35.

In the Figure 4.34 it is obvious that permeate flow rate in constant feed pressure methodology offers the highest values with least specific energy consumption over the high power range of PV system. This power range spans from the 8.8kW to 13kW and is available most of the time during the day. Total permeate produced in this scheme is 34.00 m^3 with energy consumption of 128.55kWh and operational time of 10.80 hours during the whole day. The times providing the power less than 8.8kW (corresponds to solar time before 6.40 am and after 5.20pm), RO operation at constant pressure will be driven outside the operational limits. Another noticeable advantage of this strategy is the small variation of permeate concentration. In this methodology 78.26% day time is used and 90.02% of total available energy is utilized. This technique uses an excellent range of PV power with average SEC of 3.78 kWh/m^3.

Constant permeate recovery ratio strategy exhibits the longest permeate flow rate line and is shown in Figure 4.34. It corresponds to the effective utilization of wide range of PV power. Total permeate produced in this scheme is 37.27 m^3 with energy consumption of 141.56 kWh and operational time of 12.80 hours during the whole day. In this methodology 92.75% day time is used and 99.13% of total available PV energy is utilized.

In contrary to the constant feed pressure methodology, this strategy exhibits slightly higher SEC for upper values of PV power. The overall consumable PV power range in this strategy spans from 2.95kW to 13.04kW. The RO operation below 2.95kW (time before 5.40 am and after 6.20pm) PV power, will not be possible due to the restriction imposed by the minimum retentate flow rate.

Constant retentate flow rate strategy provides the utilization of PV power range that is comparable to the constant recovery ratio methodology (2.95kW to 13.04kW). Total permeate produced in this scheme is 35.74 m^3 with energy consumption of 140.91kWh with operational time of 12.60 hours during the whole day. In this methodology 91.30% day time is utilized and 98.68% of total available energy is consumed. At the low operational point the recovery is only 8.5% which causes the increased SEC at this point. Optimal SEC is exhibited when the PV power is high. With the reduction in PV power, SEC increases sharply to an unacceptable value. Another disadvantage of this strategy is increase in the clean water salinity when RO is operated at reduced PV power.

As for as the constant feed flow rate methodology is concerned, it's SEC is significantly high, even higher than the constant retentate flow rate, when RO is operated at low PV power. Total permeate produced in this scheme is 34.60 m^3 with energy consumption of 140.11 kWh and operational time of 12.40 hours during the whole day. In this methodology 89.86% day time is utilized and 98.12% of total available energy is consumed. Moreover, the utilization of wide range of PV power is less than the constant recovery and constant retentate flow rate strategies, but better than the constant pressure methodology.

Utilization of broad range of PV power can be ensured by varying the feed pressure and feed flow rate accordingly to achieve the optimum operation for the selected operational methodology. For the high PV power most of the day time, constant feed pressure methodology is more feasible due to its least SEC. For double axis tracked PV panels, the variation of PV power is more significant at morning and evening time. To accommodate the RO operation at low PV power, the constant recovery ratio methodology is more appropriate for optimal operation.

A third option can also be considered, that will make use of constant pressure and constant RR methodology together. In this option at lower PV power RO system is to be operated at constant recovery ratio methodology and for the higher PV power constant pressure methodology is more feasible choice. The combined operation methodology is depicted out in Figure 4.36 along with other methodologies. In this combined methodology, total permeate produced is 38.10 m^3 with energy consumption of 141.56kWh and operational time of 12.80 hours during the whole day. In this methodology 92.75% day time is utilized and 99.13% of total available energy is consumed. In summary, the permeate collected for all methodologies during the whole day PVRO operation is shown in Figure 4.37. The overall energy consumption, day time usage, SEC and total permeate collected is detailed in Table 4.13.

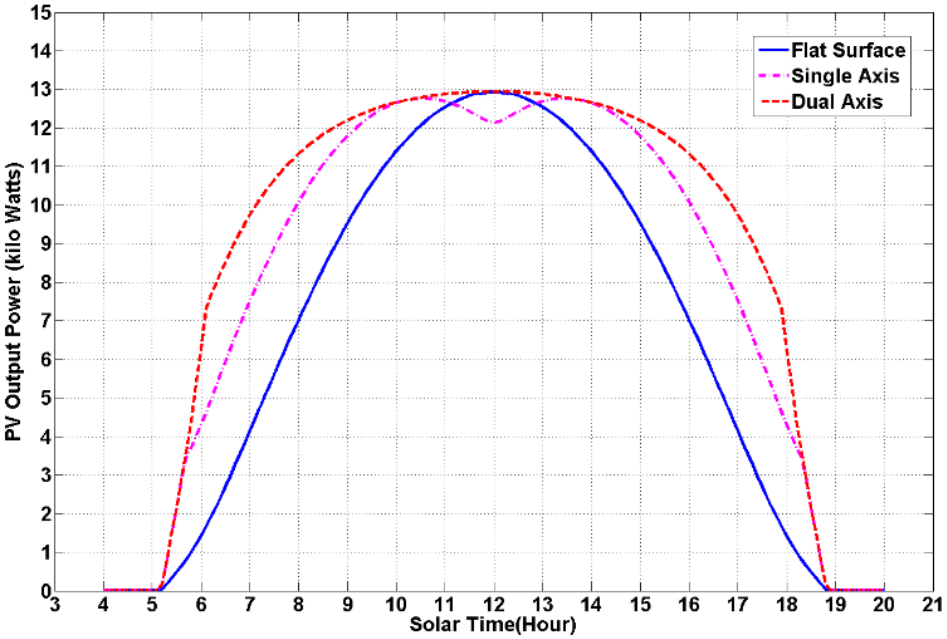

Figure 4.33: Flat and tracked PV output power profile

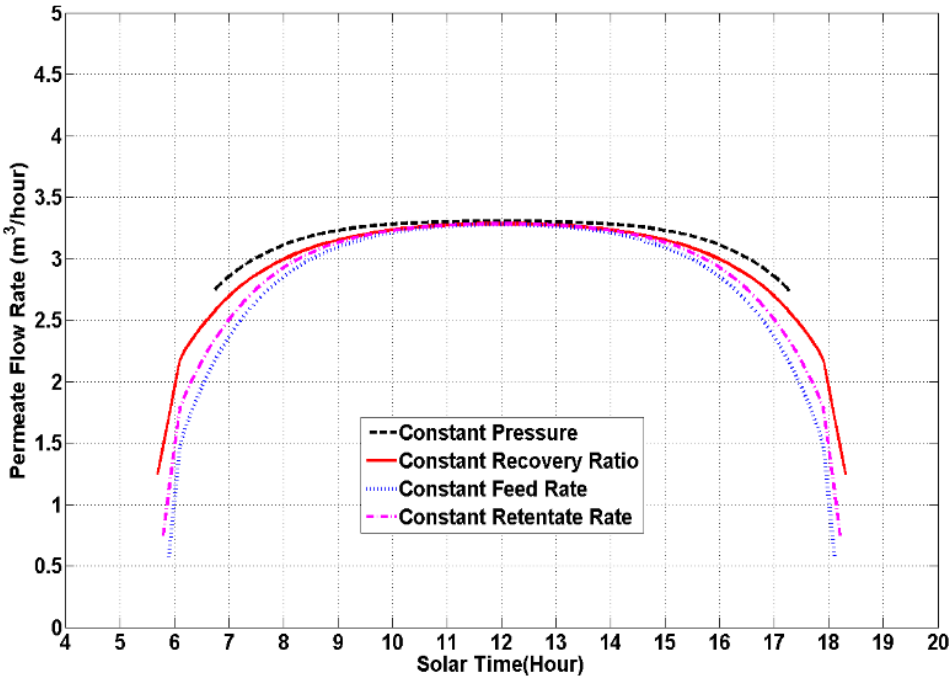

Figure 4.34: Permeate flow rate for different methodologies during the whole day (single axis PV tracking)

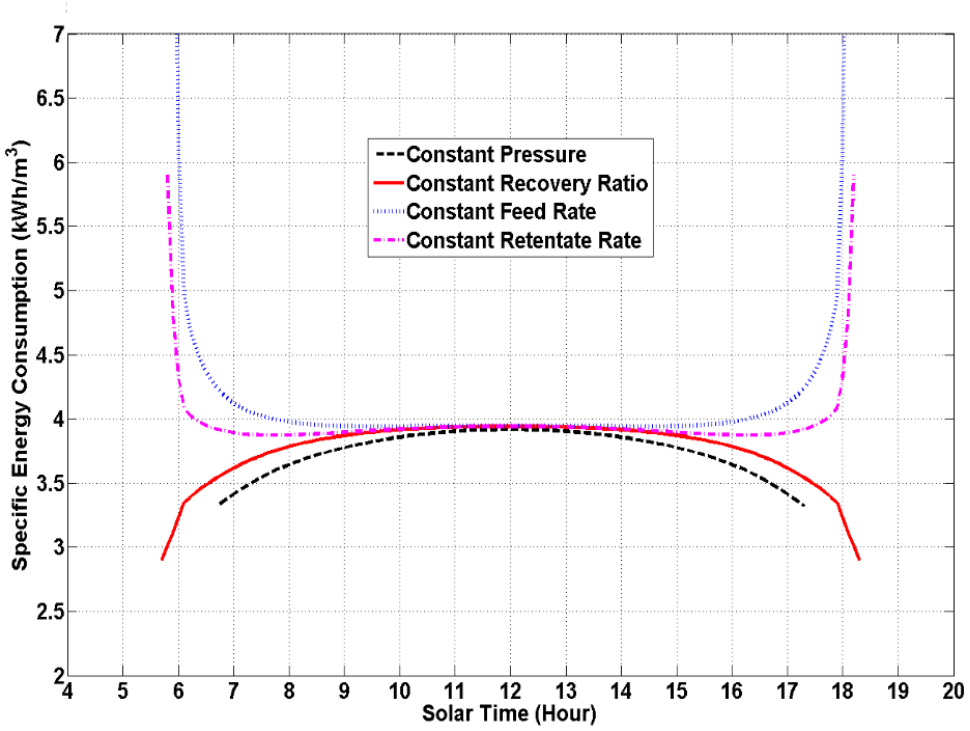

Figure 4.35: SEC comparison of different methodologies for double axis tracked PV panels

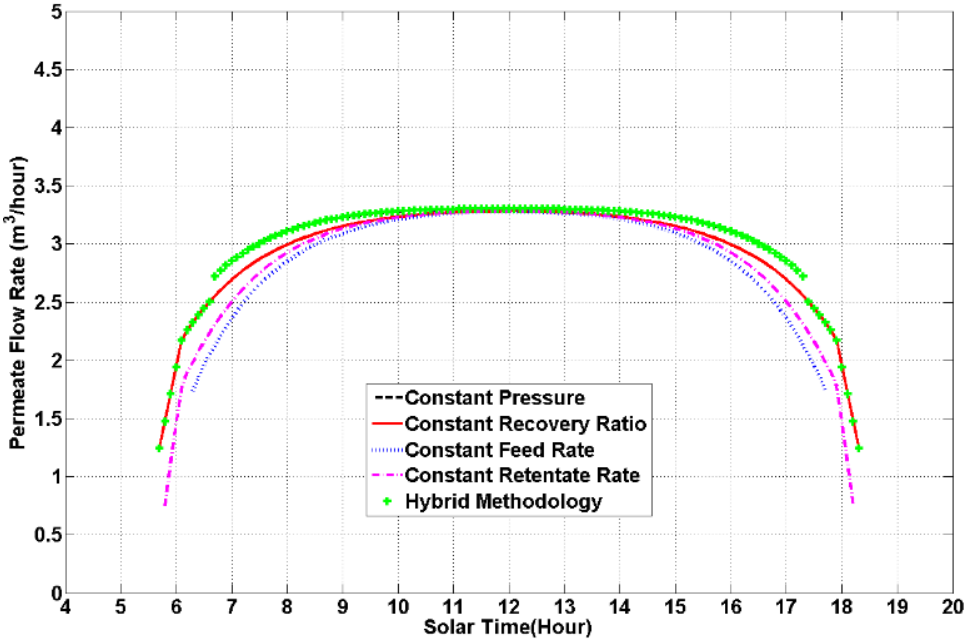

Figure 4.36: Permeate flow rata analysis of hybrid methodology with other methodologies (single axis PV tracking)

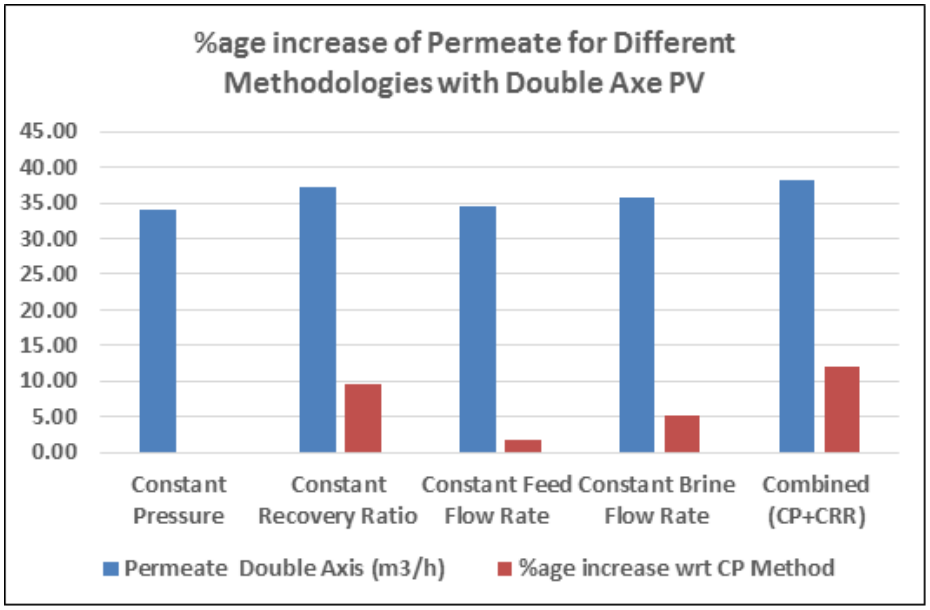

Figure 4.37: Percentage increase of permeate with double axis PV tracking

Table 4.13: Permeate and SEC for different methodologies operated with double axis tracking PV panels

	Permeate Produced (1000 Liters)	Energy Consumed (kWatt Hour)	Day Time Consumed (Hours)	Average SEC (kWatt Hour/m3)	%age Energy Used	%age Day Time Used
Constant Pressure Methodololy	34.00	128.55	10.80	3.78	90.02	78.26
Constant Recovery Ratio Methodology	37.27	141.56	12.80	3.80	99.13	92.75
Constant Feed Flow Rate Methodology	34.60	140.11	12.40	4.05	98.12	89.86
Constant Brine Flow Rate Methodology	35.74	140.91	12.60	3.94	98.68	91.30
Combined (CP+CRR) Methodolgy	38.10	141.56	12.80	3.72	99.13	92.75

4.7.4 Comparative analysis for SEC

For the whole day operation of PVRO under different operational methodologies and with the provision of flat, single axe and double axis tracked PV panels, SEC is computed and shown in the Figure 4.38. It is obvious that the SEC for the constant pressure methodology for all the cases of PV tracking is almost same and is around 3.77 kWh/m^3. The reason behind this consistency is that PVRO operation at constant pressure methodology is feasible at high PV power and more permeate is produced. The ratio between consumed energy and produced permeate remains the constant. The difference only lies in the PVRO operation duration, which is maximum in the double axis tracking PV system and minimum in the flat PV panels.

The constant permeate recovery ratio methodology exhibits the maximum duration of PVRO operation under all PV panel configurations. SEC in this scheme is 3.66, 3.73 and 3.80 kWh/m3 for the fixed PV, single and double axis tracking PV panels respectively. SEC of constant feed flow rate and constant brine scheme are higher than constant pressure and constant recovery schemes and definitely these schemes are not attractive for PVRO operation. The last option is the combined (CP+CRR) methodology that exhibits the SEC of 3.58, 3.65 and 3.72 kWh/m^3 in the fixed PV, single and double axis schemes respectively. This schemes offers the least amount of SEC than other methodologies and is most suitable for PVRO operation.

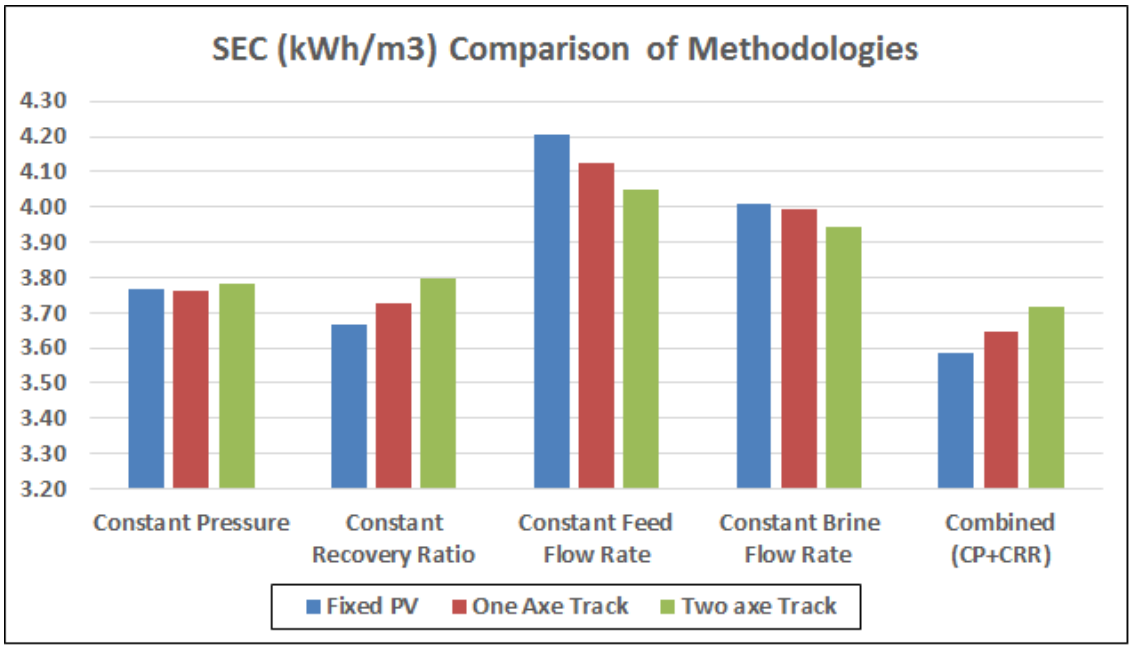

Figure 4.38: Average SEC of methodologies for fixed and tracked PV panels

4.8 Optimal feed and pressure set points for PVRO Control

In the previous section it is clear that the attractive operational schemes are the constant pressure, constant recovery and combined methodologies. Based upon the PV power and its profile any of the above mentioned schemes may be used to operate PVRO system. Based upon the selected operation methodology, optimal control system will acquire the available power from the PV system and computes the optimal feed flow rate and system pressure set points. These values will be send to the local feed flow control loop and pressure control loop as reference values. These controller will make use of feedback control system to track the reference values effectively. The inclusion of local feed and pressure control loops within the whole PVRO system is shown in Figure 4.39.

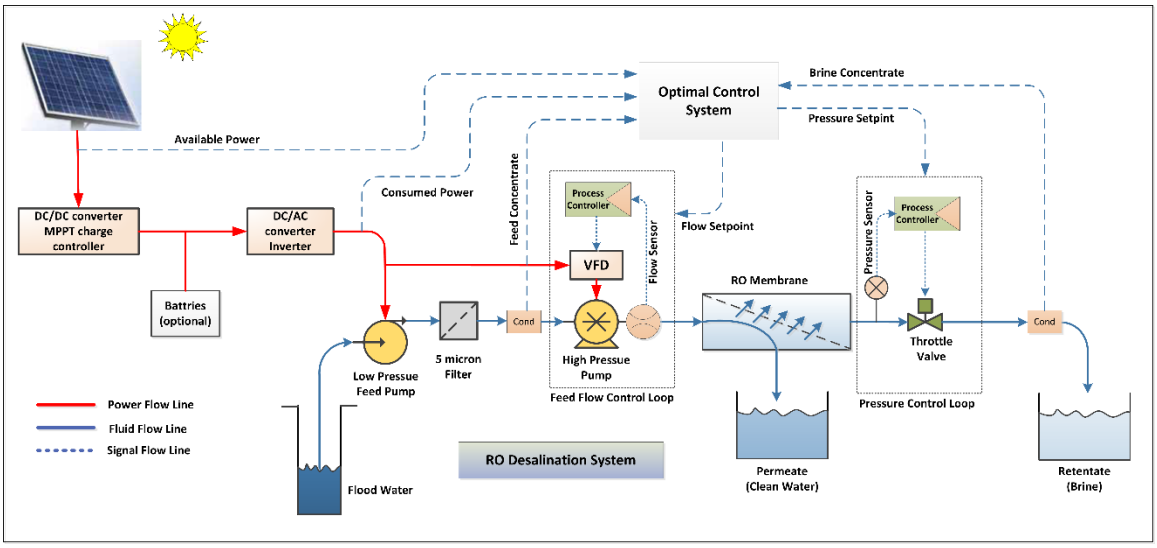

Figure 4.39: Control structure of PVRO system with optimal set point generation

4.8.1 Feed and pressure reference signals for fixed PV panels

Optimal control system will compute the reference feed and pressure signals for the local controllers. For the fixed PV panels and constant pressure methodology, these reference signals are computed and shown in the Figure 4.40. In this plot details of the sunshine time, usable and unusable range by CP are provided. Within the usable range pressure and feed flow signals are shown. Obviously during this operation the pressure signal will be constant at 61.4 bar but feed flow signal will start at 6.9 m^3/h and will increase up to 10.8 m^3/h (solar noon) and then it will decrease to low value. The pressure signal will be used to manipulate the brine valve position to adjust the system pressure whereas the feed flow signal will be used to manipulate the speed of the pump to ensure the requested feed flow rate.

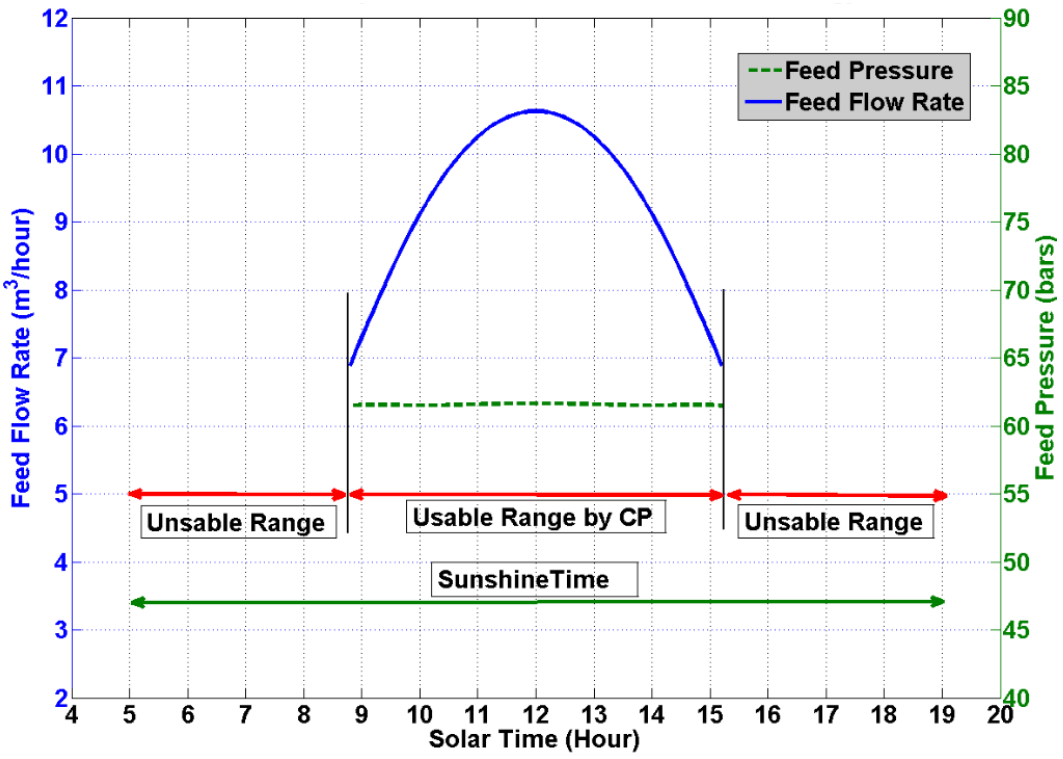

Figure 4.40: Feed and pressure set points for constant pressure method, fixed PV panels

For the fixed PV panels and constant permeate recovery methodology, the feed and pressure reference signals are computed and shown in the Figure 4.41. In this plot details of the sunshine time, usable and unusable range by CRR are provided. Within the usable range pressure and feed flow signals are shown. During the operation the pressure signal starts from 44.2 bar and increases up to 61.4 bar (at noon time) and then decrease to low value. The feed flow signal will start at 3.5 m^3/h and increases up to 10.8 m^3/h (solar noon) and then it will decrease to low value. These two signal are manipulated in such a way to keep the RR constant. The pressure signal is used to manipulate the brine valve position to adjust the system pressure whereas the feed flow signal will be used to manipulate the speed of the pump to ensure the requested feed flow rate. For the fixed PV panels and combined methodology, the feed and pressure reference signals are computed and shown in the Figure 4.42. In this plot details of the sunshine time, usable and unusable range by CP and CRR are provided.

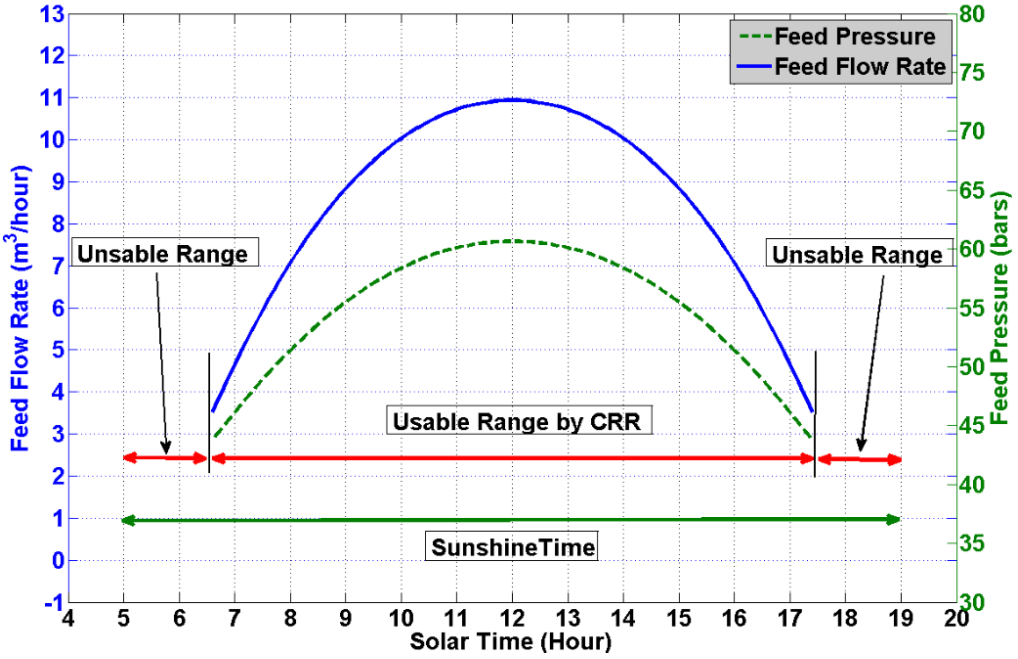

Figure 4.41: Feed and pressure set points for constant recovery method, fixed PV panels

Within the usable range, pressure and feed flow signals are shown for the CP and CRR methodologies. In this combined mode of operation the system will start in constant RR mode. In this operation the pressure signal starts from 44.2bar and increases up to 54.4bar (at 8:40am). The feed flow signal starts at 3.5 m^3/h and increases to 8.2 m^3/h (at 8:40am). After 8:40am the system will switch to constant pressure mode and feed pressure will make a step input form 54.4bar to 61.4bar and this value persists until 3:20pm. During the switching the feed flow rate will reduce from 8.2 to 7.08 m^3/h, then this value will increase to maximum value at 10.8 m^3/h (at noon time) and then it will decrease to 7.08 m^3/h at 3:20pm. After 3:20pm the system will switch from CP to CRR mode. During this switching process, pressure will be reduced and feed flow rate will be increased. During the CRR mode of operation both pressure and feed flow rate has the decreasing trend until its operational range is finished. In the combined methodology, pressure signal profile is used to manipulate the brine valve position to adjust the system pressure whereas the feed flow signal will be used to manipulate the speed of the pump to ensure the requested feed flow rate.

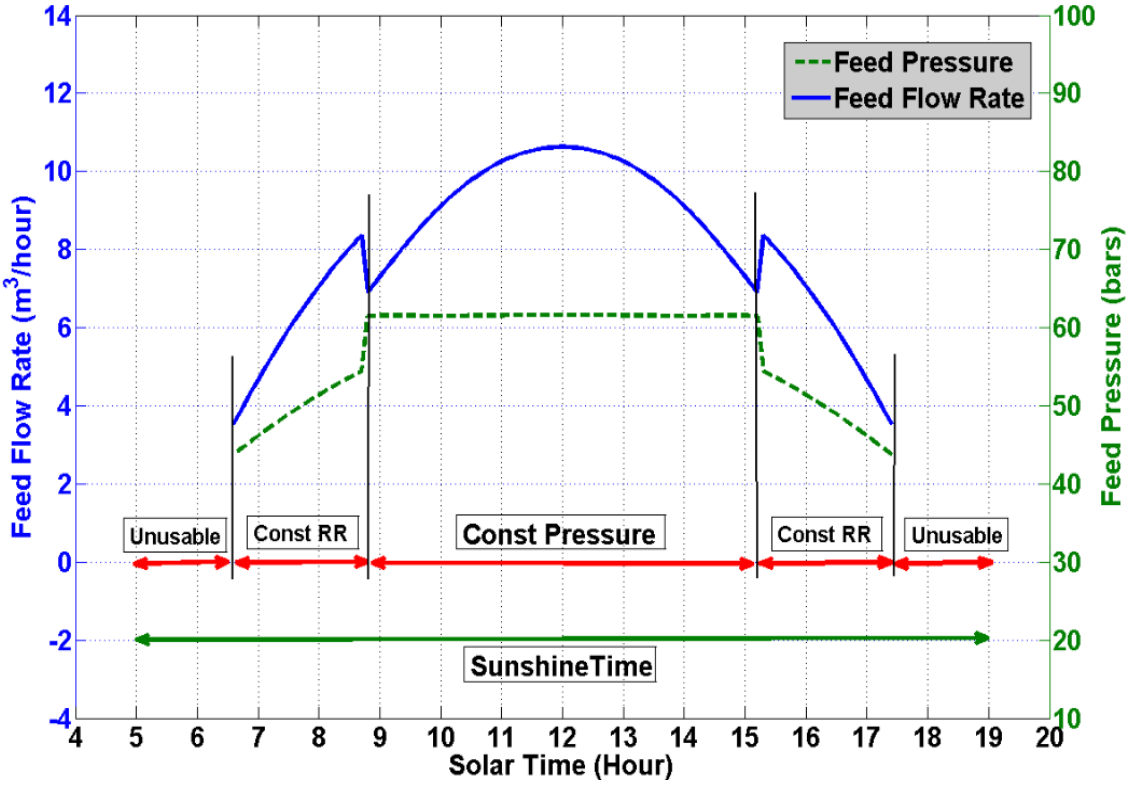

Figure 4.42: Feed and pressure set points for combined method (CP+CRR), fixed PV panels

4.8.2 Feed and pressure reference signals for single axe tracking PV

For the single axis tracked PV panels and constant pressure methodology, pressure and feed flow rate reference signals are computed and shown in the Figure 4.43. In this plot details of the sunshine time, usable and unusable range by CP are provided. Within the usable range pressure and feed flow signals are shown. Obviously during this operation the pressure signal will be constant at 61.4 bar but feed flow signal will start at 6.9 m^3/h and will increase up to 10.8 m^3/h (peak power at 10:30 m) and then it will decrease to low value 9.9 m^3/h (at solar noon). The feed flow rate profile exhibits two peaks one before the noon time and other after and resembles the PV power profile. The pressure signal will be used to manipulate the brine valve position to adjust the system pressure whereas the feed flow signal will be used to manipulate the speed of the pump to ensure the requested feed flow rate.

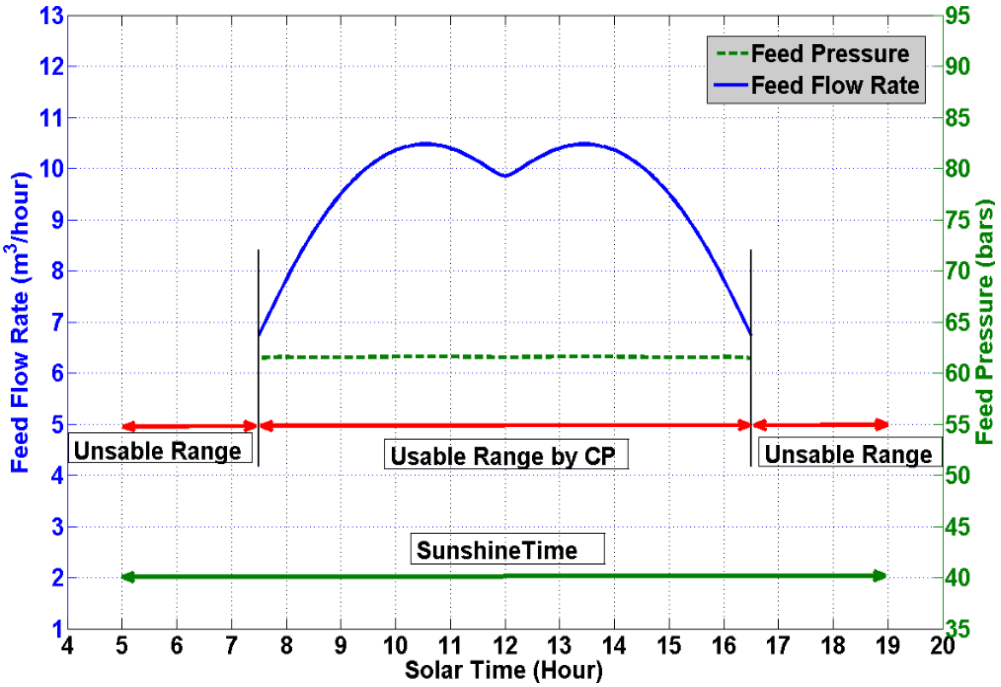

Figure 4.43: Feed and pressure set points for constant pressure method, single axe PV tracking

For the single axis tracking PV panels and constant permeate recovery methodology, the feed and pressure reference signals are computed and shown in the Figure 4.44. In this plot details of the sunshine time, usable and unusable range by CRR are provided. Within the usable range pressure and feed flow signals are shown. During the operation the pressure signal starts from 44.2 bar and increases up to 61.4 bar (at 10:30 am) and then decrease to low value of 58 bar (at solar noon). The feed flow signal will start at 3.5 m^3/h and increases up to 10.9 m^3/h (at 10:30 am) and then it decreases to low value of 10.4 m^3/h (at solar noon). After solar noon, values of both signals increases and then decreases. These two signal are manipulated in such a way to keep the RR constant during the operation. The pressure signal is used to manipulate the brine valve position to adjust the system pressure whereas the feed flow signal will be used to manipulate the speed of the pump to ensure the requested feed flow rate.

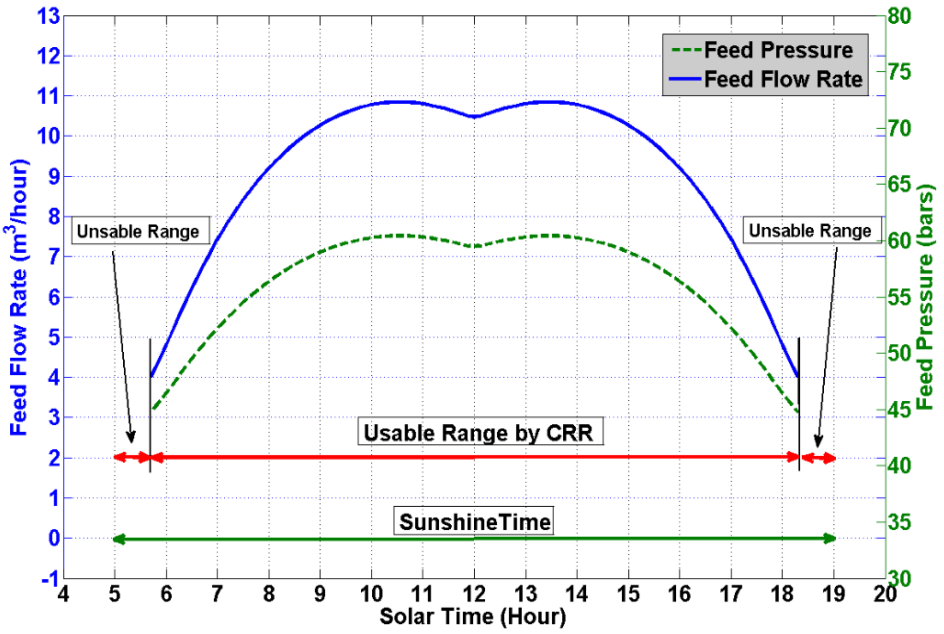

Figure 4.44: Feed and pressure set points for constant recovery method, single axe PV tracking

For the single axis tracked PV panels and combined methodology, the feed and pressure reference signals are computed and shown in the Figure 4.45. In this plot details of the sunshine time, usable and unusable range by CP and CRR are provided. Within the usable range, pressure and feed flow signals are shown for the CP and CRR methodologies. In this combined mode of operation the system will start in constant RR mode. In this operation the pressure signal starts from 44.2bar and increases up to 54.4bar (at 7:30am). The feed flow signal starts at 4.0 m^3/h and increases to 8.2 m^3/h (at 7:30am). After 7:30am the system will switch to constant pressure mode and feed pressure will make a step input form 54.4bar to 61.4bar and this value persists until 4:30pm. During the switching the feed flow rate will reduce from 8.2 to 7.08 m^3/h, then this value will increase to maximum value at 10.45 m^3/h (at 10:30 am) and then it will decrease to 9.8 m^3/h at solar noon. After 4:30pm the system will switch from CP to CRR mode. During this switching process, pressure will be reduced and feed flow rate will be increased. During the CRR mode of operation both pressure and feed flow rate has the decreasing trend until its operational range is finished. In the combined methodology, pressure signal profile is used to manipulate the brine valve position to adjust the system pressure whereas the feed flow signal will be used to manipulate the speed of the pump to ensure the requested feed flow rate.

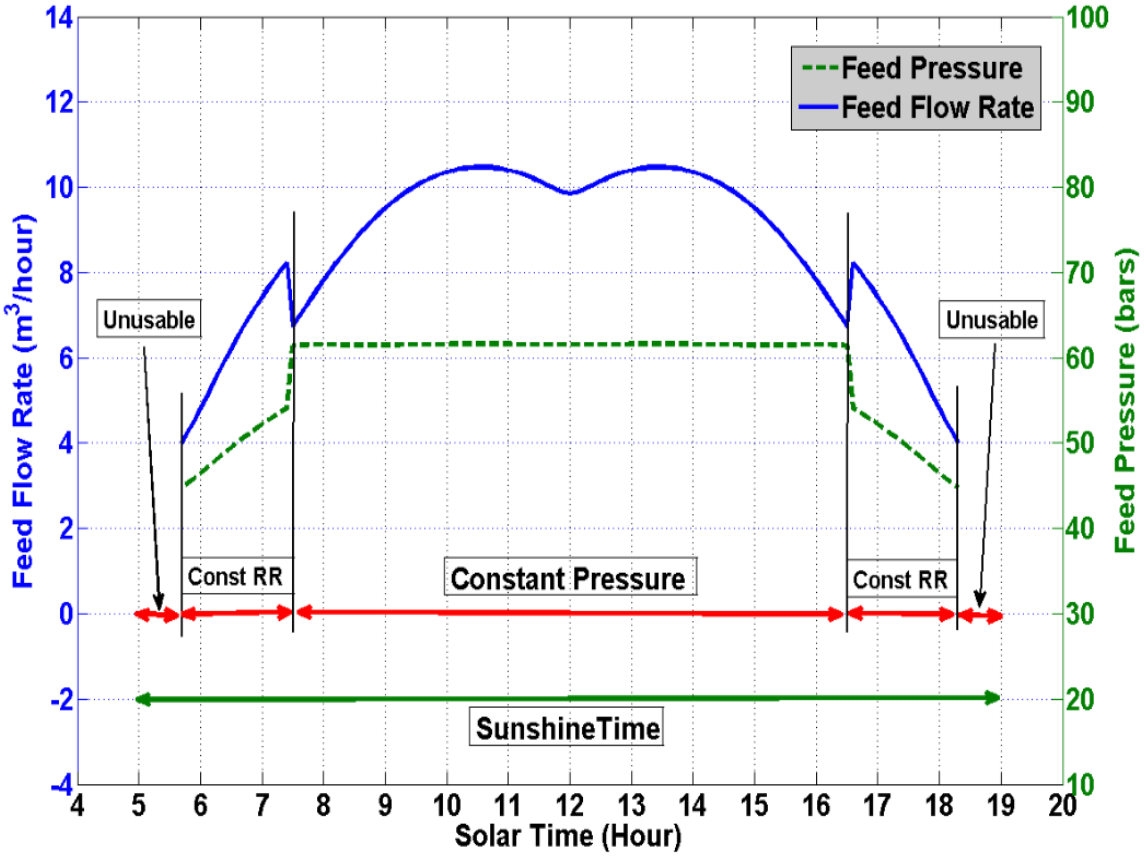

Figure 4.45: Feed and pressure set points for combined method (CP+CRR), single axe PV tracking

4.8.3 Feed and pressure reference signals for double axis tracking PV

For the double axis tracked PV panels and constant pressure methodology, the feed and pressure reference signals are computed and shown in the Figure 4.46. In this plot details of the sunshine time, usable and unusable range by CP are provided. Within the usable range pressure and feed flow signals are shown. Obviously during this operation the pressure signal will be constant at 61.4 bar but feed flow signal will start at 6.9 m^3/h and will increase up to 10.8 m^3/h (solar noon) and then it will decrease to low value. The pressure signal will be used to manipulate the brine valve position to adjust the system pressure whereas the feed flow signal will be used to manipulate the speed of the pump to ensure the requested feed flow rate.

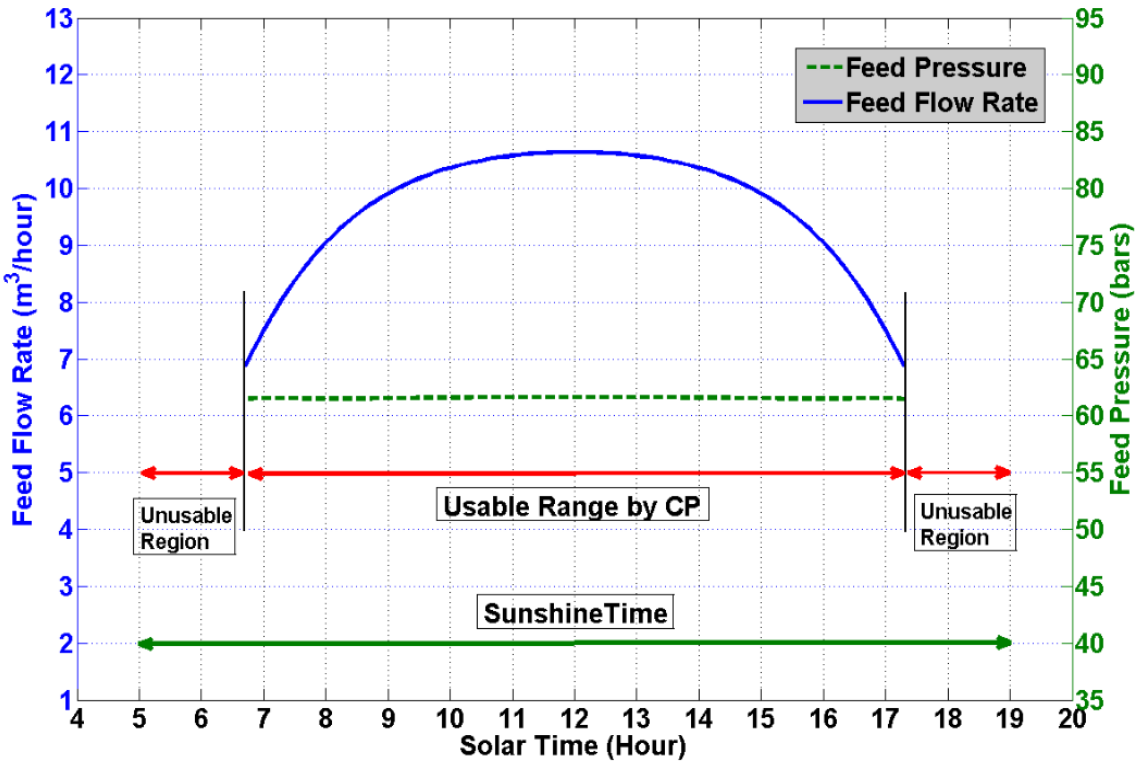

Figure 4.46: Feed and pressure set points for constant pressure method, double axis PV tracking

For the double axis tracked PV panels and constant permeate recovery methodology, the feed and pressure reference signals are computed and shown in the Figure 4.47. In this plot details of the sunshine time, usable and unusable range by CRR are provided. Within the usable range pressure and feed flow signals are shown. During the operation the pressure signal starts from 45.2 bar and increases up to 61.4 bar (at noon time) and then decrease to low value. The feed flow signal starts at 4.1 m^3/h and increases up to 10.8 m^3/h (solar noon) and then it decrease to low value. These two signal are manipulated in such a way to keep the RR constant. The pressure signal is used to manipulate the brine valve position to adjust the system pressure whereas the feed flow signal will be used to manipulate the speed of the pump to ensure the requested feed flow rate.

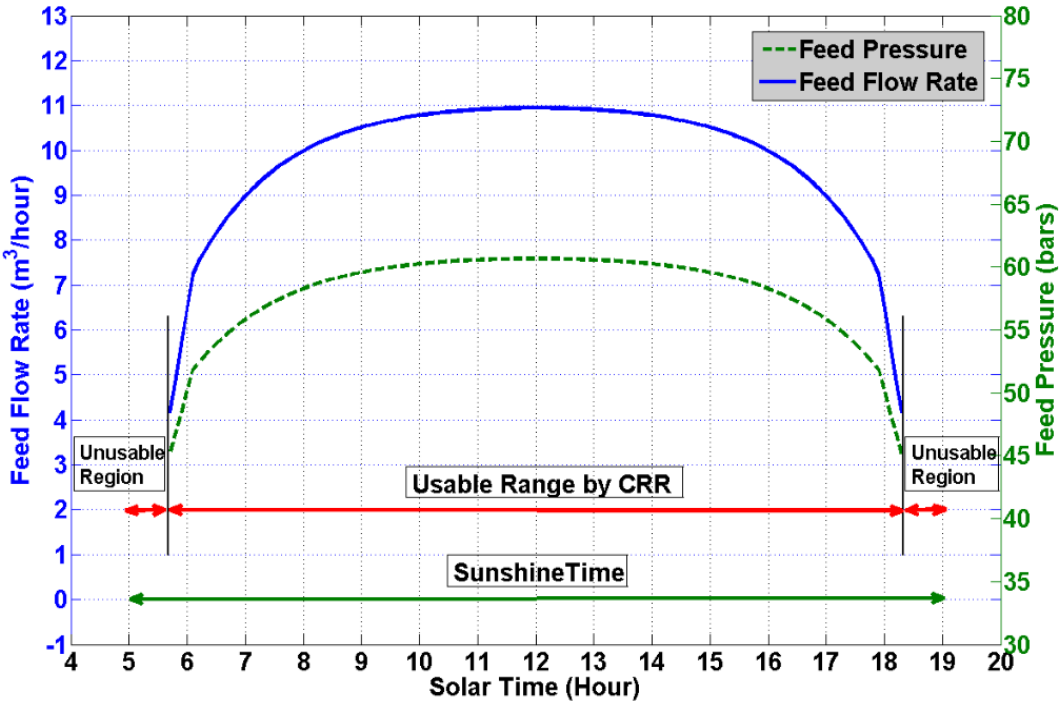

Figure 4.47: Feed and pressure set points for constant recovery method, double axis PV tracking

For the double axis tracked PV panels and combined methodology, the feed and pressure reference signals are computed and shown in the Figure 4.48. In this plot details of the sunshine time, usable and unusable range by CP and CRR are provided. Within the usable range, pressure and feed flow signals are shown for the CP and CRR methodologies. In this combined mode of operation the system will start in constant RR mode. In this operation the pressure signal starts from 44.2bar and increases up to 54.4bar (at 6:40am). The feed flow signal starts at 4.3 m^3/h and increases to 8.2 m^3/h (at 6:40am). After 8:40am the system will switch to constant pressure mode and feed pressure will make a step input form 54.4bar to 61.4bar and this value persists until solar noon time. During the switching the feed flow rate will reduce from 8.2 to 7.08 m^3/h, then this value will increase to maximum value at 10.8 m^3/h (at noon time) and then it will decrease to 7.08 m^3/h at 5:20pm. After 5:20pm the system will switch from CP to CRR mode. During this switching process, pressure will be reduced and feed flow rate will be increased. During the CRR mode of operation both pressure and feed flow rate has the decreasing trend until its operational range is finished. In the combined methodology, pressure signal profile is used to manipulate the brine valve position to adjust the system pressure whereas the feed flow signal will be used to manipulate the speed of the pump to ensure the requested feed flow rate.

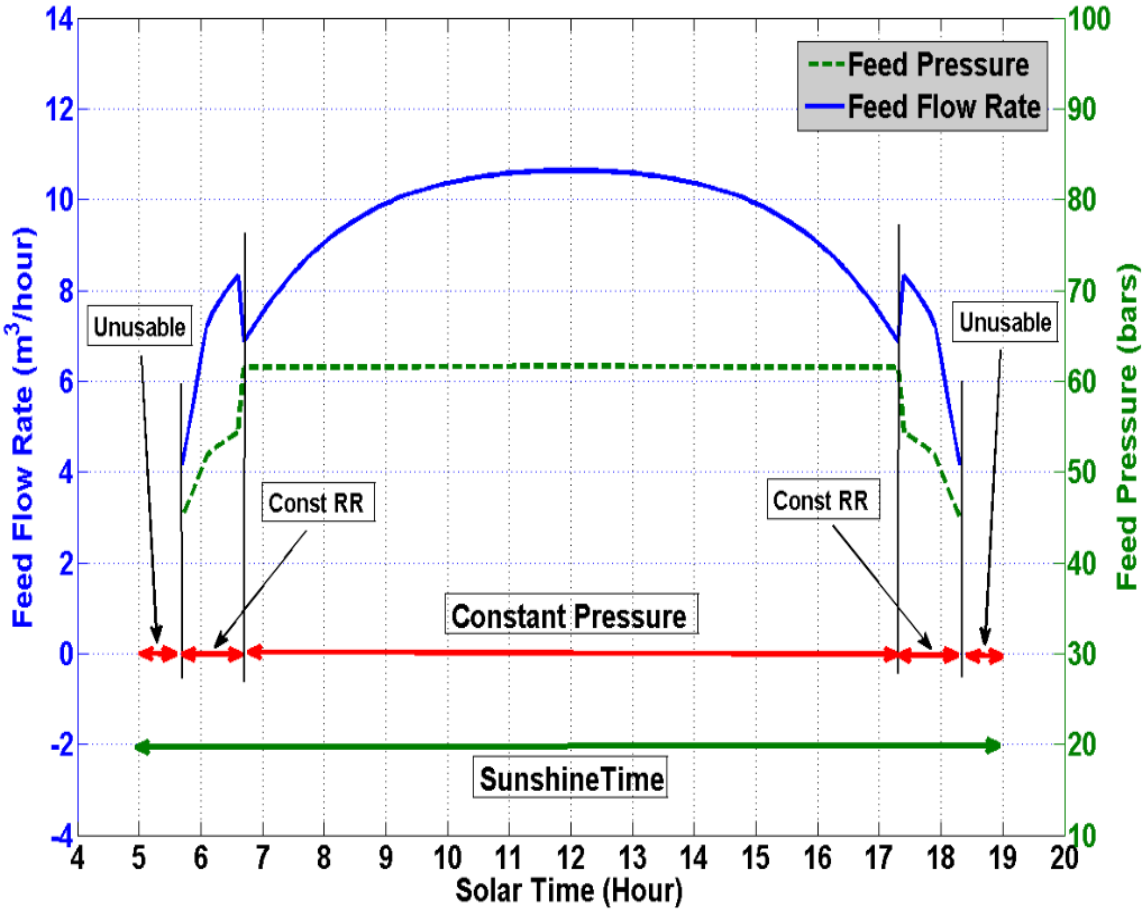

Figure 4.48: Feed and pressure set points for combined method (CP+CRR), double axis PV tracking

4.9 Summary

The purpose of this work is to make a parametric analysis of PVRO system for its optimal operation that would minimize the SEC and utilize the complete range of available PV power during the whole day. A complete mathematical model is carved out and simulated by satisfying the various constraints provided by the membrane manufacturer to determine the different operational limits of RO system. The variation of the hydraulic/process parameters within the operational window causes the change in power consumption. Four different operational methodologies are investigated for SEC while considering the feed, retentate and permeate flow rates and their salinities and permeate recovery ratio. The permeate flow rate for all the methodologies with different PV tracking options are discussed. Moreover the feed and pressure reference signals for control system applications are determined for all methodologies under different PV tracking options.

- The constant feed pressure methodology exhibits the smallest usage of PV available energy.
- The constant recovery ratio and constant retnetate flow rate topologies offers the broadest usage of PV available power range.
- The constant feed pressure and constant recovery ratio methodology offers low specific energy consumption over their respective PV power ranges.
- Constant feed flow rate topology exhibits the largest SEC for the lower PV energy and offers no significant advantage over the other methodologies.

By taking the consideration of SEC, wide range of PV energy, feed flow and pressure variation and permeate quality, the constant recovery ratio operational methodology seems to be the good selection choice to drive the RO system with varying

PV output especially when sun trackers are not installed. For the tracking PV panels, installed with single or double axis trackers, PV power variation is reduced and constant pressure methodology is more attractive. The feed and pressure set points of RO system are calculated based upon the selected operational methodology and available PV power (fixed PV, single or double axis tracked panels) profile and then are used to drive the local feed and pressure control loops to drive the RO system.

Chapter 5

Environment friendly aspects

Surface water suck from the sea or any well to be processed by the PVRO desalination system contains organic matter, which comprises living or dead particulate material and dissolved molecules, leads to the biological growth and causes biofilm within the system [117]. Therefore feed water is disinfected with the help of biocides. Most common biocide in RO systems is chlorine and concentration of up to 1 mg/L is sustained by a continuous dosage in the feed water. The removal of suspended solids is essential for a good membrane performance. For this purpose coagulants and poly-electrolytes are added for coagulation-flocculation and resulting flocs are hold back by dual media sand anthracite filters. Coagulant substances are ferric chloride, ferrous sulphate and ferric chloride sulphate or aluminum chloride. To sustain the efficiency of the filters, they are backwashed regularly [117].

The main scale forming species in RO systems are calcium carbonate, calcium sulphate and barium sulphate. Acid treatment and anti scalant dosage are used for scale control. Sulphuric acid is commonly used but alternative use of anti scanlants such as plyphosphates or polycarbonic acid has become very common in RO systems. Low concentrations of about 2mg/l are sufficient. After the pre prefiltration residues of the chlorine added for the disinfection are present and it can damage the RO membrane. It is vital to remove this chlorine by the dechlorination. The removal of chlorine is performed with sodium bisulfite, which is continuously added to reach a concentration three to four

times higher than the chlorine concentration. After the filtration process by the RO permeate is disinfected (any living organism is destroyed), pH is adjusted and remineralized (addition of some salts) to improve its quality. The additives of the conventional RO process are depicted out is the following Figure 5.1 at each stage.

The common sea water/brackish contaminants and their removal method along with their advantages and disadvantages are summarized in Table 5.1.

Table 5.1: Conventional water treatment and its environmental effects [118]

Water Contaminants	**Removal Method**	**Advantages**	**Disadvantages (Environmental Effect)**
Biological Contaminations	Disinfection, filtration to remove systs/nutrients	Effective removal, upto 99%	By products of chlorine, unreacted chlorine, Brine Disposal
Dissolved/suspended solids	Flocculant, Coogulant, Softners	Easily available, reliable	Chemical waste of $FeCl_3$, etc.(chlorides, acids) in back wash
Metals/Minerals	Iron Filters, Softners, RO, Antiscalant	Reduce Brine wastewater	Chemical waste in brine, volumes needed.
Scaling	Antiscaling (Anticarbonic Acid)	Cheaper, reduces brine waste by antiscaling the membrane	Permeate have some antiscalant. Needs some acid dosing to prevent biofouling
Organic compounds	Membrane Bioreactor, RO	MBR is natural removal	Time and maintain ideal conditions, unpleasant odor

Significant amount of research has been carried out to identify the new methods of purifying water which have the following properties [119].

- Lower cost and consumes less energy
- Minimizing the use of chemicals
- Without stressing the environment
- Without endangering the human health by treatment itself.

Based upon these objectives following design is proposed and studied.

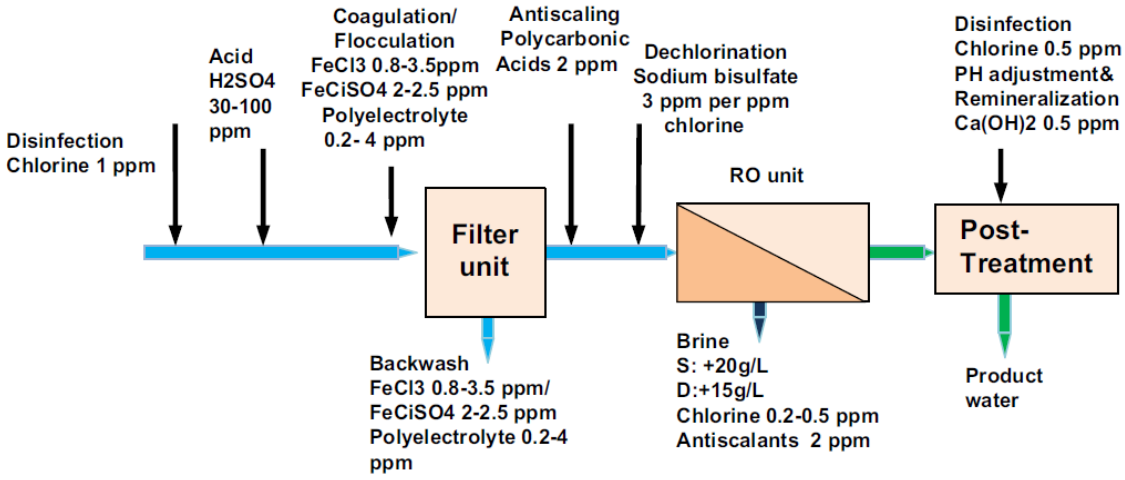

Figure 5.1: Conventional dosing of chemicals for disinfection [117]

5.1 UF and NF pretreatment with backwash utility

Based on the literature survey it is evident that state of the art PV RO community scale systems could be developed by carefully identifying the components needed and assembled and optimizing its various function as well as an integrated system for minimum environmental impacts. As a first step of filtration pre-treatment microfiltration (MF) can be applied to remove colloids and suspended matter larger than 0.1 μm. For metal membrane MF system ozone backwashing is applicable having proven to be more effective than permeate or air backwashing [119].

Ultrafiltration (UF) can be an effective pre-treatment against fouling of RO membranes as it retains colloids and dissolved organics. Depending on the operation scheme, a benefit for the environment is the reduction of RO membrane cleaning frequency consequently it will reduce the consumption of chemicals [120]. Another benefit of UF filtration is the elimination of chlorine, sodium bisulfite for dechlorination and coagulants (which are normally used in conventional filtration process) [121]. If the UF membrane is backwashed regularly and thoroughly with permeate, the use of chemicals both in the UF and the RO step can be eliminated completely [122].

Nanofiltration (NF) removes very fine suspended matter and residual bacteria, but above all it is a water softening treatment as it retains divalent ions. As these ions, e.g. Ca^{2+} and SO^{2-}, contribute significantly to scaling, nanofiltration prevents the formation of scales and replaces the conventional softening treatment [123]-[124]. Nanofiltration can be considered as revolution in scale inhibition, as it prevents scale formation like no other treatment method [125]. Such a system was studies and reported that 95-99% removal of additives from feed water is observed in experiments but 20-30% more investment is

required in NF-UF pre filtration and backwash equipment [126]. Moreover it consumed 20-30% more energy in NF UF pre filtration and backwash process. Therefore the design concept of pre-treatment filtration is shown in Figure 5.2. UF and NF filter cleaning can be carried out effectively by backwashing without chemicals. The salient features of UF and NF based prefiltration system is as follows.

- Nano-filtration system eliminates colloids, viruses and hardness. As these ions are largely removed no antiscalants are necessary.
- The nano-filtration system comprises a permeate buffer tank where the filter permeate is stored for membrane backwashing.
- Backwashing is the essential measure to retain the performance of the NF membrane and has to be done regularly with a sufficient backwash flow rate. The backwash brine is blended with the RO brine.

Pretreatment unit with backwash option needs an efficient control system to monitor the filtration performance. The control system will initiate the backwash process to recover the filtration performance of NF-UF filter. In this pursuit pressure and flow rates are sensed before and after the NF membrane and are monitored continuously.

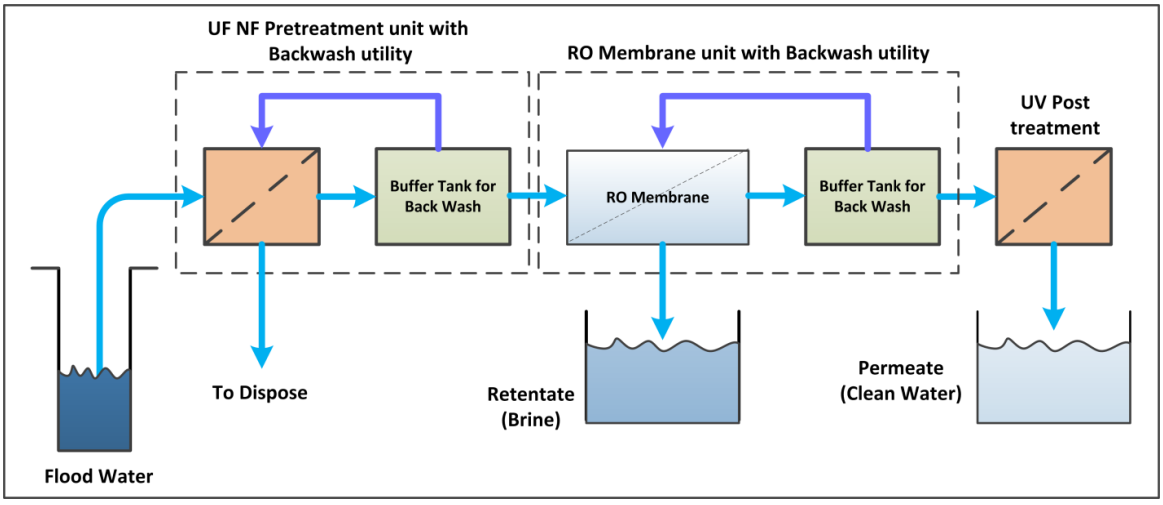

Figure 5.2: Environment friendly UF NF pretreatment system.

5.2 UV photo catalysis based pretreatment

Solar photo catalysis is an efficient method for the decontamination and disinfection of the polluted water. Solar photo catalysis aims at mineralizing the contaminants into carbon dioxide, water and inorganics, and treatment of industrial waste water seems to be one of the most promising fields of application of solar photo catalysis [127]. The solar photo catalytic detoxification process consists of making use of the near-ultraviolet (UV) band of the solar spectrum (wavelength shorter than 400 nm), to photo-excite a semiconductor catalyst in contact with water and in the presence of oxygen [128]. Hydroxyl radicals, OH^- produced due to the photo generated holes, attack oxidizable contaminants, are generated producing a progressive break-up of molecules yielding CO_2, H_2O and diluted inorganic acids.

Based upon the advantages of the solar photo catalysis based disinfection, it is envisaged to design a disinfection reactor for PV RO system (as well as standalone system when water only needs disinfection). In the design of reactor feed flow rate, exposure time to the radiation, process temperature, medium pH, turbidity, batch mode operation or continuous operation, concentration and type of pathogens in feed water and control aspects of the reactor are to be considered into account for its integration to the PV RO system. The potential use of UV disinfection at pretreatment and at post treatment is shown in the Figure 5.3. UV disinfection can be completely solar assisted through custom developed disinfection units, or to use a commercially available UV sterilizer light.

A lot of research and development efforts have been carried out in the field of semiconductor photo catalysis for disinfection of water especially by considering the sustainability and environment friendly aspects into account. Nano catalysis using solar UV radiation is one of the potential techniques for this emerging application. In this work solar based photo reactor of different geometries and configurations for the disinfection of waste water has been designed and tested. In this context mainly two types of solar photo reactor have been investigated, stair type open exposure and concentrated solar radiation reactors. In the stair type reactor stairs are coated with TiO_2 using sole gel method whereas in the parabolic type concentrator titania coated rod is used as photo reactor. In the testing of reactors, bacterial inactivity, exposure time and irradiation are closely monitored. Water samples are collected at different intervals to investigate the bacterial deactivation. Contrary to commercial slurry based photo reactor, thin film titania coated reactors have been introduced in this work. Moreover detailed designed aspects of the reactors, process parameters and reactor working are presented.

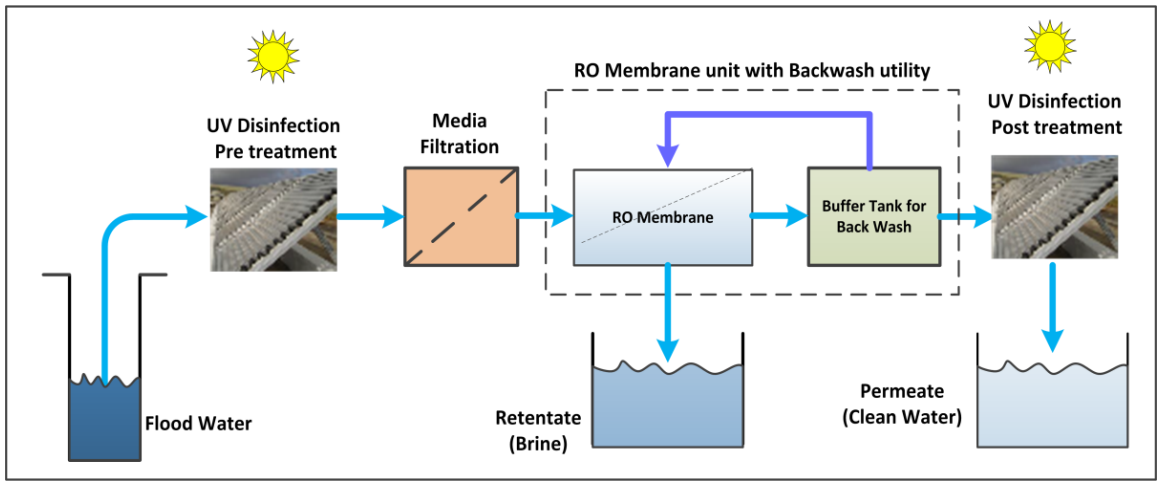

Figure 5.3: Solar UV disinfection at pretreatment and at post treatment

5.3 Fundamentals of photocatalysis

The long term consequences of the conventional decontamination and disinfection treatments have necessitated the rapid research and development in the field of "Advanced Oxidation Processes (AOP)" as innovative water treatment technologies [129]. This process involves the generation of highly reactive species e.g., hydroxyl radical ($OH^{\bullet}$), H_2O_2 and $O_2^{\bullet -}$, which mineralizes the organic compounds, disinfects the pathogens and other living organism. Many oxidation processes, such as TiO_2/UV, H_2O_2/UV and ozone (O_3, O_3/UV, and $O3/H_2O_2$) are currently employed for this purpose. The used of AOPs for water treatment has been studied extensively by UV radiation generated by UV lamps or ozone production but they are expensive [130]. So the future applications of these processes could be improved through the uses of catalysis by solar energy. Therefore, research is focusing more and more on those AOPs which can be driven by solar irradiation, photo-Fenton and heterogeneous catalysis with UV/TiO_2 [130]. Among the semiconductor catalysts, titanium dioxide (TiO_2) has received the greatest interest in R&D of photo catalysis technology. The TiO_2 is the most active photo catalyst under the photon energy of 300 nm$< \lambda <$ 390 nm and remains stable after the repeated catalytic cycles, whereas CdS or GaP are degraded along to produce toxic products. Titania slurry based bacterial disinfection using compound parabolic concentrator is reported in [131] and by using stair photo catalytic reactor is provided by [130]. The main disadvantage of slurry based photoreaction after the successful disinfection process is to remove the slurry by post treatment filtration process. In our work a thin film is coated photo reactor in stair case and compound parabolic reactor is introduced. In the stair case design all the stairs are coated with titania thin film where as a titania coated rod is used as photo reactor in parabolic

concentrator design. During the photo catalytic disinfection process with supported titania, the equipment does not require any post filtration process, consequently the whole apparatus is simple and economical to use.

In our both reactors the disinfection process is carried out by solar radiation. Solar radiation spectrum contains 52% infrared, 43% visible light and 5% ultraviolet radiation [130]. This meager amount of 5% ultraviolet radiation collection is primarily used for photo catalysis disinfection purpose. This spectrum lies in the region of 400nm to 300nm wavelength. Hence one requires the systems that collect more sunlight (consequently more UV light) to enhance the photo catalysts activity for disinfection process. Design and development of both type of reactors, non-concentrating and with concentrating capability is carried out and experimental results are presented and analyzed.

The photo catalytic process for decontamination and disinfection is carried out in the presence of semiconductor photo catalyst (TiO_2, ZnO_2), a UV light source and oxygen or air as an oxidizing agent. The photons from the solar radiation with energy greater than the band gap energy (ΔE of TiO_2) is illuminated onto its surface, it excites the lonely valance band electron to the conduction band in femtosecond. This photonic excitation leads to the formation of a positive hole (h+) in the valence band and an electron in (e-) in the conduction band. The positive hole oxidizes either the water molecules to produce the hydroxyl radicals (OH) or organic contaminants directly. Electron in the conduction band causes the reduction of the absorbed oxygen on the photo catalyst layer.

From the first studies to date, there seems to be a consensus in the mechanism of destruction of bacteria by photo catalysis. For the photo catalysis disinfection process, the microorganism outer wall is thought to be first site of attack by highly reactive hydroxyl

radicals. Rapid leakage of potassium ions from the bacteria parallel to the decrease in cell viability was reported by [132]. Maness reported results that can be explained by peroxidation of the polyunsaturated phospholipid component of the cell membrane leading to a loss of essential cell functions, e.g., respiratory activity, and in the end, to cell death [133]. In another literature cell inactivity is explained that damage takes place on the lipopolysaccharides layer of the external cell wall and on the peptidoglycan layer. Next the peroxidation of the lipid membrane (the radicals oxidize to fatty acids), the oxidation of the proteins membrane (amino acids) and of polysaccharides take place, consequently leading to cell death [134].

5.4 Experimental setup

5.4.1 Non-concentrating or stair type collectors

Non-concentrating stair type or flat plate collector is one sun collector and they are the cheapest among all other type of collectors because they do not concentrate the radiation. They have no moving parts i.e. sun tracking system and moving support mechanisms. Due to the simple design, the manufacturing costs are lower, low capital cost and reduce operational maintenance. Stair type or flat plat collector requires simple support structure and case reactor is shown in the following Figure 5.4.

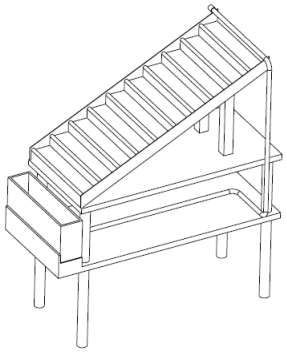

Figure 5.4: Wire frame model of the stair case photoreactor design

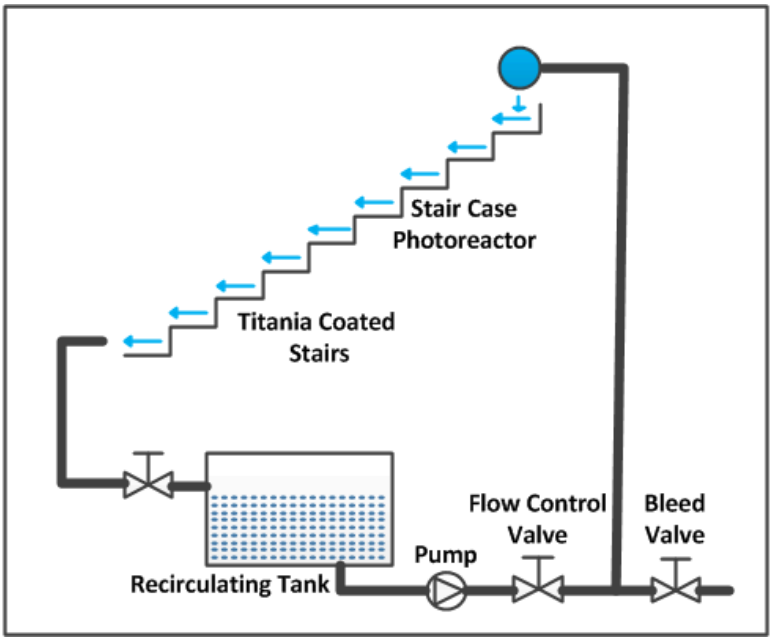

Figure 5.5: Process flow schematic of stair case photoreactor design

Figure 5.6: Experimental setup of stair case design

Stairs and its support surfaces along with water storage rectangular vessel are made of stain less steel. The reactor may be covered with Pyrex glass (UV transparent) to protect it from the environmental dust and to inhibit the water evaporation. Solar radiation collector area of the photo reactor is 7500cm^2 and in mounted on a portable table top surface. The table top surface has the provision to be tilted and it is usually kept as the latitude of the site for maximum collection of direct radiation. Although one-sun collector designs possess important advantages, the design of a robust one-sun photo reactor is not trivial, due to the need for weather-resistant and chemically inert ultraviolet-transmitting reactors [130]. Moreover non-concentrating flat plate collector systems require significantly more photo reactor area than other concentrating designs. Consequently large scale commercial system is envisaged to be designed to bear the operating pressures of the fluid during operation. Flat plate collector design are simple, robust, and economical in manufacturing and be able to withstand the fluid pressure during operation. Salient feature of the designed and manufactured stair case one sun collector are following. The dimensions of the each stair are 50, 10.2 and 5.14cm in length, width and height respectively. To cover the area of 7500cm^2, 10 stairs are fabricated and wire frame drawing is shown in the Figure 5.4. Stairs angle is set according to the latitude of the site, 26.08^o degrees due south for the maximum collection of solar radiation. A complete flow control mechanism for water flow is devised and installed in the system as shown in the Figure 5.5. Installed pump circulates the water throughout the whole reactor whereas the flow control valve is used to regulate the water flow for continuous mode of reactor operation. The complete experimental setup ready for experimental run is illustrated in the Figure 5.6.

5.4.2 Concentrating collectors

The parabolic trough collector consists of a structure that contains reflective concentrating parabolic surface. An absorber tube is fixed to at the geometrical focal line of the parabolic trough on which all the reflected radiation is concentrated. The structure is usually driven by one axis to two axis servo motors for active sun tracking to keep the parabolic collector aperture perpendicular to the solar radiation. The solar radiation reaching the ground level without being scattered or absorbed are known as direct radiation, while the radiation which are scattered or absorbed before reaching the ground are known as diffuse radiation. The sum of direct and diffuse radiation is called global radiation. Figure 5.7 shows the path for direct solar radiation unit it enters the absorber tube for the photo catalytic process.

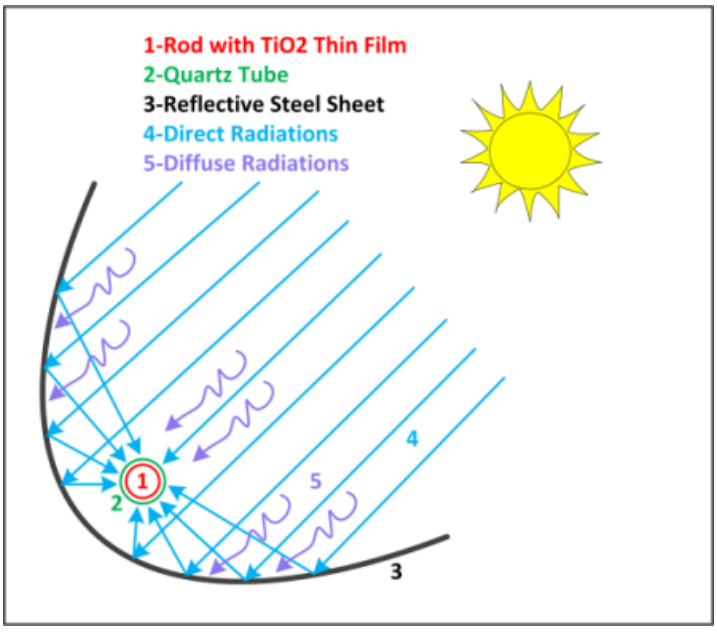

Figure 5.7: Parabolic concentrator photo reactor radiation path

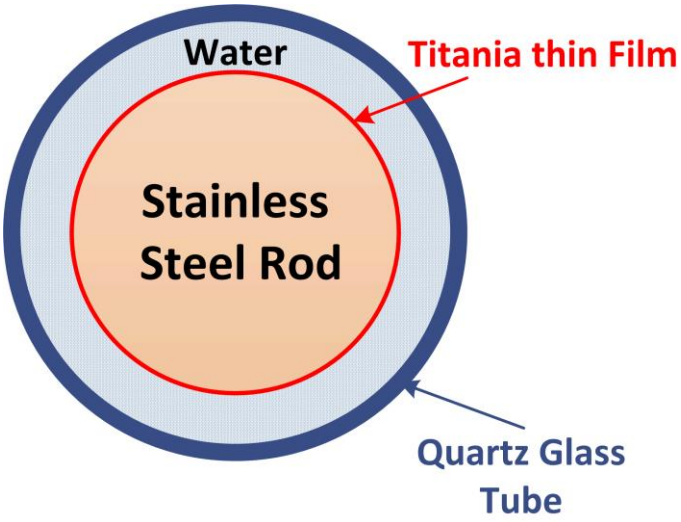

Figure 5.8: Details of thin film titania supported rod for PTC photoreactor

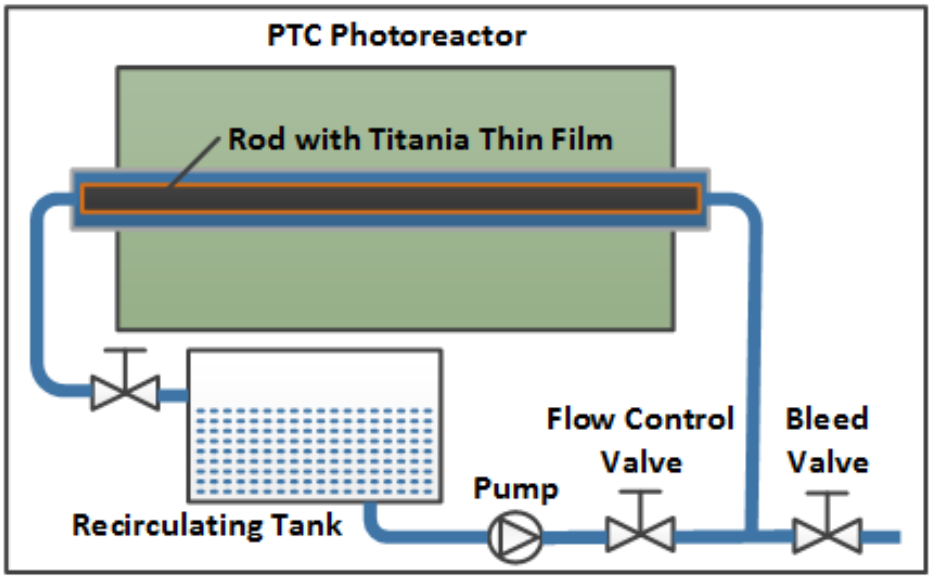

Figure 5.9: Process flow schematic of PTC photo reactor

Only the direct radiation falling on the collector surface would be able to be reflected and concentrated on the absorber tube. Two factors are considered to calculate the optical efficiency of the reactor, first the mirror reflectivity, second the UV transmisivity of the absorber tube material. Moreover the parabolic trough concentration factor (ratio of surface area of the parabola to the surface of the absorber tube Sp/Sa) must be taken into account. The global radiation are only collected by the absorber tube directly and are only affected by the transmisivity of the absorber glass tube. Within the glass absorber tube, a solid rod supporting titania thin film is inserted for the photo catalysis reaction and shown in Figure 5.8. To attain the better optic efficiency of the parabolic concentrator the ratio of the inner diameter of the tube to the diameter of the rod should be close to the refraction index of the introduced water. In our experiment (n=31.5/24.5=1.285), rod diameter is 24.5mm and the glass tube has the 36.5mm outer diameter with 2.5mm of rod thickness. For supported catalyst in these reactors a smaller amount of surface area is used for photo catalysis as compared to the nonconcentrating system for the same solar collector area. Major pros and corns of the two type of designed reactor are summarized in the Table 1. A water circulation mechanism and flow control aspects are designed and installed to operate the reactor in continuous or batch mode. The complete schematic of water flow control is shown in the Figure 5.9. Completer parabolic trough concentrator along with tracker system and flow control aspects ready for experiment is shown in Figure 5.10.

Table 5.2: Pros and corns of stair case and PTC photoreactor

	Advantages	Disadvantages
Stair type or Flat plate collectors	Makes use of direct and diffuse radiation Simple construction, low mfg. cost Low capital and maintenance cost No water heating High optical efficiency High quantum efficiency	Laminar flow of the fluid Covers more area Reactant contamination
Parabolic Concentrator	Turbulent flow(High mass transfer) practical use of supported catalyst Smaller reactor area (absorber tube area)	High cost due to sun trakcing High capital and maintenance cost High manufacturing cost Makes use of only direct radiation. Low optical and quantum efficiency. Tube and water is overheated

Figure 5.10: Experimental setup of parabolic trough concentrator for photocatalysis

5.4.3 Photocatalyst preparation

In order to investigate the effect of TiO_2 as a photo catalyst, a stable coating of the titania was deposited in both reactors. Uniform microstructure coating of TiO_2 on stairs (346L Steel) and on rod (304L Steel) was carried out by sole gel method using Tetra n Butyle Titanat (TBT) as alkoxide material. TiO_2 solution was prepared from TBT ($C_{16}H_{36}O_4Ti$) as a starting material. 91 mole % of ethanol (C_2H_5OH) and 2 mole % of ethyl aceto acetate (EAcAc, $C_6H_{15}O_3$) were mixed at room temperature and then 4 mole % of TBT was added. The formed solution was stirred for 8 hours continuously and aged for 24 hours to complete the reaction.

Steel stair structure and rod surfaces were prepared by grinding them with 1500 emery paper followed by polishing with $0.3\mu m$ Al_2O_3 powder. The surfaces were cleaned by ethanol and acetone and prepared them for dip coating. Steel rod was dipped into the solution for 10 seconds, removed back and allowed to dry at room temperature. Steel stairs were coated using pressurized spray gun to provide a thin layer of solution and dried at room temperature. After natural drying at room temperature, both photo reactors were heated at 150 ^{0}C for 30 minutes and then calcinated at 450 ^{0}C for one hour to remove the organic residuals. The prepared rod was inserted and fixed into the quarts glass tube. The tube and rod assembly was installed within the parabolic structure at its focal point.

5.4.4 Bacterial preparation and enumeration

E. coli K12 wild-type (MG 1655) bacteria was used in our studies due to its widespread used as a faecal indicator. First nutrient broth media were sterilized at 121 ^{o}C at 2 bar pressure for 30 min duration and then its 8 gram amount was dissolved into 1000 ml of distilled water (pH adjusted to 7.5). Later on 15 gram of nutrient agar was added to

the nutrient broth media and sterilized. The whole agar media was kept to cool down before pouring into petri dishes that is further used to test the bacteria. Single colony of bacteria was grown overnight in the nutrient broth at 37 ◦C on a rotary shaker (160 rpm). Aliquots of the pre-culture were inoculated into fresh medium and incubated. The culture was harvested by centrifugation at 4000 rpm for 15 min at 4◦C, washed twice with a sterile 0.9% NaCl solution at 4◦C to ensure the elimination of broth medium. Finally pellet was resuspended to a final concentration of $1x10^9$CFU/ml in sterile water. The calculated amount (one milliliter) of bacteria is added in the each liter of water used in the experiment to have the initial concentration of $1x10^6$ CFU/ml.

Viable cells of bacteria in the samples taken during the experiment were analyzed by plating them on nutrient agar plates after serial dilution in 0.9% saline. Colonies were counted after 18h incubation at 37^{o}C.

5.4.5 Photo catalytic bacteria removal studies

All the experiments were carried out under the sunlight having insolation 650-750 W/m^2 (700W/m^2 average) at Dhahran (Latitude 26.28 N, Longitude 50.21 W), Saudi Arabia. The stair type photo reactor was kept due south with inclination angle (26.28^o) equal to the latitude of the site where as the PTC was tracked to keep its aperture perpendicular to the sun during the experimental data acquisition. A centrifugal type pump was used to circulate the water from reservoir to the reactor continuously and flow control valve is used to adjust the water flow rate at 1.45L/min for both reactors.

At the start of experiment both reactors ware cleaned and 20 liter of filtered water was admitted into the reservoir tank of each reactor. 20 ml of cultured E.Coli bacteria was

added to the each reservoir tank and its water was circulated through the reactor for 10 minutes in the dark until the uniform bacterial concentration of 10^6CFU/ml was attained in the whole reactor. Each of the experiment is characterized as continuously stirred tank reactor in series with the plug flow solar photo reactor. The initial uniform bacterial concentration in each experiment was 10^6CFU/ml. At the beginning of each experiment, water sample was taken from the reservoir at t=0, photo reactor was uncovered and solar light was allowed to incident upon the collectors. The collected sample was marked and kept in the complete dark as a control throughout the whole experimental run to ensure that the bacteria die off in the samples was only due to the solar photocatalytic reactions and not from the other mechanism such as heat or any contamination etc. The water was recirculated in the reactor with sunlight exposure for two hours. Water samples were collected after every 20 minutes duration and taken directly to the laboratory for bacteria enumeration. It was ensured that the no bacteria die-off takes place outside the photo reactor tube. Each reactor was operated in continuous mode of operation. The average UV intensity in the solar radiation was taken the 5% of the whole solar spectrum and it comes out to be 30-35 W/m_2 at the site of experiment.

5.5 Results and discussion

Before we present the results, it is worth mentioning to describe the killing phenomenon of bacteria. the electron hole pairs, generated by photo excitation can move to the surface of semiconductor particle to form a highly oxidizing radicals like .OH (hydroxyl radical) and –O2 (super-oxide radical) and these radicals effectively oxidize the cell membrane and damage the microbial organism. The hydroxyl radical generate oxygen while H+ ions form hydrogen by capturing conduction band electrons. The super-oxide radical (-O2) and ($OH^{\cdot}$)

generated through solar radiation induced photo-catalysis process as described in equations (5.1-5.5) kill the bacteria in contaminated water i.e.

$$SC(semiconductorcatalyst) \xrightarrow{h\upsilon > E_g} SC(h_{vb}^{+} + e_{cb}^{-}) \tag{5.1}$$

$$H_2O + h_{vb}^{+} \rightarrow H_2O^{+} \rightarrow OH^{\bullet} + H^{+} \tag{5.2}$$

$$OH^{\bullet} + OH^{\bullet} \rightarrow H_2O + \tfrac{1}{2}O_2 \tag{5.3}$$

$$H^{+} + e_{cb}^{-} \rightarrow H^{\bullet} + H^{\bullet} \rightarrow H_2 \tag{5.4}$$

$$O_2 + e^{-}_{cb} \rightarrow O_2^{-\bullet} \tag{5.5}$$

Moreover the extent of microbial damage depends on how effectively the cell walls and cell membrane succumb to the oxidative process [135]. Data collected from the experimental runs in both reactors were plotted. Figure 5.11 and Figure 5.12 shows the survival of bacteria population (normalized values, actual bacterial concentration / initial bacterial concentration) as a function of time for the stair case and PTC reactor respectively. For the stair case photo reactor, it took about 20 minutes to disinfect the 28% of starting value of bacteria concentration. As the time progressed bacterial deactivation was increasing and approached to 93% after 140 minutes. Bacterial disinfection rate for PTC was faster than the stair case. Using the PCT 75% decrease in the deactivation of bacteria is observed in the first 20 minutes of the experiment and it approached to 97% after 140 minutes of photo activity. The initial fast decay in inactivation activity is attributed due to the high insolation flux at the photo reactor tube leading to more photo catalytic activity.

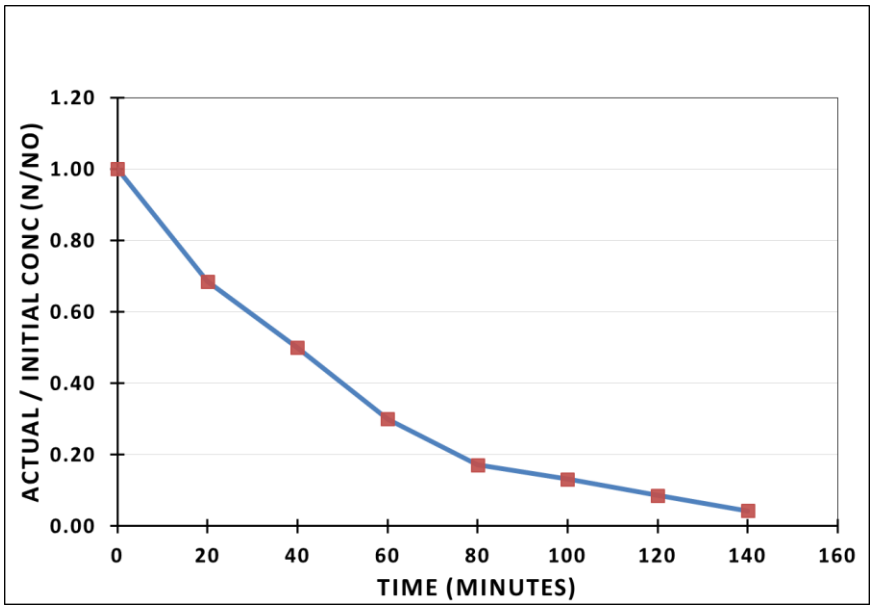

Figure 5.11: Bacterial disinfection activity in stair case reactor

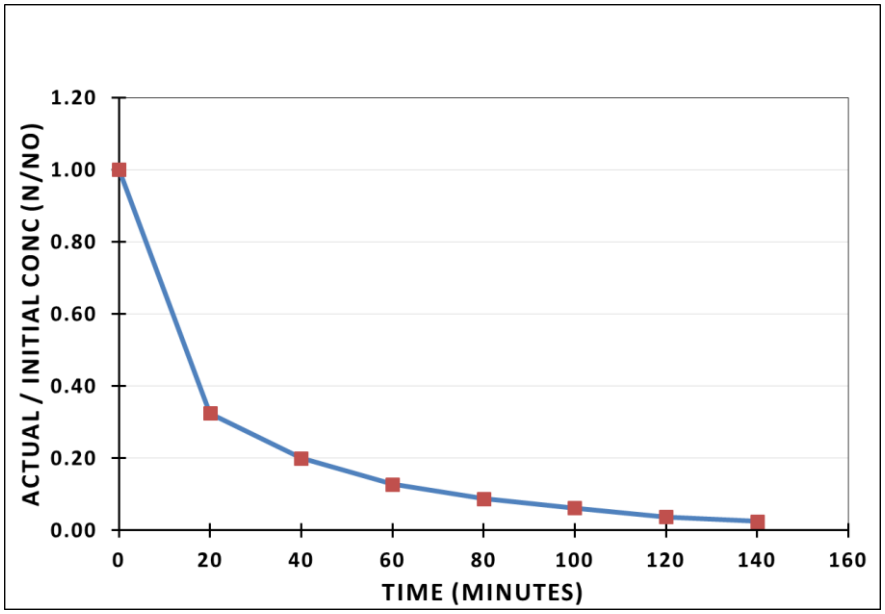

Figure 5.12: Bacterial disinfection activity in both parabolic trough concentrator

The bacterial inactivation against the cumulative solar UV radiation is also calculated according to the following relation.

$$Q_{UV_n} = Q_{UV_{n-1}} + \frac{\Delta t_n UV_{GN} A}{V_T}, \Delta t_n = t_n - t_{n-1} \quad (5.6)$$

In this equation Q_{UV_n} and $Q_{UV_{n-1}}$ are the cumulative received UV energy per liter in the samples at time n and $n-1$. Δt_n is the time interval between two collected samples. UV_{GN} is the average incident ultraviolet radiation on the photo reactor during the experimental run and its value is taken as 30 W/m^2. A is the irradiated area and V_T is the total volume (20 liters in each reactor) of the circulated fluid in the reactor. Figure 5.13 and Figure 5.14 shows the bacterial inactivation as a function of the cumulated solar UV radiation in the stair case and PTC photo reactors respectively. The plotted results reveal that PTC reactor performs more efficiently than the stair case reactor. The results showed that 1.75 kJ/l of UV energy is required to achieve 75% reduction of bacterial population whereas only 4.1 kJ/l of UV is required to produce the same result in stair case reactor. It should be noted that these results consider the difference in collector area (and thus solar UV radiation flux) between the CP and stair reactors. The cumulative dose of UV radiation is a function of both solar intensity and collector irradiated area, consequently providing the valid comparisons between both photo reactors.

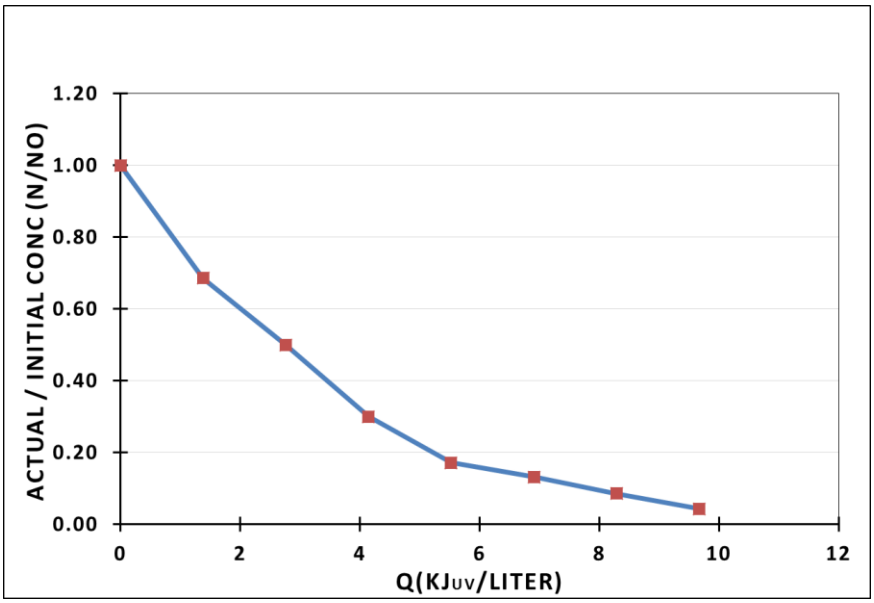

Figure 5.13: Survival of E Coli versus cumulative UV radiation for stair case reactor

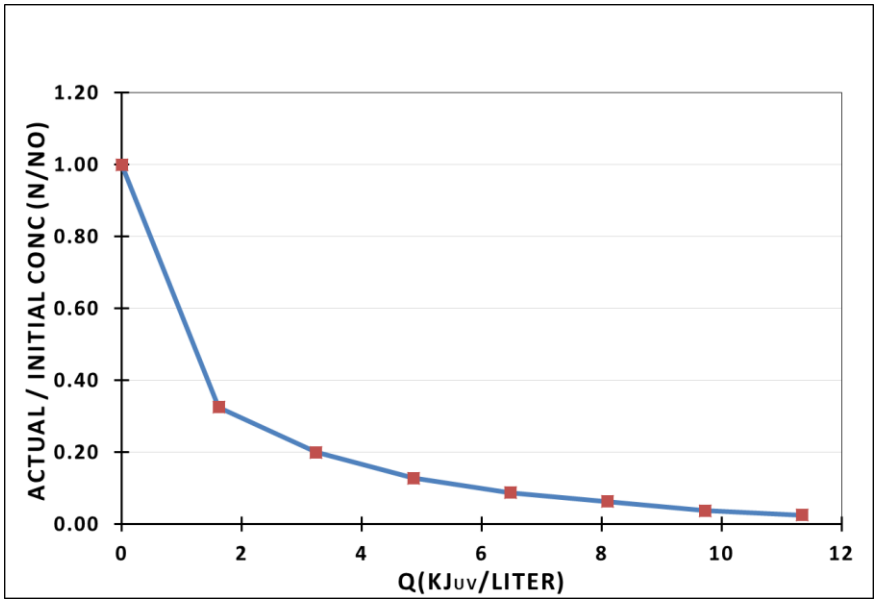

Figure 5.14: Survival of E Coli versus cumulative UV radiation for PTC Reactor

The temperature rise in the reactors during the experiment was observed from 25 C^0 to 31 C^0 in stair case reactor where as in parabolic reactor it increased from $25C^0$ to $40C^0$ degree. Literature shows that any temperature related die-off bacteria starts to have synergetic effect at minimum level of 45 ^{0}C [136]. The observed photo catalytic disinfection of the bacteria is due to the overall effect of solar irradiation and oxidant species produced by the supported titania in form of thin layer through photo catalytic process and not due to the rise of temperature.

These experiments clearly reveal the benefits of PTC photo reactor over the stair case one and confirms that the PTC profile is the optimum collector configuration for the disinfection purpose. The relative difference of these two collector geometries need some further investigation in terms of full/large scale implementation while considering the manufacturing/fabrication, reflective material quality, tracking cost and overall system cost.

5.6 Summary

Two solar disinfection photo reactors, stair case and parabolic trough concentrator (PTC) were designed, fabricated and demonstrated for disinfection of E Coli bacteria. The results reveal that adequate disinfection is attained using sunlight with the use of supported catalyst in both reactors. Both collector profiles in continuous mode of flow operation were evaluated, with the PTC demonstrating a clear advantage over the stair case in terms of disinfection efficiency. Experimental results reveal that 28% and 75% of the initial bacterial concentration is disinfected in stair case and PTC photo reactor respectively during the first 20 minutes of operation. Moreover results show that 1.75 kJ/l of UV energy is required to achieve 75% reduction of initial bacterial population whereas 4.1 kJ/l of UV is required to produce the same result in stair case reactor. The fast decay in inactivation activity in PTC is attributed due to the high insolation flux at the tube leading to more photo catalytic activity. The attained results was only for a single bacterial species and more work is envisaged to assess the photo catalytic disinfection process on other strains of bacteria and pathogenic organism i.e. protozoa and viruses.

Chapter 6

Concluding remarks and recommendations

6.1 Concluding remarks

- A comprehensive literature review is carried out that includes the introduction to PVRO system, its different components and its technical and economic feasibility in the solar radiation rich areas. Different installed PVRO systems in the various locations of the globe are explored in the literature review with the emphasis on their design configuration and control aspects. Based upon this literature review research objectives are determined.
- A customized design of PVRO system was manufactured and installed in the premises of KFUPM, Dhahran, Saudi Arabia.
- For the installed PVRO system, instrumentation, data acquisition along with graphical user interface is designed, developed and installed successfully for monitoring and performance evaluation purposes.
- Installed instrumentation in PV system encompasses the different sensors for the accurate measurement of the solar radiation, ambient temperatures, PV cell temperature, panel voltage and current at various points.
- Instrumentation at RO section encompasses the flow, pressure and conductivity sensors for the measurement of feed water flow rate, permeate flow rates and their pressures and salinities.

- The experimental investigation of installed PVRO system is carried out by using LabVIEW interface capabilities. The developed graphical user interface system reveals and stores the pronounced impact of measured variables of the PV output power and specific energy consumption of the RO filtration system. More than 18 different variable are measured and stored for the PVRO performance analysis.
- A detailed set of physics based models of whole PVRO system are meticulously developed. In photovoltaic system, solar radiation and PV generation modeling is done and investigation of the effect of fixed and tracking PV panel on the collected insolation and PV power is carried out. For the RO system, complete model of RO membrane is developed that estimates the feed water pressure and permeate flow rate.
- The developed PV and RO system modeling technique (independent PV and RO, and integrated PVRO) is validated using the KFUPM experimental PVRO facility.
- Validated PVRO model is used to study the effect of slope and azimuth angle of the PV panel on the permeate flow rate for the whole year. The increments in the clean water flow rate for the yearly tilt, monthly tilt, single and double axis tracking PV panels with respect to traditional flat panel are computed.
- It was revealed from the literature review that for community scale application the optimized RO network is single stage with single pass configuration. Within RO network, RO operational design space was determined by considering the RO membrane data provided by its manufacturer as membrane operational constraints. These constraints are the maximum allowable permeate flux, maximum feed flow rate, maximum recovery ratio and minimum concentrate flow rate for specific RO stage configuration.

- Within the developed RO operational design space, PV output power (ranging from minimum to maximum available power from PV source) lines are drawn to determine the feasible operational area of PVRO system.
- Within the computed feasible PVRO operational regime, design variables (feed flow rate and system pressure) are manipulated in such a way to keep the RO operation at optimum operational methodology while taking the wide range of PV power utilization into consideration.
- The investigated operational methodologies are constant feed water flow rate, constant feed pressure, constant retentate flow rate, constant recovery ratio, maximum PV utilization scheme and constant permeate concentration. For each of this methodology specific energy consumption (SEC) of RO unit over the whole range of available PV power is computed.
- The analysis of the results revealed that least SEC of the RO system is achieved by constant feed pressure methodology when the available PV power is sufficient enough to drive the RO pump. Constant recovery ratio methodology is preferable with slightly higher SEC than constant feed pressure methodology's SEC as it provides relatively broader range of available PV power utilization.
- The proposed optimal/hybrid operational methodology produces 28.14%, 17.79% and 6.4% more water than constant pressure methodology when operated by Fixed PV, single axis and double axis tracking PV panels.
- For the selected optimum operational methodology (constant pressure, constant recovery ratio, optimal/hybrid), reference signals of feed flow rate and RO pressure are computed according to the available PV power from the fixed and tracked PV panels.

These generated signals will be used as reference signals for local control loops in RO system.

- Environmental effects of conventional water treatment are elaborated. To make the PVRO operation environmental friendly, UV photo catalysis based pretreatment process is discussed in detail. In pursuit of this, solar photo catalysis based stair case and parabolic trough concentrator photo reactor are designed and tested for the bacterial disinfection for the pretreatment and post treatment section of RO system.

6.2 Highlights of thesis contribution

- A detailed and comprehensive model of PVRO system is developed and validated through the experimental PVRO facility installed at the KFUM premises.
- PV system output power profiles are determined and elaborated with fixed and tracking PV panels for different days of the year.
- For single stage single pass RO network configuration, RO operational design space is constructed by taking the RO membrane operational constraints into consideration.
- Within the developed RO operational design space, PV output power lines are drawn to come up with feasible operational area of PV and RO systems.
- Within the PVRO feasible operational area, different operational methodologies are discussed for reduced SEC and maximum utilization of wide range of available PV power.

- For the selected optimum operational methodology, reference signals of feed flow rate and RO system pressure are computed for control application according to the available PV power from the fixed and tracked PV panels.

- To make the PVRO operation environmental friendly, solar photo catalysis based stair case and parabolic trough concentrator photo reactor are designed and tested for the bacterial disinfection for the pretreatment and post treatment section of RO system.

6.3 Recommendations for future work

In our work we have used LabVIEW based data acquisition system to monitor and evaluate the performance analysis of whole PVRO system. For the commercial application, a smart microcontroller based handy and portable system is envisaged to design and develop. It should have the following capabilities.

- It should measure the environmental variables (ambient temperature, solar radiation), PV panel slope and its azimuth angle for PV tracking.
- Power available from and PV panels, power flow through the batteries and power consumed by the RO system should also by measured.
- Its embedded control capabilities should be able to construct the operational design space from the given RO operational constraints by user interface panel.
- Within the RO design space provisions of selection of different operational methodology should also be given.
- By considering the PV available power, power flow through the batteries (as a measure to check under loading and overloading state of the PV

panels), optimum RO operational parameter (RO system pressure and feed flow rate) are to be generated. The switching of methodology within the optimal operation regime must be done within 30-60 seconds to limit the rate of change of pressure and feed flow rate for the membrane safety.

Construction the RO operational design space for fixed feed salinity and feed temperature for a specific RO membrane type was carried out. For brackish water salinity is 10345 ppm and for sea water 35647 ppm is considered with temperature of 25^{o}C. To accommodate the salinity variations of the feed water, RO design space is to be computed for different feed water salinities. It would generate the relevant data to see the impact of salinity variation on the RO design space dimensions and it can be further used to streamline the optimal operational methodology. Moreover, the temperature variation effect (while keeping the feed salinity constant) may also be studied to see its effect on RO design space dimensions.

Another important area of research is to investigate the optimal sizing of battery in autonomously driven PVRO system. The battery storage is used to monitor the current flowing through it to access the PV panel under loading or over loading conditions. By measuring and manipulating these storage signals, RO parameters are to be adjusted actively to keep the RO running at the available PV power.

The full scale designing, developing and testing of solar based UV disinfection unit is also envisaged that can by integrated to the RO unit in pretreatment and post treatment stage for bacterial disinfection. The attained results was only for a single bacterial species and more work is envisaged to assess the photo catalytic disinfection process on other strains of bacteria and pathogenic organism i.e. protozoa and viruses.

References

[1] V. Gewin, Industry lured by the gains of going green, *Nature* 436 (2005) 173.

[2] M.A. Shannon, P.W. Bohn, M. Elimelech, J.G. Georgiadis, B.J. Marinas, A.M. Mayes, Science and technology for water purification in the coming decades. *Nature* 452 (2008) 301-310.

[3] R.W. Baker, Membrane Technology and Applications, 2nd ed., John Wiley & Sons, Chichester, New York, 2004.

[4] Al-Karaghouli, Ali, David Renne, and Lawrence L. Kazmerski. "Solar and wind opportunities for water desalination in the Arab regions." Renewable and Sustainable Energy Reviews 13.9 (2009): 2397-2407.

[5] A.P. Rao, N.V. Desai, R. Rangarajan, Interfacially synthesized thin film composite RO membrane for seawater desalination, *J. Membr. Sci*. 124 (1997) 263.

[6] A.M.K. El-Ghonemy, "Future sustainable water desalination technologies for the Saudi Arabia: A review "Renewable and Sustainable Energy Reviews 16 (2012) 6566–6597

[7] Ali Al-Karaghouli, David Renne, Lawrence L. Kazmerski "Technical and economic assessment of photovoltaic-driven desalination systems." Renewable Energy 35 (2010) 323–328

[8] Ali, Muhammad Tauha, Hassan ES Fath, and Peter R. Armstrong. "A comprehensive techno-economical review of indirect solar desalination." *Renewable and Sustainable Energy Reviews* 15.8 (2011): 4187-4199.

[9] Bilton, Amy M., Richard Wiesman, A. F. M. Arif, Syed M. Zubair, and Steven Dubowsky. "On the feasibility of community-scale photovoltaic-powered reverse osmosis desalination systems for remote locations." Renewable Energy 36, no. 12 (2011): 3246-3256.

[10] Alawaji, Saleh, Mohammed Salah Smiai, Shah Rafique, and Byron Stafford. "PV-powered water pumping and desalination plant for remote areas in Saudi Arabia." Applied energy 52, no. 2 (1995): 283-289.

[11] Franca, K. B., H. M. Laborde, and H. Neff. "Design and performance of small scale solar powered water desalination systems, utilizing reverse osmosis."*Journal of solar energy engineering* 122.4 (2000): 170-175.

[12] Herold, Dirk, and Apostolos Neskakis. "A small PV-driven reverse osmosis desalination plant on the island of Gran Canaria." *Desalination* 137.1 (2001): 285-292.

[13] Joyce, António, David Loureiro, Carlos Rodrigues, and Susana Castro. "Small reverse osmosis units using PV systems for water purification in rural places."Desalination 137, no. 1 (2001): 39-44.

[14] Thomson, Murray, and David Infield. "A photovoltaic-powered seawater reverse-osmosis system without batteries." *Desalination* 153.1 (2003): 1-8.

[15] Espino, Tomas, Baltasar Penate, Gonzalo Piernavieja, Dirk Herold, and Apostel Neskakis. "Optimised desalination of seawater by a PV powered reverse osmosis plant for a decentralised coastal water supply." Desalination156, no. 1 (2003): 349-350.

[16] Richards, Bryce S., and Andrea I. Schäfer. "Photovoltaic-powered desalination system for remote Australian communities." *Renewable Energy* 28.13 (2003): 2013-2022.

[17] Oliveira Jr, Demercil S., Douglas Bressan Riffel, and Ricardo Gildo V. de Oliveira. "Mathematical Model of a Photovoltaic Powered Reverse Osmosis Plant without Batteries." - World Climate & Energy Event, 15-17 February 2005, Rio de Janeiro, Brazil

[18] Schäfer, A. I., Andreas Broeckmann, and B. S. Richards. "Renewable energy powered membrane technology. 1. Development and characterization of a photovoltaic hybrid membrane system." *Environmental science & technology* 41.3 (2007): 998-1003.

[19] Mohamed, Essam Sh, G. Papadakis, E. Mathioulakis, and V. Belessiotis. "A direct coupled photovoltaic seawater reverse osmosis desalination system toward battery

based systems—a technical and economical experimental comparative study." Desalination 221, no. 1 (2008): 17-22.

[20] Richards, B. S., D. P. S. Capão, and A. I. Schäfer. "Renewable energy powered membrane technology. 2. The effect of energy fluctuations on performance of a photovoltaic hybrid membrane system." *Environmental science & technology* 42.12 (2008): 4563-4569.

[21] Kim, Seung Joon, Sanghoun Oh, Young Geun Lee, Moon Gu Jeon, In S. Kim, and Joon Ha Kim. "A control methodology for the feed water temperature to optimize SWRO desalination process using genetic programming." Desalination247, no. 1 (2009): 190-199.

[22] Qiblawey, Hazim, Fawzi Banat, and Qais Al-Nasser. "Laboratory setup for water purification using household PV-driven reverse osmosis unit." *Desalination and Water Treatment* 7.1-3 (2009): 53-59.

[23] Riffel, Douglas B., and Paulo Carvalho. "Small-scale photovoltaic-powered reverse osmosis plant without batteries: Design and simulation." *Desalination*247.1 (2009): 378-389.

[24] Khayet, M., M. Essalhi, C. Armenta-Déu, C. Cojocaru, and N. Hilal. "Optimization of solar-powered reverse osmosis desalination pilot plant using response surface methodology." Desalination 261, no. 3 (2010): 284-292.

[25] Kelley, Leah C., and Steven Dubowsky. "Thermal control to maximize photovoltaic powered reverse osmosis desalination systems productivity." *Desalination* 314 (2013): 10-19.

[26] Peñate, Baltasar, Fernando Castellano, Alejandro Bello, and Lourdes García-Rodríguez. "Assessment of a stand-alone gradual capacity reverse osmosis desalination plant to adapt to wind power availability: A case study." Energy 36, no. 7 (2011): 4372-4384.

[27] Forstmeier, Markus, Wilhelm Feichter, and Oliver Mayer. "Photovoltaic powered water purification-challenges and opportunities." *Desalination* 221.1 (2008): 23-28.

[28] Gandhidasan, P., and Sultan A. Al-Mojel. "Effect of feed pressure on the performance of the photovoltaic powered reverse osmosis seawater desalination system." *Renewable Energy* 34.12 (2009): 2824-2830.

[29] Ali, M., A. Ajbar, E. Ali, and K. Alhumaizi. "Robust model-based control of a tubular reverse-osmosis desalination unit." Desalination 255, no. 1 (2010): 129-136.

[30] Alatiqi, Imad, Hisham Ettouney, and Hisham El-Dessouky. "Process control in water desalination industry: an overview." *Desalination* 126.1 (1999): 15-32.

[31] Gambier, Adrian, N. Blumlein, and Essameddin Badreddin. "Real-time fault tolerant control of a reverse osmosis desalination plant based on a hybrid system approach." *American Control Conference, 2009. ACC'09*. IEEE, 2009.

[32] Abbas, Abderrahim. "Model predictive control of a reverse osmosis desalination unit." *Desalination* 194.1 (2006): 268-280.

[33] Elshafei, Moustafa, Anwar Khalil Sheikh, and Naseer Ahmad. "Directly Driven RO System by PV Solar Panel Arrays." *Open Journal of Applied Sciences* 3.02 (2013): 35. (http://www.scirp.org/journal/ojapps)

[34] Benghanem, M. "Optimization of tilt angle for solar panel: case study for Madinah, Saudi Arabia." Applied Energy 88.4 (2011): 1427-1433.

[35] Hussein, H. M. S., G. E. Ahmad, and H. H. El-Ghetany. "Performance evaluation of photovoltaic modules at different tilt angles and orientations." Energy conversion and management 45.15 (2004): 2441-2452.

[36] Shariah, Adnan, M-Ali Al-Akhras, and I. A. Al-Omari. "Optimizing the tilt angle of solar collectors." Renewable Energy 26.4 (2002): 587-598.

[37] Duffie J.A., Beckman W.A., Solar engineering of thermal processes. Fourth Edition, New York: John Wiley and Sons; 2013.

[38] Nijegorodov, N., Devan, K. R. S., Jain, P. K., & Carlsson, S. "Atmospheric transmittance models and an analytical method to predict the optimum slope of an absorber plate, variously oriented at any latitude." Renewable Energy 4.5 (1994): 529-543.

[39] Gunerhan, Huseyin, and Arif Hepbasli. "Determination of the optimum tilt angle of solar collectors for building applications." Building and Environment 42.2 (2007): 779-783.

[40] Mousazadeh, Hossein, Alireza Keyhani, Arzhang Javadi, Hossein Mobli, Karen Abrinia, and Ahmad Sharifi. "A review of principle and sun-tracking methods for maximizing solar systems output." Renewable and Sustainable Energy Reviews 13, no. 8 (2009): 1800-1818.

[41] Zhang, Peng, Gongbo Zhou, Zhencai Zhu, Wei Li, and Zhixiong Cai. "Numerical study on the properties of an active sun tracker for solar streetlight." Mechatronics 23, no. 8 (2013): 1215-1222.

[42] Şenpinar, Ahmet, and Mehmet Cebeci. "Evaluation of power output for fixed and two-axis tracking PV arrays." Applied Energy 92 (2012): 677-685

[43] Eke, Rustu, and Ali Senturk. "Performance comparison of a double-axis sun tracking versus fixed PV system." Solar Energy 86.9 (2012): 2665-2672.

[44] Qiblawey, Hazim, Fawzi Banat, and Qais Al-Nasser. "Performance of reverse osmosis pilot plant powered by Photovoltaic in Jordan." Renewable Energy36.12 (2011): 3452-3460.

[45] Aybar, H. Ş., J. S. Akhatov, N. R. Avezova, and A. S. Halimov. "Solar powered RO desalination: Investigations on pilot project of PV powered RO desalination system." Applied Solar Energy 46, no. 4 (2010): 275-284.

[46] Schies, A., J. Went, C. Heidtmann, M. Eisele, F. Kroemke, H. Schmoch, and M. Vetter. "Operating control strategies and dimensioning of photovoltaic powered reverse osmosis desalination plants without batteries." Desalination and Water Treatment 21, no. 1-3 (2010): 131-137.

[47] Sobana, S., and Rames C. Panda. "Review on modelling and control of desalination system using reverse osmosis." Reviews in Environmental Science and Bio/Technology 10.2 (2011): 139-150.

[48] Sundaramoorthy, S., G. Srinivasan, and D. V. R. Murthy. "An analytical model for spiral wound reverse osmosis membrane modules: Part I—Model development and parameter estimation." Desalination 280.1 (2011): 403-411.

[49] Kaghazchi, Tahereh, Mahdieh Mehri, Maryam Takht Ravanchi, and Ali Kargari. "A mathematical modeling of two industrial seawater desalination plants in the Persian Gulf region." Desalination 252, no. 1 (2010): 135-142.

[50] Mane, Pranay P., Pyung-Kyu Park, Hoon Hyung, Jess C. Brown, and Jae-Hong Kim. "Modeling boron rejection in pilot-and full-scale reverse osmosis desalination processes." Journal of Membrane Science 338, no. 1 (2009): 119-127.

[51] Abbas, Abderrahim, and Nader Al-Bastaki. "Modeling of an RO water desalination unit using neural networks." Chemical Engineering Journal 114.1 (2005): 139-143.

[52] Jamal, K., M. A. Khan, and M. Kamil. "Mathematical modeling of reverse osmosis systems." Desalination 160.1 (2004): 29-42.

[53] Bartman, Alex R., Panagiotis D. Christofides, and Yoram Cohen. "Nonlinear model-based control of an experimental reverse-osmosis water desalination system." Industrial & Engineering Chemistry Research 48.13 (2009): 6126-6136.

[54] A. Gambier, Senior Member, IEEE, A. Krasnik, E. Badreddin. Dynamic Modeling of a Simple Reverse Osmosis Desalination Plant for Advanced Control Purposes, Proceedings of the 2007 American Control Conference Marriott Marquis Hotel at Times SquareNew York City, USA, July 11-13, 2007

[55] Riverol, C., and V. Pilipovik. "Mathematical modeling of perfect decoupled control system and its application: A reverse osmosis desalination industrial-scale unit." Journal of Analytical Methods in Chemistry 2005.2 (2005): 50-54.

[56] Chaaben, Abderrahmen B., Ridha Andoulsi, Anis Sellami, and Radhi Mhiri. "MIMO modeling approach for a small photovoltaic reverse osmosis desalination system." Journal of Applied Fluid Mechanics 4, no. 1 (2011): 35-41.

[57] Khayet, M., C. Cojocaru, and M. Essalhi. "Artificial neural network modeling and response surface methodology of desalination by reverse osmosis." Journal of Membrane Science 368.1 (2011): 202-214.

[58] Hossein Mousazadeh, Alireza Keyhani , Arzhang Javadi, Hossein Mobli, Karen Abrinia, Ahmad Sharifi. A review of principle and sun-tracking methods for maximizing solar systems output. Renewable and Sustainable Energy Reviews; 13 (2009); 1800‑1818

[59] Taher Maatallah, Souheil El Alimi, Sassi Ben Nassrallah, Performance modeling and investigation of fixed, single and dual-axis tracking photovoltaic panel in Monastir city, Tunisia, Renewable and Sustainable Energy Reviews 15 (2011); 4053– 4066

[60] Mondol, Jayanta Deb, Yigzaw G. Yohanis, and Brian Norton. "Solar radiation modelling for the simulation of photovoltaic systems." Renewable Energy 33.5 (2008): 1109-1120.

[61] Li, Danny HW, and Joseph C. Lam. "Predicting solar irradiance on inclined surfaces using sky radiance data." Energy Conversion and Management 45.11 (2004): 1771-1783.

[62] Posadillo, R., and R. López Luque. "Evaluation of the performance of three diffuse hourly irradiation models on tilted surfaces according to the utilizability concept." Energy Conversion and Management 50.9 (2009): 2324-2330.

[63] Chwieduk, Dorota A. "Recommendation on modelling of solar energy incident on a building envelope." Renewable Energy 34.3 (2009): 736-741.

[64] Lee, Shun Ching. "Operation analysis of a photovoltaic lighting system with battery and heater." Solar Energy 85.9 (2011): 2144-2153.

[65] Skoplaki, E., and J. A. Palyvos. "On the temperature dependence of photovoltaic module electrical performance: A review of efficiency/power correlations." Solar energy 83.5 (2009): 614-624.

[66] Benghanem, M. "Low cost management for photovoltaic systems in isolated site with new IV characterization model proposed." Energy Conversion and Management 50, no. 3 (2009): 748-755.

[67] Castañer, Luis & Santiago Silvestre Modelling Photovoltaic Systems, Using PSpice John Wiley & Sons Ltd, 2002

[68] Walker, Geoff R. "Evaluating MPPT converter topologies using a MATLAB PV model" Australasian Universities Power Engineering Conference, AUPEC '00, Brisbane, 2000

[69] Salas, V., E. Olias, A. Barrado, and A. Lazaro. "Review of the maximum power point tracking algorithms for stand-alone photovoltaic systems." Solar energy materials and solar cells 90, no. 11 (2006): 1555-1578.

[70] Houssamo, Issam, Fabrice Locment, and Manuela Sechilariu. "Maximum power tracking for photovoltaic power system: Development and experimental comparison of two algorithms." Renewable Energy 35.10 (2010): 2381-2387.

[71] Fundamentals of Salt Water Desalination by H.T. El-Sessouky and H.M.Ettouney, 2002 Elsevier science.

[72] DOW Filmtec™ Membranes. Filmtec™ Reverse Osmosis Membranes: Technical Manual. Form No. 609-00071-0705. http://www.dowwaterandprocess.com/en

[73] Lu, Yan-Yue, Yang-Dong Hu, Xiu-Ling Zhang, Lian-Ying Wu, and Qing-Zhi Liu. "Optimum design of reverse osmosis system under different feed concentration and product specification." Journal of membrane science 287, no. 2 (2007): 219-229.

[74] DOW Filmtec Membranes, Product SW30-4040 datasheet, Form No. 609-00350-0911. http://www.dowwaterandprocess.com/en

[75] Chang, Tian Pau. "Output energy of a photovoltaic module mounted on a single-axis tracking system." Applied energy 86.10 (2009): 2071-2078.

[76] Gunerhan, Huseyin, and Arif Hepbasli. "Determination of the optimum tilt angle of solar collectors for building applications." Building and Environment 42.2 (2007): 779-783.

[77] Chang, Tian Pau. "The gain of single-axis tracked panel according to extraterrestrial radiation." Applied Energy 86.7 (2009): 1074-1079.

[78] ARMINES. Technical and economic analysis of the potential for water desalination in the Mediterranean region, RENA-CT94–0063, France; 1996.

[79] Ammar Mahjoubi, Ridha Fethi Mechlouch and Ammar Ben Brahim, "A Low Cost Wireless Data Acquisition System for a Remote Photovoltaic (PV) Water Pumping System" Energies 2011, 4, 68-89; doi:10.3390/en4010068

[80] Sandro C. S. Jucá 1, Paulo C. M. Carvalho and Fábio T. Brito. "A Low Cost Concept for Data Acquisition Systems Applied to Decentralized Renewable Energy Plants" Sensors 2011, 11, 743-756; doi:10.3390/s110100743

[81] Peng Jiang, Hongbo Xia, Zhiye He and Zheming Wang. "Design of a Water Environment Monitoring System Based on Wireless Sensor Networks" Sensors 2009, 9, 6411-6434; doi:10.3390/s90806411

[82] Belmili, Hocine, Salah Med Ait Cheikh, Mourad Haddadi, and Cherif Larbes. "Design and development of a data acquisition system for photovoltaic modules characterization." *Renewable Energy* 35, no. 7 (2010): 1484-1492.

[83] M. Benghanem. "A low cost wireless data acquisition system for weather station monitoring." Renewable Energy 35 (2010) 862–872

[84] Hazim Qiblawey, Fawzi Banat, Qais Al-Nasser. "Performance of reverse osmosis pilot plant powered by Photovoltaic in Jordan." Renewable Energy 36 (2011) 3452-3460

[85] Daniel P. Clarke, Yasir M. Al-Abdeli, Ganesh Kothapalli. The effects of including intricacies in the modeling of a small-scale solar-PV reverse osmosis desalination system, Desalination 311 (2013) 127–136

[86] Bilton, Amy M., Leah C. Kelley, and Steven Dubowsky. "Photovoltaic reverse osmosis—Feasibility and a pathway to develop technology." *Desalination and Water Treatment* 31, no. 1-3 (2011): 24-34.

[87] B.S.Rrichards ,D.P.Scapão and A.I.Schafer. "Renewable Energy Powered Membrane Technology. 2. The Effect of Energy Fluctuations on Performance of a Photovoltaic Hybrid Membrane System." Environ. Sci. Technol. 2008, 42, 4563–4569

[88] Qiblawey H, Banat F, Al-Nassera Q. "Laboratory setup for water purification using household PV-driven reverse osmosis unit." Desalination and Water Treatment 2009;7:53-59.

[89] Douglas B. Riffela, Paulo C.M. Carvalhob. "Small-scale photovoltaic-powered reverse osmosis plant without batteries: Design and simulation." Desalination 247 (2009) 378–389

[90] Scrivani, A. "Energy management and DSM techniques for a PV-diesel powered sea water reverse osmosis desalination plant in Ginostra, Sicily." Desalination 183.1 (2005): 63-72.

[91] Y. Kim, S. Kim, Y. Kim, S. Lee, I. Kim, J. Kim, "Overview of systems engineering approaches for a large-scale seawater desalination plant with a reverse osmosis network" Desalination 238 (1–3) (2009) 312–332.

[92] Y.-Y. Lu, Y.-D. Hu, D.-M. Xu, L.-Y. Wu, "Optimum design of reverse osmosis seawater desalination system considering membrane cleaning and replacing" Journal of Membrane Science 282 (1–2) (2006) 7–13.

[93] M. Zhu, M. El-Halwagi, M. Al-Ahmad, "Optimal design and scheduling of flexible reverse osmosis networks" Journal of Membrane Science 129 (2) (1997) 161–174.

[94] H. See, V. Vassiliadis, D. Wilson, "Optimisation of membrane regeneration scheduling in reverse osmosis networks for seawater desalination" Desalination 125 (1–3) (1999) 37–54.

[95] M. Marcovecchio, P. Aguirre, N. Scenna, "Global optimal design of reverse osmosis networks for seawater desalination: Modeling and algorithm" Desalination 184 (1–3) (2005) 259–271.

[96] A. Villafafila, I. Mujtaba, “Fresh water by reverse osmosis based desalination: Simulation and optimization” Desalination 155 (1) (2003) 1–13.

[97] Wilf, Mark, and Craig Bartels. "Optimization of seawater RO systems design." Desalination 173, no. 1 (2005): 1-12.

[98] Wilf, Mark, and Kenneth Klinko. "Optimization of seawater RO systems design." Desalination 138, no. 1 (2001): 299-306.

[99] Lu, Yan-Yue, Yang-Dong Hu, Xiu-Ling Zhang, Lian-Ying Wu, and Qing-Zhi Liu. "Optimum design of reverse osmosis system under different feed concentration and product specification." Journal of membrane science 287, no. 2 (2007): 219-229.

[100] Lu, Yanyue, Anping Liao, and Yangdong Hu. "The design of reverse osmosis systems with multiple-feed and multiple-product." *Desalination* 307 (2012): 42-50.

[101] Sassi, Kamal M., and Iqbal M. Mujtaba. "Effective design of reverse osmosis based desalination process considering wide range of salinity and seawater temperature." *Desalination* 306 (2012): 8-16.

[102] Laborde, H. M., K. B. Franca, H. Neff, and A. M. N. Lima. "Optimization strategy for a small-scale reverse osmosis water desalination system based on solar energy." Desalination 133, no. 1 (2001): 1-12.

[103] Miranda, Marcos S., and David Infield. "A wind-powered seawater reverse-osmosis system without batteries." *Desalination* 153.1 (2003): 9-16.

[104] Liu, Clark CK, Park Jae-Woo, Reef Migita, and Qin Gang. "Experiments of a prototype wind-driven reverse osmosis desalination system with feedback control." Desalination 150, no. 3 (2002): 277-287.

[105] Manth, Thomas, Michael Gabor, and Eli Oklejas Jr. "Minimizing RO energy consumption under variable conditions of operation." *Desalination* 157.1 (2003): 9-21.

[106] Epp, Christian, and Michael Papapetrou. "Co-ordination action for autonomous desalination units based on renewable energy systems—ADU-RES." *Desalination* 168 (2004): 89-93.

[107] de la Nuez Pestana, Ignacio, Francisco Javier García Latorre, Celso Argudo Espinoza, and Antonio Gómez Gotor. "Optimization of RO desalination systems powered by renewable energies. Part I: Wind energy." Desalination160, no. 3 (2004): 293-299.

[108] Gilau, Asmerom M., and Mitchell J. Small. "Designing cost-effective seawater reverse osmosis system under optimal energy options." *Renewable energy* 33.4 (2008): 617-630.

[109] Khayet, M., M. Essalhi, C. Armenta-Déu, C. Cojocaru, and N. Hilal. "Optimization of solar-powered reverse osmosis desalination pilot plant using response surface methodology." Desalination 261, no. 3 (2010): 284-292.

[110] Poullikkas, Andreas. "An optimization model for the production of desalinated water using photovoltaic systems." *Desalination* 258.1 (2010): 100-105.

[111] SUNPOWER, 230 SOLAR PANEL, exceptional efficiency and performance, data sheet Document #001-42190 Rev*A / LTR_EN, Mar 2009.

[112] Mean Well, 500W True Sine Wave DC-AC Inverter with MPPT Solar Charger, Data Sheet for Operation. http://www.meanwell.com/search/ISI-501/default.htm

[113] Lu, Yan-Yue, Yang-Dong Hu, Xiu-Ling Zhang, Lian-Ying Wu, and Qing-Zhi Liu. "Optimum design of reverse osmosis system under different feed concentration and product specification." Journal of membrane science 287, no. 2 (2007): 219-229.

[114] DOW Filmtec™ Membranes. Filmtec™ Reverse Osmosis Membranes: Technical Manual. Form No. 609-00071-0705.

[115] DOW Filmtec™ Membranes. Filmtec™, DOW FILMTEC SW30HR LE-400i Seawater Reverse Osmosis Element with iLEC™ Interlocking Endcaps, Form No. 609-00477-1109.

[116] Pritchard, C., V. Verbeek, and Z. Rahal. "A preliminary design of a direct-driven wind-powered SWRO system." International desalination and water reuse quarterly 13.1 (2003): 29-33.

[117] A.M.K. El-Ghonemy, Water desalination systems powered by renewable energy sources: Review, Renewable and Sustainable Energy Reviews 16 (2012) 6566–6597

[118] A. Sheikh, S. Dubowsky, Design and Manufacturing of Solar Power System and Devices for Challenging Environments, Presented at 9th workshop on clean water and clean energy, 8 January 2013, KFUPM, Saudi Arabia.

[119] Malato, Sixto, P. Fernández-Ibáñez, M. I. Maldonado, J. Blanco, and W. Gernjak. "Decontamination and disinfection of water by solar photocatalysis: recent overview and trends." Catalysis Today 147, no. 1 (2009): 1-59.

[120] Kim, J.-O., Jung, J.-T., Chung, J, 2007, Treatment performance of metal membrane microfiltration and electrodialysis integrated system for wastewater reclamation, Desalination 202 (2007), 343-350, http://www.desline.com/articoli/8515.pdf

[121] Vedavyasan, C.V, 2007, Pretreatment trends – an overview, Desalination 203 (2007), 296-299, http://www.desline.com/articoli/8041.pdf

[122] Wilf, Mark, and Kenneth Klinko. "Effective new pretreatment for seawater reverse osmosis systems." Desalination 117, no. 1 (1998): 323-331.

[123] Xu, Jia, Guoling Ruan, Xizhang Chu, Ye Yao, Baowei Su, and Congjie Gao. "A pilot study of UF pretreatment without any chemicals for SWRO desalination in China." Desalination 207, no. 1 (2007): 216-226.

[124] Hassan, A.M., Al-Sofi, M.A.K., Al-Amoudi, A.S., Jamaluddin, A.T.M., Farooque, A.M., Rowaili, A., Dalvi, A.G.I., Kither, N.M., Mustafa, G.M., Al-Tisan, I.A.R., 2007, A new approach to membrane and thermal seawater desalination processes using nanofiltration membranes (Part 1), Desalination 118 (1998), 35-51.

[125] Al-Shammiri, M., Safar, M., Al-Dawas, M., "Evaluation of two different antiscalants in real operation at the Doha research plant." Desalination 128 (2000) 1-16.

[126] AQUA-CSP.In:Trieb F,SchillingsC,ViebahnP,PaulC,AltowaieH,SufianT, Alnaser W, KabaritiM, ShahinW,BennounaA, NokraschyH, KernJ,KniesG, El BassamN, HasairiI, HaddoucheA, GladeH, AliewiA.Concentrating solar power for sea water desalination. German Aerospace Center(DLR). Study for the German Ministry of

Environment. Nature Conversation and Nuclear Safety, Stuttgart;2007, /www.dlr.de/tt/aqua-csp

[127] S. Malato , Julian Blanco, Diege C Alarcon "Photocatalytic decontamination and disinfection of water with solar collector." Catalysis Today 122 (2007) 137–149

[128] Malato, Sixto, P. Fernández-Ibáñez, M. I. Maldonado, J. Blanco, and W. Gernjak. "Decontamination and disinfection of water by solar photocatalysis: recent overview and trends." Catalysis Today 147, no. 1 (2009): 1-59.

[129] Meng Nan Chong, Bo Jin, Christopher W.K. Chow, Chris Saint, "Recent developments in photocatalytic water treatment technology: A review." Water research 44 (2010)2997-3027

[130] Sixto Malato, Julia´n Blanco, Diego C. Alarco´n, Manuel I. Maldonado, Pilar Ferna´ndez-Iba´n˜ez, Wolfgang Gernjak, "Photocatalytic decontamination and disinfection of water with solar collectors." Catalysis Today 122 (2007) 137–149

[131] S. Malato Rodrı´guez, J. Blanco Ga´lvez, M.I. Maldonado Rubio, P. Ferna´ndez Iba´n˜ez, D. Alarco´n Padilla, M. Collares Pereira, J. Farinha Mendes, J. Correia de Oliveira, "Engineering of solar photocatalytic collectors." Solar Energy 77 (2004) 513-524.

[132] Ahmed, Saber, M. G. Rasul, R. Brown, and M. A. Hashib. "Influence of parameters on the heterogeneous photocatalytic degradation of pesticides and phenolic contaminants in wastewater: a short review." Journal of Environmental Management 92, no. 3 (2011): 311-330.

[133] Saito, T., T. Iwase, J. Horie, and T. Morioka. "Mode of photocatalytic bactericidal action of powdered semiconductor TiO2 on mutans streptococci." Journal of Photochemistry and Photobiology B: Biology 14, no. 4 (1992): 369-379.

[134] Maness, Pin-Ching, Sharon Smolinski, Daniel M. Blake, Zheng Huang, Edward J. Wolfrum, and William A. Jacoby. "Bactericidal activity of photocatalytic TiO2 reaction: toward an understanding of its killing mechanism." Applied and environmental microbiology 65, no. 9 (1999): 4094-4098.

[135] Barati, Nastaran, and MA Faghihi Sani. "Coating of titania nanoparticles on stainless steel using an alkoxide precursor." Prog. Color Colorants Coat 2 (2009): 71-78.

[136] T.Y. Leung, C. Y. Chan, C. Hu, J. C. Yu, P. K. Wong "Photo catalytic disinfection of marine bacteria using fluorescent light." Water research 42.19 (2008): 4827-4837.

Appendix

Data for Operational window:

		1	2	2_	3	4	5	6	7	8	9	10	11	12
pf	bar	33.01	39.92	52.86	66.18	67.61	67.98	69.73	67.14	51.8	48.5	35	33.3	33
qf	m3/h	14.08	14.08	14.08	14.08	12.34	10.86	9.08	9.21	5.23	5	4	7.83	12.1
qp,i	m3/h	0.19	0.43	0.84	1.2	1.2	1.2	1.2	1.15	0.69	0.6	0.2	0.19	0.19
yi	%age	1	3	6	9	10	11	13	13	13	12	6	2	2
qc	m3/h	13.51	12.67	11.26	10.08	8.39	7.06	5.44	5.71	3.4	3.4	3.4	7.24	11.53
cp	mg/l	500	217.9	122	95.32	100	107	119	120	215	237	500	500	500
Jw	l/m2h	3.83	9.47	18.95	26.9	26.57	25.56	24.42	23.55	12.3	10.8	4.2	3.95	3.87
y	% age	4.04	10	20	28.4	32	35	40	38	35	32	15	7.5	4.75
Po	kWh/m3	26.68	13.98	9.24	8.14	7.38	6.78	6.08	6.17	5.17	5.3	8.1	15.6	24.38

Data for Constant Pressure Methodology

	Feed Flow rate (m3/hour)	Feed Pressure (bar)	System Recovery (%age)	Concentrate Flow (m3/hour)	Concentrate Pressure (bar)	Permeate Flow (m3/hour)	Permeate Concen (mg/l)	HPP Power (kW)	Calculated Power (kW)	Recovered Power (kW)	Net Driving Power (kW)	SEC (kWh/m3)
1	6.7	**61.39**	40	4.02	60.83	2.68	159	14.36	14.28	5.43	8.85	3.30
2	7.55	**61.64**	38	4.68	60.96	2.87	145	16.25	16.16	6.34	9.82	3.42
3	8.29	**61.39**	36	5.31	60.6	2.98	136	17.77	17.67	7.15	10.52	3.53
4	9.26	**61.62**	34	6.11	60.66	3.15	127	19.93	19.81	8.24	11.58	3.68
5	10.2	**61.52**	32	6.94	60.39	3.26	120	21.91	21.79	9.31	12.47	3.83
6	11.4	**61.83**	30	7.98	60.49	3.42	112	24.62	24.47	10.73	13.75	4.02

Data for Constant Recovery Ratio

	Feed Flow rate (m3/hour)	Feed Pressure (bar)	System Recovery (%age)	Concentrate Flow (m3/hour)	Concentrate Pressure (bar)	Permeate Flow (m3/hour)	Permeate Concen (mg/l)	HPP Power (kW)	Calculated Power (kW)	Recovered Power (kW)	Net Driving Power (kW)	SEC (kWh/m3)
1	3.5	43.71	**30**	2.45	43.46	1.05	351	5.35	5.31	2.37	2.95	2.81
2	5	46.86	**30**	3.5	46.46	1.5	247	8.2	8.14	3.61	4.52	3.01
3	6.5	50.13	**30**	4.55	49.53	1.95	192	11.4	11.31	5.01	6.31	3.23
4	8	53.53	**30**	5.6	52.73	2.4	158	14.97	14.87	6.56	8.31	3.46
5	9.5	57.09	**30**	6.65	56.05	2.85	134	18.95	18.83	8.28	10.55	3.70
6	11	60.81	**30**	7.7	59.54	3.3	116.4	23.36	23.23	10.19	13.04	3.95

Data for Constant Feed Flow Rate

	Feed Flow rate (m3/hour)	Feed Pressure (bar)	System Recovery (%age)	Concentrate Flow (m3/hour)	Concentrate Pressure (bar)	Permeate Flow (m3/hour)	Permeate Concen (mg/l)	HPP Power (kW)	Calculated Power (kW)	Recovered Power (kW)	Net Driving Power (kW)	SEC (kWh/m3)
1	**11**	32.78	5	10.45	31.21	0.55	523	12.65	12.52	7.25	5.27	9.59
2	**11**	37.61	10	9.9	36.11	1.1	277	14.5	14.36	7.94	6.42	5.84
3	**11**	42.64	15	9.35	41.22	1.65	195	16.43	16.29	8.56	7.72	4.68
4	**11**	48.13	20	8.8	46.73	2.2	154	18.52	18.38	9.14	9.24	4.20
5	**11**	54.12	25	8.25	52.8	2.75	132	20.81	20.67	9.68	10.99	4.00
6	**11**	60.81	30	7.7	59.54	3.3	116	23.36	23.23	10.19	13.04	3.95

Data for Constant Concentrate Flow Rate

	Feed Flow rate (m3/hour)	Feed Pressure (bar)	System Recovery (%age)	Concentrate Flow (m3/hour)	Concentrate Pressure (bar)	Permeate Flow (m3/hour)	Permeate Concen (mg/l)	HPP Power (kW)	Calculated Power (kW)	Recovered Power (kW)	Net Driving Power (kW)	SEC (kWh/m3)
1	8.1	31.48	5	**7.7**	30.46	0.4	704	8.95	8.85	5.21	3.64	9.10
2	8.56	35.8	10	**7.7**	34.75	0.86	353	10.75	10.64	5.95	4.69	5.46
3	9.06	40.56	15	**7.7**	39.46	1.36	235	12.87	12.76	6.75	6.01	4.42
4	9.63	46.09	20	**7.7**	44.94	1.92	176	15.52	15.41	7.69	7.72	4.02
5	10.27	52.7	25	**7.7**	51.48	2.57	140	18.91	18.79	8.81	9.98	3.88
6	11	60.81	30	**7.7**	59.54	3.3	116	23.36	23.23	10.19	13.04	3.95

Thesis Publications

- **Naseer Ahmad**, Anwar Khalil Sheikh, P. Gandhidasan, Moustafa Elshafie, Modeling, Simulation and performance evaluation of a community scale PVRO Water Desalination System operated by fixed and tracking PV Panels: A case study for Dhahran city, Saudi Arabia. Renewable Energy 75 (2015) 433-447, **(Impact Factor 3.8).** http://dx.doi.org/10.1016/j.renene.2014.10.023

- Mahmood Kassas, **Naseer Ahmad**, Simulation and Implementation of Space Vector Pulse width Modulation Using look up Table. Arab J Sci Eng (2014) 39:4815–4828. http://link.springer.com/article/10.1007/s13369-014-0965-2

- M. Elshafei, A. Sheikh and **Naseer Ahmad**, "Directly Driven RO System by PV Solar Panel Arrays," Open Journal of Applied Sciences, Vol. 3 No. 2B, 2013, pp. 35-40. doi: 10.4236/ojapps.2013.32B007. http://file.scirp.org/Html/37839.html

- **Naseer Ahmad**, Anwar Khalil Sheikh, Moustafa Elshafie, Hussain Alqahtani. Design and Development of Instrumentation and Data Acquisition for a Photovoltaic Driven Community Scale RO Desalination System and Its Performance Studies, Proceedings of the 12th Biennial ASME Conference on Engineering System Design and Analysis, ESDA14, June 25-27, 2014, **Copenhagen, Denmark**. http://proceedings.asmedigitalcollection.asme.org/proceeding.aspx?articleID=1920117

- M.A.Gondal, **Naseer Ahmad**, Anwar Khalil Sheikh. Water Disinfection Strategies Using Solar Photo Catalysis and Some Prototype Devices for Small Scale Application. The Photocatalytic and Superhydrophilic Surfaces Workshop, PSS2013, **Manchester, UK**, December 2013. http://www.dri.mmu.ac.uk/pss2013/files/pss2013-poster-24-ma-gondal.pdf

- Moustafa Elshafei, Anwar Khalil Sheikh and **Naseer Ahmad**, "Directly Driven RO systems by PV Solar Panel Arrays," presented at the International Conference on Smart Grid (CSG2013), **Beijing, China**, June, 2013.

- **Naseer Ahmad**, M.A.Gondal, Anwar Khalil Sheikh, Comparative Study of Different Solar Based Photo catalytic Reactors for Disinfection of Contaminated Water. Desalination and Water treatment journal. **(Accepted for Publication)**

- **Naseer Ahmad**, Anwar Khalil Sheikh, Moustafa Elshafie, P. Gandhidasan, On The Determination of Optimal Operational Methodology for Community Scale Photovoltaic Driven Reverse Osmosis Water Desalination System, Submitted to Renewable Energy Journal. (under review)

Vitae

Name	Naseer Ahmad
Nationality	Pakistani
Date of Birth	7 Dec 1977
Email	naseer_mct@yahoo.com, nahmad@kfupm.edu.sa

EDUCATION

PhD, Mechanical Engineering, November 2014

King Fahd University of Engineering and Technology, Dhahran, Saudi Arabia.

PhD Course work GPA = 3.75 (out of 4.00).

MS, Mechatronics Engineering, March 2003

The University of Engg & Tech Lahore, Pakistan.

Thesis: *Servomechanism for Gap control of an ECM machine*.

Marks Obtained: 81% (Degree with honors)

BE, Mechanical Engineering, Dec 2000 (16 Yrs Education)

The University of Engg & Tech, Lahore, Pakistan.

Project: *Design, Fabrication & Programming of an Autonomous Vehicle*

Marks Obtained: 79% (Degree with honors)

Member Pakistan Engineering Council (PEC-MECH/17159)

PROFESSIONAL EXPERIENCE

Lecturer-B. **Sept 2009- Nov 2014**

KFUPM, Mechanical Engg Dept. Dhahran, KSA

Assistant Professor. **Nov 2004 – Sept 2009**

University of Engg & Tech. Lahore, Pakistan

- Worked as ***lab director*** of ***Instrumentation & Control*** and ***Embedded Systems*** labs in the Mechatronics & Control Engg Department.
- Diligently involved in the procurement, installation and got the training of the equipment of the following Labs in the Mechatronics & Control Engg Dept.
  - *Instrumentation & Control Lab*
  - *Embedded systems Lab*
  - *Robotics & Automation Lab*
  - *Hydraulics and Pneumatics Lab*

Lecturer/Lab Engineer **Dec'01—Nov '04**

University of Engg & Tech Lahore